

Tissue Stiffness Drives Breast Cancer Malignant Progression

by

Luke David Cassereau

DISSERTATION

Submitted in partial satisfaction of the requirements for the degree of

DOCTOR OF PHILOSOPHY

in

Bioengineering

in the

GRADUATE DIVISION

of the

UNIVERSITY OF CALIFORNIA, SAN FRANCISCO

AND

UNIVERSITY OF CALIFORNIA, BERKELEY

Dedication and Acknowledgments

This dissertation, the research in it and the process of writing it, would not have been possible without the tremendous mentors and support system I have had during my time as a PhD student. All of this was only possible with the people who taught, guided, and supported me and without them none of this would have been possible. With that in mind I would like to thank:

My PhD advisor, Dr. Valerie Weaver. Before I met Valerie, I was fairly certain I did not enjoy academic research as my previous experiences had been dull at best. However, starting work with Valerie as an undergraduate immediately inspired me and convinced me to pursue a PhD. From then Valerie has been one of my biggest supporters and has spent an inordinate amount of time teaching and instructing me and helping me develop into a better scientist. Everything from how to read a paper, how to write a paper, how to give a presentation, or how to fundamentally drive a scientific project Valerie has gone out of her way and beyond what is required for her to help me and be a mentor for me.

My dissertation and qualification exam committee, Dr. Tejal Desai, Dr. Dan Fletcher, Dr. Sanjay Kumar, and Dr. Nancy Boudreau. The two toughest challenges in the PhD program are easily the qualifying exam and the dissertation; yet my committee, through their support and accessibility, made the process an excellent learning experience and while still a challenge it never felt impossible. Additionally, all four of my committee members serve as tremendous examples for me of scientific excellence and professionalism and I hope to live up their example as I move on in my career.

My PhD lab, the Weaver lab. In many aspects the PhD is a test of endurance but I was fortunate to work among a group of people that consistently brought an excellent work ethic and enthusiasm making it much easier to keep up consistently strong effort. Moreover, surrounded by so many talented scientists set my personal standards much higher and was also a terrific environment for learning a diverse set of experimental skills. As such, in a less broad and interdisciplinary group I would not have learned or accomplished anywhere near as much as I did.

My golden bear family. While it has been several years since we were all in school together, I have been fortunate to stay in close touch with all of you. In particular, every get together we have, whether just a hangout, a holiday ski trip, or everyone coming to my first bodybuilding contest, seeing you all and spending time together is always a nice break and chance to recharge.

My girlfriend and best friend, Jeni Lee. Throughout this whole process, both highs and lows, you have been my closest confidant and supporter. Earning the PhD has been so much easier having someone I am so close to that can directly relate to the experience. Moreover, you are not just supportive but you push me to be better to not settle and always striving to improve. I can't wait to see what the next chapter of our careers will be like and to work through it with you by my side.

My family. Long before I was writing my PhD and nearing completion of this degree, the support and encouragement from my parents, grandparents, uncles and aunts convinced me I could accomplish whatever I set my mind to. Through this whole process whether through words of encouragement or direct financial support to help me be slightly less of a starving student, the help from my family was integral to my success in school culminating in the completion of my PhD. In particular, I would like to thank my grandparents as their emphasis on education and their encouragement absolutely set in motion my path towards graduate school. To my Grandpa and Mamie, I know you both would have been proud to see my finish my degree and I hope you both know how important you were to my achievements.

Last but not least, I would like to especially thank my parents. There was a time in which school did not interest me and it showed in my performance. Yet, my parents still believed in my potential and when I realized I wanted to focus on my education they were there encouraging me and often directly helping me study. That work together, their investment in me ultimately made me into the student I am today and without their belief in me I wouldn't have made it this far by a long shot.

Abstract

Breast cancer is the most common cancer of women worldwide and the second leading cause of cancer death in women in the United States. Despite new therapies that show efficacy in treating the primary tumor there is a significant lack of therapies that treat metastasis, the most common cause of death. This deficit underscores the necessity for a new perspective in the study of breast cancer metastasis. Breast cancer malignant progression coincides with drastic tissue extracellular matrix (ECM) remodeling and stiffening. Previous work in our lab has shown that ECM stiffening is both necessary and sufficient to drive tumor aggression and metastasis *in vivo*. Consistently, our lab has demonstrated ECM mechanical properties act through integrin focal adhesions to regulate cell functions critical to tumor aggression such as cell proliferation, survival, and motility. Yet, how ECM structural changes occur with tumor progression and which signaling mechanisms downstream of cell-ECM adhesions are critical for tumor aggression remains unclear. In this thesis I address the overarching hypothesis that ECM mechanical properties influence tumor malignant progression through integrin focal adhesion signaling and subsequent downstream signaling affecting tumor motility and invasion, tumor metabolism, and immune cell response. To address this hypothesis I used a combination of isolated mammary epithelial cells with 2D and 3D mechanically tunable substrates *ex vivo*, *in vivo* breast cancer models, and human breast cancer tissues samples to robustly quantify the physical and structural ECM changes with tumor progression, identify through which integrin signaling mechanisms tumor cells sense these changes, and determine how tumor cell mechanosensing alters cell signaling to regulate tumor metastasis. From this work I found that tumor cell malignant phenotype is enhanced by ECM stiffness specifically via $\alpha 5\beta 1$ – FN integrin

binding which enhances pro-tumorigenic cell signaling to enhance tumor cell invasion and migration and alter tumor cell metabolism. Additionally, ECM stiffness alters tumor cytokine secretion and inflammatory signaling to regulate immune system response which I show in both *in vivo* models and human samples plays a critical role in tumor malignant progression. Thus, this work provides new mechanistic insight into how the physical microenvironment regulates tumor malignant progression.

Table of Contents

| | |
|--|-----|
| Chapter 1: Introduction | 1 |
| Chapter 2: A 3D Tension Bioreactor Platform to Study the Interplay between ECM Stiffness and Tumor Phenotype | 21 |
| Chapter 3: Force-Dependent Malignancy Requires the Fibronectin Synergy Site to Engage Integrin Signaling and Activate PI3 Kinase | 43 |
| Chapter 4: Altered Tumor Cell Metabolism is Correlated with Breast Cancer Metastasis and Dependent on ECM Stiffness and Integrin Signaling. | 99 |
| Chapter 5: Human Breast Cancer Invasion and Aggression Correlates with ECM Stiffening and Immune Cell Infiltration | 141 |
| Chapter 6: Investigating a link between tissue mechanics and tumor immune response in breast cancer | 182 |
| Chapter 7: Conclusions & Future Directions | 210 |
| Appendix 1: Tension bioreactor schematics and protocols | 234 |
| Appendix 2: List of PCR primers used | 236 |

List of Figures and Illustrations

Chapter 2:

| | |
|------------|----|
| Figure 2.1 | 26 |
| Figure 2.2 | 28 |
| Figure 2.3 | 30 |
| Figure 2.4 | 32 |
| Figure 2.5 | 34 |
| Figure 2.6 | 35 |

Chapter 3:

| | |
|-------------|----|
| Figure 3.1 | 50 |
| Figure 3.2 | 53 |
| Figure 3.3 | 55 |
| Figure 3.4 | 57 |
| Figure 3.5 | 60 |
| Figure 3.6 | 61 |
| Figure 3.7 | 64 |
| Figure 3.8 | 65 |
| Figure 3.9 | 67 |
| Figure 3.10 | 69 |
| Figure 3.11 | 72 |
| Figure 3.12 | 73 |
| Figure 3.13 | 76 |

Chapter 4:

| | |
|-------------|-----|
| Figure 4.1 | 103 |
| Figure 4.2 | 104 |
| Figure 4.3 | 106 |
| Figure 4.4 | 107 |
| Figure 4.5 | 111 |
| Figure 4.6 | 112 |
| Figure 4.7 | 115 |
| Figure 4.8 | 116 |
| Figure 4.9 | 119 |
| Figure 4.10 | 120 |
| Figure 4.11 | 122 |
| Figure 4.12 | 124 |
| Figure 4.13 | 125 |

Chapter 5:

| | |
|------------|-----|
| Figure 5.1 | 148 |
| Figure 5.2 | 150 |
| Figure 5.3 | 153 |
| Figure 5.4 | 155 |
| Figure 5.5 | 157 |
| Figure 5.6 | 159 |
| Figure 5.7 | 161 |
| Figure 5.8 | 163 |
| Figure 5.9 | 165 |

Chapter 6:

| | |
|------------|-----|
| Figure 6.1 | 188 |
| Figure 6.2 | 190 |
| Figure 6.3 | 193 |
| Figure 6.4 | 195 |
| Figure 6.5 | 197 |

Chapter 1: Introduction

Breast cancer is the most common neoplasia of women worldwide and the second leading cause of cancer death in women in the United States, with the vast majority of these deaths due to metastasis^{1,2}. Critically, the number of deaths from breast cancer is not decreasing despite better screening techniques, public awareness, and new therapies that show efficacy in treating the primary tumor for certain patients¹. This suggests a severe deficit in therapies that treat metastasis, the most common cause of death from breast cancer. The process of metastasis requires multiple steps, including tumor cell invasion through the basement membrane, tumor cell migration through the collagen- (Col) and fibronectin- (FN) rich stroma toward circulatory vessels, intravasation and survival in circulation, and finally extravasation and proliferation in a secondary site^{3,4}. While the events that occur during metastasis are well described, the underlying regulation of these steps remains unclear. Thus, a better understanding of this process is essential and a pressing modern health issue and could benefit from a new perspective in addition to traditional tumor cell signaling—focused research.

In human patients, breast cancer malignant progression is coincident with profound extracellular matrix (ECM) remodeling and stiffening^{5-10,11}. Importantly, my lab has previously shown that this altered ECM is both sufficient and necessary for tumor progression, aggression, and metastasis *in vivo*^{12,13}. Consistently, previous work from my lab and others has implicated ECM mechanical and structural changes as key drivers of cell behaviors important to tumor progression, such as tumor cell proliferation, survival, and motility, as well as effects on stromal cells such as fibroblasts and immune cells¹²⁻¹⁸. However, how cells sense and respond to ECM

mechanical properties and how ECM remodeling alters cell signaling to influence tumor metastatic progression are not yet fully understood.

Multiple mechanisms have been proposed by which cells sense and respond to exogenous mechanical cues¹⁹⁻²¹. Integrins and integrin adhesions play a central role in sensing and transmitting biophysical stimuli from the ECM to alter cell and tissue phenotype. Integrins consist of 24 distinct transmembrane heterodimers that relay cues from the surrounding ECM to regulate cell growth, survival, motility/invasion, and differentiation²²⁻²⁴. Integrins function through their ability to assemble cytoplasmic adhesion signaling complexes, modulating cytoskeletal organization and tension through interaction with actin linker proteins and cytoskeletal remodeling enzymes such as the RhoGTPases^{18,20,25}. Interestingly, we and others have determined that extracellular stiffness and cell contractility cooperate to regulate integrin adhesion assembly and signaling, and these combined effects then modulate cell and tissue behavior^{18,24}. We have also showed that when matrix stiffness or cell contractility is elevated, tissue integrity is compromised and tissues exhibit a "malignant-like" phenotype, with reinforced integrin signaling and destabilized cell-cell junctions^{6,13,15,17,18,26}. We and others have also implicated adhesion signaling in mediating ErbB receptor signaling, a commonly modified and upregulated pathway in human breast tumors²⁷⁻²⁹.

Thus, while there is an abundance of support for ECM mechanics and integrin mechanosignaling in driving malignant progression, several key questions and technical challenges remain:

1. How do we engineer and implement an *ex vivo* system that recapitulates the complex heterogeneity, structure, and mechanics of the tumor ECM while still being highly controllable for the study of tumor cell—ECM interactions?
2. In considering integrin-based mechanosignaling driving tumor aggression, are there specific integrin dimer—ligand combinations that are key for malignant progression?
3. Downstream of integrin signaling, what cell signaling pathways are regulated by ECM mechanics and which are pertinent to tumor cell invasion and malignant phenotype?
4. In the remodeled ECM of the stroma, how are other cell types affected and how do they contribute to tumor aggression?
5. How can we accurately measure and assess the mechanical changes and remodeling that occur with tumor progression and can we relate specific modifications to malignant progression?

With these questions in mind, the central theme of my research project was a rigorous quantitative approach to understand the physical and structural changes in the ECM with tumor progression and how these modifications alter cell signaling to potentiate malignant progression. Specifically, in this thesis I address the overarching hypothesis that ECM mechanical properties influence tumor malignant progression through integrin focal adhesion signaling and subsequent downstream signaling affecting tumor motility and invasion, tumor metabolism, and immune cell response. This hypothesis is tested and addressed in five separate sections:

1. The development of a bioreactor to study mechanically sensitive cell–ECM interactions in 3D
2. The role of $\alpha 5$ integrin—FN interactions in tumor malignant phenotype
3. The impact of ECM mechanics on tumor cell metabolism and its effect on metastasis
4. A quantitative mechanical and structural analysis of human tumor tissue remodeling accompanying malignant transformation
5. An investigation into a link between tissue mechanics and tumor immune response in breast cancer malignant progression

Development of a bioreactor to study mechanically sensitive cell–ECM interactions in 3D

The lack of understanding of the role of mechanics in tumor progression is partially due to the current lack of experimental systems that successfully combine the manipulability and control of *in vitro* platforms with the relevant composition and structural complexity of native tissue and allow for dynamic real-time data collection^{26,30–36}. To address this gap, a variety of synthetic hydrogel systems has been designed to study the impact of ECM composition, density, mechanics, and topography on cell and tissue phenotype. However, these synthetic systems fail to accurately recapitulate the biological properties and structure of the native tissue ECM. Natural three-dimensional (3D) ECM hydrogels, such as collagen or hyaluronic acid, feature many of the chemical and physical properties of tissue, yet these systems have limitations, including the inability to independently control biophysical properties such as stiffness and pore size. Here I have designed a 3D tension bioreactor system that permits precise mechanical tuning of collagen hydrogel stiffness while maintaining consistent composition and pore size,

which I then validated by analyzing the impact of substrate stiffness on pre-malignant and malignant tumor cell organoid invasion.

The role of $\alpha 5$ integrin—FN interactions in tumor malignant phenotype

While the role of integrin signaling in driving tumor malignant phenotype is well appreciated^{16,22,37–40}, making integrin signaling an attractive potential therapeutic target, there exist 24 unique integrin—ligand combinations, making specificity difficult. Moreover, not all specific integrin—ligand pairs potentiate a malignant phenotype, as previous work has shown even the most abundant integrin—ligand interaction in breast cancer cells, $\alpha 2\beta 1$ —collagen I, in fact blunts tumor aggression⁴¹. With this in mind I aimed to determine if there were other pertinent integrin—ligand pairs that were key drivers of malignant progression. Previous work has demonstrated that with tumor development or oncogenic transformation of epithelial cells *in vitro* there is a specific upregulation of $\alpha 5\beta 1$ integrin and its ligand fibronectin (FN) and that $\alpha 5\beta 1$ —FN binding has a key functional role in tumor cell invasion and migration *in vitro* and tumor progression *in vivo*^{42,43}. Critically, $\alpha 5\beta 1$ overexpression has been correlated with poor survival in human patients⁴⁴, and thus elucidating the role of $\alpha 5\beta 1$ —FN in tumor aggression has direct clinical applications and is the focus of this section. I aimed to assess the specific role of $\alpha 5\beta 1$ —FN in potentiating tumor cell invasion, migration, and malignant phenotype relative to other relevant integrin—ligand pairs in breast cancer cells. In particular, $\alpha 5\beta 1$ —FN demonstrates a unique synergy site binding relative to other integrin—dimer ligand interactions, and I wanted to assess whether this drives tumor cell invasion, migration, and malignant phenotype^{43,45,46}. Specifically, I tested the effects of $\alpha 5\beta 1$ —FN synergy site binding on adhesion strength and focal

adhesion assembly, cell contractility, and subsequent effects on cell signaling to potentiate tumor cell invasion and migration relative to other integrin—ligand pairs.

Tumor metabolism is tuned by ECM mechanical properties and a key mediator of tumor invasion and metastasis

Tumors exhibit altered cellular metabolism supportive of continuous cell growth and invasion^{47,48}. Importantly, this altered metabolism significantly correlates with poor patient prognosis^{48,49}. Nevertheless, the fundamental molecular mechanisms through which tumors adapt their metabolism and how this altered metabolism regulates tumor behavior remain unclear. What is known is that there is a wide variety of cell signaling mechanisms that regulate metabolic state (Hif1a^{50,51}, MYC^{52,53}, mTor^{54,55}, Akt^{53,56}) and that all solid tumors demonstrate some form of aberrant cell metabolism (i.e., upregulation of glycolysis, mitochondrial dysfunction, overactive biogenesis, and ROS production)^{57–63,49}. Previously we demonstrated a distinct role for ECM stiffness and integrin signaling in several of the pathways^{11,17,64} that have a capacity to control cell metabolism, and as such I hypothesized that elevated ECM stiffness potentiates cell metabolism by increasing the expression and activity of key metabolic targets driven by enhanced pro-tumorigenic signaling via integrin activity to regulate malignant progression. To test this hypothesis, I profiled metabolic markers using a combination of quantitative RT-PCR, immunoblotting and immunofluorescence of MMTV-PyMT transgenic tumors (\pm ECM cross-linking), and breast tumor mammary epithelial cells grown on tunable hydrogel substrates *in vitro*. I then used pharmacological inhibitors targeting glycolysis or

oxidative phosphorylation to assess the interplay among ECM stiffness, metabolism, and tumor cell behavior, including invasion, migration, and proliferation.

A quantitative mechanical and structural analysis of human tumor tissue remodeling accompanying malignant transformation

The correlation between tissue and extracellular matrix stiffness in human breast cancer progression and aggression is well established, but how this remodeling occurs and which properties influence malignant progression remains unclear^{5,6,8,9,65,66}. Here I undertook a biophysical and biochemical assessment of stromal–epithelial interactions in noninvasive, invasive, and normal adjacent human breast tissue and in breast cancers of increasingly aggressive subtype. Specifically, I utilized a combination of atomic force microscopy (AFM), second harmonic generation (SHG) collagen imaging via two-photon microscopy, and immunofluorescence imaging to assess physical and structural changes of the stroma surrounding the tumor and the resulting effects on tumor cell signaling and aggression. Additionally, several stromal cell populations such as fibroblasts and immune cells have been implicated with the dramatic ECM remodeling seen *in vivo*^{67,12,68,69}. With this in mind I also assessed the changes in stromal cell populations accompanying ECM remodeling and tumor malignant progression. Critically, I observed a significant increase in collagen deposition and bundling and consequently increased ECM stiffness with tumor progression and in the most aggressive breast cancer subtypes. These changes in the ECM were accompanied by significantly increased infiltrate of macrophage into the tumor stroma and pro-fibrotic signaling

through TGF β ^{70,71}. This suggested a possible causative relationship among immune cell infiltrate, ECM remodeling, and tumor malignant progression.

Investigating a link between tissue mechanics and tumor immune response in breast cancer malignant progression

Having established a positive correlation between the number and location of infiltrating CD45 and CD68 immune cells and ECM stiffness in human breast tumors, I aimed to assess the impact of this immune infiltrate in tumor progression. Infiltrating immune cells have been previously implicated in ECM remodeling associated with mammary gland development and tumorigenesis^{67,72–74}. This led me to hypothesize that immune cells promote tumor-associated fibrosis that induces inflammatory signaling, resulting in a feed-forward loop to stimulate a pro-tumor immune response. To test this I used the MMTV-PyMT transgenic tumor model in which I could modulate ECM stiffness, macrophage infiltration, and inflammatory signaling in the tumor and then measure ECM remodeling and mechanics with tumor progression as well as tumor cell invasion and metastasis. Additionally, I isolated both macrophage and tumor cells and via an adaptation to my tension bioreactor assessed the role of ECM stiffness in controlling tumor cell—immune cell interactions in a co-culture model.

Combined, these projects demonstrated a potent effect of tissue mechanical properties in regulating tumor malignant. Ultimately, this work provides new insight into how tumor malignant progression occurs, in particular with regards to the importance of ECM mechanical properties. These insights are a framework for future translational work, which could lead to better diagnostic techniques revolving around tumor mechanical properties as well as therapies

specifically targeting pathways we have shown are needed for robust metastasis, ECM mechanical properties directly, cell contractility, alpha 5—FN integrin binding, metabolic adaptation, and inflammatory signaling. The future challenge will revolve around demonstrating that these trends hold in large human patient cohorts as well as their clinical efficacy when attempting to treat human breast tumors.

Works Cited

1. Cancer of the Breast —SEER Stat Fact Sheets. At
<<http://seer.cancer.gov/statfacts/html/breast.html>>
2. Boyd, N. F., Lockwood, G. A., Byng, J. W., Trichler, D. L. & Yaffe, M. J. Mammographic densities and breast cancer risk. *Cancer Epidemiol Biomarkers Prev* **7**, 1133–44 (1998).
3. Quail, D. F. & Joyce, J. A. Microenvironmental regulation of tumor progression and metastasis. *Nat Med* **19**, 1423–37 (2013).
4. Erler, J. T. & Weaver, V. M. Three-dimensional context regulation of metastasis. *Clin Exp Metastasis* **26**, 35–49 (2009).
5. Chang, J. M. *et al.* Stiffness of tumours measured by shear-wave elastography correlated with subtypes of breast cancer. *Eur Radiol* **23**, 2450–58 (2013).
6. Lopez, J. I., Kang, I., You, W.-K., McDonald, D. M. & Weaver, V. M. In situ force mapping of mammary gland transformation. *Integr Biol (Camb)* **3**, 910–21 (2011).
7. Plodinec, M. *et al.* The nanomechanical signature of breast cancer. *Nat Nanotechnol* **7**, 757–65 (2012).
8. Samani, A., Zubovits, J. & Plewes, D. Elastic moduli of normal and pathological human breast tissues: an inversion-technique-based investigation of 169 samples. *Phys. Med. Biol.* **52**, 1565–76 (2007).

9. Venkatesh, S. K. *et al.* MR elastography of liver tumors: preliminary results. *AJR Am J Roentgenol* **190**, 1534–40 (2008).
10. Barr, R. G. Elastography in clinical practice. *Radiol Clin North Am* **52**, 1145–62 (2014).
11. Mouw, J. K. *et al.* Tissue mechanics modulate microRNA-dependent PTEN expression to regulate malignant progression. *Nat Med* **20**, 360–67 (2014).
12. Pickup, M. W. *et al.* Stromally derived lysyl oxidase promotes metastasis of transforming growth factor- β -deficient mouse mammary carcinomas. *Cancer Res* **73**, 5336–46 (2013).
13. Levental, K. R. *et al.* Matrix crosslinking forces tumor progression by enhancing integrin signaling. *Cell* **139**, 891–906 (2009).
14. Paszek, M. J. *et al.* The cancer glycocalyx mechanically primes integrin-mediated growth and survival. *Nature* **511**, 319–25 (2014).
15. Yeung, T. *et al.* Effects of substrate stiffness on cell morphology, cytoskeletal structure, and adhesion. *Cell Motil. Cytoskeleton* **60**, 24–34 (2005).
16. Weaver, V. M. *et al.* Reversion of the malignant phenotype of human breast cells in three-dimensional culture and in vivo by integrin blocking antibodies. *J Cell Biol* **137**, 231–45 (1997).

17. Rubashkin, M. G. *et al.* Force engages vinculin and promotes tumor progression by enhancing PI3K activation of phosphatidylinositol (3,4,5)-triphosphate. *Cancer Res* **74**, 4597–611 (2014).
18. Samuel, M. S. *et al.* Actomyosin-mediated cellular tension drives increased tissue stiffness and β -catenin activation to induce epidermal hyperplasia and tumor growth. *Cancer Cell* **19**, 776–91 (2011).
19. Vogel, V. & Sheetz, M. Local force and geometry sensing regulate cell functions. *Nat Rev Mol Cell Biol* **7**, 265–75 (2006).
20. Huang, S. & Ingber, D. E. Cell tension, matrix mechanics, and cancer development. *Cancer Cell* **8**, 175–6 (2005).
21. Janmey, P. A., Wells, R. G., Assoian, R. K. & McCulloch, C. A. From tissue mechanics to transcription factors. *Differentiation* **86**, 112–20 (2013).
22. Desgrosellier, J. S. & Cheresch, D. A. Integrins in cancer: biological implications and therapeutic opportunities. *Nat Rev Cancer* **10**, 9–22 (2010).
23. Kadler, K. E., Hill, A. & Canty-Laird, E. G. Collagen fibrillogenesis: fibronectin, integrins, and minor collagens as organizers and nucleators. *Curr Opin Cell Biol* **20**, 495–501 (2008).
24. Gallant, N. D., Michael, K. E. & García, A. J. Cell adhesion strengthening: contributions of adhesive area, integrin binding, and focal adhesion assembly. *Mol Biol Cell* **16**, 4329–40 (2005).

25. Keely, P. J. Mechanisms by which the extracellular matrix and integrin signaling act to regulate the switch between tumor suppression and tumor promotion. *J Mammary Gland Biol Neoplasia* **16**, 205–19 (2011).
26. Cassereau, L., Miroshnikova, Y., Ou, G., Lakins, J. & Weaver, V. M. A 3D tension bioreactor platform to study the interplay between ECM stiffness and tumor phenotype. *J Biotechnol* **193**, 66–9 (2014).
27. Tornillo, G. *et al.* p130Cas promotes invasiveness of three-dimensional ErbB2-transformed mammary acinar structures by enhanced activation of mTOR/p70S6K and Rac1. *Eur J Cell Biol* **90**, 237–48 (2011).
28. Hasebe, T., Tsuda, H., Tsubono, Y., Imoto, S. & Mukai, K. Fibrotic focus in invasive ductal carcinoma of the breast: a histopathological prognostic parameter for tumor recurrence and tumor death within three years after the initial operation. *Jpn J Cancer Res* **88**, 590–9 (1997).
29. Perou, C. M. *et al.* Molecular portraits of human breast tumours. *Nature* **406**, 747–52 (2000).
30. Ulrich, T. A., de Juan Pardo, E. M. & Kumar, S. The mechanical rigidity of the extracellular matrix regulates the structure, motility, and proliferation of glioma cells. *Cancer Res* **69**, 4167–74 (2009).

31. Shi, Q. *et al.* Rapid disorganization of mechanically interacting systems of mammary acini. *Proc Natl Acad Sci U S A* **111**, 658–63 (2014).
32. Miroshnikova, Y. A. *et al.* Engineering strategies to recapitulate epithelial morphogenesis within synthetic three-dimensional extracellular matrix with tunable mechanical properties. *Phys Biol* **8**, 26013 (2011).
33. Guo, C.-L. *et al.* Long-range mechanical force enables self-assembly of epithelial tubular patterns. *Proc Natl Acad Sci U S A* **109**, 5576–82 (2012).
34. Tse, J. R. & Engler, A. J. Preparation of hydrogel substrates with tunable mechanical properties. *Curr Protoc Cell Biol* **Chapter 10**, Unit 10.16 (2010).
35. Provenzano, P. P., Eliceiri, K. W., Inman, D. R. & Keely, P. J. Engineering three-dimensional collagen matrices to provide contact guidance during 3D cell migration. *Curr Protoc Cell Biol* **Chapter 10**, Unit 10.17 (2010).
36. Gautieri, A., Vesentini, S., Redaelli, A. & Buehler, M. J. Hierarchical structure and nanomechanics of collagen microfibrils from the atomistic scale on. *Nano Lett* **11**, 757–66 (2011).
37. Guo, W. & Giancotti, F. G. Integrin signalling during tumour progression. *Nat Rev Mol Cell Biol* **5**, 816–26 (2004).
38. Yao, E. S. *et al.* Increased beta1 integrin is associated with decreased survival in invasive breast cancer. *Cancer Res* **67**, 659–64 (2007).

39. Maschler, S. *et al.* Tumor cell invasiveness correlates with changes in integrin expression and localization. *Oncogene* **24**, 2032–41 (2005).
40. Nam, J.-M. *et al.* β 1-Integrin via NF- κ B signaling is essential for acquisition of invasiveness in a model of radiation treated in situ breast cancer. *Breast Cancer Res* **15**, R60 (2013).
41. Zutter, M. M., Santoro, S. A., Staatz, W. D. & Tsung, Y. L. Re-expression of the alpha 2 beta 1 integrin abrogates the malignant phenotype of breast carcinoma cells. *Proc Natl Acad Sci U S A* **92**, 7411–5 (1995).
42. Mosher, D. F. Cross-linking of fibronectin to collagenous proteins. *Mol Cell Biochem* **58**, 63–8 (1984).
43. Friedland, J. C., Lee, M. H. & Boettiger, D. Mechanically activated integrin switch controls alpha5beta1 function. *Science* **323**, 642–4 (2009).
44. Stoeltzing, O. *et al.* Inhibition of integrin alpha5beta1 function with a small peptide (ATN-161) plus continuous 5-FU infusion reduces colorectal liver metastases and improves survival in mice. *Int J Cancer* **104**, 496–503 (2003).
45. Li, F., Redick, S. D., Erickson, H. P. & Moy, V. T. Force measurements of the alpha5beta1 integrin-fibronectin interaction. *Biophys J* **84**, 1252–62 (2003).
46. Dingemans, A.-M. C. *et al.* Integrin expression profiling identifies integrin alpha5 and beta1 as prognostic factors in early stage non-small cell lung cancer. *Mol Cancer* **9**, 152 (2010).

47. Cairns, R. A., Harris, I. S. & Mak, T. W. Regulation of cancer cell metabolism. *Nat Rev Cancer* **11**, 85–95 (2011).
48. Pinheiro, C. *et al.* GLUT1 and CAIX expression profiles in breast cancer correlate with adverse prognostic factors and MCT1 overexpression. *Histol Histopathol* **26**, 1279–86 (2011).
49. Lüftner, D. *et al.* Tumor type M2 pyruvate kinase expression in advanced breast cancer. *Anticancer Res* **20**, 5077–82
50. Muniyappa, H., Song, S., Mathews, C. K. & Das, K. C. Reactive oxygen species-independent oxidation of thioredoxin in hypoxia: inactivation of ribonucleotide reductase and redox-mediated checkpoint control. *J Biol Chem* **284**, 17069–81 (2009).
51. Denko, N. C. Hypoxia, HIF1 and glucose metabolism in the solid tumour. *Nat Rev Cancer* **8**, 705–13 (2008).
52. Doherty, J. R. *et al.* Blocking lactate export by inhibiting the Myc target MCT1 disables glycolysis and glutathione synthesis. *Cancer Res* **74**, 908–20 (2014).
53. Mukherjee, J. *et al.* Pyruvate kinase M2 expression, but not pyruvate kinase activity, is up-regulated in a grade-specific manner in human glioma. *PLoS One* **8**, e57610 (2013).
54. Chou, C.-C. *et al.* AMPK reverses the mesenchymal phenotype of cancer cells by targeting the Akt-MDM2-Foxo3a signaling axis. *Cancer Res* **74**, 4783–95 (2014).

55. Zakikhani, M., Dowling, R., Fantus, I. G., Sonenberg, N. & Pollak, M. Metformin is an AMP kinase-dependent growth inhibitor for breast cancer cells. *Cancer Res* **66**, 10269–73 (2006).
56. Elstrom, R. L. *et al.* Akt stimulates aerobic glycolysis in cancer cells. *Cancer Res* **64**, 3892–9 (2004).
57. Semenza, G. L. Tumor metabolism: cancer cells give and take lactate. *J Clin Invest* **118**, 3835–7 (2008).
58. Leone, A., Di Gennaro, E., Bruzzese, F., Avallone, A. & Budillon, A. New perspective for an old antidiabetic drug: metformin as anticancer agent. *Cancer Treat Res* **159**, 355–76 (2014).
59. Diehn, M. *et al.* Association of reactive oxygen species levels and radioresistance in cancer stem cells. *Nature* **458**, 780–3 (2009).
60. Morais-Santos, F. *et al.* Differential sensitivities to lactate transport inhibitors of breast cancer cell lines. *Endocr Relat Cancer* **21**, 27–38 (2014).
61. Asghar Butt, S. *et al.* Monitoring mammary tumor progression and effect of tamoxifen treatment in MMTV-PyMT using MRI and magnetic resonance spectroscopy with hyperpolarized [1-(13) C]pyruvate. *Magn Reson Med* (2014). doi:10.1002/mrm.25095
62. Chandel, N. S. Mitochondria as signaling organelles. *BMC Biol* **12**, 34 (2014).

63. Schumacker, P. T. Reactive oxygen species in cancer cells: live by the sword, die by the sword. *Cancer Cell* **10**, 175–6 (2006).
64. Paszek, M. J. *et al.* Tensional homeostasis and the malignant phenotype. *Cancer Cell* **8**, 241–54 (2005).
65. Provenzano, P. P., Inman, D. R., Eliceiri, K. W. & Keely, P. J. Matrix density-induced mechanoregulation of breast cell phenotype, signaling and gene expression through a FAK-ERK linkage. *Oncogene* **28**, 4326–43 (2009).
66. Balleyguier, C. *et al.* Breast elasticity: principles, technique, results: an update and overview of commercially available software. *Eur J Radiol* **82**, 427–34 (2013).
67. Pollard, J. W. Macrophages define the invasive microenvironment in breast cancer. *J Leukoc Biol* **84**, 623–30 (2008).
68. Hasebe, T. Tumor-stromal interactions in breast tumor progression—significance of histological heterogeneity of tumor-stromal fibroblasts. *Expert Opin Ther Targets* **17**, 449–60 (2013).
69. Lijnen, P. & Petrov, V. Transforming growth factor-beta 1-induced collagen production in cultures of cardiac fibroblasts is the result of the appearance of myofibroblasts. *Methods Find Exp Clin Pharmacol* **24**, 333–44 (2002).
70. Pickup, M., Novitskiy, S. & Moses, H. L. The roles of TGF β in the tumour microenvironment. *Nat Rev Cancer* **13**, 788–99 (2013).

71. Curran, C. S. & Keely, P. J. Breast tumor and stromal cell responses to TGF- β and hypoxia in matrix deposition. *Matrix Biol* **32**, 95–105 (2013).
72. Assoian, R. K. *et al.* Expression and secretion of type beta transforming growth factor by activated human macrophages. *Proc Natl Acad Sci* **84**, 6020–4 (1987).
73. Walker, R. A., Dearing, S. J. & Gallacher, B. Relationship of transforming growth factor beta 1 to extracellular matrix and stromal infiltrates in invasive breast carcinoma. *Br J Cancer* **69**, 1160–5 (1994).
74. Rudnick, J. A. & Kuperwasser, C. Stromal biomarkers in breast cancer development and progression. *Clin Exp Metastasis* **29**, 663–72 (2012).

Chapter 2: A 3D Tension Bioreactor Platform to Study the Interplay between ECM Stiffness and Tumor Phenotype

Luke Cassereau^{1,2}

In collaboration with: Yekaterina Miroshnikova^{1,2}, Guanqing Ou^{1,2}, Johnathon Lakins¹

Under the supervision of: Valerie M Weaver^{1,3,4,5}

¹Center for Bioengineering and Tissue Regeneration, Department of Surgery, UCSF, San Francisco, California, USA.

²University of California San Francisco/University of California Berkeley Joint Graduate Group in Bioengineering, San Francisco, CA, USA.

³Department of Anatomy, and Department of Bioengineering and Therapeutic Sciences, UCSF, San Francisco, California, USA.

⁴Eli and Edythe Broad Center of Regeneration Medicine and Stem Cell Research, UCSF, San Francisco, California, USA.

⁵UCSF Helen Diller Comprehensive Cancer Center, UCSF, San Francisco, California, USA.

Adapted from previously published work: Cassereau et al., Journal of Biotechnology January 2015

Abstract:

Extracellular matrix (ECM) structure, composition, and stiffness have profound effects on tissue development and pathologies such as cardiovascular disease and cancer. Accordingly, a variety of synthetic hydrogel systems have been designed to study the impact of ECM composition, density, mechanics, and topography on cell and tissue phenotype. However, these synthetic systems fail to accurately recapitulate the biological properties and structure of the native tissue ECM. Natural three dimensional (3D) ECM hydrogels, such as collagen or hyaluronic acid, feature many of the chemical and physical properties of tissue, yet, these systems have limitations including the inability to independently control biophysical properties such as stiffness and pore size. Here, I present a 3D tension bioreactor system that permits precise mechanical tuning of collagen hydrogel stiffness, while maintaining consistent composition and pore size. I achieved this by mechanically loading collagen hydrogels covalently-conjugated to a polydimethylsiloxane (PDMS) membrane to induce hydrogel stiffening. I validated the biological application of this system with oncogenically transformed mammary epithelial cell organoids embedded in a 3D collagen I hydrogel, either uniformly stiffened or calibrated to create a gradient of ECM stiffening, to visually demonstrate the impact of ECM stiffening on transformation and tumor cell invasion. As such, this bioreactor presents the first tunable 3D natural hydrogel system that is capable of independently assessing the role of ECM stiffness on tissue phenotype.

Introduction

The biophysical properties of the extracellular matrix (ECM) are important determinants of cell and tissue behavior, as shown by prior studies that highlight effects on cell migration, proliferation, survival, and tissue morphogenesis^{1,2}. In particular, ECM rigidity and organization play essential roles in biological processes such as stem cell differentiation, wound healing, and pathologies such as cancer³⁻⁵. Nevertheless, how cells sense and respond to these biophysical cues from the ECM remains poorly understood.

Studies examining the relationship between ECM mechanics and cell phenotype have thus far been hampered by limitations in the experimental approaches used to manipulate biophysical properties of the ECM. Current state-of-the-art systems predominantly employ mechanically tunable two-dimensional (2D) polymer hydrogels conjugated with ECM ligands (e.g., collagen, fibronectin, laminin, etc.)^{6,7}. These 2D substrates, unfortunately, fail to model the heterogeneous and three-dimensional (3D) structure of native tissue. More recent approaches that employ 3D hydrogel substrates are fraught with limitations, including the failure to control for pore size, lack of ECM remodeling, and gel inconsistencies. For instance, while synthetic polymer systems are amenable to careful tuning of mechanical properties and ECM presentation, these systems fail to recapitulate the complex, multicomponent composition of native tissue, do not enable cells to remodel the matrix, and lack the architecture of natural ECM hydrogels^{8,9}. By contrast, the use of native ECM materials such as type I collagen, fibrin, or hyaluronic acid for 3D hydrogel studies more faithfully reconstitute the native tissue matrix composition and function, including the binding and presentation of growth factors and cell-mediated matrix remodeling¹⁰. However, the use of native hydrogels is

compromised by lack of uniformity and consistency and the profound changes in pore size and ligand binding induced when protein concentration or cross-linking are used to modify biophysical properties^{11,12}.

To address this, I engineered a 3D tension bioreactor system using a collagen I hydrogel which allows tuning of mechanical properties independently of structural changes and features the biocompatibility inherent to natural hydrogels. I validated and optimized this system using a combination of mechanical and structural testing via atomic force microscopy (AFM) and scanning electron microscopy (SEM) followed by cell invasion studies using breast tumor cells to demonstrate a potential biological application of the system.

Design and Validation of 3D Tension Bioreactor System.

I developed a novel tension bioreactor system that employs a native collagen I (Col I) hydrogel and permits consistent manipulation of ECM stiffness in the absence of modifications to the structure, composition, or pore size of the gel. Briefly, my method involves casting a polydimethylsiloxane (PDMS) membrane using a 3D printed negative mold to create a membrane with wells of defined depth to accommodate the collagen hydrogel and a surrounding media reservoir. The PDMS membrane is surface activated through a combination of plasma cleaning, a (3-Aminopropyl)triethoxysilane (APTES) incubation, followed by glutaraldehyde incubation, as previously described¹³. Following surface activation, Col I solution is prepared by neutralizing acid-solubilized rat tail collagen I (BD Bioscience) with 1N NaOH and a DMEM buffer, and polymerized at 37°C within wells in the PDMS membrane. After polymerization, the PDMS membrane is attached to an aluminum-loading frame, which, through connections to a sliding rail system, permits uniaxial stretching of the membrane and the attached collagen gel up to 10% strain (Figure 2.1).

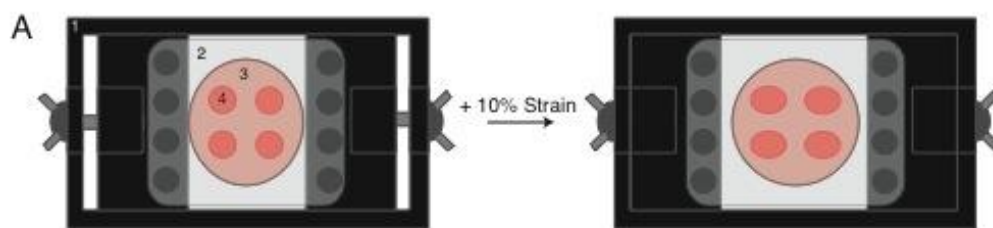


Figure 2.1: Schematic of tension bioreactor

A) Schematic of tension bioreactor system, consisting of 1) Stretching frame 2) PDMS stretchable membrane 3) media reservoir 4) Col I hydrogels.

Using atomic force microscopy (AFM) with a Bio-AFM (Asylum Research) and a beaded silicon tip (5mm diameter, Novascan), I measured the elastic modulus of the Col I hydrogel under 0 and 10% applied strain over a range of Col I concentrations (1–7 mg/ml). Force measurements were performed at 1 pN indentation with 100 measurements per condition and force curves were fitted with the Hertz model and averaged to determine the gel elastic modulus. Using these measurements, I observed that, depending on collagen concentration, upon stretching of the PDMS membrane, I was able to increase the ECM elastic modulus up to fourfold (Figure 2.2). Samples were retested 7 days later and showed no change in elastic modulus, suggesting that the stiffening effect is permanent due to collagen strain hardening as previously described¹⁴.

I then used scanning electron microscopy (SEM) to determine the effect of strain on hydrogel architecture, porosity, and organization. Collagen gels were fixed and prepared as previously described⁸, then imaged on a JEOL JCM-6000 Neoscope SEM (JEOL USA Inc., Peabody, MA). SEM images were used to determine hydrogel porosity and organization with ctFire analysis software (LOCI, UW Madison), with porosity defined as the ratio of fiber surface area to total image area and gel organization determined by the average individual fiber orientation and straightness. With this analysis, I concluded that porosity and fiber organization do not significantly change with mechanical loading for a given Col I concentration (evaluated by Student's t-test). Thus, I have the first 3D natural material hydrogel system in which I can alter the ECM stiffness independently of the ECM structure across a range of different substrate concentrations (Figure 2.2).

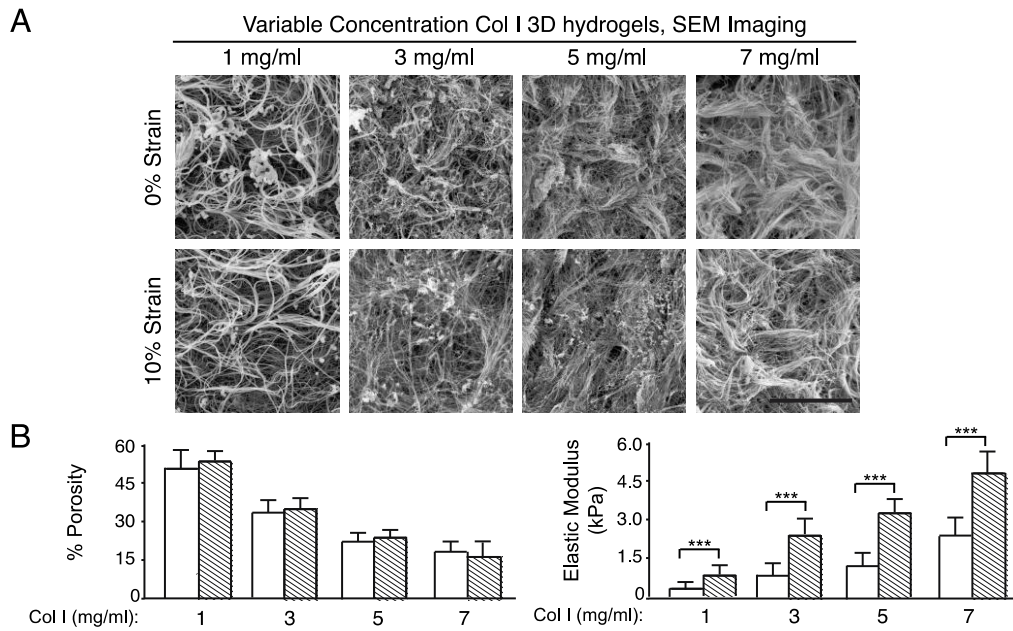


Figure 2.2: Characterization of collagen hydrogel mechanics and structure in tension bioreactor

A) SEM images of Col I hydrogels of varying collagen concentration at 0% and 10% strain in the bioreactor system (scale bar = 2 μ m). B) Quantification of gel pore size and elastic modulus as a function of Col I concentration and the application of uniaxial strain (error bars represent standard deviation, *** denotes $p < .05$ evaluated by t-test).

Biological Applications of the Tension Bioreactor in Cancer Biology

My group and others have previously demonstrated that ECM remodeling and stiffening can potentiate tumor malignant progression^{15,16}. Thus, to demonstrate the biological applications of my system, I aimed to determine the impact of altered ECM stiffness on tumor cell migration and invasion in a 3D context independently of structural changes to the ECM. I cultured oncogenically transformed (Ha-Ras) pre-malignant mammary epithelial cell organoids (pregrown for 8 days in rBM) embedded in Col I hydrogels of varying concentrations supplemented with FN (1 ug/ml) and rBM (5%) and in the tension bioreactor with 0 or 10% strain for up 2 days. To assess the extent and penetrance of tumor cell invasion and migration, I paraformaldehyde fixed and stained Col I hydrogels with propidium iodide and AlexaFluor 488-phalloidin and imaged the gels using a 2-photon microscope (Olympus upright microscope, Olympus 20X .95 NA objective). Organoid invasion and tumor cell migration were quantified by thresholding fluorescence images for signal above 3x background and measuring colony spread area and circularity with ImageJ¹⁷.

These experiments revealed that increasing collagen concentration to increase the ECM rigidity initially induced tumor cell invasion. However, once collagen concentration reached 5 mg/ml, cell invasion was greatly reduced, likely due to decreasing pore size^{18,19}. In marked contrast, I quantified a profound increase in tumor cell invasion induced by increasing ECM stiffness via my bioreactor, illustrating that when pore size is not limiting, ECM stiffness independently enhances tumor cell invasion and migration (Figure 2.3).

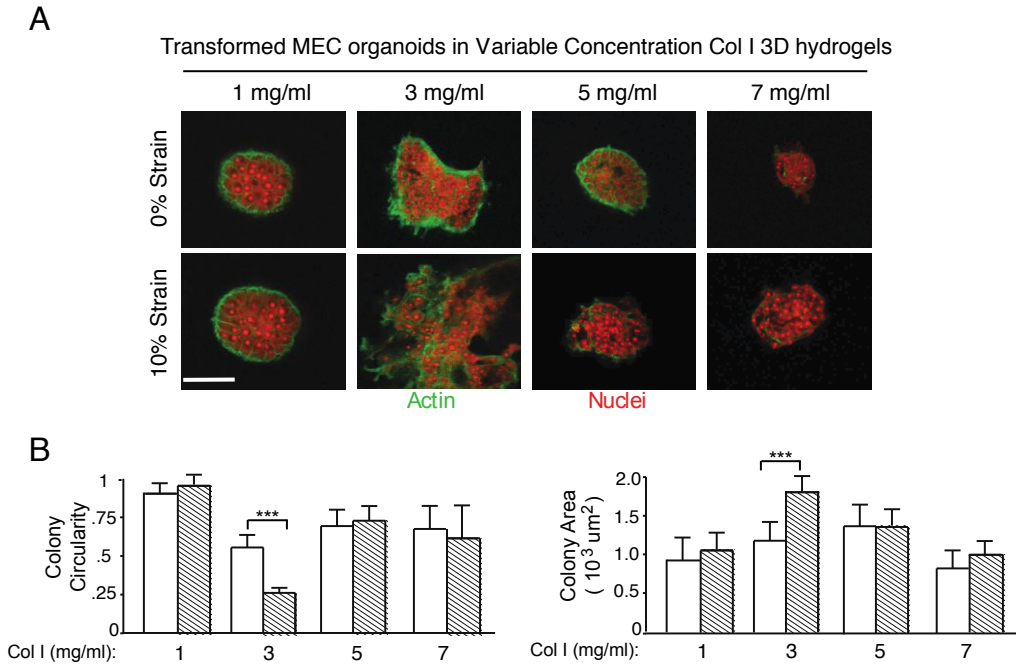


Figure 2.3: Characterization of biological application of tension bioreactor with transformed mammary epithelial cell migration

A) Premalignant mammary epithelial cells pre-grown in rBM as spherical multicellular organoids embedded in Col I hydrogels of varying concentration and then placed under either 0% or 10% strain in the tension bioreactor. After two days cultures were fixed and stained for actin cytoskeleton and nuclei to assess the extent of tumor cell invasion and migration (scale bar = 20 μm). B) Quantification of organoid spread area and circularity.

Following these studies, I aimed to assess the effect of ECM stiffness in my system with malignant tumor cells. I isolated tumor cells from 11 week MMTV-PyMT transgenic tumor model mice and grew the tumor cells as organoids prior to embedding in 3mg/ml collagen gels, the optimum composition for premalignant cell invasion, in the bioreactor. As with premalignant organoids, cultures were fixed and stained after 2 days. From these studies I found that ECM stiffness was not necessary to induce tumor cell invasion but did accelerate organoid dissociation. (Figure 2.4)

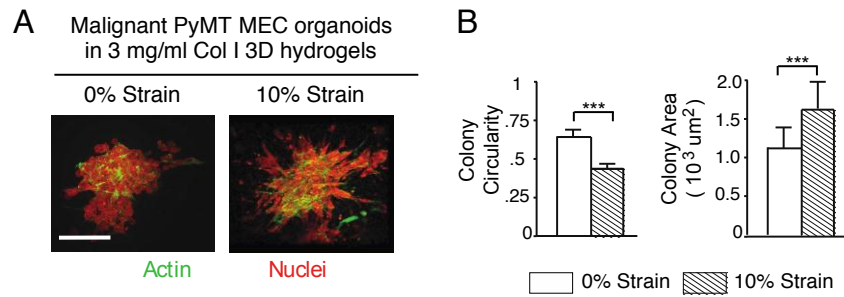


Figure 2.4: Characterization of biological application of tension bioreactor with malignant mammary epithelial tumor cell migration

A) Malignant mammary epithelial cells isolated from transgenic mouse models (MMTV-PyMT) and then pre-grown in rBM as spherical multicellular organoids embedded in 3mg/ml Col I hydrogels and then placed under either 0% or 10% strain in the tension bioreactor. After 2 days cultures were fixed and stained for actin cytoskeleton and nuclei to assess the extent of tumor cell invasion and migration (scale bar = 20 μm). B) Quantification of PyMT organoid spread area and circularity.

Prior work suggests that the structural heterogeneity of native tissue may create gradients in ECM stiffness, which promotes morphogenetic processes such as branching morphogenesis and pathologies such as cancer^{2,20,21}. To address this possibility, I leveraged the unique mechanical loading principle of my system and designed an alternative PDMS membrane to allow for generation of ECM stiffness gradients. This was achieved by modifying the PDMS membrane connections to the loading apparatus by stepwise increases in the major axis length of each set of connections across the width of the membrane, consequently decreasing the maximum possible strain and mechanical loading of the hydrogel in a gradient fashion (Figure 2.5A). Testing this modification with a 3 mg/ml Col I hydrogel, I was able to demonstrate with AFM and SEM that I am able to create a gradient of ECM stiffness ranging from (0.4–4 kPa, 0.12 kPa/mm) independently of structural changes (Figure 2.5B). To illustrate a biological application of the gradient mechanical loading tension bioreactor, I again used oncogenically transformed (Ha-Ras) mammary epithelial cell organoids embedded in a Col I hydrogel (3 mg/ml). Organoids were fixed, stained, and imaged as described in uniform stiffness experiments. ECM stiffness for a given gel region was determined by measuring the length of the gel in the direction of the applied strain relative to the initial length to calculate the local strain and then fit to AFM elastic modulus measurements for that specific strain.

Consistent with my previous results in uniform-stiffness collagen gels, increasing ECM stiffness potentiated tumor cell migration. Yet, in my gradient system, I was also able to observe ranges of cell behavior within the same hydrogel in response to increasing stiffness (Figure 2.6A–B). These data show that I generated a tractable system for creating gradients of mechanical stiffness in collagen hydrogels without altering ECM structure or organization.

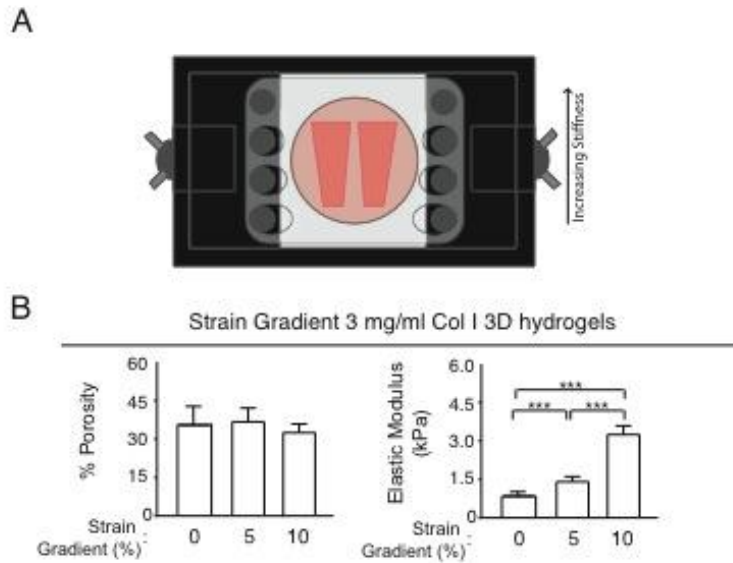


Figure 2.5: Design and characterization of gradient tension bioreactor

A) Schematic of gradient strain tension bioreactor. B) Quantification of pore size based on SEM imaging (not shown) and elastic modulus across strain gradient (error bars represent standard deviation, *** denotes $p < .05$ evaluated by pairwise t-test).

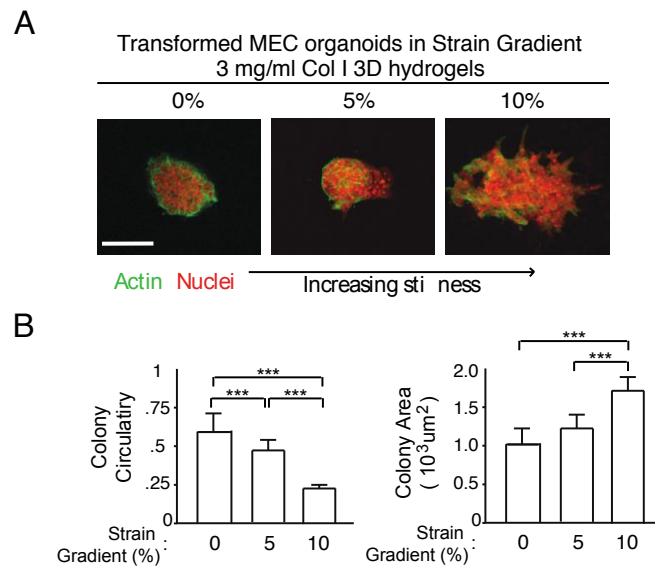


Figure 2.6: Biological application of gradient tension bioreactor

A) Premalignant mammary epithelial cells pre-grown in rBM as spherical multicellular organoids embedded in gradient stiffness Col I hydrogels. After two days cultures were fixed and stained for actin cytoskeleton and nuclei to assess the extent of tumor cell invasion and migration (scale bar = 20 μm). B) Quantification of organoid spread area and circularity.

Discussion

Here, I have outlined a new strategy for the design and implementation of a 3D bioreactor that can be used to accurately manipulate the stiffness of type I collagen hydrogels without changing substrate concentration or altering pore size. The system also can be adopted to generate shallow gradients of ECM stiffening in 3D. I have described the validation of my system and demonstrated how it can be used to study malignant transformation and the invasive and migratory phenotype of tumor cells in response to ECM stiffness. In the next stage of my thesis research I then aimed to explore what cell signaling mechanisms might be critical in the role of ECM mechanics as a driver of tumor malignant phenotype.

As is, this system is amenable for rapid incorporation into research programs aimed at clarifying the impact of ECM stiffness on tissue morphogenesis, wound healing, and a range of other tissue functions. However to improve on this system, future projects incorporating multiple cell types, fibroblasts, immune cells, endothelial cells as vascularity, would better represent the physiological conditions of native tissue. Thus for cancer research allow more meaningful insights into factors driving tumor cell invasion and malignant phenotype.

Materials and Methods

Design and construction of PDMS inserts and tension loading frame

Solidworks was used to design negative molds for PDMS inserts. Briefly, dimensions were set such that each insert collagen gel well fit 250ul total and a media reservoir for 1ml of cell culture media. For the gradient tension insert, the media reservoir was maintained but the 4 250ul wells were replaced by two rectangular 1ml wells with a long axis perpendicular to the direction of strain. The negative mold was then created using an Objet 3D printer with Vera White construction material. After 3D printing, negative molds were washed in tap water at 37°C for 72 hours. To create the insert, PDMS was then mixed 1:10 base to cross-linker and degassed for 1 hour. After degassing PDMS was poured into negative mold and the insert was polymerized overnight at 60°C. Post polymerization, the PDMS inserts were washed in distilled water at 37°C for 72 hours.

The tension loading frame was also designed with Solidworks and 3D printed for design of the prototype. The final system was then made of aluminum by the UC Berkeley Department of Physics machine shop. Full schematics for tension bioreactor system components are detail in Appendix 1.

Surface activation and collagen gel casting in PDMS inserts

To allow protein binding to the PDMS insert, I adapted a protocol developed previously detailed. Briefly, I use a three-step activation process: 1) Plasma cleaning for 5 minutes 2) 200ul 10% APTES in EtOH in each collagen gel well and then incubated at 60°C for 1 hour followed by extensive washing in distilled water (5x 10 minutes) 3) 200ul 5% glutaraldehyde in PBS in each

collagen gel well and then incubated at room temperature for 30 minutes followed by extensive washing in distilled water (5x 10 minutes). Post activation I diluted and pH neutralized a collagen I solution in a 10X DMEM buffer and 1M NaOH for a final concentration of 1-7mg/ml depending on the experiment (2.5-3mg/ml was found to be the best for mammary epithelial cells) with an additional supplement of FN or laminin depending on the experiment. In general FN was used at 1 ug/ml in all experiments with laminin used at 0.5% - 5% depending on the cell source (primary normal cells require significantly higher laminin to insure viability). After the collagen gel solution was prepared 200ul was added to each well and polymerized at 37°C for 30 minutes. If cells were to be embedded, the collagen gel was added in two layers, first a cell free 100ul layer polymerized at 37°C for 30 minutes followed by a cell collagen gel mixture added as the remaining 100ul and polymerized at 37°C for 30 minutes followed by the addition of media. After media addition the 10% strain would be applied to the appropriate experimental group. Exact recipes and protocols are detailed in full in Appendix 2.

Cell Invasion Studies

For cell invasion studies, MMTV PyMT mice were sacrificed at 11 week and the #4 mammary glands were collected for a tumor cell source or MCF10AT cells were cultured in matrigel as previously detailed for growth of acini. For PyMT cells, mammary glands were digested and tumor organoids isolated as previously described. For both cell types once acini were generated or isolated they were seeded in the collagen bioreactor and cultured for 2 days. After 2 days they were paraformaldehyde fixed and stained with propidium iodide and alexa488 phalloidin for imaging on the two-photon microscope.

Acknowledgements

I wish to thank Dr. Jan Liphardt Stanford University for helpful suggestions. Work was supported by NIH F31CA183255 and the ARCS Foundation to LC, NSF GRFP and NIH F31CA180422 to YAM, NSF GRFP to GO, NIH R01 CA138818, DoD W81XWH-13-1-0216, NIH U01ES019458, and NIH R01 CA085492 to VW

Works Cited:

- [1] M. J. Paszek, N. Zahir, K. R. Johnson, J. N. Lakins, G. I. Rozenberg, A. Gefen, C. A. Reinhart-King, S. S. Margulies, M. Dembo, D. Boettiger, D. A. Hammer and V. M. Weaver, "Tensional homeostasis and the malignant phenotype", *Cancer Cell*, 8, no. 3, p. . 241-54, 2005.
- [2] C. -L. Guo, M. Ouyang, J. -Y. Yu, J. Maslov, A. Price and C. -Y. Shen, "Long-range mechanical force enables self-assembly of epithelial tubular patterns", *Proc Natl Acad Sci U S A*, 109, no. 15, p. . 5576-82, 2012.
- [3] A. J. Engler, S. Sen, H. L. Sweeney and D. E. Discher, "Matrix elasticity directs stem cell lineage specification", *Cell*, 126, no. 4, p. . 677-89, 2006.
- [4] P. Lu, K. Takai, V. M. Weaver and Z. Werb, "Extracellular matrix degradation and remodeling in development and disease", *Cold Spring Harb Perspect Biol*, 3, no. 12, 2011.
- [5] J. K. Mouw, Y. Yui, L. Damiano, R. O. Bainer, J. N. Lakins, I. Acerbi, G. Ou, A. C. Wijekoon, K. R. Levental, P. M. Gilbert, E. S. Hwang, Y. -Y. Chen and V. M. Weaver, "Tissue mechanics modulate microRNA-dependent PTEN expression to regulate malignant progression", *Nat Med*, 20, no. 4, p. . 360-7, 2014.
- [6] J. R. Tse and A. J. Engler, "Preparation of hydrogel substrates with tunable mechanical properties", *Curr Protoc Cell Biol*, Chapter 10, no., p. . Unit 10.16, 2010.
- [7] J. L. Young and A. J. Engler, "Hydrogels with time-dependent material properties enhance cardiomyocyte differentiation in vitro", *Biomaterials*, 32, no. 4, p. . 1002-9, 2011.
- [8] Y. A. Miroshnikova, D. M. Jorgens, L. Spirio, M. Auer, A. L. Sarang-Sieminski and V. M. Weaver, "Engineering strategies to recapitulate epithelial morphogenesis within

- synthetic three-dimensional extracellular matrix with tunable mechanical properties", *Phys Biol*, 8, no. 2, p. . 026013, 2011.
- [9] J. S. Miller, C. J. Shen, W. R. Legant, J. D. Baranski, B. L. Blakely and C. S. Chen, "Bioactive hydrogels made from step-growth derived PEG-peptide macromers", *Biomaterials*, 31, no. 13, p. . 3736-43, 2010.
- [10] K. M. Yamada and E. Cukierman, "Modeling tissue morphogenesis and cancer in 3D", *Cell*, 130, no. 4, p. . 601-10, 2007.
- [11] T. A. Ulrich, A. Jain, K. Tanner, J. L. MacKay and S. Kumar, "Probing cellular mechanobiology in three-dimensional culture with collagen-agarose matrices", *Biomaterials*, 31, no. 7, p. . 1875-84, 2010.
- [12] P. P. Provenzano, K. W. Eliceiri, D. R. Inman and P. J. Keely, "Engineering three-dimensional collagen matrices to provide contact guidance during 3D cell migration", *Curr Protoc Cell Biol*, Chapter 10, no., p. . Unit 10.17, 2010.
- [13] P. -J. Wipff, H. Majd, C. Acharya, L. Buscemi, J. -J. Meister and B. Hinz, "The covalent attachment of adhesion molecules to silicone membranes for cell stretching applications", *Biomaterials*, 30, no. 9, p. . 1781-9, 2009.
- [14] A. Gautieri, S. Vesentini, A. Redaelli and M. J. Buehler, "Hierarchical Structure and Nanomechanics of Collagen Microfibrils from the Atomistic Scale Up", *Nano Lett*, 11, no. 2, p. . 757-766, 2011.
- [15] P. P. Provenzano, D. R. Inman, K. W. Eliceiri and P. J. Keely, "Matrix density-induced mechanoregulation of breast cell phenotype, signaling and gene expression through a FAK-ERK linkage", *Oncogene*, 28, no. 49, p. . 4326-43, 2009.

- [16] K. R. Levental, H. Yu, L. Kass, J. N. Lakins, M. Egeblad, J. T. Ertler, S. F. T. Fong, K. Csiszar, A. Giaccia, W. Weninger, M. Yamauchi, D. L. Gasser and V. M. Weaver, "Matrix crosslinking forces tumor progression by enhancing integrin signaling", *Cell*, 139, no. 5, p. . 891-906, 2009.
- [17] C. A. Schneider, W. S. Rasband and K. W. Eliceiri, "NIH Image to ImageJ: 25 years of image analysis", *Nature Methods*, 9, no. 7, p. . 671-675, 2012.
- [18] K. Wolf, M. Te Lindert, M. Krause, S. Alexander, J. Te Riet, A. L. Willis, R. M. Hoffman, C. G. Figdor, S. J. Weiss and P. Friedl, "Physical limits of cell migration: control by ECM space and nuclear deformation and tuning by proteolysis and traction force", *J Cell Biol*, 201, no. 7, p. . 1069-84, 2013.
- [19] A. Haeger, M. Krause, K. Wolf and P. Friedl, "Cell jamming: Collective invasion of mesenchymal tumor cells imposed by tissue confinement", *Biochim Biophys Acta*, no., 2014.
- [20] B. C. Isenberg, P. A. Dimilla, M. Walker, S. Kim and J. Y. Wong, "Vascular smooth muscle cell durotaxis depends on substrate stiffness gradient strength", *Biophys J*, 97, no. 5, p. . 1313-22, 2009.
- [21] J. I. Lopez, I. Kang, W. -K. You, D. M. McDonald and V. M. Weaver, "In situ force mapping of mammary gland transformation", *Integr Biol (Camb)*, 3, no. 9, p. . 910-21, 2011.

Chapter 3: Force-Dependent Malignancy Requires the Fibronectin Synergy Site to Engage Integrin Signaling and Activate PI3 Kinase

Cassereau, L.¹

In collaboration with: Miroshnikova, Y.A.^{1*}, Rozenberg, G. I.^{2,3}, Ou, G¹, Lopez, J.¹, Friedland, J.², Templeman, K.L.⁴, Elloumi-Hannachi, I.⁴, Calvo, J.C.³, Mies, C.⁵, Davidson, M.⁶, Gooch, K.^{2,7}, Sarang- Sieminski, A.L.^{2,8}, García, A.J.⁴

Under the supervision of: Weaver V.M.^{1,9,10}

¹Department of Surgery, Center for Bioengineering and Tissue Regeneration, University of California, San Francisco, San Francisco, CA, 94143

²Institute for Medicine and Engineering, University of Pennsylvania, Philadelphia, PA 19104

³University of Buenos Aires, Department of Biological Sciences, Buenos Aires, Argentina

⁴Woodruff School of Mechanical Engineering, Petit Institute for Bioengineering and Bioscience, Georgia Institute of Technology, Atlanta, GA 30332

⁵Department of Pathology, University of Pennsylvania, Philadelphia, PA 19104

⁶National High Magnetic Field Laboratory, Department of Biological Sciences, Florida State University, Tallahassee, FL 32310

⁷Current Address: Department of Biomedical Engineering, The Ohio State University, Columbus, OH 43210

⁸Current Address: Franklin W. Olin College of Engineering, Needham, MA, 02492

⁹Department of Anatomy, Department of Bioengineering and Therapeutic Sciences, Eli and Edythe Broad Center of Regeneration Medicine and Stem Cell Research and Helen Diller Family Comprehensive Cancer Center, University of California San Francisco, San Francisco, CA 94143

Abstract

Tumors are mechanically-corrupted tissues. Although a role for tissue force in malignancy is slowly becoming appreciated, the molecular mechanisms underlying this phenotype remain poorly understood. Tumors contain abundant cross-linked collagen that increases tissue tension to promote malignant transformation by inducing focal adhesions and potentiating PI3 kinase signaling. Importantly, collagen cross-linking requires fibronectin and tumors contain abundant fibronectin and frequently express high levels of $\alpha5\beta1$ integrin. Using transgenic and xenograft models and tunable two and three dimensional substrates, I found that fibronectin-bound $\alpha5\beta1$ integrin is essential for collagen-dependent, stiffness-driven malignant transformation. I also observed that collagen-dependent tension is transduced to tumor cells via force-dependent unfolding of fibronectin, which reveals the cryptic synergy binding site. Indeed, I found that ligation of $\alpha5\beta1$ integrin by the synergy site of fibronectin is necessary and sufficient for malignant transformation. Quantitative analysis and high resolution imaging revealed that ligation of the synergy site of fibronectin permits tumor cells to develop sufficient intracellular myosin-dependent tension to engage a zyxin-stabilized, vinculin force clutch that permits nucleation of PIP3 and facilitates PI3 kinase-dependent invasion and the persistent migration linked to malignant transformation. These data explain how a rigid collagen-rich matrix facilitates tissue transformation and they explain why $\alpha5\beta1$ integrin and fibronectin are consistently up-regulated in tumors and correlate with cancer aggression.

Introduction

Tumors are highly fibrotic¹⁻⁴. Fibrotic tumors contain abundant quantities of extracellular matrix (ECM) proteins, such as type I collagen, fibronectin (FN), tenascin (TN), and assorted proteoglycans, and cancerous tissues typically exhibit altered levels and activities of ECM receptors like integrins^{5,6}. Consistently, elevated β 1 integrin expression and focal adhesion kinase (FAK) activity correlate positively with high tumor grade and is predictive of poor patient prognosis⁶. Moreover, inhibiting β 1 integrin ligand binding represses the malignant phenotype of tumor cells *in vitro* and *in vivo*, and transgenic ablation of β 1 integrin or focal adhesion kinase (FAK) prevent oncogene-induced malignant transformation and metastasis^{7,8}. These findings emphasize the importance of interplay between tissue fibrosis and integrin signaling in malignancy.

Tumors are also mechanically corrupted and exhibit high interstitial pressure, elevated compression, ECM stiffening, and increased cellular tension^{3,9-11}. Highly fibrotic and stiff tumors are associated with increased aggression and high mortality^{7,10,12-15}. Consistently, elevating cell tension or stiffening the ECM via increased deposition and crosslinking of ECM components like collagen promotes the malignant transformation of a tissue¹³. Conversely, reducing cell tension, interstitial pressure, or preventing matrix stiffening decreases tumor incidence and aggression and improves treatment efficacy^{8,16-18}. Cell tension and ECM stiffness promote focal adhesion assembly, and integrin signaling is necessary for force-dependent malignant transformation^{15,19-21}. Thus, tissue tension promotes tumor progression via integrin signaling. However, the relationship between the high force environment of a tumor and

selective expression of specific integrins and their ECM ligands has yet to be determined. Indeed, while deposition and crosslinking of collagen promotes ECM stiffening and tumor progression, its major receptor, $\alpha 2\beta 1$ integrin, is tumor-suppressive rather than tumor promoting¹⁴.

Fibronectin (FN) levels are frequently elevated at both the primary and metastatic tumor sites and aggressive tumors express abundant FN^{6,22-24}. Moreover, elevated levels of the major FN receptor, $\alpha 5\beta 1$ integrin, are associated with tumor progression and tumors expressing high $\alpha 5\beta 1$ integrin are more aggressive⁶. Intriguingly, $\alpha 5\beta 1$ integrin and FN are frequently up-regulated in primary tumors, which we and others have shown are significantly stiffer than normal tissue^{6,16,25}. Indeed, high expression of $\alpha 5$ integrin and FN and elevated tissue tension independently correlate with poor patient prognosis^{3,6,13,16,20,25,26}. By way of explanation, FN is assembled with type I collagen and cross-linked collagen increases FN unfolding to reveal cryptic binding sites for $\alpha 5\beta 1$ integrin ligation^{27,28}. $\alpha 5\beta 1$ integrin is a unique transmembrane ECM receptor that is able to simultaneously engage both the RGD and synergy sites of FN and by doing so is able to significantly elevate intracellular tension^{29,30}. We and others showed that high actomyosin-mediated cell contractility potentiates ERK and PI3 kinase signaling and promotes tumor cell growth, survival and invasion^{15,31,32}. This raises the possibility that a stiffened, cross-linked type I collagen matrix promotes tissue transformation by inducing FN deposition and $\alpha 5$ integrin expression and thereafter mechanically priming FN to facilitate the catch-bond mediated ligation of $\alpha 5\beta 1$ integrin to drive tumor cell invasion. Here, I describe a series of studies in which I employed transgenic and xenograft mouse models of mammary cancer, two dimensional (2D) substrates and three dimensional (3D) organotypic

hydrogels, a novel bioreactor with tuned ECM stiffness, and quantitative imaging approaches to test this hypothesis. My findings revealed that ligation of the RGD and synergy sites of FN is necessary and sufficient to permit mammary tumor cells to develop high enough levels of intracellular myosin-dependent tension to be able to engage a zyxin-stabilized, vinculin force clutch that is required for the nucleation of PIP3 to facilitate PI3 kinase-dependent invasion and malignant transformation.

Results

Mammary malignancy is associated with increased expression of integrins that ligate fibronectin

Malignant transformation in mammary tissue is associated with altered expression of integrins and ECM proteins, ECM stiffening, and elevated cell tension, all of which promote tumor progression^{8,19,33–35}. Here, I examined which integrins are functionally linked to force-dependent malignant transformation.

Consistent with previous studies functionally implicating a multitude of integrins in tumor progression, Second Harmonic Generation (SHG) and immunofluorescence analysis indicated increased fibronectin (green) deposition along collagen tracks (indicated in white) in the invading fronts (sparse PI staining indicating cell strands protruding from tumor border) of highly stiffened, late stage PyMT tumors (Figure 3.1A). Indeed, the collagen network is the main ECM component that undergoes remodeling and altered crosslinking, leading to elevated extracellular matrix stiffness in tumors. Paradoxically, $\alpha 2\beta 1$ integrin, the main collagen receptor in mammary cells, is thought to be tumor suppressive, while the fibronectin receptor, $\alpha 5\beta 1$ integrin, is highly upregulated in aggressive and metastatic tumors^{1,9,13,36}. These findings intrigued me and led to me to investigate whether collagen-mediated ECM-stiffening promotes fibronectin secretion at stiff ECM sites, where it then engages $\alpha 5\beta 1$ integrin in a tension-dependent manner. This would provide a rationale for selective expression of $\alpha 5\beta 1$ integrin in the context of a stiffened ECM of a tumor. To determine whether tissue stiffness, malignant transformation, and $\alpha 5\beta 1$ integrin expression are linked, I examined tissue harvested from a cohort of Her2/Neu and PyMT mice treated with and without either a function blocking

antibody or a pharmacological inhibitor of lysyl oxidase (Lox) that prevents collagen cross-linking and ECM stiffening^{10,13}. Confocal immunofluorescence imaging of mammary tumor tissue from these mice revealed strong p³⁹⁷FAK and elevated pMLC in the epithelium of the non-treated invasive Her2/Neu (Figure 1B) and PyMT (not shown) tumors, and low to non-detectable levels in tissue from mice that had been treated with Lox inhibitor (Figure 3.1B). Coincident with the elevated focal adhesion signaling and high cytoskeletal tension detected in untreated mammary tumors, I also observed a significant increase in FN deposition in these tissues and robust reduction in the Lox inhibited tissue (Figure 3.1B). I additionally observed high levels of $\alpha 5$, $\alpha 2$ integrin and αV integrin in the invasive tumors and determined that their expression appeared lower when ECM stiffening and tumor tension were inhibited, whereas no differences in levels of $\alpha 2$ integrin were detectable (Figure 3.1B). These findings established a positive and specific association between collagen-mediated FN deposition, the expression of its integrin receptors $\alpha 5\beta 1$ and $\alpha V\beta 3$, and tissue tension and mammary malignancy *in vivo*.

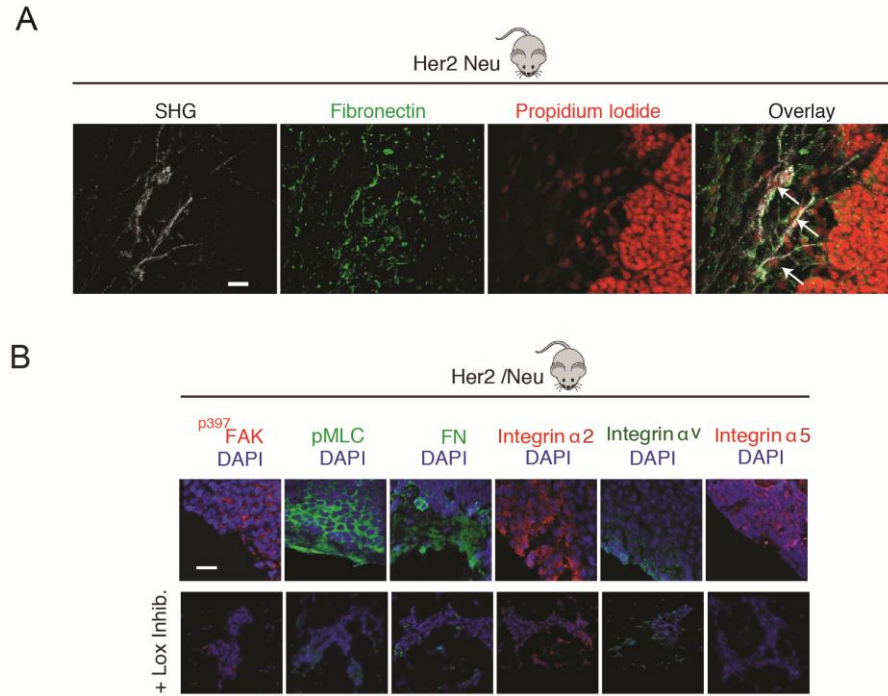


Figure 3.1 A) Second Harmonic Generation (SHG) images of collagen (grey), fibronectin (green), and nuclei (red) in the 7 month old PyMT tumors at the invasive front. Scale Bar 20µm. Arrows indicate cells migrating along FN-coated collagen fibers. **B)** Confocal immunofluorescence images of mammary tissue stained for ^pMLC, ^{p397}FAK, fibronectin (FN) and α5β1 integrin, α2 integrin and αv integrin in tissue excised from 7 month old control (Her2/Neu) or lysyl oxidase inhibitor treated (Lox inhibitor) Her2/Neu transgenic mice. Scale Bar 10µm

To explore the impact of tissue tension, FN, and its integrin receptors $\alpha 5\beta 1$ and $\alpha V\beta 3$ on breast malignancy, I used the nonmalignant S1 and malignant T4-2 mammary epithelial cells (MECs) from the HMT3522 human breast cancer progression series³⁷. The T4-2 MECs from this series exert significantly more traction force than their nonmalignant counterparts¹⁹. Moreover, as shown previously, upon embedment into a reconstituted basement membrane (rBM), the low force-exerting S1 MECs from this series formed polarized, growth-arrested acini-like structures demonstrated by lack of Ki-67 nuclear staining, robust β -catenin localization to cell-cell junctions, apical-lateral actin, basally localized $\beta 4$ integrin, and basally deposited laminin V. By contrast, the highly contractile, malignant T4-2 derivative MECs formed continuously growing, disorganized, and invasive colonies, as illustrated by elevated nuclear Ki-67 and disrupted localization of β -catenin, $\alpha 6 \beta 4$ integrin, and laminin V. However, inhibition of $\beta 1$ integrin, using a ligand function-blocking antibody, reverted the malignant phenotype of the contractile T4-2 colonies towards that of a growth-arrested, noninvasive, and more differentiated structure indicated by absence of detectable nuclear Ki-67, restoration of cell-cell localized β -catenin, apical-lateral actin, and basally localized $\alpha 6 \beta 4$ integrin and laminin V (8,19) (Figure 3.2A). Consistent with an association between tumor tension and ligation of the FN integrins $\alpha 5\beta 1$ and $\alpha V\beta 3$ and malignancy, FACS analysis revealed that the highly contractile T4-2 tumor cells expressed high levels of αV , $\alpha 5$, and $\beta 1$ but not $\alpha 2$ (Figure 3.2C) or $\beta 3$, $\beta 5$, $\beta 6$, $\alpha 1$ $\alpha 5\beta 1$, $\alpha 3$ or $\alpha 6$ integrin at their surface (not shown). Further, immunoblot analysis showed that following phenotypic reversion via blocking $\beta 1$ integrin, both $\alpha 5$ integrin and αV integrin levels were substantially reduced (Figure 1E). Moreover, immunostaining revealed that while the T4-2 MECs deposited abundant FN, expression of this ECM protein was lost in the reverted

structures (Figure 3.2A). These findings establish an association between tissue tension, expression of FN and its integrin receptors $\alpha5\beta1$ and $\alphaV\beta3$, and mammary malignancy.

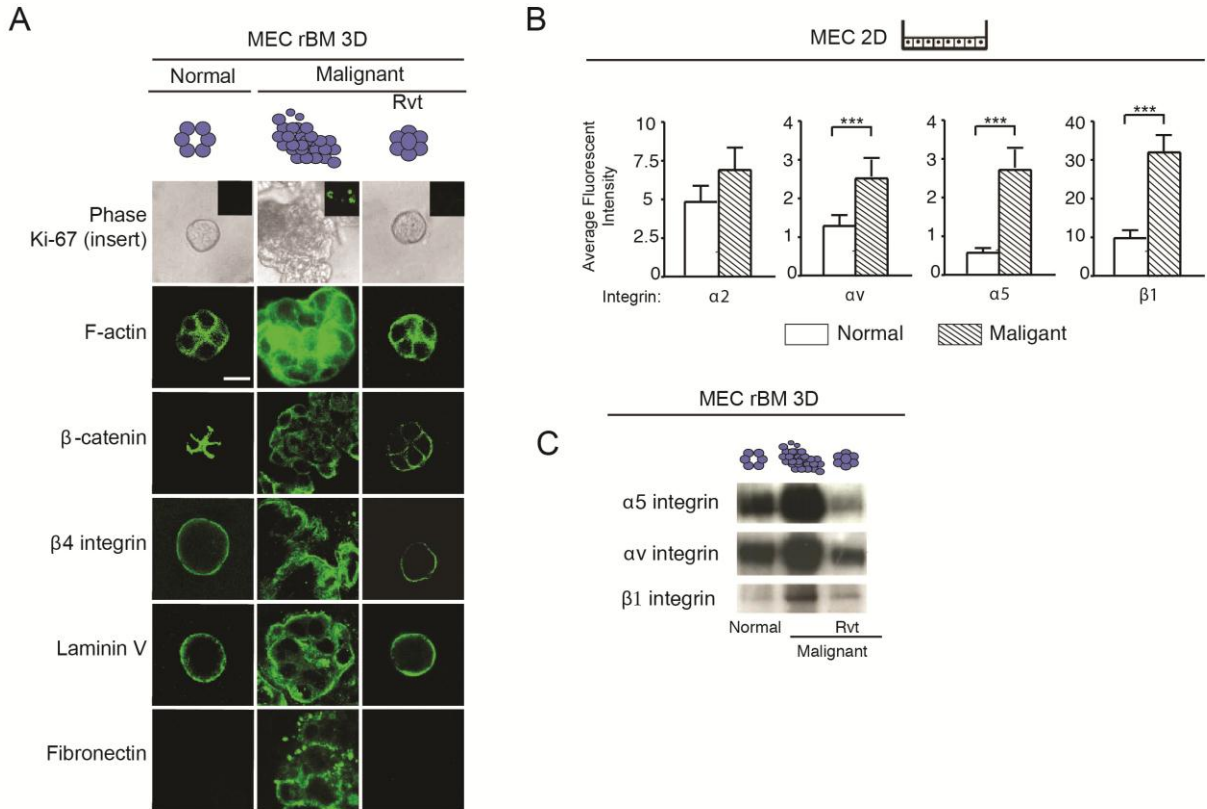


Figure 3.2 A) Phase contrast and confocal immunofluorescence images of Ki-67 (insert), Phalloidin (F-actin), β -catenin, β 4 integrin, laminin-5, and fibronectin stained colonies of nonmalignant (S-1), malignant (T4-2) and phenotypically-reverted (T4 Rvt) HMT-3522 human mammary epithelial cells (MECs) grown within a reconstituted basement membrane (rBM) for two weeks. Scale Bar 10 μ m. **B)** Bar graphs of FACS analysis of membrane localized integrins in S-1 compared to T4-2 MECs. **C)** Representative immunoblot image of α 5, α v and β 1 integrin in lysates from S-1, T4-2 and T4 Rvt 3D rBM colonies shown in A. ($n > 50$ acini). Results are the mean \pm S.E.M. of 3 separate experiments (* $p < 0.05$; ** $p < 0.01$; *** $p < 0.001$).

FN-ligated $\alpha 5\beta 1$ integrin is necessary and sufficient for expression of the malignant phenotype *in vitro* and *in vivo*

To directly explore the functional relationship among FN and its integrin receptors $\alpha 5\beta 1$ and $\alpha V\beta 3$, and mammary tissue transformation, I treated 3D rBM cultures of T4-2 mammary epithelial cells, which secrete copious amounts of FN (Figure 3.2A), with $\alpha 5$ or αV function-blocking antibodies and compared effects of the function blocking to malignant MECs treated with $\alpha 2$, $\alpha 3$, and $\beta 1$ function blocking antibodies. Data revealed that although blocking ligand binding to $\alpha 2$ (Figure 3.3A), αV , or $\alpha 3$ integrin (not shown) had little to no effect on the behavior of the T4-2 MECs, inhibiting $\alpha 5$ integrin repressed their malignant phenotype, similar to that observed following inhibition of $\beta 1$ integrin ligand binding (Figure 3.3A; 3.2A). Thus, while T4-2 MECs treated with either IgG isotype matched control, $\alpha 2$ or αV function blocking antibodies in forming continuously growing, large, disorganized and invasive colonies in rBM, as indicated by aberrantly localized $\alpha 6$ integrin, β -catenin and actin, the tumor cells pre-treated with function blocking antibodies against $\alpha 5$ or $\beta 1$ integrin assembled growth arrested, polarized structures reminiscent of differentiated mammary acini (Figure 3.3A) that were at least 60-70 percent smaller than the non-treated colonies (Figure 3.3B). Moreover, preventing $\alpha 5$ or $\beta 1$ integrin ligand binding in the T4-2 tumor cells significantly impaired anchorage independent growth and survival in soft agar (Figure 3.3C). These data indicate that FN-ligated $\alpha 5\beta 1$ integrin is necessary for expression of the malignant phenotype in cultured human mammary epithelial tissue-like structures.

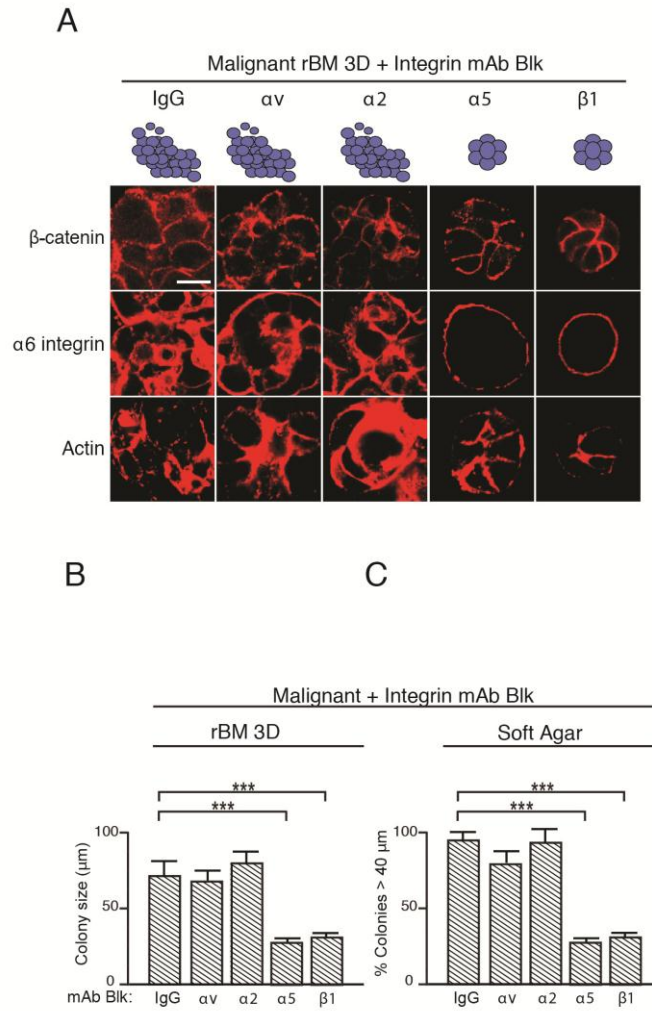


Figure 3.3 **A)** Confocal immunofluorescence images of β -catenin, $\alpha 6$ integrin and actin (Phalloidin) staining of malignant (T4-2) MEC colonies grown for two weeks in rBM in the presence of a function-blocking antibody (mAb) to αv , $\alpha 2$, $\alpha 5$ or $\beta 1$ or an IgG isotype matched control mAb. Scale Bar 30 μm . **B)** Bar graph showing relative size of the T4-2 colonies shown in A. **C)** Bar graph showing percentage of tumor colonies formed in soft agar (40+ microns) following treatment with function-blocking mAbs to αv , $\alpha 2$, $\alpha 5$ or $\beta 1$ integrin or an IgG isotype matched control mAbs.

I next determined whether FN-ligated $\alpha 5\beta 1$ integrin was sufficient to promote mammary malignancy. I expressed a tetracycline (tet)-regulated eGFP-tagged $\alpha 5$ or $\alpha 2$ integrin in nonmalignant S1 MECs (which express negligible $\alpha 5$ integrin) and assayed their response to FN. Immunoblot and fluorescence-activated cell sorting (FACS) analysis confirmed a tet-modulated increase in $\alpha 5$ and $\alpha 2$ integrin (data not shown) and showed that neither ectopic expression of $\alpha 5$ nor $\alpha 2$ integrin significantly altered the cell surface expression of any of the other integrin receptors in HMT-3522 S1 MECs (not shown). Moreover, 10-14 days following their embedment within a three dimensional (3D) rBM, nonmalignant S1 MECs expressing either elevated cell surface $\alpha 2$ or $\alpha 5$ integrin assembled growth-arrested (Figure 3.4B-C), polarized mammary acini with cleared lumens, as indicated by cell-cell localized β -catenin, basally-localized $\alpha 6 \beta 4$ integrin, and basally deposited collagen IV (Figure 3.4A). However, following FN engagement, the S1 MECs expressing high $\alpha 5$ integrin not only continued growing (Figure 3.4B), but also failed to clear their lumens, showed diffuse cell-cell localized β -catenin and lacked basal polarity (Figure 3.4A). Indeed, in the presence of exogenous FN, nonmalignant S1 MECs expressing elevated $\alpha 5$ integrin formed mammary colonies that were 30-40 percent larger than S1 MECs expressing elevated $\alpha 2$ integrin, despite the availability of abundant collagen (Figure 3.3B). These findings demonstrate that FN-ligated $\alpha 5\beta 1$ integrin is both necessary and sufficient for expression of the malignant phenotype of MECs *in vitro*

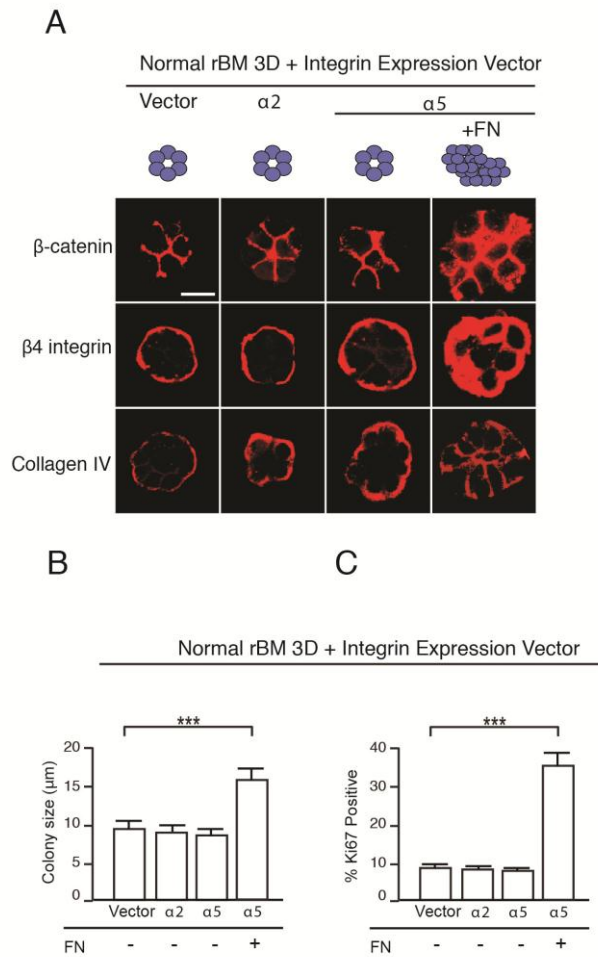
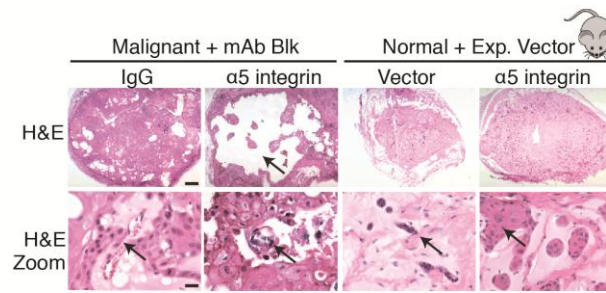


Figure 3.4 A) Confocal immunofluorescence images of β -catenin, $\beta 4$ integrin and collagen IV staining of colonies of nonmalignant (S-1) vector (Ctrl) MECs and MECs expressing elevated $\alpha 2$ or $\alpha 5$ integrin grown in rBM with or without the addition of fibronectin (+FN) for two weeks. Scale Bar 10 μm . **B)** Bar graph showing relative size of S-1 MEC colonies shown in **C)** Bar graph showing percent Ki-67 positive S-1 MEC colonies shown in **A**.

To further implicate FN-ligation of $\alpha 5\beta 1$ integrin in mammary malignancy, I manipulated $\alpha 5$ integrin expression and/or function in nonmalignant and malignant MECs and assayed for effects on tumorigenesis *in vivo*. I inoculated nonmalignant S1 MECs expressing eGFP (nonmalignant control) or high levels of $\alpha 5$ integrin (+ $\alpha 5$ integrin), as well as T4-2 tumorigenic MECs that had been treated with either an $\alpha 5$ integrin function blocking monoclonal antibody ($\alpha 5$ integrin inhibited) or an isotype IgG control antibody (tumor control), into the rear flanks of Balb/c nu/nu mice. Two months following MEC inoculation, the control tumors had formed large, actively growing, invasive, and highly angiogenic tumor masses, as indicated by elevated PCNA, negligible activated caspase 3, a clearly visible vasculature (confirmed by strong CD34 tissue staining), and histopathological analysis that showed invasive cell masses (Figures 3.5, 3.6A-B). However, T4-2 cells treated with the $\alpha 5$ integrin function blocking antibody formed only small, non-proliferating tumor colonies that stained positively for the apoptosis marker activated caspase 3, lacked a vasculature, had no CD34 staining, and showed histopathological evidence of cystic degeneration and necrosis (Figures 3.5, 3.6A-B). As expected, the majority of the nonmalignant S1 MECs failed to survive, and those that did formed ductal-like differentiated tissue structures. By contrast, those S1 MECs expressing high levels of $\alpha 5$ integrin not only survived but grew to form hyperplastic/dysplastic cell masses that activated an angiogenic response, as indicated by a visible vasculature and positive CD34 tissue staining (Figures 3.5, 3.6A-B). Indeed, a 3D *in vitro* co-culture angiogenesis assay (Figure 3.6C) revealed that blocking $\alpha 5$ or $\beta 1$ integrin binding activity in the T4-2 malignant MECs prevented endothelial network formation and showed that nonmalignant MECs expressing elevated FN-ligated $\alpha 5$ integrin, but not collagen-ligated $\alpha 2$ integrin, induced endothelial networks.

Consistently, the FN-ligated $\alpha 5\beta 1$ integrin MECs expressed abundant VEGF and inhibiting $\alpha 5$ or $\beta 1$ integrin in the T4-2 malignant MECs reduced VEGF levels (Figure 3.6B). These findings indicate that FN-ligated $\alpha 5\beta 1$ integrin is both necessary and sufficient for expression of the malignant phenotype of MECs *in vitro* and *in vivo*.

A



B

| Cell Description | Lesion Mass (g) | Histological Features | | | |
|---------------------------------|----------------------|-----------------------|-----------------------|-----------|---------------|
| | | Acinar/Ductal | Hyperplasia/Dysplasia | Carcinoma | Cyst/Necrosis |
| Non-Malignant | 6/8 (0.018±0.013) | ++++ | - | - | 0/8 |
| Non-Malignant + α5 integrin | 8/8 (0.028±0.011) | ++ | +++ | - | 0/8 |
| Malignant + IgG | 8/8 (0.236±0.078) | - | - | +++++ | 1/8 |
| Malignant + α5 integrin mAb Blk | 8/8 (0.341±0.324) | - | - | ++ | 7/8 |

Figure 3.5 A) Phase contrast images of low (top panel) and high (second panel) magnification of H & E sections of tissue excised two months following injection of malignant T4-2 MECs with IgG or a function blocking antibody to $\alpha 5$ integrin and nonmalignant S-1 MECs expressing empty vector or an $\alpha 5$ integrin. Scale Bar 10 μ m. **B)** Table summarizing tumor score and histological features. Scale Bar 10 μ m. (* $p < 0.05$; ** $p < 0.01$; *** $p < 0.001$).

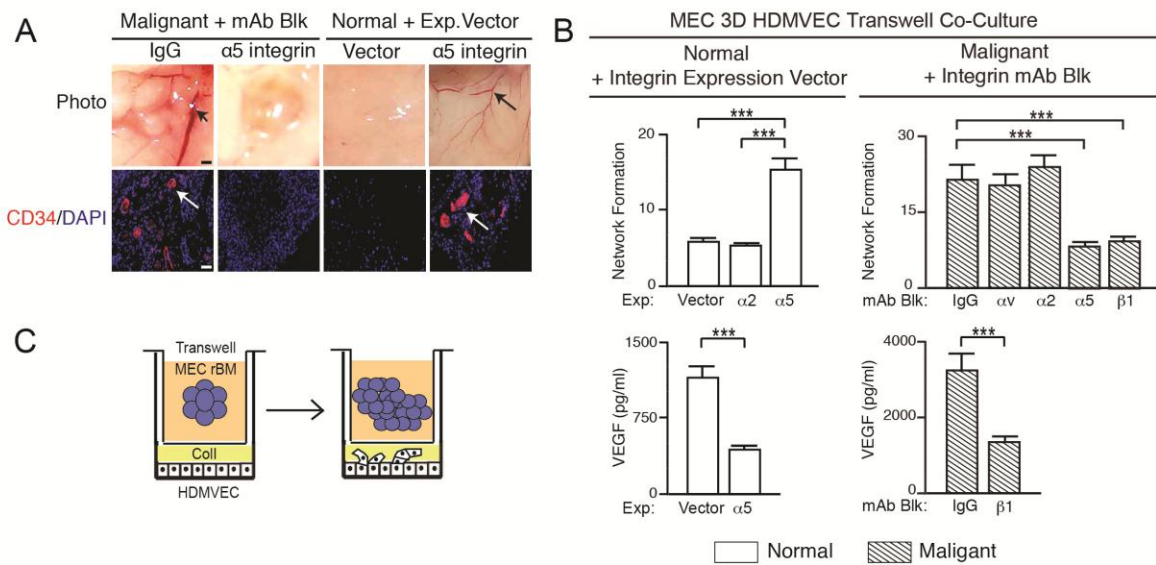


Figure 3.6 A) (upper panel) Photomicrographs of vasculature in tissue from injected malignant T4-2 MECs with and without $\alpha 5$ integrin inhibition and nonmalignant S-1 MECs expressing empty vector or elevated $\alpha 5$ integrin. Scale Bar 10 mm. (lower panel) Immunofluorescence images of tissue stained for the endothelial marker CD34. Results are the mean \pm S.E.M. of 3 separate experiments. **B)** *In vitro* network formation of HDMVECs is (top left) greatly increased in a co-culture setting with non-malignant MECs over-expressing $\alpha 5$ integrin and is (top right) highly reduced when either $\beta 1$ or $\alpha 5$ integrins are functionally-blocked in the malignant MECs, but not $\alpha 2$ or αv ; (bottom left) nonmalignant MECs overexpressing $\alpha 5$ integrin secrete higher levels of VEGF and (bottom right) function-blocking of $\alpha 5$ integrin in malignant MECs reduces their VEGF. **C)** Schematic of an *in vitro* endothelial network formation model system by human dermal microvascular endothelial cells (HDMVECs) co-cultured with MECs.

Fibronectin-ligated $\alpha5\beta1$ integrin increases cell tension to promote mammary malignancy

To directly test if FN-ligation of $\alpha5\beta1$ integrin could promote mammary malignancy by increasing cell tension, I treated 3D collagen-FN cultures of MCF10A MECs expressing either elevated $\alpha5$ or $\alpha2$ integrin with either a ROCK inhibitor (Figure 3.7A) or myosin inhibitor (not shown). Examination of FN-doped 3D collagen cultures of nonmalignant MCF10A MECs expressing elevated $\alpha5$ integrin showed that inhibition of ROCK activity or actomyosin contractility normalized their tissue structure to that assembled by control nonmalignant MECs or nonmalignant MECs expressing elevated $\alpha2$ integrin (Figure 3.7A). While $\alpha5\beta1$ integrin expressing nonmalignant MECs formed disorganized, invasive, proliferating large colonies, those cultures in which cell tension was reduced were growth-arrested and formed smaller colonies (Figure 3B) that exhibited apical-lateral actin networks and $\beta1$ integrin, basally-localized laminin, and exhibited evidence of active luminal clearance as indicated by elevated activated caspase 3 (Figure 3.7A; left panel). Similarly, T4-2 mammary tumor cells treated with these force inhibitors also formed smaller (Figure 3.7C), growth-arrested, phenotypically-reverted tissue-like structures similar to those generated in the presence of a function blocking antibody to $\alpha5$ integrin and in marked contrast to the significantly larger, highly proliferative, invading, and disorganized colonies observed in the IgG isotype-treated or vehicle-treated control cells or those in which $\alpha2$ integrin was inhibited (Figure 3.7A; right panel). Furthermore, I directly implicated tension-dependent and $\alpha5\beta1$ -FN-mediated cellular invasion and disorganization of acini using a 3D tension bioreactor. To better recapitulate the evolving microenvironment of the tumor, I embedded acini in a soft, non-stretched collagen gels with or without fibronectin, then uniaxially stretched and stiffened the matrix as described previously

³⁸. Similarly to static growth culture 3D studies, acini only disorganized and invaded (indicated by arrows) in a context of a stiff environment upon high expression of $\alpha 5$ integrin and its ligation to fibronectin (Figure 3.7D). Interestingly, although they did not fully invade, $\alpha 5$ overexpressing acini began to form protrusions on the basal side in the context of exogenous FN even in a soft, non-stretched collagen (as indicated by arrows) (Figure 3.8).

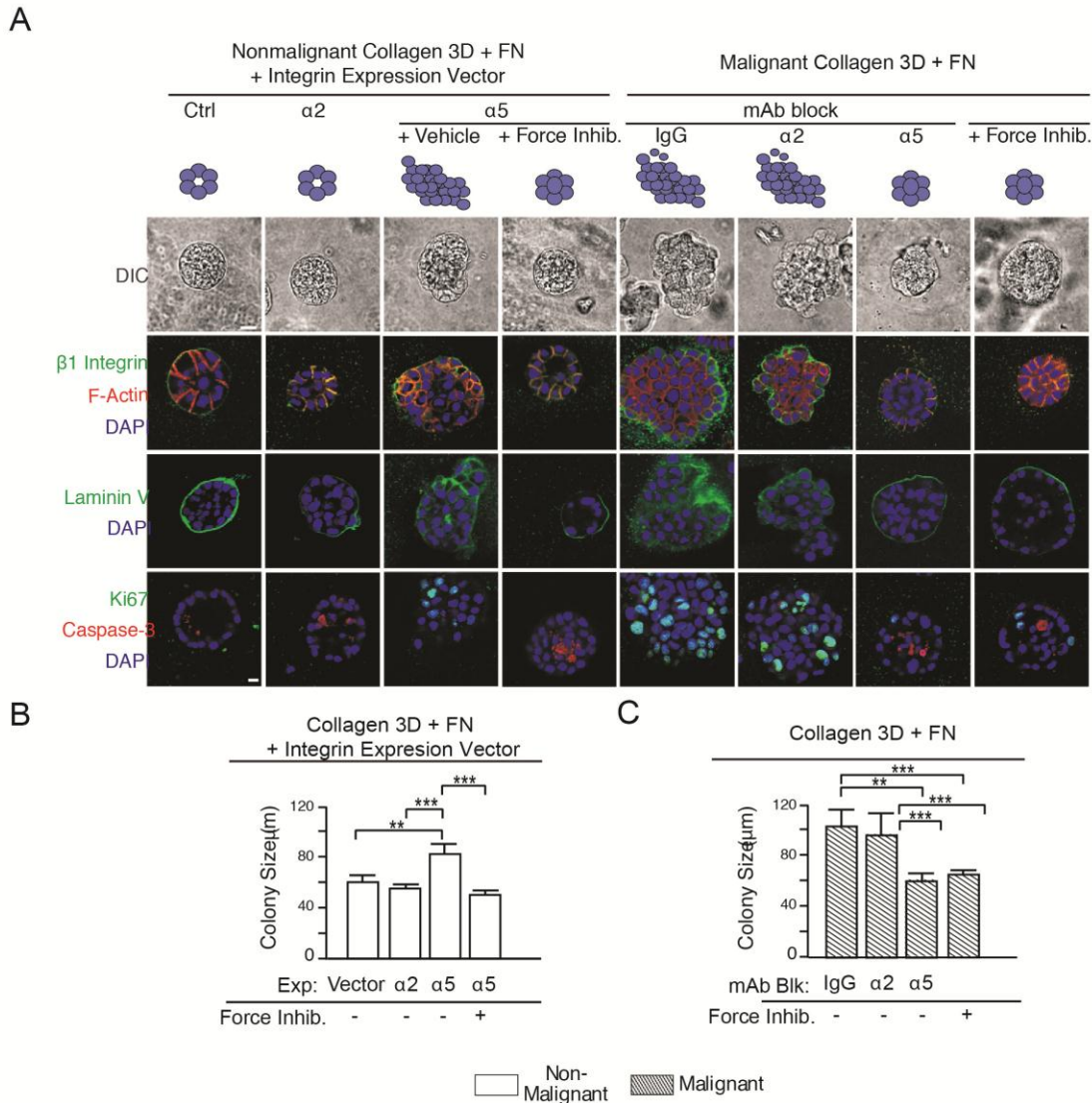


Figure 3.7 A) Phase contrast and confocal immunofluorescence images of $\beta 1$ integrin, Phalloidin (F-actin), laminin V, Ki-67 and activated caspase 3 (Caspase-3) and DAPI (nuclei) stained colonies of nonmalignant (MCF10A) human mammary epithelial cells (MECs) expressing empty vector or elevated $\alpha 2$ or $\alpha 5$ integrin treated with or without a ROCK inhibitor and malignant (HMT-3522 T4-2) incubated with nonspecific IgG or function blocking antibodies to $\alpha 2$ or $\alpha 5$ integrin or treated with or without a ROCK inhibitor grown within a collagen gel with added fibronectin (FN) for two weeks. Scale Bar 8 μm . **B)** Bar graph showing relative size of the non-malignant colonies shown in A. **C)** Bar graph showing relative size of the malignant colonies shown in A.

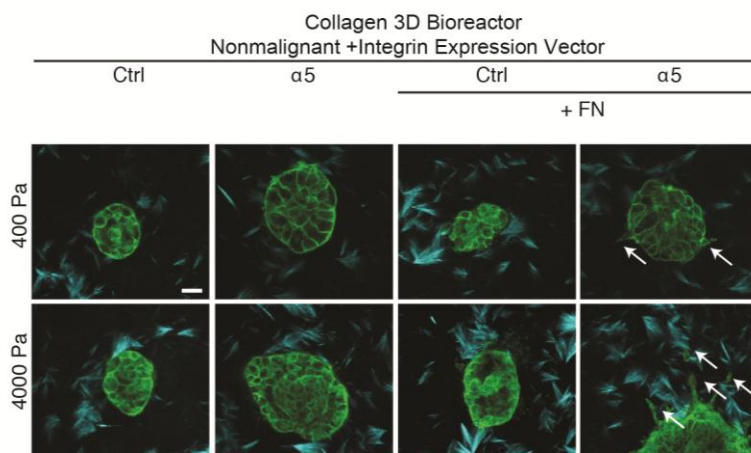


Figure 3.8 Second Harmonic Generation images of nonmalignant (MCF10A) human mammary epithelial day 20 acini (green) expressing empty vector or elevated $\alpha 5$ integrin with or without FN embedded in collagen (blue) and installed into a 3D tension bioreactor system and subjected either to 0% (400Pa) or 10% (4000Pa) stretch, as described previously³⁸. Arrows indicate invasive cells. Results are the mean \pm S.E.M. of 3-5 separate experiments. (** $p < 0.01$; *** $p < 0.001$).

Fibronectin-ligated $\alpha5\beta1$ integrin and not collagen-ligated $\alpha2\beta1$ integrin increases MEC tension

I next asked how FN-ligated $\alpha5\beta1$ integrin promoted mammary tissue malignancy. Examination of the adhesions assembled by MECs plated on either FN or collagen coated glass slides revealed that nonmalignant MECs with FN-ligated $\alpha5\beta1$ integrin had larger numbers of prominent, peripheral adhesions (Figures 3.9B) with more p^{397} FAK (Figure 3.9A) and recruited greater quantities of the force-activated molecules vinculin and zyxin (Figure 3.9C-F) as compared to MECs expressing collagen-ligated $\alpha2\beta1$ integrin (Figures 3.9A-F) or FN-ligated $\alphaV\beta3$ integrin (not shown). Importantly, I also determined that $\alpha5\beta1$ -expressing MECs contained higher levels of nuclear yes-associated protein (YAP), which reflects enhanced activity of the mechanoactivated Hippo pathway³⁹ (Figure 3.9G). These findings show that FN-ligation of $\alpha5\beta1$ integrin in MECs increases their tension at matrix adhesions and elevates their mechano-signaling.

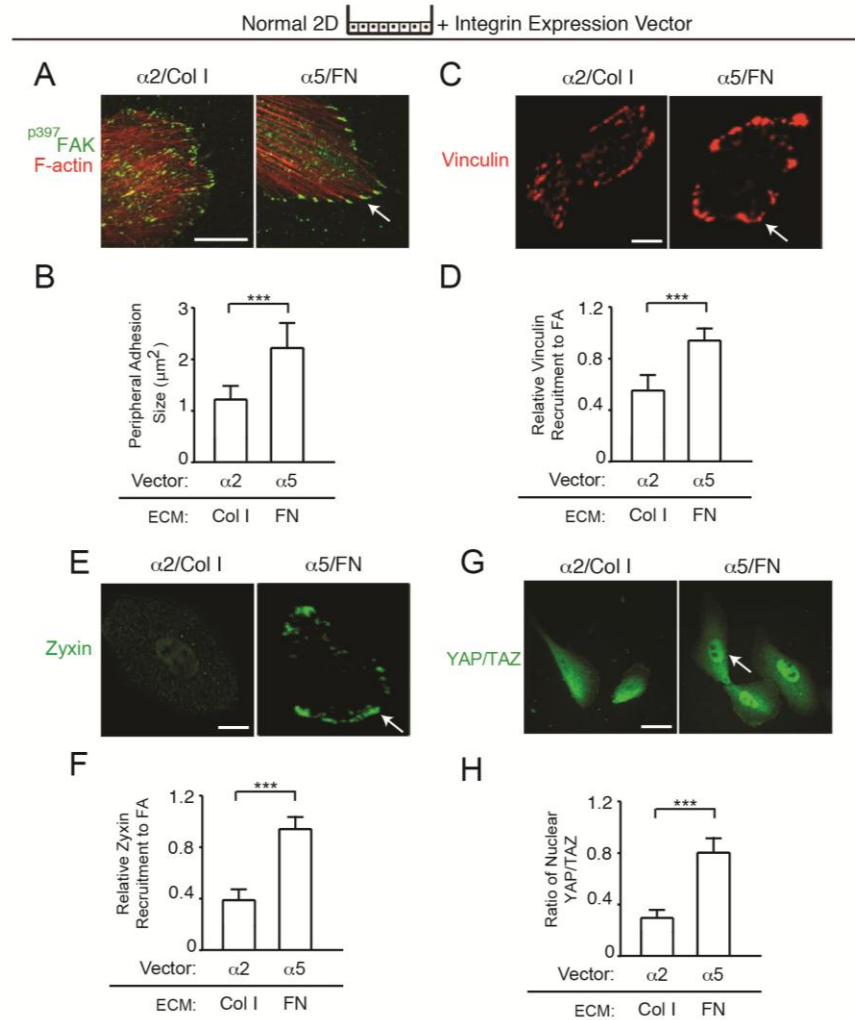


Figure 3.9 **A**) Immunofluorescence confocal images of nonmalignant mammary epithelial cells (MECs) expressing either exogenous $\alpha 2$ integrin plated on type 1 collagen ($\alpha 2/\text{Col I}$) or exogenous $\alpha 5$ integrin plated on fibronectin ($\alpha 5/\text{FN}$) stained for $p^{397}\text{FAK}$ ($p^{397}\text{FAK}$; green) or with phalloidin (F-actin; red). Scale Bar 10 μm . **B**) Bar graph quantifying size of peripheral adhesions shown in **A**. **C**) Immunofluorescence confocal images of $\alpha 2/\text{Col I}$ and $\alpha 5/\text{FN}$ nonmalignant MECs stained for vinculin (Vinculin; red) Scale Bar 3 μm . **D**) Bar graphs showing quantification of relative amount of vinculin recruited to focal adhesions in MECs shown in **C**. **E**) Immunofluorescence confocal images of $\alpha 2/\text{Col I}$ and $\alpha 5/\text{FN}$ nonmalignant MECs stained for zyxin (Zyxin; green) Scale Bar 3 μm . **F**) Bar graphs showing quantification of relative zyxin recruited to focal adhesions in MECs shown in **E**. **G**) Immunofluorescence images of $\alpha 2/\text{Col I}$ and $\alpha 5/\text{FN}$ nonmalignant MECs stained for YAP (arrow indicating nuclear localization of YAP). Scale Bar 15 μm **H**) Bar graphs quantifying percent nuclear YAP in MECs shown in **H**

Consistent with the hypothesis that FN-ligated $\alpha 5\beta 1$ integrin enhances tension in MECs, confocal immunofluorescence imaging revealed that the aberrant colonies assembled by the FN-ligated $\alpha 5\beta 1$ integrin expressing nonmalignant MECs showed high levels of ROCK activity, as indicated by more activated p^{1696} MYPT (myosin phosphatase binding protein), an observation that is consistent with high cell contractility and elevated actomyosin activity. By contrast, the nonmalignant MECs expressing collagen-ligated $\alpha 2 \beta 1$ integrin did not stain positively for p^{696} MYPT and formed small, polarized acini-like structures with apical-lateral β -catenin and basally-deposited the basement membrane (BM) protein laminin V (Figure 3.10A). Moreover, MECs expressing $\alpha 5$ integrin contracted 3D collagen gels to a greater extent (Figure 3.10B) than those expressing $\alpha 2$ integrin. Indeed, traction force microscopy demonstrated that MECs which had FN-ligated $\alpha 5\beta 1$ integrin exhibited higher maximum cell traction force on their ECM as compared to $\alpha 2$ integrin-expressing MECs plated on collagen I-activated polyacrylamide gels (Figure 3.10C). These findings indicate that FN-ligated $\alpha 5\beta 1$ integrin and not collagen-ligated $\alpha 2 \beta 1$ integrin specifically increases tension and mechano-signaling in MECs.

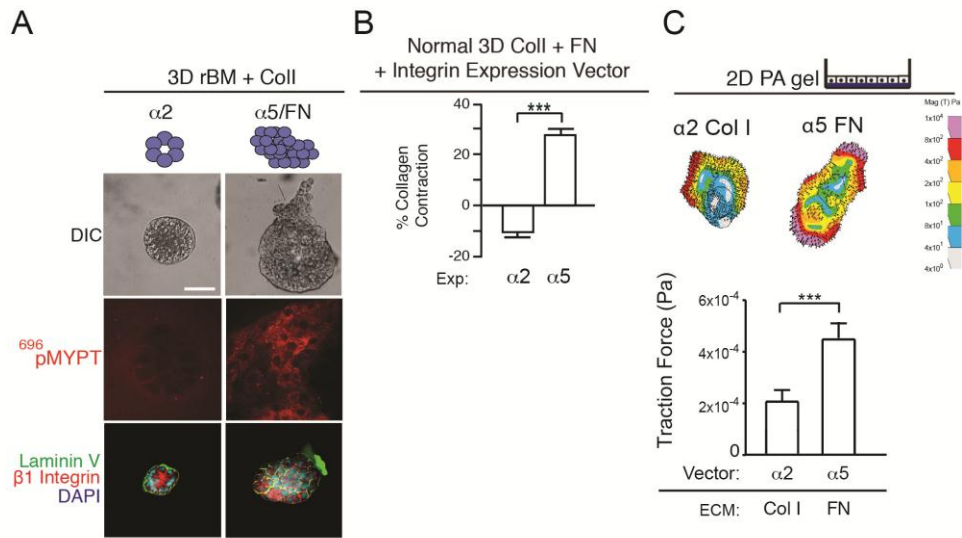


Figure 3.10 A) Immunofluorescence confocal images (top and bottom panels) and phase contrast images (middle panel) of three dimensional cultures of $\alpha 2/Col 1$ and $\alpha 5/FN$ nonmalignant MECs stained for the ROCK target ⁶⁹⁶MYPT (top) or $\beta 1$ integrin (red) and laminin V (green) and DAPI (blue). Scale Bar 50 μm . **B)** Quantification of collagen gel contraction of normal mammary epithelial cells + either $\alpha 2$ or $\alpha 5$ integrin and embedded in a 3D collagen gel for 3 days. **C)** Force maps of $\alpha 2/Col 1$ and $\alpha 5/FN$ nonmalignant MECs and bar graphs showing maximum traction generated by MECs at the cell edge. Arrows in A), C), and E) indicate peripheral localization of adhesion molecules. Results are the mean \pm S.E.M. of 3 separate experiments. (***) $p < 0.001$.

The $\alpha 5\beta 1$ integrin catch bond enhances mechanotransduction in MECs

Unlike αV integrin, $\alpha 5$ integrin binds to both the PHSRN synergy and RGD sites of fibronectin, and only FN bound $\alpha 5\beta 1$, not $\alpha V\beta 3$ integrin, exhibits a unique catch-bond phenotype in which ligand binding is strengthened in response to force⁴⁰ (Figure 3.11A). Consistently, shear force adhesion studies showed that $\alpha 5\beta 1$ integrin expressing MECs attached to either full length (not shown) or a recombinant 9-10 domain FN bound with much greater strength compared to MECs plated on recombinant 9-10 domain FN in which the PHSRN domain was mutated (Figure 3.11A). Indeed, MECs expressing elevated $\alpha 5$ integrin bound with at least twice as much strength to recombinant 9-10 domain FN as compared to MECs expressing elevated $\alpha V\beta 3$ integrin ligated to the same ECM or $\alpha 2\beta 1$ integrin expressing MECs ligated to a GFOGER Col I substrate or $\alpha 5\beta 1$ integrin expressing MECs ligated to recombinant 9-10 FN in which the synergy site region was mutated (Figure 3.11A-B). The adhesions assembled by MECs with $\alpha 5$ integrin interacting with recombinant 9-10 FN also showed that in the absence of the synergy site the size of peripheral adhesions was greatly diminished (Figure 3.11D) as was the amount of p³⁹⁷FAK (Figure 3.11D) and the quantity of vinculin and zyxin at the integrin adhesions (Figure 3.11D-E, 3.12A-B). There was also a significant reduction in the amount of zyxin recruited to actin stress fibers at the $\alpha 5\beta 1$ integrin adhesions in the MECs plated on the recombinant FN lacking the PHSRN synergy domain (Figure 3.12C-D) and less nuclear YAP, indicating that there was reduced mechano-signaling³⁹ (Figure 3.12E-F). Consistently, in the absence of the synergy site FN ligation of $\alpha 5\beta 1$ integrin in MECs showed a significant reduction in vinculin-mediated FRET signaling indicative of reduced mechano-transduction (Figure 3.11H-I). Moreover, only

the $\alpha 5\beta 1$ integrin expressing MECs ligated a synergy site intact recombinant FN, and not $\alpha 2\beta 1$ integrin expressing MECs on collagen I or $\alpha V\beta 3$ expressing MECs on fibronectin, demonstrated strong directional migration (durotaxis) in response to gradient ECM stiffness (3.11C). Finally, while the $\alpha 5\beta 1$ integrin expressing MECs formed continuously growing, large, and disorganized colonies with high levels of nuclear YAP when embedded in rBM doped with either recombinant 9-10 FN (Figure 3.12G) or a wild type full length FN (data not shown), in the absence of the synergy site the structures grew less, these same MECs barely activated YAP and they formed significantly smaller, polarized structures that showed evidence of active luminal clearance (Figure 3.12G). Furthermore, I directly tested the role of fibronectin's synergy site in the tension $\alpha 5\beta 1$ -integrin-dependent cellular invasion and disorganization of acini using the 3D tension bioreactor described above³⁸. Similarly to 2D findings and conventional 3D culture, acini disorganized and invaded in the context of a stiff environment only upon high expression of $\alpha 5$ integrin and its ligation to full length fibronectin (indicated by arrows; Figure 3.12H). Colony invasiveness was abrogated with the inhibition of fibronectin's synergy site using a small molecule inhibitor ATN-161 (Figure 3.12H). These findings indicate that FN-ligated $\alpha 5\beta 1$ integrin, by virtue of its unique ability to bind to the FN synergy site to enhance cell tension and mechano-signaling, promotes the force-dependent malignancy of MECs.

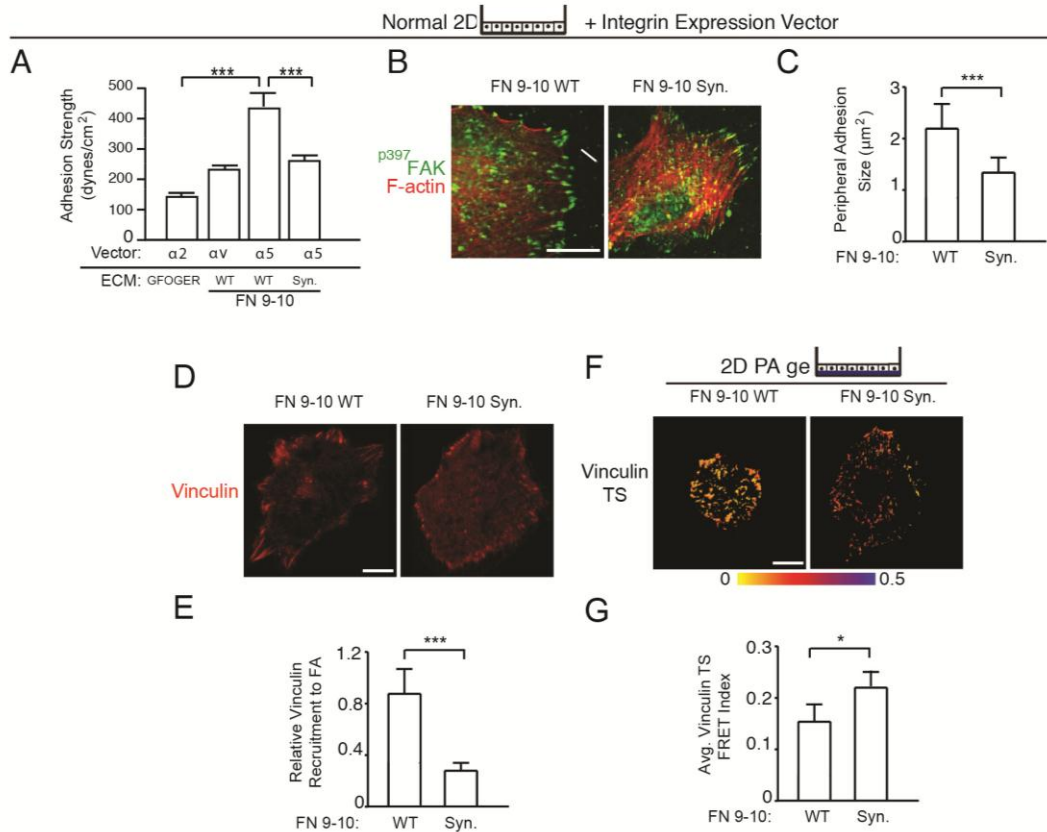


Figure 3.11 A) Bar graphs showing adhesion strength of nonmalignant mammary epithelial cells (MECs) expressing integrins $\alpha 2$ plated on GFOGER, αv or $\alpha 5$ plated on recombinant fibronectin 9-10 (FN 9-10 WT), and $\alpha 5$ plated on recombinant fibronectin 9-10 with the synergy site mutated (FN 9-10 Syn). **B)** Fraction of MECs overexpressing remaining adherent with linearly increased applied hydrodynamic fluid shear force. **C)** Top: MEC directional migration when plated on polyacrylamide gels (PA) of gradient stiffness (140-60,000 Pa) **B)** Immunofluorescence confocal images of MECs expressing $\alpha 2$ integrin plated on FN 9-10 WT or FN 9-10 Syn stained for p³⁹⁷FAK (p³⁹⁷FAK; green) and actin with phalloidin (F-actin; red). Scale Bar 10 μ m. **C)** Bar graph quantifying size of peripheral adhesions shown in B. **D)** Immunofluorescence confocal images of MECs expressing $\alpha 2$ integrin plated on FN 9-10 WT or FN 9-10 Syn stained for vinculin. Scale Bar 3 μ m. **E)** Bar graphs showing quantification of relative amount of vinculin recruited to focal adhesions in MECs shown in D. **F)** FRET images of MECs expressing $\alpha 5$ integrin and the vinculin force sensor plated on polyacrylamide gels conjugated with FN 9-10 WT or FN 9-10 Syn. Scale Bar 5 μ m. **G)** Bar graphs showing quantification of FRET index at focal adhesions in MECs shown in F.

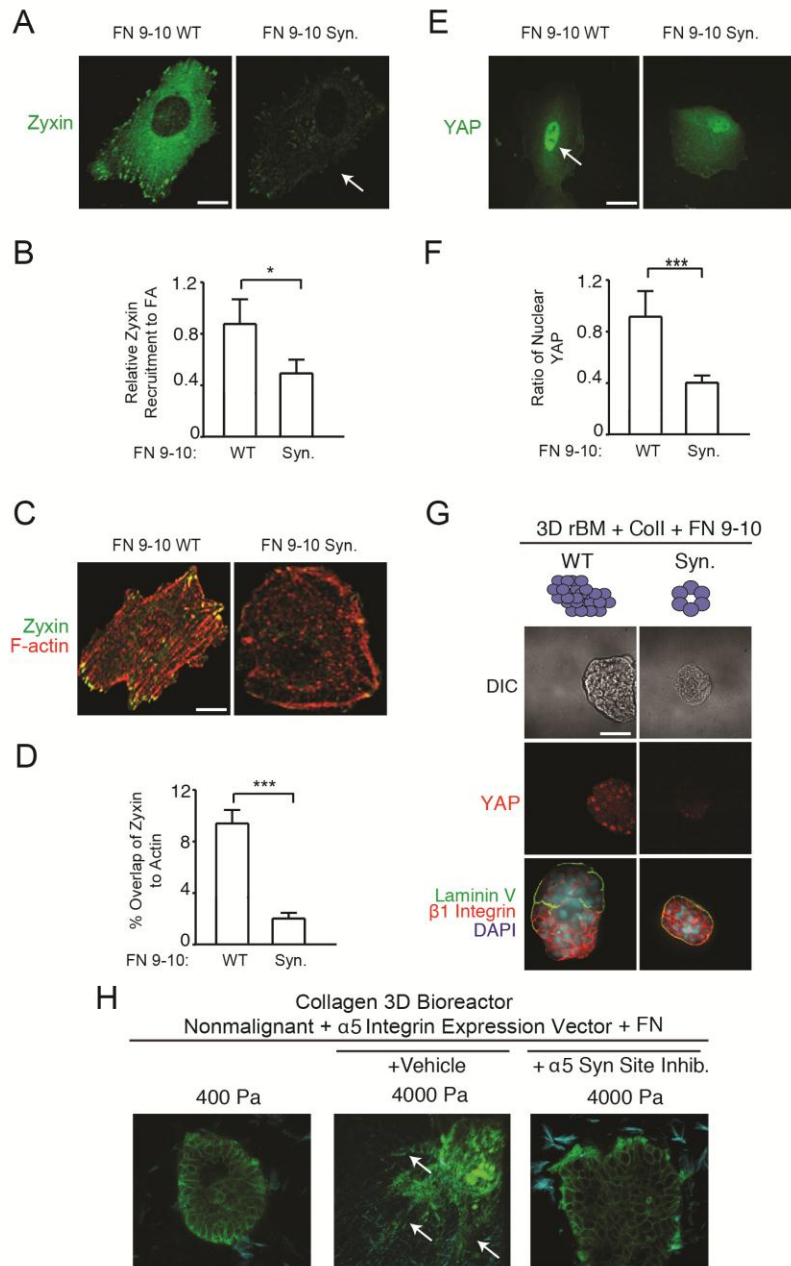


Figure 3.12 **A)** MECs expressing α 5 integrin stained for zyxin. Scale Bar 3 μ m **B)** Quantification of zyxin. **C)** MECs expressing α 5 integrin double-stained for zyxin and F-actin. Scale Bar 3 μ m. **D)** Quantification of zyxin co-localization to actin. **E)** MECs expressing α 5 integrin stained for YAP. Scale Bar 15 μ m. **F)** Quantification nuclear YAP in MECs shown in E. **G)** Immunofluorescence images of MEC organoids embedded in collagen **H)** MEC organoids embedded in collagen gels tuned to 400PA or 4kPA. Arrows indicating invading cells. Scale Bar 50 μ m.

The fibronectin synergy site-ligated $\alpha 5\beta 1$ integrin increases MEC tension and promotes malignancy by amplifying PI3K signaling

I next examined how an increase in cell tension mediated by FN-ligation of $\alpha 5\beta 1$ integrin could induce the malignant behavior of MECs. Growth factor receptor (GFR) signaling enhances MEC growth and survival by activating PI3K and ERK, and oncogenic transformation requires PI3K and ERK activity³¹. Consistently, I observed greatly reduced $p^{202/204}$ ERK and p^{473} Akt levels in the mammary epithelium of Her2/Neu mice in which collagen cross-linking and ECM stiffening had been prevented by inhibiting lysyl oxidase activity (Figure 3.13A), and this reduction in PI3K and ERK signaling correlated with lower p^{397} FAK, p MLC, $\alpha 5$ integrin and FN expression *in vivo* (Figure 3.1B). I also observed that FN-ligation of $\alpha 5\beta 1$ integrin increased the levels and duration of epidermal growth factor receptor (EGFR) stimulated p^{473} Akt and $p^{202/204}$ ERK activity in both nonmalignant and tumorigenic MECs in culture¹³. Thus, FN-ligated, nonmalignant HMT-3522 S1 MECs expressing $\alpha 5$ integrin showed a three hundred percent increase in p^{473} Akt and a two hundred percent increase in $p^{202/204}$ ERK ninety minutes following EGF treatment, as compared to control cells expressing empty vector (Figure 3.13B left). Similarly, treating HMT-3522 T4-2 MECs plated on wildtype FN with a function-blocking antibody to $\alpha 5$ integrin significantly decreased p^{473} Akt and $p^{202/204}$ ERK activation in response to EGF stimulation (Figure 3.13B; right). Moreover, while S1 MECs cultured in 3D rBM gels doped with wildtype FN formed disorganized, invasive and non-polarized colonies, inhibition of PI3K, as well as EGFR or MEK (data now shown), activity reverted their phenotype to that exhibited by control nonmalignant MECs (Figure 3.13C; left panels) and significantly decreased colony size (Figure 3.13D; left). Treatment of T4-2 MECs with these same inhibitors also reverted their phenotype

to that exhibited by noninvasive, growth-arrested, polarized nonmalignant MECs (Figure 3.13C; right panels) and significantly decreased their colony size (Figure 3.12D; right). Importantly, the $\alpha 5\beta 1$ integrin-mediated increase in ERK and PI3 kinase signaling required ligation of the synergy site of FN because nonmalignant $\alpha 5\beta 1$ integrin expressing MCF10A MECs showed a profound and sustained increase in EGF-stimulated ERK and Akt activation only when the cells were attached to recombinant FN that contained a synergy site (Figure 3.12E).

I recently found that a force-stabilized vinculin-talin-actin-zyxin scaffolding complex facilitates PI3-kinase mediated conversion of phosphatidylinositol (3,4)-bisphosphate (PIP2) into phosphatidylinositol (3,4,5)-triphosphate (PIP3)¹⁵. I therefore asked whether the force-mediated stabilization of the vinculin-talin-actin-zyxin scaffolding complex by FN-ligation of $\alpha 5\beta 1$ integrin led to enrichment of PIP3 at adhesions. Consistently, more mKO2-PH-Grp1 (a PIP3 localization reporter¹⁵) was localized to the focal adhesions (indicated by vinculin mEmerald) in response to EGF in $\alpha 5\beta 1$ -overexpressing MCF10As, but only when they were ligated to a FN in which the synergy site was intact (Figure 3.13F). These findings demonstrate that the unique mechanical behavior of a FN-ligated $\alpha 5\beta 1$ integrin increases cell tension to stabilize a vinculin-talin-actin-zyxin scaffolding complex that promotes mammary malignancy by amplifying GFR signaling through PI3 kinase.

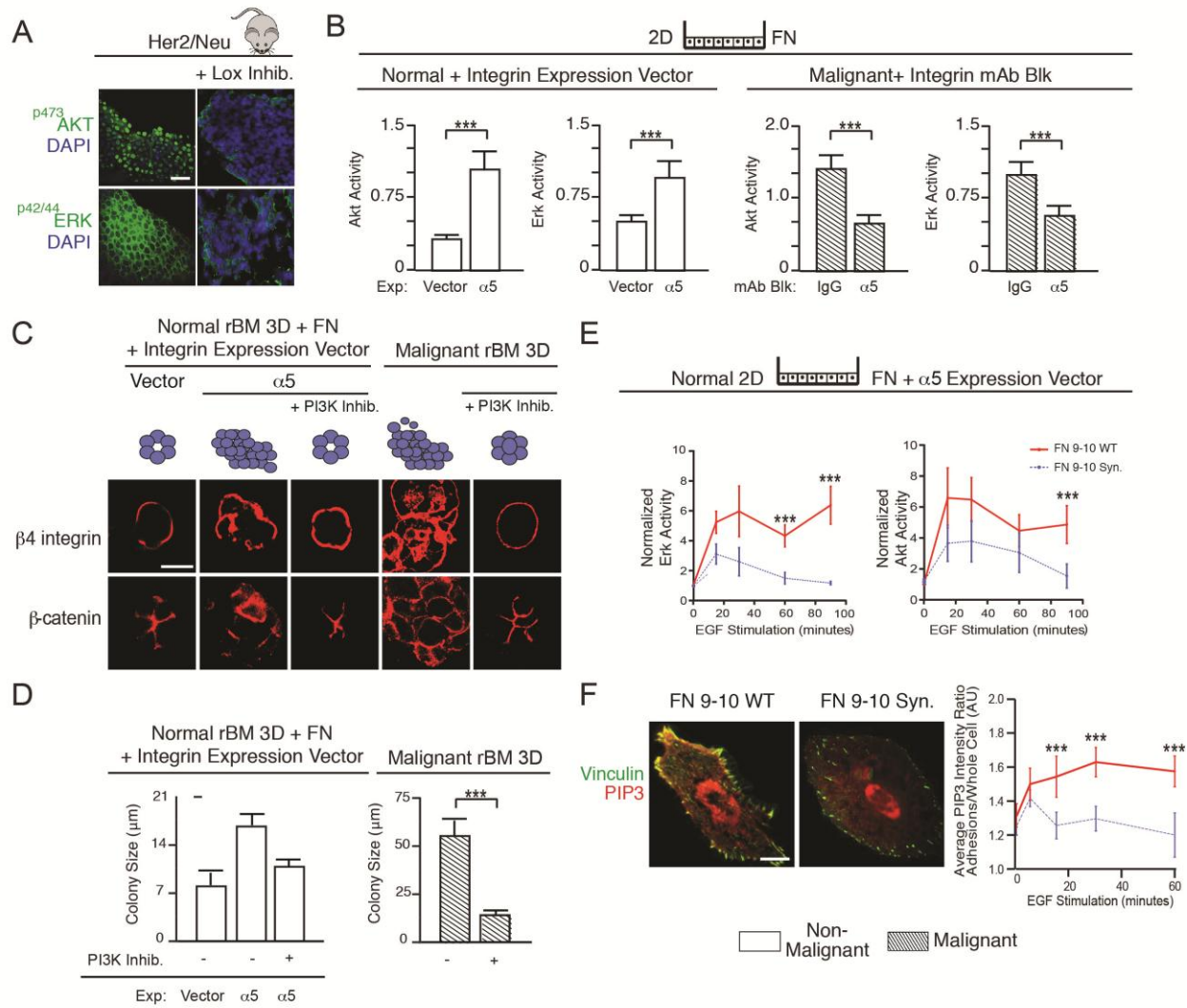


Figure 3.13 A) Tissue staining of Her2/Neu mice +/- LOX inhibition for p^{473} Akt, $p^{Thr202/pTyr204}$ ERK. Scale Bar 10 μ m. **B)** Bar graphs showing level of p^{473} Akt and $p^{Thr202/pTyr204}$ ERK normalized to total cellular Akt and ERK in control or $\alpha 5$ expressing non-malignant MECs and in malignant MECs treated with either IgG or a $\alpha 5$ blocking antibody. **C)** Images of organoids of non-malignant MECs +/- $\alpha 5$ and in malignant organoids +/- a PI3 kinase inhibitor. Scale Bar 10 μ m. **D)** Quantification of colony size in C. **E)** Line graphs showing time course of EGF stimulated $p^{Thr202/pTyr204}$ ERK and p^{473} Akt levels normalized to total ERK and Akt in MECs +/- $\alpha 5$ plated on wildtype (WT) or synergy site mutated (Syn) fibronectin. **F)** Confocal images of MECs + $\alpha 5$ plated on wildtype (WT) or synergy site mutated (Syn) fibronectin. Scale Bar 3 μ m. Line graphs showing time course of EGF-stimulated PIP3 recruited to focal adhesions. Measurements of all pixels in adhesions were averaged over whole cell. (** $p < 0.01$; *** $p < 0.001$).

Discussion

I determined that stiff mammary tumors express high levels of $\alpha 5\beta 1$ integrin and FN and that reducing tissue tension decreases these levels. Through a series of *in vitro* studies, I could show that when $\alpha 5\beta 1$ integrin is bound to a mechanically-primed FN, this ligation is able to promote malignant transformation through engagement of a zyxin-vinculin tension clutch that nucleates PIPs to potentiate PI3 kinase activation. Using 2D and 3D culture assays, a 3D tension bioreactor, and mouse models I showed that FN-ligated $\alpha 5\beta 1$ integrin, by virtue of its ability to enhance cell tension, is both necessary and sufficient for expression of the malignant phenotype of MECs *in vitro* and *in vivo*. My findings provide a plausible explanation for why $\alpha 5\beta 1$ integrin and its ligand FN are so frequently elevated in solid tumors, where interstitial pressure and tension are also elevated, and in contractile primary and metastatic cancer cell lines and tumor cells with high Rho and ROCK activity^{19,21,41,42}. My data are also consistent with prior results which showed that cancer cell lines expressing abundant FN, when sorted for high membrane $\alpha 5$ integrin levels, migrate faster and contract collagenous matrices to a greater extent²⁹ and studies showing that blocking the activity of RGD-binding receptors is critical for expression of the malignant phenotype of cultured breast cancer cells^{18,6,43}. Here, I not only identified $\alpha 5\beta 1$ integrin as the key the RGD receptor, but I also rigorously demonstrated that the ability of $\alpha 5\beta 1$ integrin to promote the malignant phenotype of MECs requires binding to both the RGD and synergy site of FN (Figure 3.13). Importantly, $\alpha 5\beta 1$ integrin exists in a relaxed state and requires tension to unfold the otherwise hidden synergy site on FN in order to full engage $\alpha 5\beta 1$ and induce downstream signaling through FAK^{44,45}. My data imply that collagen-mediated ECM stiffening likely promotes malignancy by fostering $\alpha 5\beta 1$ integrin binding to the

FN synergy site along stiff collagen fibrils that allow for the force-dependent exposure of the synergy site on FN molecules^{27,46,47}.

Tumors contain abundant quantities of type I collagen, and cross-linked, remodeled type I collagen contributes critically to the tensile strength of a tissue^{10,13}. Nevertheless, I failed to quantify differences in $\alpha 2$ integrin in either Her2/Neu mouse mammary tissue or in the 3D organotypic cultures of malignant MECs in which the tension had been reduced (Figure 3.1; Figure 3.12A). Instead, I established a relationship between cell tension and ECM stiffness and elevated expression of the FN receptor $\alpha 5\beta 1$ integrin in mouse mammary tissue and mammary organoids. I determined that MECs with FN-ligated $\alpha 5\beta 1$ integrin, but not collagen I-ligated $\alpha 2\beta 1$, exerted higher traction forces and were able to contract collagen gels more (Figure 3.9). My data are consistent with prior studies suggesting that $\alpha 2\beta 1$ integrin represses expression of the malignant phenotype of MECs in culture and is a tumor suppressor in the mammary gland *in vivo*¹⁴ and recent data indicating that $\alpha 2\beta 1$ integrin activates FAK by a force-independent mechanism. Interestingly, FN and collagen are often secreted and processed in tandem, and a FN matrix can serve as a scaffold to guide collagen assembly⁴⁸. Indeed, just as FN deposition and unfolding requires a collagen scaffold, collagen assembly and remodeling require FN⁴⁹, during which time FN can be crosslinked to collagen⁴⁸⁻⁵⁰. FN fibril assembly and collagen-remodeling form a feedback loop, with collagen-mediated ECM stiffness and cell contractility inducing conformational changes in FN that reveal hidden binding sites required for FN matrix assembly, which then further facilitate collagen remodeling. Thus, my data are consistent with a paradigm where the highly crosslinked collagen form the scaffold upon which a FN meshwork is laid. This stiffened ECM, by virtue of its ability to modify FN, would then drive malignancy by

permitting $\alpha 5\beta 1$ integrin binding to enhance tension-dependent signaling in tumors. Nevertheless, it is also feasible that FN bound $\alpha 5\beta 1$ integrin could collaborate with other transmembrane collagen receptors such as the discoidin receptor (DDR) or syndecans to foster malignant progression, particularly since DDRs are also tension regulated⁴⁴.

PI3 kinase (PI3K) and ERK regulate cell growth, survival and invasion, and the levels and activity of these kinases are frequently elevated in tumors^{31,32,51}. Accordingly, an assortment of pharmacological inhibitors has been developed to target these kinases and their associated signaling molecules to treat (and cure) various cancers with varying degrees of clinical success⁵¹. Here, I determined that while the Her2/Neu tumors, which are surrounded by a stiffened ECM, have elevated ERK and PI3K activity as expected, that merely preventing collagen crosslinking and stiffening by inhibiting Lox activity significantly reduced both ERK and Akt activity, and did so in tandem with a reduction in $\alpha 5$ integrin and FN. I also observed that that MECs with $\alpha 5\beta 1$ integrin ligated by a wild-type, but not a synergy-site mutated FN, nucleated more vinculin-talin-actin-zyxin scaffolds and recruited more PIP3 to amplify EGF-dependent activation of Akt and ERK. Inhibiting PI3K or ERK repressed the malignant behavior of FN-ligated mammary MEC 3D tissue-like structures expressing elevated $\alpha 5\beta 1$ integrin. My findings thereby revealed how mechanical signals from stiffened tumor stroma or elevated cancer cell contractility can amplify oncogenic signaling by modifying GFR signaling via ligation of $\alpha 5\beta 1$ integrin by the FN synergy site. The data thereby provide one plausible explanation for why in some instances targeted molecular therapies are less effective and suggest that combinatorial treatments that target both the mechanical properties of the cell or tissue and specific oncogenic signaling pathways might prove to be a better therapeutic option. My findings are

therefore clinically relevant, as they identify a tumor-specific mechanical signature, since the synergy site is only engaged in a high-force environment, such as that of a tumor. Thus, inhibiting the ability of $\alpha 5\beta 1$ integrin to ligate the synergy site of fibronectin could prove to be a potent cancer-specific therapy⁴⁵. And since ECM mechanics and mechanotransduction are necessary for progression to malignancy but cannot be targeted directly in patients, targeting the pathways that are critical for mechanosensing and mechanotransduction, in addition to targeting relevant oncogenic pathways, might prove to be tractable therapeutic approaches with which to treat cancer. The data also suggest that strategies to detect the FN synergy site in tumor biopsies might be useful biomarkers to identify patients with potential kinase treatment resistance⁵².

Materials and Methods

Cell culture

Phenotypic reversion of T4-2 cells was as described⁸. To inhibit integrin function the 3D multicellular structures were pre-incubated with anti- $\alpha 2$, $\alpha 5$, or αv integrin-blocking antibodies or IgG isotype matched control mAb (20 μ g/ml). Colony size and morphology were measured after 10-12 days in culture. Adult human dermal microvascular endothelial cells (HDMVECs) were grown on collagen type I-coated flasks (Collaborative Biomedical) in EGM-2 bullet kit media (Bio-Whitaker). Angiogenesis induction by MECs was assayed by co-culturing 3D rBM generated mammary organoids in cell culture inserts (0.45 μ m pore size; Biocoat, BD Labware) with HDMVECs that had been overlaid with a 1-mm-layer of acellular collagen type I (BD Pharmingen). HDMECs invasion through the collagen overlay and network formation was assessed after 2 days by staining with toluidine blue. Anchorage-independent growth was assessed using a soft agar assay⁵³. Briefly, 20,000 cells in 1.0 ml 0.35% agarose with or without integrin blocking antibodies, as indicated, were overlaid with 1.0 ml 0.5% agarose containing 1X growth media, and colonies larger than 40 μ m in diameter were scored positive after 21 days.

Cell and Tissue Staining

3D rBM gels, as well as tissue sections, were prepared by mixing cultures with fresh collagen following embedment and freezing in sucrose with Tissue-Tek OCT compound (Miles Laboratories), then sectioned in 10-20 μ m thick slices for analysis. All samples were incubated with primary mAbs followed directly by either FITC-, Texas red-, or AlexaFluor- conjugated secondary Abs. Nuclei were counterstained with diaminophenyl- indole (Sigma). Images were

compared and quantified based on fluorescence intensity signal following minimal thresholding to subtract background. For mouse studies, when mice were sacrificed, lesions were photographed, dissected, measured, macroscopically analyzed, fixed in 4% paraformaldehyde, and paraffin embedded. H&E sections were evaluated for histopathological evidence of tumor phenotype and tissue sections were analyzed by immunofluorescence as described.

Image Acquisition & Microscopy Setup

All immunofluorescence images were recorded at 20-120X magnification and conventional images were recorded at 40-60X magnification. FRET images were acquired using a 60X WI 1.2NA Plan Apo objective.

Immunofluorescence and FRET images were acquired using an Olympus IX81 Epifluorescence microscope with Spot color CCD camera, Nikon TE2000-U inverted microscope, Bio-Rad MRC 1024 laser scanning confocal microscope attached to a Nikon Diaphot 200 microscope, and a spinning disc/TIRF microscope setup with Andor's iXon3 EMCCD camera with the Yokogawa CSU-X1 confocal scanner, a Nikon TIRF illuminator, and a MOSAIC module for FRAP and photo-activation on a motorized Nikon Ti-E inverted microscope base.

Flow Cytometry

Cells were isolated, blocked with 1% bovine serum albumin in PBS for 60 minutes, incubated with saturating concentrations of primary mAb for 60 minutes, washed three times, and labeled with FITC- or Phycoerythrin-conjugated goat IgG (Millipore). Stained cells were washed three

times and immediately analyzed on a FACScan (BD Pharmingen). All manipulations were conducted at 4°C.

PIP3 localization analysis

Stable lines of MCF10A cells expressing tagged- $\alpha 5$ integrin and transiently transfected with vinculin-mEmerald and KO2-PH-Grp1 (a fluorescent PIP3 probe courtesy Keith Mostov) were plated on recombinant FN 9-10 or recombinant FN 9-10 with the synergy site mutants. Images were quantified by creating a mask for areas of cell-ECM adhesion based on the vinculin-mEmerald signal. PIP3-probe fluorescence intensity in masked areas was then compared with that in the whole cell to evaluate enrichment of PIP3 at focal adhesions.

Mouse Studies

Starting at 5 months of age, mice were treated with BAPN (3mg/kg; Spectrum) in the drinking water or a Lox function-blocking polyclonal antibody (3mg/kg; OpenBiosystems) injected intraperitoneally twice per week¹³. Mice were sacrificed at 7-8 months of age, at which time the 4th mammary gland was paraformaldehyde fixed; paraffin sections were analyzed for histology and parallel sections were stained as described. Four week-old BalbC nu/nu mice were subcutaneously injected in the rear flanks (5E6 cells/injection, together with Matrigel with or without addition of function-blocking antibody or IgG isotype control), and palpable lesions were detected, measured, and monitored biweekly for 2 months (Instant read-out digital calipers; Electron Microscopy Sciences).

Retroviral and lentiviral infections and vectors

Standard retroviral and lentiviral infection procedures were utilized. For detailed description of lentiviral and retroviral constructs and vectors, please refer to the Appendix 4.

Western and ELISA Procedures

Equal amounts of cell protein lysate (either RIPA or Laemmli lysate; BCA; Pierce) were separated on reducing SDS-PAGE gels, transferred to nitrocellulose or PVDF membranes, and probed with primary antibody. Bands were visualized and quantified using a Fujifilm Gel Documentation system, in combination with HRP-conjugated secondary antibodies and ECL-Plus system (Amersham Pharmacia). Specific activity for Akt and Erk was calculated by normalizing densitometric values of phosphorylated to total AKT or ERK and E-cadherin. Integrin protein levels were assessed using non-reducing SDS-PAGE gels. VEGF, Il-8 and bFGF levels in the media of 10-12 day three dimensional rBM cultures of MECs were measured using sandwich ELISA (R&D systems), according to the manufacturer's instructions. O.D. measurements were performed using a Fluoroskan Ascent FL (Labsystems).

RT-PCR analysis

Random-primed cDNA was prepared from total isolated RNA using Trizol reagent (Invitrogen) and target cDNA sequences were quantified via real-time PCR using SYBR Green I reagent (Roche) according to the manufacturer's protocol. Eppendorf Realplex2 quantitative PCR machine was used for all studies. Please refer to Appendix 3 for primer sequences.

Cell contractility, migration, and durotaxis assays

Collagen gel contraction was measured by imaging projected gel areas of cell-embedded collagen gels as described previously¹⁹. Traction force microscopy studies were performed as described by Dr. Dembo and colleagues and processed using LIBTRC-2.0 software¹⁹. For durotaxis studies, brightfield images were captured every 5 minutes over 12 hours using gradient stiffness polyacrylamide gel⁵⁴. Cell migration time course images were compiled and cell speed, persistence, distance, and directionality were analyzed on a single cell basis with Image J. (NIH) and the Chemotaxis plugin. 3D collagen gel invasion assays were performed as previously described.³⁸

Substrate Preparation

ECM-crosslinked PA gels were prepared and mechanically analyzed as described; single stiffness substrates⁵⁵ and mechanically gradient substrates⁵⁶. Briefly, two droplets, each containing 12.5 μ l of a soft (100 Pa) or stiff (60,000 Pa) acrylamide/bis-acrylamide mixture, are placed adjacent to each other on a large hydrophobic coverglass (no. 1, 45 mm \times 50 mm; Fisher Scientific) and then covered with a small circular activated coverglass (no. 1, 18-mm diameter; Fisher Scientific) to merge the drops. By carefully maintaining the interface, a uniform gradient of 3.33Pa/ μ m along the length of substrate is achieved. Regions of different rigidities were distinguished by using a fluorescently labeled bis-acrylamide in the stiff solution creating a gradient of fluorescence correlated with the mechanical gradient.

Substrate elastic modulus was measured via atomic force microscopy (Asylum Research) using the Hertz model⁵⁷. Briefly, a silicon beaded tip cantilever (5µm diameter, 0.07 N/m, silicon nitride) was used to measure 90 µm by 90 µm elastic modulus maps down the length of the gel along the mechanical gradient while simultaneously measuring fluorescence intensity with a inverted epi-fluorescence microscope. I used these measurements to assess the mechanical gradient and also develop an algorithm for determining the elastic modulus of the gel from solely the fluorescent intensity. This model allowed me to determine the particular surface stiffness seeded cells were adhered to when tracking cell motility.

Adhesion strength

Preparation of adhesive ligands: the previously described Promega Pinpoint vector containing the sequence for a fragment spanning the 7th to 10th type III repeat of human fibronectin (FN7-10)⁵⁸ was cut with NruI and ligated to yield an expression vector for a fragment spanning the 9th to 10th type III repeat of human fibronectin (FN9-10). The synergy site mutant PHSAN (FN9-10(PHSAN)) was generated using the Stratagene QuikChange Site Directed Mutagenesis kit and primers 5'-GGGTGCCCCACTCTGCGAATTCATCACCC-3' (forward) and 5'-GGGTGATGGAATTCGCAGAGTGGGGCACCC-3' (reverse). Constructs were verified by DNA sequencing. Proteins were expressed in JM109 cells (Promega) in the presence of d-biotin and purified by affinity chromatography⁵⁸. Protein concentration and purity were confirmed by Western blotting and Coomassie blue staining. The GFOGER collagen-mimetic peptide was synthesized as previously described⁵⁹.

Preparation of micropatterned substrates: micropatterned substrates were generated by microcontact printing of self-assembled monolayers of alkanethiols on gold⁶⁰ using a PDMS stamp (Sylgard 184/186 elastomer kit) with circular patterns (10 μm diameter circles, 75 μm center to center spacing). Arrays of methyl-terminated alkanethiol [$\text{HS}-(\text{CH}_2)_{11}-\text{CH}_3$; Sigma] circles were stamped onto Au-coated glass coverslips. The remaining exposed areas were functionalized with a tri(ethylene glycol)-terminated alkanethiol [$\text{HS}-(\text{CH}_2)_{11}-(\text{CH}_2\text{CH}_2\text{O})_3-\text{OH}$; ProChimia Surfaces] to generate a cell adhesive-resistant background. Patterned substrates were coated with purified adhesive ligands (20 $\mu\text{g}/\text{ml}$), blocked with 1% heat-denatured bovine serum albumin, incubated in PBS ($\text{Ca}^{2+}/\text{Mg}^{2+}$), then seeded with cells at a density of 210 cells/ mm^2 and incubated for 16 hours at 37°C.

Cell adhesion assay description: cell adhesion to fibronectin-coated islands was measured using a hydrodynamic spinning disk system. Micropatterned substrates with adherent cells were spun in PBS supplemented with 2 mM dextrose for 5 min at constant speeds. The applied shear stress (τ) is given by the formula $\tau = 0.8r(\rho\mu\omega^3)^{1/2}$, where r is the radial position and ρ , μ and ω are the fluid density, viscosity and rotational speed respectively. After spinning, cells were fixed in 3.7% formaldehyde, permeabilized in 1% Triton X-100, stained with ethidium homodimer-1 (Invitrogen). Adherent cells were counted at specific radial positions using a 10X objective lens in a Nikon TE300 microscope equipped with a Ludl motorized stage, Spot-RT camera and an Image-Pro analysis system. A total of 61 fields (80–100 cells per field before spinning) were analyzed and cell counts were normalized to the number of cell counts at the center of the disk. The fraction of adherent cells (f) as a function of shear stress τ (force/area) was then fitted to a sigmoid curve $f = f_0/[1 + \exp[b(\tau - \tau_{50})]]$, where τ_{50} is the shear stress for 50% detachment, b is

the inflection slope, and f_0 is the y-intercept. τ_{50} represents the mean adhesion strength for the cell population.

Vinculin tension sensor and FRET

FRET images were collected and analyzed as previously described⁶¹. Briefly, images were background subtracted and adjusted for spectral bleed through. Relative FRET index was calculated by taking the ratio of pixel intensity in the FRET image (donor excitation and acceptor emission) to pixel intensity in the donor image (donor excitation and emission). Average cell FRET index was calculated for each cell in a sample of 25-30 cells. Cell averages were then used to calculate a sample average, which was then used in student t-tests to evaluate whether the sampled populations had different means.

Statistical Analysis

Statistical analysis was performed using Prism/GraphPad Software (La Jolla, CA) at indicated p-values. Unless otherwise stated, two-tailed Student's t-tests were used for significance testing. Means were presented as +/- s.e.m of at least three independent experiments. Unless otherwise noted, sample size, n, was n=3 and statistical significance was considered at p<0.05. Adhesion strength values were specifically analyzed via ANOVA and Tukey's post-hoc test with a p-value < 0.05 considered significant.

Acknowledgements

I thank H.P. Erickson for fibronectin mutants [70], K. Mostov for the fluorescent PIP3 probe [37], M.J Paszek for lentiviral α V and α 5 expression constructs, and M. Dembo for the LIBTRC 2.0 traction force software. This work was supported by NIH grants R01CA138818-01A1 (VMW), 2R01CA085482-11A1 (H Moses and VMW); U54CA143836-01 (J Liphardt and VMW); U01 ES019458-01 (Z Werb and VMW); U54CA163155-01 (G Berger and VMW), DOD BCRP grants W81XWH-05-1-0330 and BC122990 (VMW); NSF GRFP 1144247 and NIH/NCI F31CA180422 (YAM) and NSF GRFP 1106400 (GO); NIH R01 GM065918 (AJG).

Works Cited

1. Samani, A., Zubovits, J. & Plewes, D. Elastic moduli of normal and pathological human breast tissues: an inversion-technique-based investigation of 169 samples. *Phys. Med. Biol.* **52**, 1565–76 (2007).
2. Nakagawa, H. *et al.* Loss of liver E-cadherin induces sclerosing cholangitis and promotes carcinogenesis. *Proc. Natl. Acad. Sci. U. S. A.* 2–7 (2014). doi:10.1073/pnas.1322731111
3. Venkatesh, S. K. *et al.* MR elastography of liver tumors: preliminary results. *AJR. Am. J. Roentgenol.* **190**, 1534–40 (2008).
4. Shimosato, Y. *et al.* Prognostic implications of fibrotic focus (scar) in small peripheral lung cancers. *Am. J. Surg. Pathol.* **4**, 365–373 (1980).
5. Ioachim, E. *et al.* Immunohistochemical expression of extracellular matrix components tenascin, fibronectin, collagen type IV and laminin in breast cancer: their prognostic value and role in tumour invasion and progression. *Eur. J. Cancer* **38**, 2362–2370 (2002).
6. Nam, J.-M., Onodera, Y., Bissell, M. J. & Park, C. C. Breast cancer cells in three-dimensional culture display an enhanced radioresponse after coordinate targeting of integrin alpha5beta1 and fibronectin. *Cancer Res.* **70**, 5238–48 (2010).
7. Nimwegen, M. J. Van, Verkoeijen, S., Buren, L. Van, Burg, D. & Water, B. Van De. Requirement for Focal Adhesion Kinase in the Early Phase of Mammary Adenocarcinoma

- Lung Metastasis Formation Mammary Adenocarcinoma Lung Metastasis Formation.
4698–4706 (2005).
8. Weaver, V. M. *et al.* Reversion of the malignant phenotype of human breast cells in three-dimensional culture and in vivo by integrin blocking antibodies. *J. Cell Biol.* **137**, 231–45 (1997).
 9. Plodinec, M. *et al.* The nanomechanical signature of breast cancer. *Nat. Nanotechnol.* **7**, 757–65 (2012).
 10. Lopez, J. I., Kang, I., You, W.-K., McDonald, D. M. & Weaver, V. M. In situ force mapping of mammary gland transformation. *Integr. Biol. (Camb)*. **3**, 910–21 (2011).
 11. Heldin, C.-H., Rubin, K., Pietras, K. & Ostman, A. High interstitial fluid pressure - an obstacle in cancer therapy. *Nat. Rev. Cancer* **4**, 806–13 (2004).
 12. Ewald, A. J., Werb, Z. & Egeblad, M. Dynamic, long-term in vivo imaging of tumor-stroma interactions in mouse models of breast cancer using spinning-disk confocal microscopy. *Cold Spring Harb. Protoc.* **2011**, pdb.top97 (2011).
 13. Levental, K. R. *et al.* Matrix crosslinking forces tumor progression by enhancing integrin signaling. *Cell* **139**, 891–906 (2009).
 14. Maschler, S. *et al.* Tumor cell invasiveness correlates with changes in integrin expression and localization. *Oncogene* **24**, 2032–41 (2005).

15. Rubashkin, M. G. *et al.* Force engages vinculin and promotes tumor progression by enhancing PI3K activation of phosphatidylinositol (3,4,5)-triphosphate. *Cancer Res.* **74**, 4597–611 (2014).
16. Yao, E. S. *et al.* Increased beta1 integrin is associated with decreased survival in invasive breast cancer. *Cancer Res.* **67**, 659–64 (2007).
17. Stoeltzing, O. *et al.* Inhibition of integrin alpha5beta1 function with a small peptide (ATN-161) plus continuous 5-FU infusion reduces colorectal liver metastases and improves survival in mice. *Int. J. Cancer* **104**, 496–503 (2003).
18. Park, C. C. *et al.* Beta1 integrin inhibitory antibody induces apoptosis of breast cancer cells, inhibits growth, and distinguishes malignant from normal phenotype in three dimensional cultures and in vivo. *Cancer Res.* **66**, 1526–35 (2006).
19. Paszek, M. J. *et al.* Tensional homeostasis and the malignant phenotype. *Cancer Cell* **8**, 241–54 (2005).
20. Ulrich, T. a, de Juan Pardo, E. M. & Kumar, S. The mechanical rigidity of the extracellular matrix regulates the structure, motility, and proliferation of glioma cells. *Cancer Res.* **69**, 4167–74 (2009).
21. Samuel, M. S. *et al.* Actomyosin-mediated cellular tension drives increased tissue stiffness and β -catenin activation to induce epidermal hyperplasia and tumor growth. *Cancer Cell* **19**, 776–91 (2011).

22. Kaplan, R. N. *et al.* VEGFR1-positive haematopoietic bone marrow progenitors initiate the pre-metastatic niche. *Nature* **438**, 820–7 (2005).
23. Quail, D. F. & Joyce, J. A. Microenvironmental regulation of tumor progression and metastasis. *Nat. Med.* **19**, 1423–37 (2013).
24. Liu, D., Aguirre Ghiso, J., Estrada, Y. & Ossowski, L. EGFR is a transducer of the urokinase receptor initiated signal that is required for in vivo growth of a human carcinoma. *Cancer Cell* **1**, 445–57 (2002).
25. Dingemans, A.-M. C. *et al.* Integrin expression profiling identifies integrin alpha5 and beta1 as prognostic factors in early stage non-small cell lung cancer. *Mol. Cancer* **9**, 152 (2010).
26. Huang, S. & Ingber, D. E. Cell tension, matrix mechanics, and cancer development. *Cancer Cell* **8**, 175–6 (2005).
27. Baneyx, G., Baugh, L. & Vogel, V. Fibronectin extension and unfolding within cell matrix fibrils controlled by cytoskeletal tension. **2002**, (2002).
28. Vogel, V. & Sheetz, M. Local force and geometry sensing regulate cell functions. *Nat. Rev. Mol. Cell Biol.* **7**, 265–75 (2006).
29. Mierke, C. T., Frey, B., Fellner, M., Herrmann, M. & Fabry, B. Integrin $\alpha 5\beta 1$ facilitates cancer cell invasion through enhanced contractile forces. *J. Cell Sci.* **124**, 369–83 (2011).

30. García, A. J., Huber, F. & Boettiger, D. Force required to break alpha5beta1 integrin-fibronectin bonds in intact adherent cells is sensitive to integrin activation state. *J. Biol. Chem.* **273**, 10988–93 (1998).
31. Weber, G. *et al.* Roles of the RAF/MEK/ERK and PI3K/PTEN/AKT pathways in malignant transformation and drug resistance. *Adv. Enzyme Regul.* **46**, 249–279 (2006).
32. Wong, K.-K., Engelman, J. A. & Cantley, L. C. Targeting the PI3K signaling pathway in cancer. *Curr. Opin. Genet. Dev.* **20**, 87–90 (2010).
33. Guo, W. & Giancotti, F. G. Integrin signalling during tumour progression. *Nat. Rev. Mol. Cell Biol.* **5**, 816–26 (2004).
34. Yeung, T. *et al.* Effects of substrate stiffness on cell morphology, cytoskeletal structure, and adhesion. *Cell Motil. Cytoskeleton* **60**, 24–34 (2005).
35. Desgrosellier, J. S. & Cheresch, D. a. Integrins in cancer: biological implications and therapeutic opportunities. *Nat. Rev. Cancer* **10**, 9–22 (2010).
36. Zutriner, M. M., Santoro, S. A., Staats, W. D. & Tsung, Y. L. Re-expression of the 02131 integrin abrogates the malignant phenotype of breast carcinoma cells. **92**, 7411–7415 (1995).
37. Briand, P., Petersen, O. W. & Deurs, B. A new diploid nontumorigenic human breast epithelial cell line isolated and propagated in chemically defined medium. *Vitr. Cell. Dev. Biol.* **23**, 181–188 (1987).

38. Cassereau, L., Miroshnikova, Y., Ou, G., Lakins, J. & Weaver, V. M. A 3D tension bioreactor platform to study the interplay between ECM stiffness and tumor phenotype. *J. Biotechnol.* **193**, 66–69 (2014).
39. Dupont, S. *et al.* Role of YAP/TAZ in mechanotransduction. *Nature* **474**, 179–183 (2011).
40. Kong, F., García, A. J., Mould, a P., Humphries, M. J. & Zhu, C. Demonstration of catch bonds between an integrin and its ligand. *J. Cell Biol.* **185**, 1275–84 (2009).
41. Bachman, H., Nicosia, J., Dysart, M. & Barker, T. H. Utilizing Fibronectin Integrin-Binding Specificity to Control Cellular Responses. *Adv. wound care* **4**, 501–511 (2015).
42. Cao, L. *et al.* Phage-based molecular probes that discriminate force-induced structural states of fibronectin in vivo. *Proc. Natl. Acad. Sci. U. S. A.* **109**, 7251–6 (2012).
43. Martin-Belmonte, F. *et al.* PTEN-mediated apical segregation of phosphoinositides controls epithelial morphogenesis through Cdc42. *Cell* **128**, 383–97 (2007).
44. Seong, J. *et al.* Distinct biophysical mechanisms of focal adhesion kinase mechanoactivation by different extracellular matrix proteins. *Proc Natl Acad Sci U S A* **110**, 19372–19377 (2013).
45. Friedland, J. C., Lee, M. H. & Boettiger, D. Mechanically activated integrin switch controls alpha5beta1 function. *Science* **323**, 642–4 (2009).

46. Martino, M. M. *et al.* Controlling integrin specificity and stem cell differentiation in 2-D and 3-D environments through regulation of fibronectin domain stability. **30**, 1089–1097 (2010).
47. Barker, T. H. *et al.* SPARC regulates extracellular matrix organization through its modulation of integrin-linked kinase activity. *J. Biol. Chem.* **280**, 36483–93 (2005).
48. Kadler, K. E., Hill, A. & Canty-Laird, E. G. Collagen fibrillogenesis: fibronectin, integrins, and minor collagens as organizers and nucleators. *Curr. Opin. Cell Biol.* **20**, 495–501 (2008).
49. Mosher, D. F. Cross-linking of fibronectin to collagenous proteins. *Mol. Cell. Biochem.* **58**, 63–68 (1984).
50. Singh, P., Carraher, C. & Schwarzbauer, J. E. Assembly of fibronectin extracellular matrix. *Annu. Rev. Cell Dev. Biol.* **26**, 397–419 (2010).
51. Engelman, J. A. Targeting PI3K signalling in cancer: opportunities, challenges and limitations. *Nat. Rev. Cancer* **9**, 550–62 (2009).
52. Redick, S. D., Settles, D. L., Briscoe, G. & Erickson, H. P. Defining Fibronectin ' s Cell Adhesion Synergy Site by Site-directed Mutagenesis. **149**, 521–527 (2000).
53. Gilbert, P. M. *et al.* HOXA9 regulates BRCA1 expression to modulate human breast tumor phenotype. *J. Clin. Invest.* **120**, 1535–50 (2010).

54. Isenberg, B. C., Dimilla, P. A., Walker, M., Kim, S. & Wong, J. Y. Vascular smooth muscle cell durotaxis depends on substrate stiffness gradient strength. *Biophys. J.* **97**, 1313–22 (2009).
55. Reinhart-King, C. A., Dembo, M. & Hammer, D. A. Endothelial Cell Traction Forces on RGD-Derivatized Polyacrylamide Substrata †. *Langmuir* **19**, 1573–1579 (2003).
56. Lo, C.-M., Wang, H.-B., Dembo, M. & Wang, Y. Cell Movement Is Guided by the Rigidity of the Substrate. *Biophys. J.* **79**, 144–152 (2000).
57. Radmacher, M., Tillamnn, R., Fritz, M. & Gaub, H. From molecules to cells: imaging soft samples with the atomic force microscope. *Science (80-.).* **257**, 1900–1905 (1992).
58. Petrie, T. A., Capadona, J. R., Reyes, C. D. & García, A. J. Integrin specificity and enhanced cellular activities associated with surfaces presenting a recombinant fibronectin fragment compared to RGD supports. *Biomaterials* **27**, 5459–70 (2006).
59. Reyes, C. D. & García, A. J. Engineering integrin-specific surfaces with a triple-helical collagen-mimetic peptide. *J. Biomed. Mater. Res. A* **65**, 511–23 (2003).
60. Gallant, N. D., Michael, K. E. & García, A. J. Cell adhesion strengthening: contributions of adhesive area, integrin binding, and focal adhesion assembly. *Mol. Biol. Cell* **16**, 4329–40 (2005).

61. Graham, D. L., Lowe, P. N. & Chalk, P. A. A method to measure the interaction of Rac/Cdc42 with their binding partners using fluorescence resonance energy transfer between mutants of green fluorescent protein. *Anal. Biochem.* **296**, 208–17 (2001).

Chapter 4: Altered Tumor Cell Metabolism is Correlated with Breast Cancer Metastasis and Dependent on ECM Stiffness and Integrin Signaling.

Luke Cassereau^{1,2}

In collaboration with: Janna Mouw¹, Matthew Barnes¹, Ori Maller¹ Johnathon Lakins¹

Under the supervision of: Valerie M Weaver^{1,3,4,5}

¹Center for Bioengineering and Tissue Regeneration, Department of Surgery, UCSF, San Francisco, California, USA.

²University of California San Francisco/University of California Berkeley Joint Graduate Group in Bioengineering, San Francisco, CA, USA.

³Department of Anatomy, and Department of Bioengineering and Therapeutic Sciences, UCSF, San Francisco, California, USA.

⁴Eli and Edythe Broad Center of Regeneration Medicine and Stem Cell Research, UCSF, San Francisco, California, USA.

⁵UCSF Helen Diller Comprehensive Cancer Center, UCSF, San Francisco, California, USA.

Abstract:

Tumors exhibit altered cellular metabolism supportive of continuous cell growth. Nevertheless, the fundamental molecular mechanisms through which altered metabolism regulates tumor behavior remain unclear. Our lab previously demonstrated that elevated ECM stiffness and epithelial cell tension drive squamous carcinoma and mammary transformation. We further identified integrin signaling as a key conduit of ECM mechanical cues and a potent regulator of pro-tumorigenic signaling. I hypothesized that elevated ECM stiffness alters cell metabolism through integrin signaling mediated pro-tumorigenic signaling to drive tumor metastasis. To test this hypothesis, I profiled metabolic markers using a combination of, quantitative RT-PCR, immunoblotting and immunofluorescence of MMTV-PyMT transgenic tumors (\pm ECM crosslinking) and breast tumor mammary epithelial cells grown on tunable hydrogel substrates *in vitro*. I then used pharmacological inhibitors targeting glycolysis or metabolic adaptation to assess the interplay between ECM stiffness, metabolism and tumor cell behavior, including invasion, migration, and proliferation. My data suggest that ECM stiffening induces tumor cell glycolysis downstream of integrin signaling by targeting key regulators of glycolysis such as the glucose and lactate transporters and lactate dehydrogenase. Additionally, inhibitors of metabolism abrogated tumor cell proliferation and invasion *in vitro* and tumor growth, EMT, and metastasis *in vivo*. My data therefore suggest that elevated ECM stiffness may regulate tumor aggression in part by modulating tumor cell metabolism. Additional studies are underway to further clarify how ECM-driven metabolic dysregulation drives tumor behavior

Introduction:

Breast cancer development and malignant progression is associated with profound tissue extracellular matrix (ECM) remodeling and stiffening¹⁻⁷. Critically, previous work in our lab and others has demonstrated that physical changes to the ECM is a potent drive of tumor malignant phenotype and metastasis *in vivo*⁸⁻¹⁵. In particular, integrin focal adhesions have been implicated as essential signaling complexes in controlling cell response to altered ECM mechanics and driving tumor cell invasion and motility in support of tumor cell malignant phenotype and metastasis^{5,11,12,16-21}. Consistently, previous work by our lab and others and in Chapter 3 of this thesis, enhanced integrin signaling mediated by ECM stiffness has been shown to directly alter pro-tumorigenic signaling, specifically potentiating Akt and Erk signaling intensity and duration (Figure 3.13)^{11,12}. Building on this data, I next aimed to explore the further downstream effects of integrin signaling and how this contributes to tumor cell malignant phenotype.

Importantly, Akt and Erk signaling have both been implicated as key regulators of cell metabolism²²⁻²⁷. Moreover, previous work in our lab has also implicated ECM stiffness and integrin signaling as regulating MYC activity, another essential metabolic regulator, to drive tumor metastasis²⁸. To expand on these observations, I aimed to explore the role of ECM stiffness and integrin signaling in regulating tumor cell metabolism and to determine the role of cell metabolism in tumor aggression and metastasis.

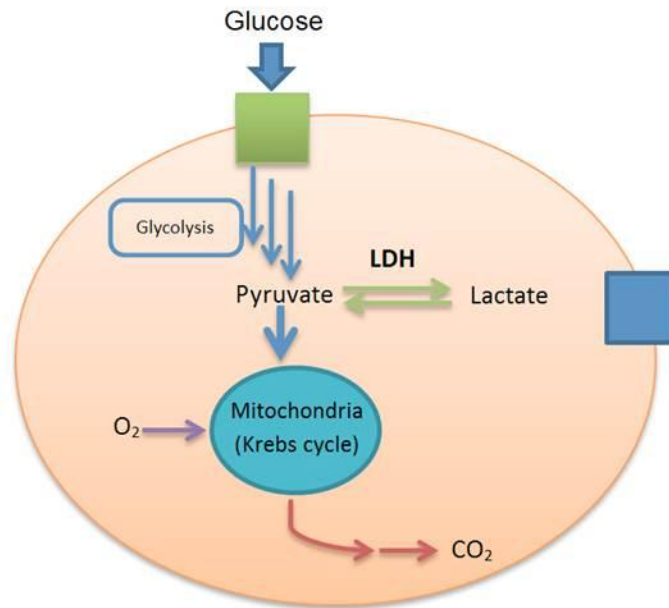
Critically, tumor cell metabolism has been shown to have an effect on several key tumor cell behaviors such as proliferation, drug resistance, invasion, motility, and ECM remodeling^{27,29-37}. Consistently, several key metabolic regulators, Glut1 (glucose transport),

MCT1 (lactate transport), LDHA (lactic acid fermentation), PKM2 (biogenesis), and Ca9 (pH regulation) have been associated with poor clinical outcomes in multiple tumor indications³⁸⁻⁴⁰. Yet, the underlying mechanisms of how and when tumor cell metabolism is altered and its specific role in tumor malignant progression is not fully understood.

When considering breast cancer specifically, the metabolic changes closely follow the Warburg Effect (Figure 4.1). Specifically, breast carcinomas have been seen to up regulate glucose transport into the cell, glycolysis, and to use the abundant pyruvate generated for lactic acid fermentation as opposed to oxidative phosphorylation in the mitochondria^{24,29,41}. However how tumor cells switch to this type of metabolism and how this aberrant metabolism contributes to tumor cell malignant phenotype remains unclear.

This is complicated by multiple signaling mechanisms having overlapping impacts on cell metabolism, with AKT, MYC, Hif1a, and mTor all having regulating cell metabolic state^{24,35,37,41-43} (Figure 4.2). This emphasizes the clear importance of cell metabolism as there exist many redundant mechanisms, which control it, as well as the potential impact of a stimulus that could alter many of these pathways simultaneously.

Normal Cell



Cancer Cell

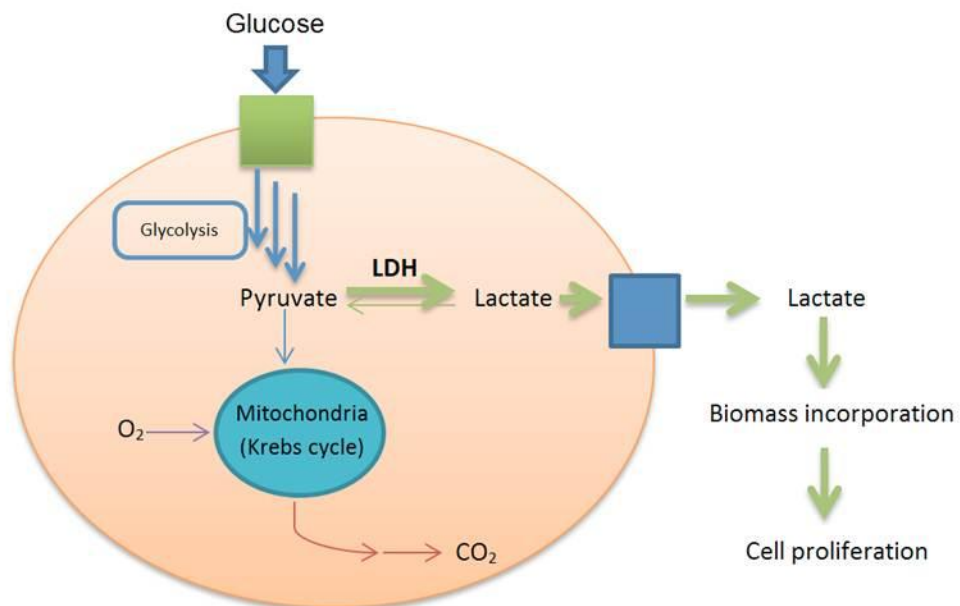


Figure 4.1 In certain cancer indications, such as breast cancer, tumor cells demonstrate an up regulation of glucose transport and glycolysis but rather than rely on oxidative phosphorylation, excess pyruvate is converted to lactate by LDHA. Lactate can be subsequently transported out of the cell where it can be taken up by other cell types or other tumor cells to support biogenesis and cell proliferation.

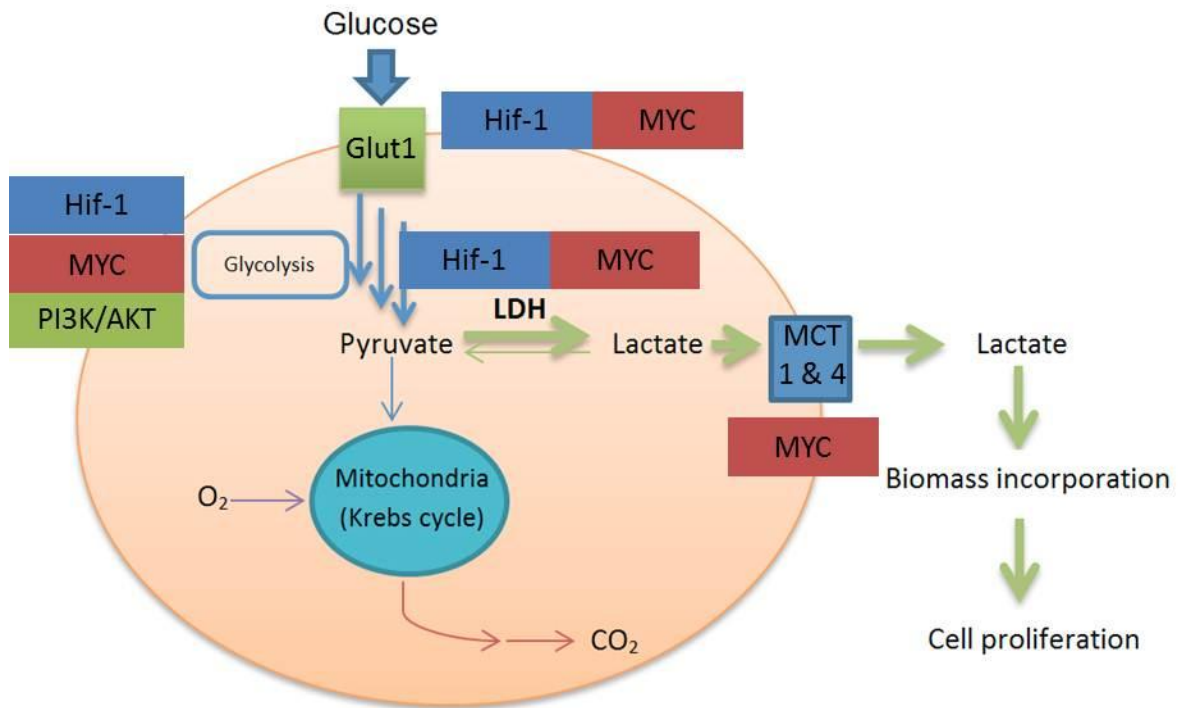


Figure 4.2 Cell metabolism is regulated by several different signaling mechanisms. Glucose uptake and Glycolysis is controlled by Hif1, MYC, and AKT signaling. In the case of a tumor cell, over active lactate production and transport is also regulated by Hif1 and MYC signaling.

Thus the previous work from our lab and others demonstrating ECM mechanical properties via integrin focal adhesions can potentiate AKT^{11,44} and MYC^{28,45,46}, both key mediators of glycolysis in breast epithelial cells, provides strong support for ECM mechanics as a potential regulator of cell metabolism. Moreover, preliminary data showed ECM cross-linking directly regulates Hif1a *in vivo*, a major regulator of cell metabolism. Importantly we demonstrated that inhibiting collagen cross-linking in transgenic MMTV PyMT mice significantly blunts hypoxia and subsequent Hif1a signaling (Figure 4.3A) and subsequently prevents metastasis (Figure 4.3B). Consistently, transgenic PyMT Hif1a knockout tumors also have significantly reduced tumor cell invasion and blunted metastases stressing the importance of Hif1a in tumor malignancy (Figure 4.4 A-B). Thus, we have preliminary data showing ECM stiffness can directly regulate key mediators of cell metabolic state and that these signaling mechanisms are essential for tumor metastasis.

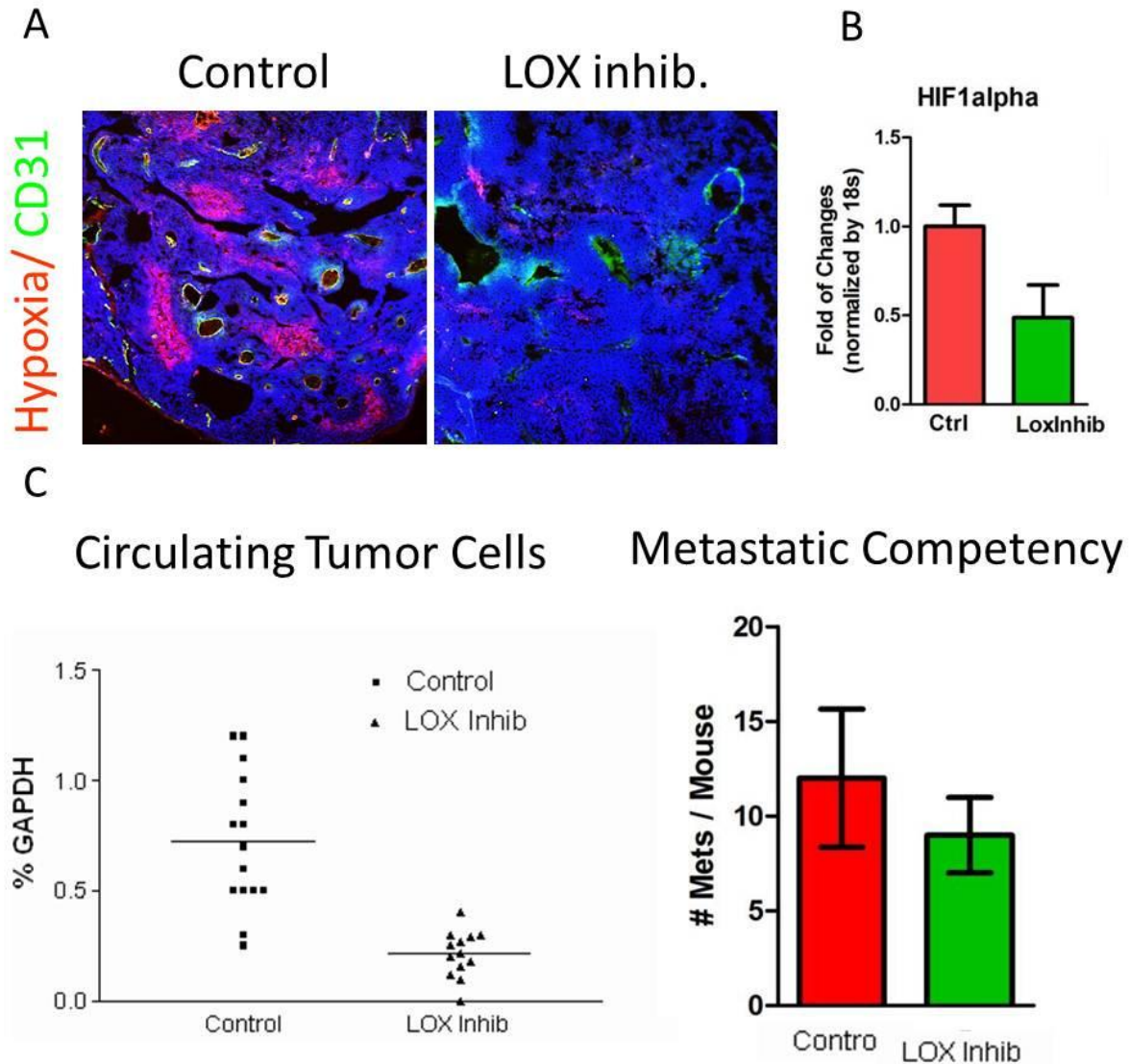


Figure 4.3 **A)** PyMT tumors demonstrate significantly increased hypoxia with collagen crosslinking intact. **B)** Increased hypoxia causes an increase in Hif1a transcription factor expression, a key pathway in cell signaling changes in response to low oxygen. **C)** Loss of collagen cross-linking correlates with significantly reduced circulating tumor cell levels, but equal metastatic competency when tumor cells are directly injected into the tail vein of untreated mice suggesting collagen cross-linking inhibition directly hinders tumor cell invasion, migration, and intravasation.

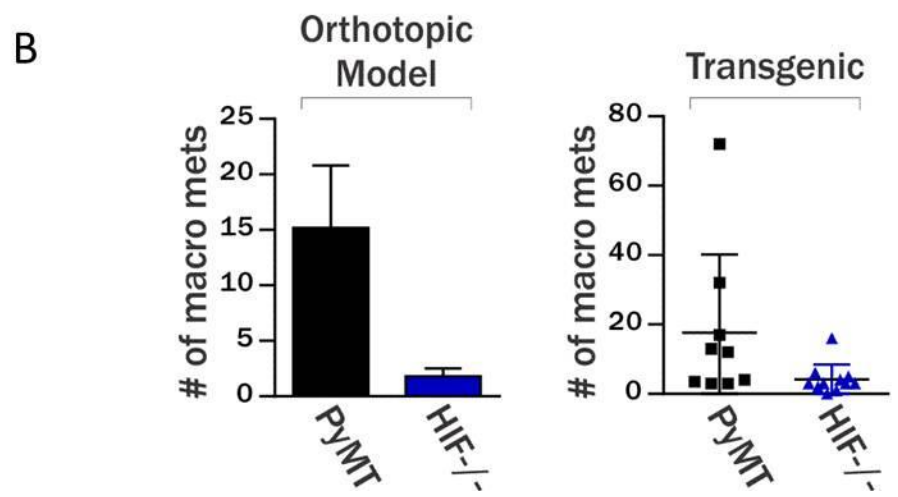
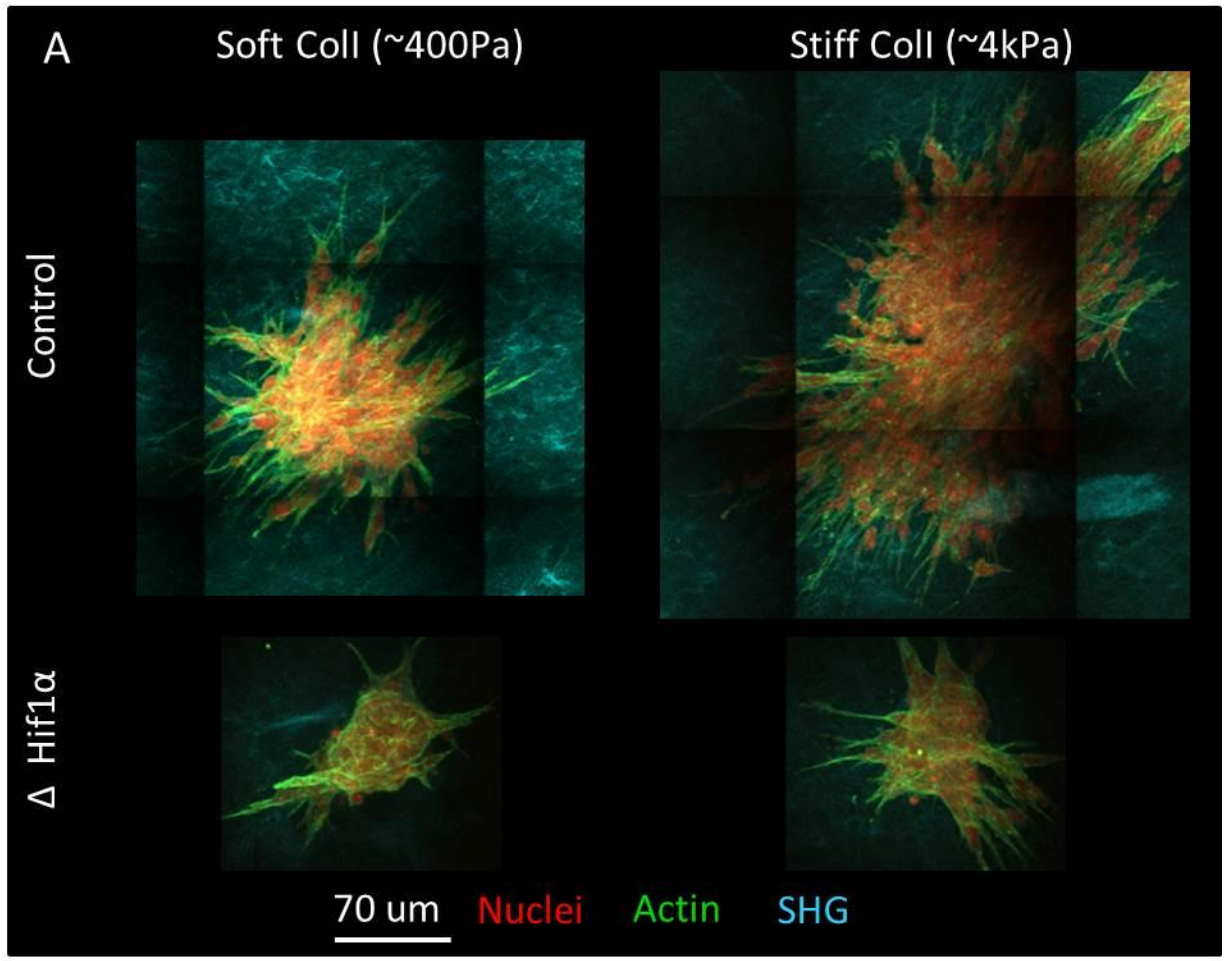


Figure 4.4 A) Hif1a signaling is critical to tumor cell invasion as Hif1a knockout tumor cells have blunted invasion in both soft and stiff collagen gels *ex vivo* **B)** Orthotopic or transgenic mouse models show loss of metastatic progression without Hif1a signaling.

In this project I planned to build on these data and address how ECM stiffness regulates tumor cell metabolism and the role of altered cell metabolism in tumor cell metastasis. Specifically I aimed to test the following hypothesis: the stiffened ECM associated with tumor progression enhances integrin signaling to alter cell metabolism by increasing the expression and activity of key metabolic targets to support tumor metastasis. I tested this hypothesis using mammary tumor cell lines isolates from transgenic tumor models in combination with mechanically tunable substrates in which I measured relative levels and activity of key metabolic regulators. To address, how tumor cell metabolism influences malignant phenotype, I assessed *in vitro* tumor cell invasion and migration in the presence of metabolic inhibitors, 2-deoxyglucose (2DG, a glucose mimic which cannot be metabolized inhibiting glycolysis^{35,37}) and metformin (a diabetic drug that activates AMPk , which inhibits mTor, MYC, and Hif1a to normalize cell metabolism and has recently been implicated as having anti-tumor effects^{33,42,47,48}). Finally, I then performed an *in vivo* study using metformin with MMTV-PyMT transgenic mice to determine the effects of metabolic inhibition in preventing metastasis.

My data shows robustly that ECM stiffness can in fact directly alter cell metabolism and that this adaptation allows cells to better cope with nutrient stress, such as mimicked by 2DG, but also more sensitive to drugs which directly target upstream regulators of metabolism, such as metformin. Importantly, the effect of metformin in preventing tumor cell malignant phenotype translates *in vivo* and significantly inhibits metastasis.

Results:

Protein and expression level of key metabolic markers are reduced with inhibition of ECM stiffness *in vivo* and regulated by substrate stiffness *in vitro*.

Having previously demonstrated the impact of ECM stiffness via collagen cross-linking in potentiating tumor metastasis *in vivo* dependent on Hif1a signaling (Figure 4.3,4.4), I aimed to examine metabolic changes associated with collagen cross linking inhibition. I first assessed the impact of collagen cross linking on protein level of the pertinent glucose transporters⁴¹ (Glut1 and Glut3 for mammary epithelial cells) via immunofluorescence imaging (Figure 4.5A) in MMTV PyMT tumors +/- BAPN¹² (collagen cross-linking inhibitor). Consistent with the loss of Hif1a signaling, a key driver of glucose transporter expression, when inhibiting collagen cross-linking I observed significant reduction in Glut1 fluorescent intensity. This result suggests blunted glycolysis when reducing ECM stiffness via inhibiting collagen cross-linking as the steep concentration gradient of glucose across the cell membrane causes glucose transporter levels to directly correlate with glucose influx into the cell.

To assess the overall state of tumor metabolism and the role of ECM stiffness I next profiled mRNA expression level of several key metabolic regulators in MMTV PyMT tumors +/- BAPN. Interestingly, I found that tumors with collagen cross-linking intact has significantly higher expression levels of key regulators of glycolysis: glucose transporters (Glut1) lactic acid fermentation enzymes, lactic acid transporters (MCT1 and MCT4), and cellular pH buffering capacity (Ca9) (Figure 4.5B). Overall, these results suggest with a stiffened ECM, PyMT tumors are highly glycolytic, which has several potential benefits for tumor development as the excess lactate produced allows for abundant material for biogenesis supporting proliferation and

acidifies the extracellular space enhancing ECM remodeling (See Figure 4.5C). These changes are consistent with previous clinical observations showing a correlation between high expression of glucose metabolism and glycolysis regulators and poor patient prognosis as preventing collagen cross-linking both blunts glycolysis and metastasis in MMTV PyMT mice. However, how these changes occur and whether they are solely due to ECM mechanical properties cannot be determined solely from these data due to the complex nature of *in vivo* tumor models and the potential secondary effects of systemic treatment with BAPN.

To determine the effects of substrate stiffness specifically on tumor cell metabolic regulation I isolated MMTV PyMT and seeded these cells on 2D mechanically tunable polyacrylamide (PA) gels representing a range of stiffnesses from healthy to tumor associated breast tissue. In agreement with my *in vivo* results, I observed that stiffened substrates resulted in increased expression of key protein regulators of glucose transport, glycolysis, and biogenesis (Figure 4.6). This result again supports the notion that substrate stiffness has key role in determining tumor cell metabolism, specifically switching mammary tumor cells towards glycolysis. As has been previously shown, tumor cells on stiffened substrates demonstrate significantly higher migration and proliferation likely supported by this enhanced metabolism.

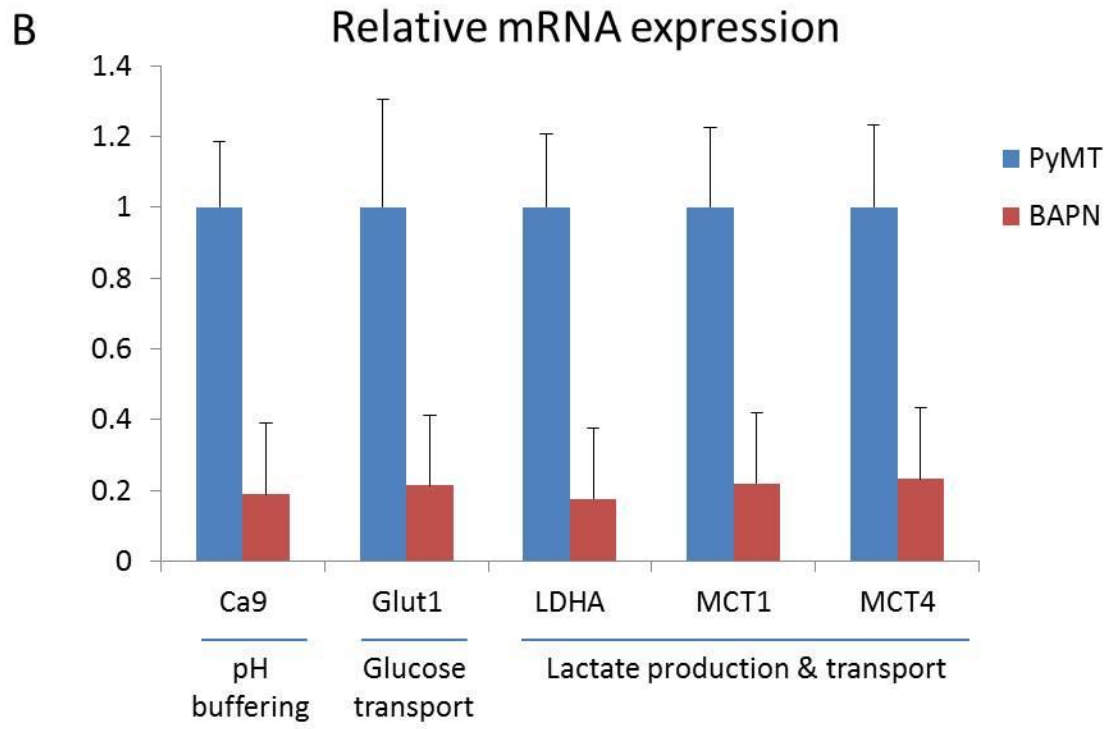
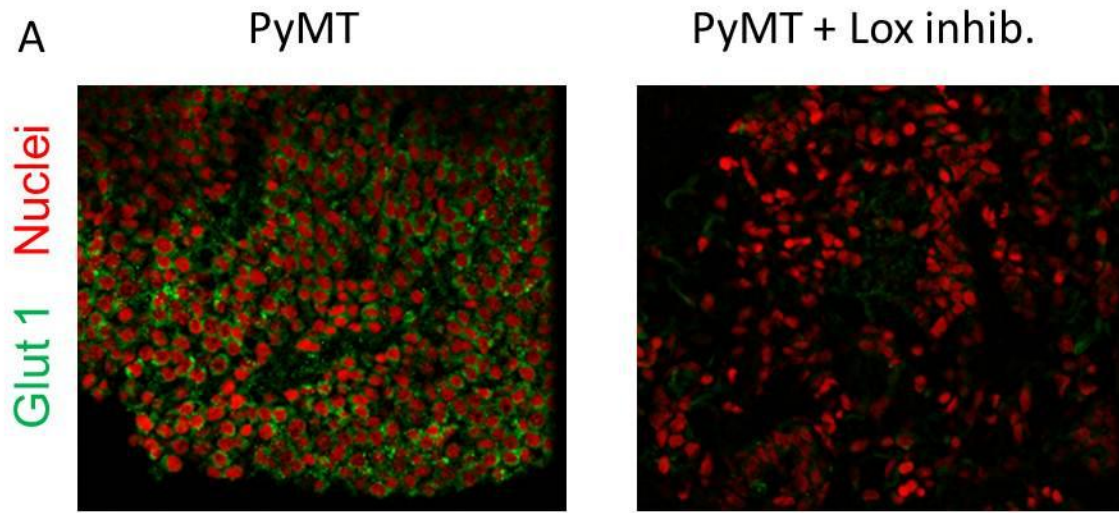


Figure 4.5 A) Glut1 protein levels assessed with immunofluorescence in PyMT tumors +/- lysyl oxidase (LOX) inhibition (via BAPN treatment) to prevent collagen crosslinking. Scale Bar 70um
B) Expression analysis of cellular pH buffering capacity, glucose transporters, and lactate production and transport mechanisms, from PyMT tumors +/- collagen cross-linking inhibition (BAPN).

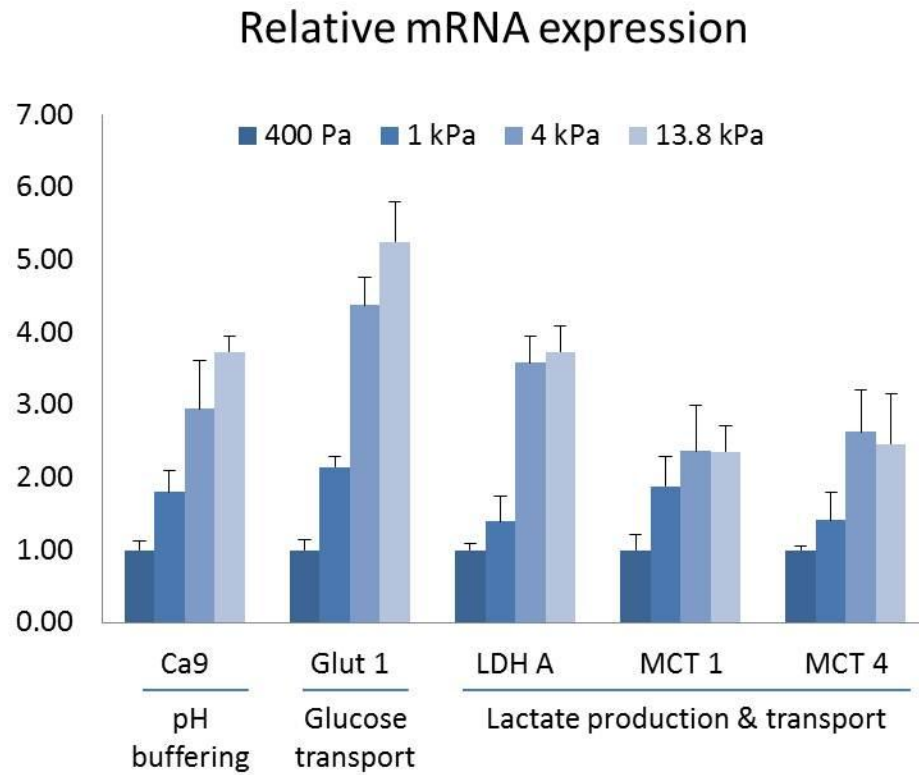


Figure 4.6 mRNA expression analysis of metabolic targets in isolated tumor cells seeded on polyacrylamide gels of increasing stiffness.

Inhibiting tumor cell metabolism blunts tumor cell invasion dependent on ECM mechanical properties.

Having established a role for ECM mechanics in altering tumor cell metabolism, I next aimed to elucidate the importance of metabolism in tumor cell behavior and in particular tumor invasion and malignant phenotype. I first examined the importance of glycolysis in tumor cell invasion using a combination of 2-deoxyglucose (2DG) and my 3D tension bioreactor described previously. Briefly, 2DG is a molecule structurally similar to glucose such that it is transported into the cell just equimolar to glucose through the glucose transporters; however, because of its chemical structure it cannot be metabolized past the first reaction of glycolysis (Figure 4.7). Consequently increasing concentrations of 2DG supplemented into cell culture media represent a model of nutrient stress similar to what might occur in a poorly vascularized tumor.

To assess the effects of 2DG I isolated PyMT organoids from five MMTV PyMT mice and seeded each separately in a 3D collagen gels as previously described⁸. After 24 hours of culture I then added 2DG into the culture media ranging from (500uM to 5mM). After two days of culture with 2DG I fixed and stained tumor cell nuclei to visualize tumor cell invasion and growth. Consistent with previous experimental results^{43,49} organoids from three animals showed reduced invasion and proliferation with increasing concentrations of 2DG (Figure 4.7). Yet, two animals in this study showed significantly reduced sensitivity to 2DG even at the highest doses (Figure 4.7). I next used qPCR expression analysis to determine why certain animals did or did not respond. Interestingly, I found that animals with reduced sensitivity had significantly higher levels of key metabolic regulators associated with glycolysis, suggesting that

tumors from these animals were better able to handle doses of 2DG due to increased flux of glucose and subsequent glycolysis (Figure 4.7).

Having shown previously that ECM mechanics can directly regulate expression and protein levels of key metabolic regulators and that high levels of proteins associated with glycolysis permitted certain tumor cells to have reduced sensitivity to 2DG, I aimed to determine if ECM stiffness could alter mammary tumor cell sensitivity to nutrient stress. As in my initial studies with 2DG, I seeded primary PyMT organoids from five MMTV PyMT mice seeded in my collagen tension bioreactor but now tuned to either 400 Pa or 4 kPa, healthy or tumor like stiffness respectively. After two days, cultures were fixed and stained with phalloidin propidium iodide and then imaged with a two-photon microscope to visualize tumor cell invasion and migration. Intriguingly, a stiffened matrix significantly reduced cell death and allowed persistent invasion and migration even with high doses of 2DG relative to the low stiffness condition (Figure 4.8). These results provide an interesting new insight into the potential importance of ECM mechanics in tumor metabolism and the functional benefits of this aberrant metabolism to tumor development, especially in low nutrient environments such as those early in development prior to extensive angiogenesis, avascular tumors, or tumors with poor blood perfusion.

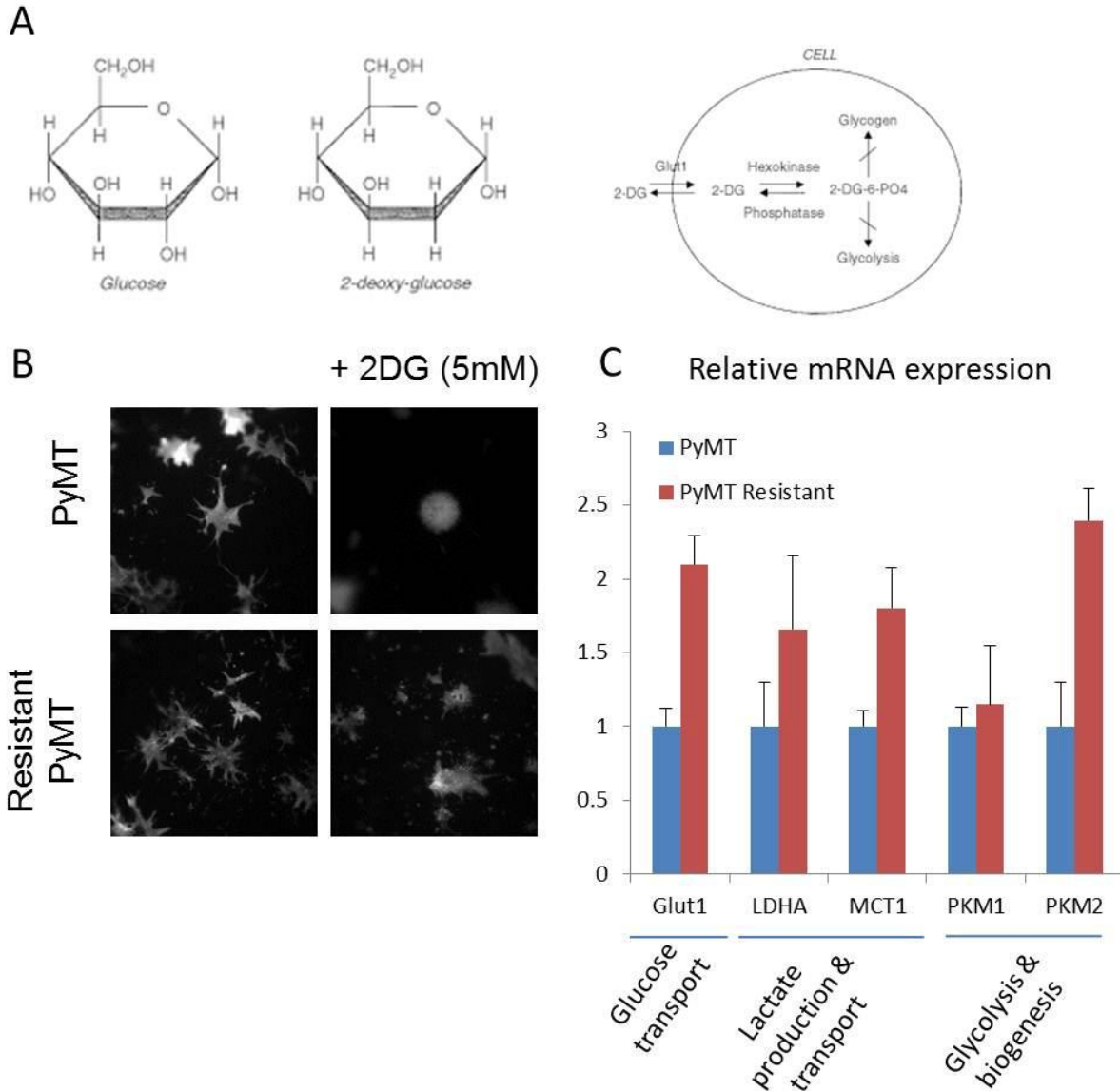


Figure 4.7 **A**) Schematic of 2-deoxyglucose (2DG) chemical structure relative to glucose and mechanism by which it inhibits glycolysis. **B**) PyMT tumor organoids seeded in collagen gels, imaged after two days of culture to assess invasion with or without 2DG treatment. Top panel represents biological replicates which responded to 2DG treatment, while the bottom panel replicated which still showed an invasive phenotype with 2DG. Scale bar 100um **C**) mRNA expression analysis of metabolic targets in PyMT organoids and PyMT organoids which were resistant to 2DG.

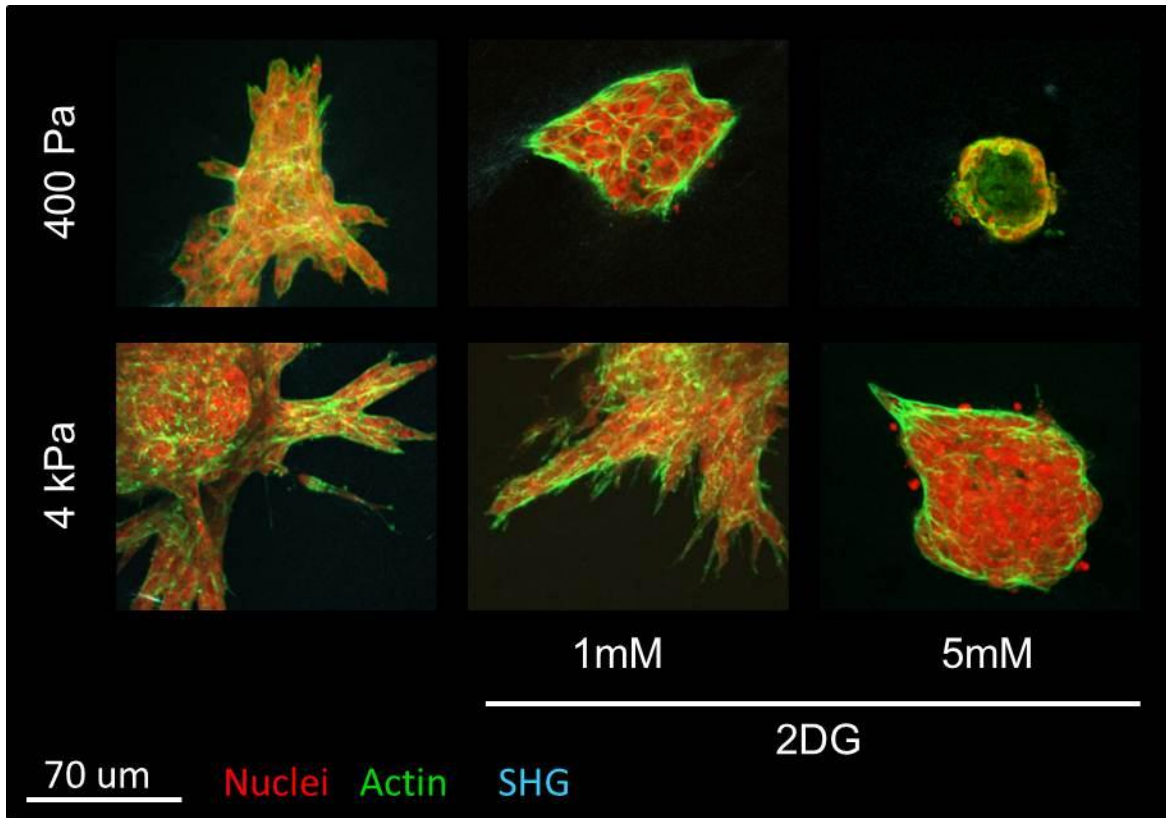


Figure 4.8 PyMT organoids seeded in collagen I gels in the tension bioreactor tuned to either 400Pa or 4kPa (healthy or tumor associated stiffness respectively) and cultured with increasing doses of 2DG. After two days cultures were fixed and imaged to assess invasion.

Building on my data showing ECM stiffness potentiating metabolic adaptations, I next aimed to target cell signaling mechanisms responsible for this metabolic switch. AMPk signaling is a key metabolic sensor in healthy normal cells that serves this very purpose by keeping cell division and biogenesis in line with nutrient availability. Specifically, AMPk is activated by low intracellular ATP allowing the cell to sense poor nutrient availability and in turn AMPk deactivates Hif1a, MYC, and mTor to slow glucose uptake and glycolysis as well as reduce cellular biogenesis and subsequent cell division^{23,33,38,42}. It is for this reason that I aimed to test the impact of a pharmacological activator of AMPk, metformin⁴², in regulating tumor cell phenotype.

As in studies with 2DG I isolated primary tumor organoids from five MMTV PyMT mice and seeded in my collagen tension bioreactor tuned to either 400 Pa or 4 kPa and cultured with metformin in the culture media at either 10 or 50mM as previously described. Intriguingly, results from my bioreactor studies show the reverse trend from studies with 2DG, with the stiffened condition increasing sensitivity to AMPk activation causing blunting proliferation and invasion and inducing cell death with higher concentration (Figure 4.9). To develop more mechanistic insight on the effects of metformin and the role of ECM stiffness on tumor malignant phenotype I next seeded PyMT tumor cells on 2D PA gels and assessed cell morphology via immunofluorescence and cell signaling changes with qPCR expression analysis and western blotting of key signaling proteins. Western blot and qPCR results confirmed metformin was having the expected pharmacological effects of activating AMPk and inhibiting mTor and MYC expression. Consistently, downstream targets of these pathways such as pS6 and metabolic targets (Glut1, LDHA, and MCT1) were also downregulated. (Figure 4.9).

Interestingly and in line with 3D invasion results, stiffened matrices dramatically sensitized tumor cells to subsequent downstream effects with both pFak 397 and pHistone H3 levels significantly reduced (Figure 4.10). Importantly this sensitivity also translates to significant changes in cell morphology as demonstrated with actin cytoskeleton staining, with metformin preventing effective actin stress formation and resulting in a more rounded cell shape. (Figure 4.10). These results clearly demonstrate an impact of metformin on cell behavior in signaling and in particular in a stiffened environment, making metformin a potentially attractive therapeutic option for highly fibrotic tumors.

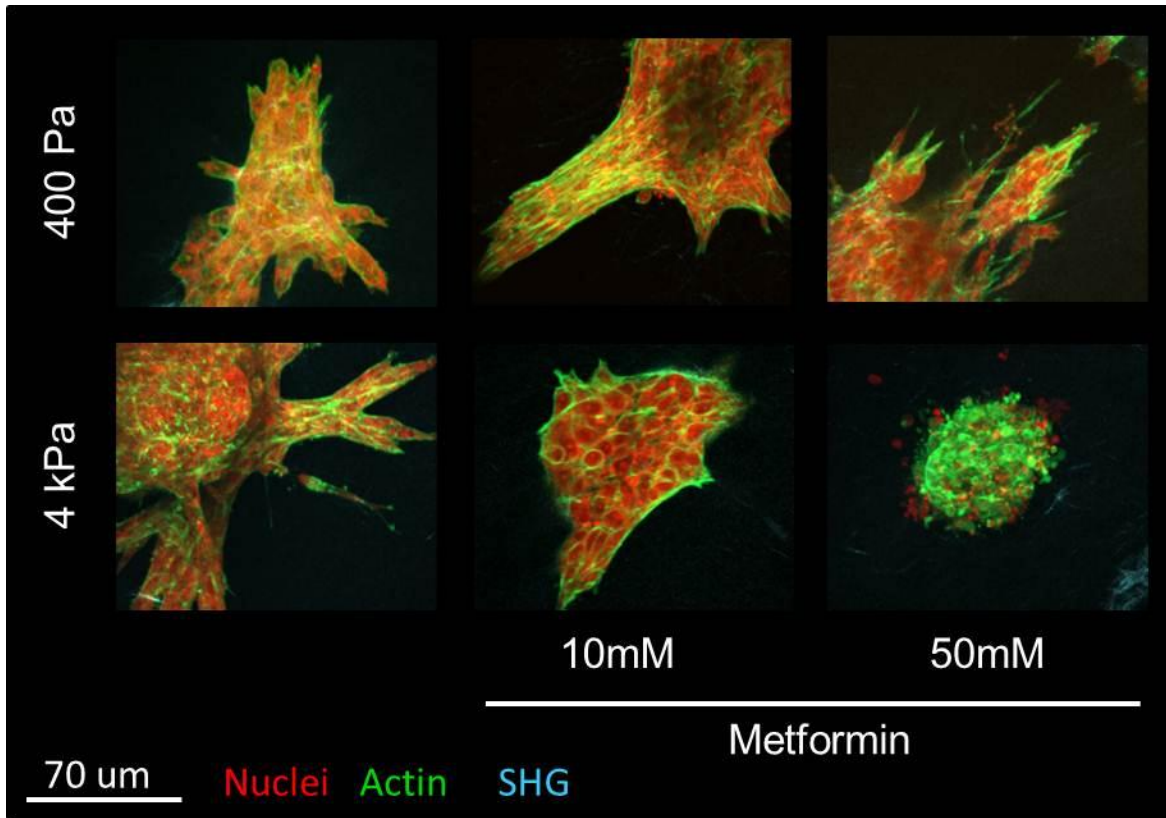


Figure 4.9 PyMT organoids seeded in the tension bioreactor tuned to either 400Pa or 4kPa (healthy or tumor associated stiffness respectively) and cultured with increasing doses of metformin. After two days cultures were fixed and imaged to assess invasion.

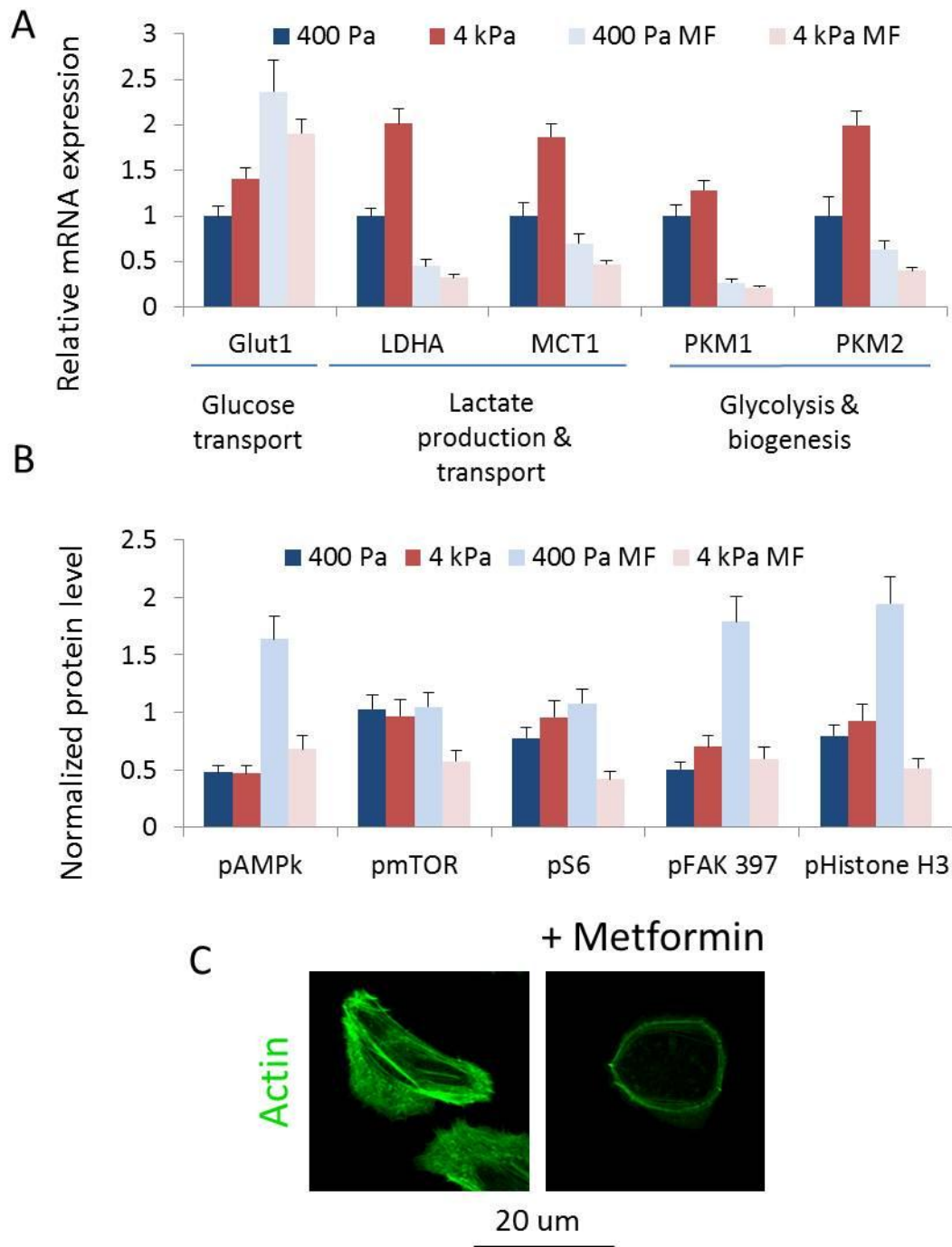


Figure 4.10 **A)** mRNA expression analysis of metabolic targets in isolated tumor cells seeded on polyacrylamide gels of varying stiffness with or without metformin treatment. **B)** Immunoblot analysis of protein targets in isolated tumor cells seeded on polyacrylamide gels of varying stiffness with or without metformin treatment. **C)** Actin cytoskeleton staining of isolated PyMT tumor cells with or without metformin treatment.

Metformin slows tumor growth, inhibits pro-invasion tumor signaling, and prevents lungs metastasis in malignant breast cancer *in vivo*.

Building on my *in vitro* work demonstrating the impact of metformin in preventing tumor cell invasion in stiffened environments I next aimed to explore whether this effect translates *in vivo*. My study design included 20 MMTV PyMT mice; a spontaneous tumor model with rapidly progresses with robust fibrosis and metastasis. Ten mice received metformin (0.5mg/ml in water) and ten served as a control group receiving only water. Mice were euthanized for tissue collection at two time points, early tumor progression (11 weeks of age) and late tumor progression (upon tumors reaching the 2mm³ total tumor burden IACUC limit) (Figure 4.10).

Tumor growth based on caliper measurements and time required to reach 2mm³ were significantly reduced with metformin treatment consistent with previous results using orthotopic tumor models. (Figure 4.11) Importantly, despite all animals with or without treatment ultimately reaching the same size, animals treated with metformin had significantly reduced metastasis to the lungs suggesting despite substantial tumor growth with metformin there is a substantial difference in metastatic competence.

To explore why metformin prevented metastasis I first assessed the impact of treatment on overall tissue structure and organization with H&E and picrosirius tissue staining I postulated that metformin may have anti-fibrotic effects in the mammary gland as has been described previously in other tissues (cardiac) and in agreement with my previous data demonstrating anti-fibrotic drugs blunting metastasis in this tumor model. However, I found in both tissues

equal amount of collagen remodeling and structural changes with tumor progression (Figure 4.11).

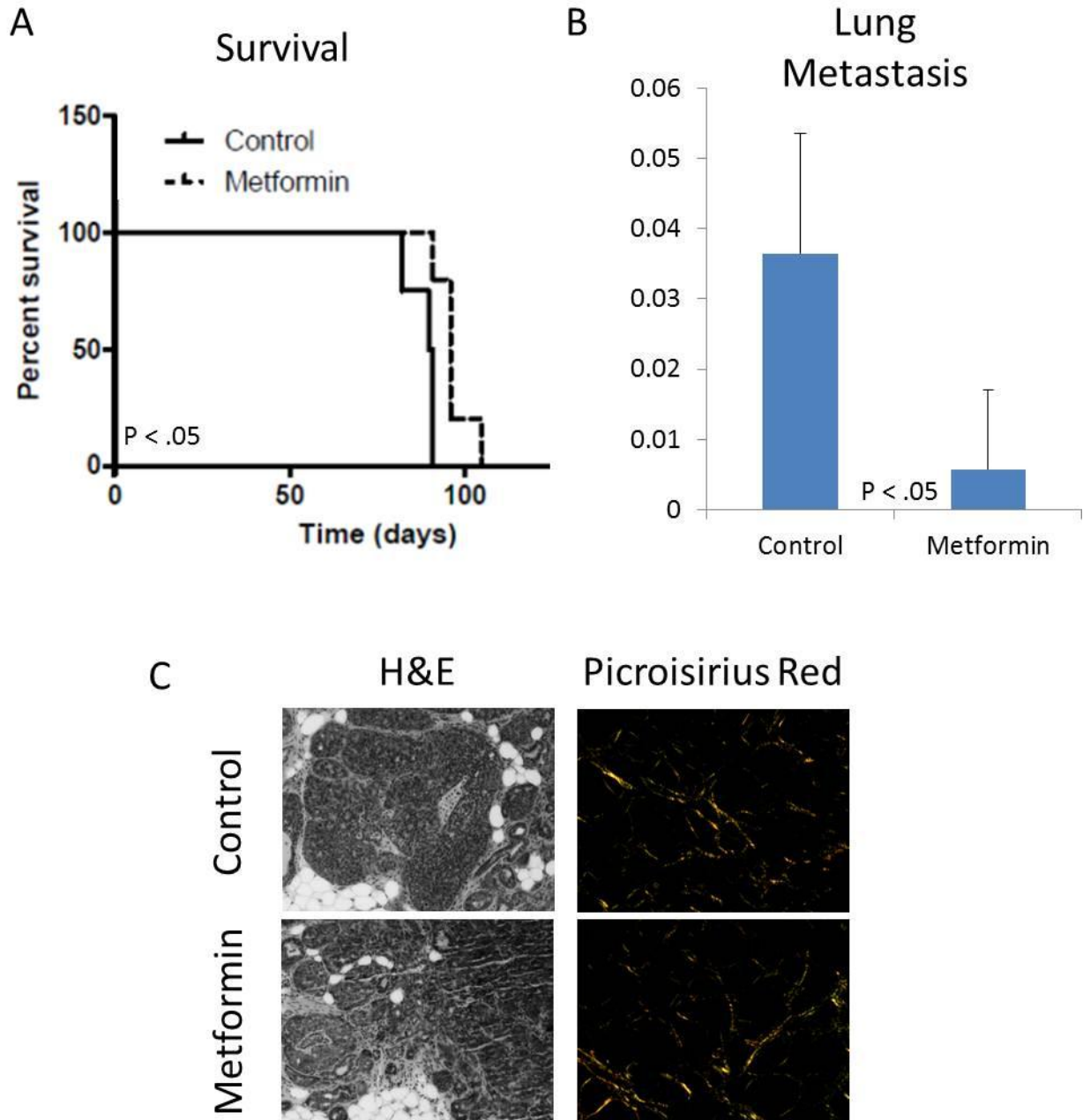


Figure 4.11 **A)** Kaplan-meyer curve showing percent survival of late stage PyMT mice +/- metformin. Mice were euthanized at a total tumor burden of 2mm^3 . **B)** mRNA expression analysis of PyMT transgene in mouse lung tissue of late stage PyMT mice as an assessment of metastasis. **C)** H&E and Picrosirius Red staining of 11 week PyMT tumors +/- metformin.

These results then suggested the difference may be inherent to the tumor cells themselves and accordingly I isolated PyMT organoids from animals with and without treatment and seeded them in my tension bioreactor to assess their invasion and growth potential (Figure 4.12). Interestingly, while organoids from both animals had similar proliferation and multicellular streaming migration, only organoids from non-treated animals demonstrated single cell invasion.

Following this I next assessed differences in tumor expression patterns from the primary tumors to suggest signaling changes, which might be driving this difference. As expected with metformin treatment tumors showed significantly lower expression of metabolic targets downstream of Hif1a, MYC, and mTor such as Glut1, MCT1, LDHA, and PKM2 suggesting metformin treatment switches PyMT tumor metabolism away from glycolysis and more toward oxidative phosphorylation as in normal cells (Figure 4.13). Interestingly, there was also a significant decrease in expression of transcription factors (Snail1 and Snail2) and cytoskeletal elements (vimentin) associated with EMT and a corresponding increase in cell-cell junctions (e-Cadherin) suggesting a loss of the pro-invasion phenotype of control tumors^{23,50,51}. Both the metabolic change and the down regulation of EMT signaling was also supported by immunostaining of tissue sections with Glut 1 and vimentin protein levels down with metformin treatment. Consistently, pS6 levels are also decreased with metformin treatment suggesting decreased mTOR signaling as expected. Interestingly, I also observed loss of pMLC with metformin treatment suggesting tumor cells are potentially less contractile and less mechanically activated (Figure 4.13).

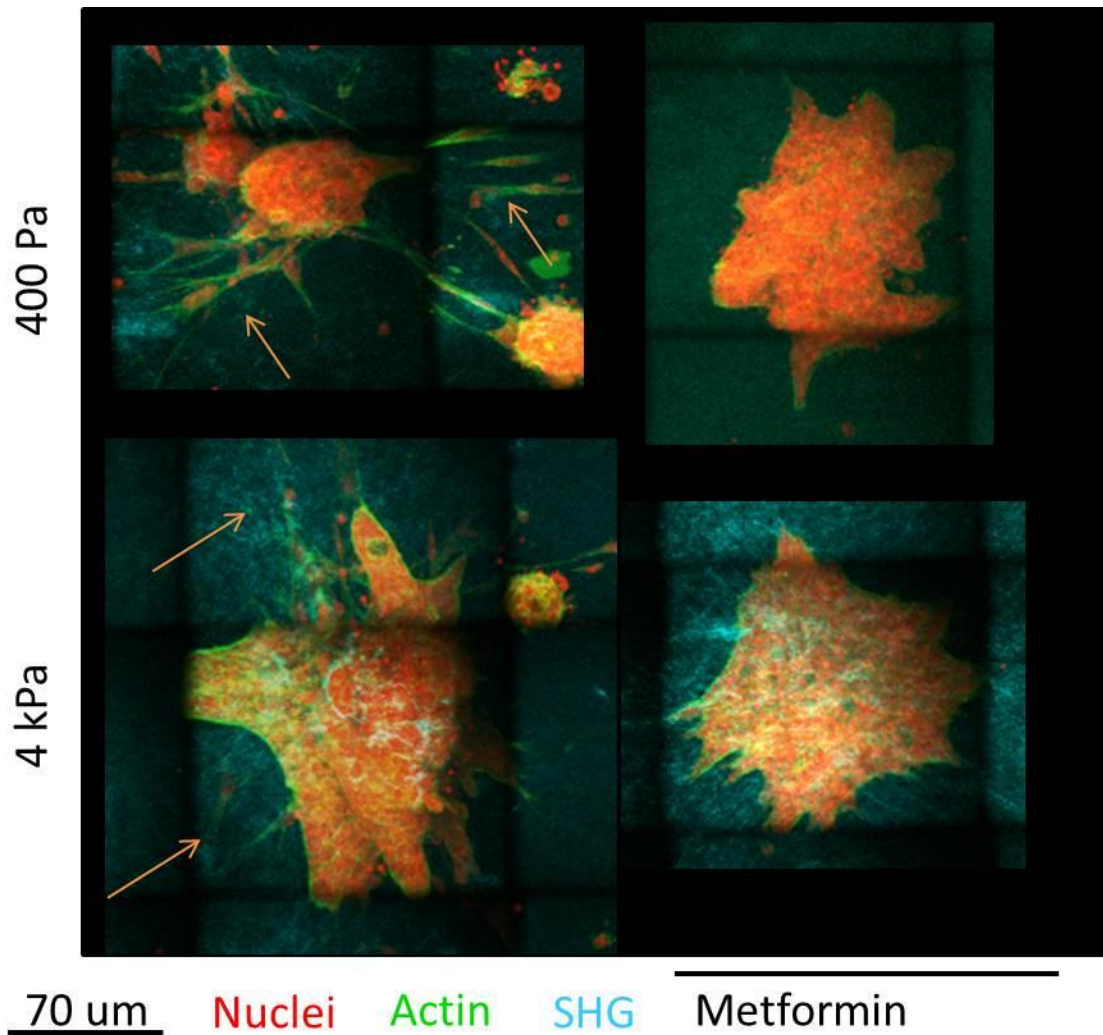


Figure 4.12 PyMT organoids isolated from 11 week MMTV PyMT mice +/- metformin and seeded in the tension bioreactor tuned to either 400Pa or 4kPa (healthy or tumor associated stiffness respectively). After two days cultures were fixed and imaged to assess invasion.

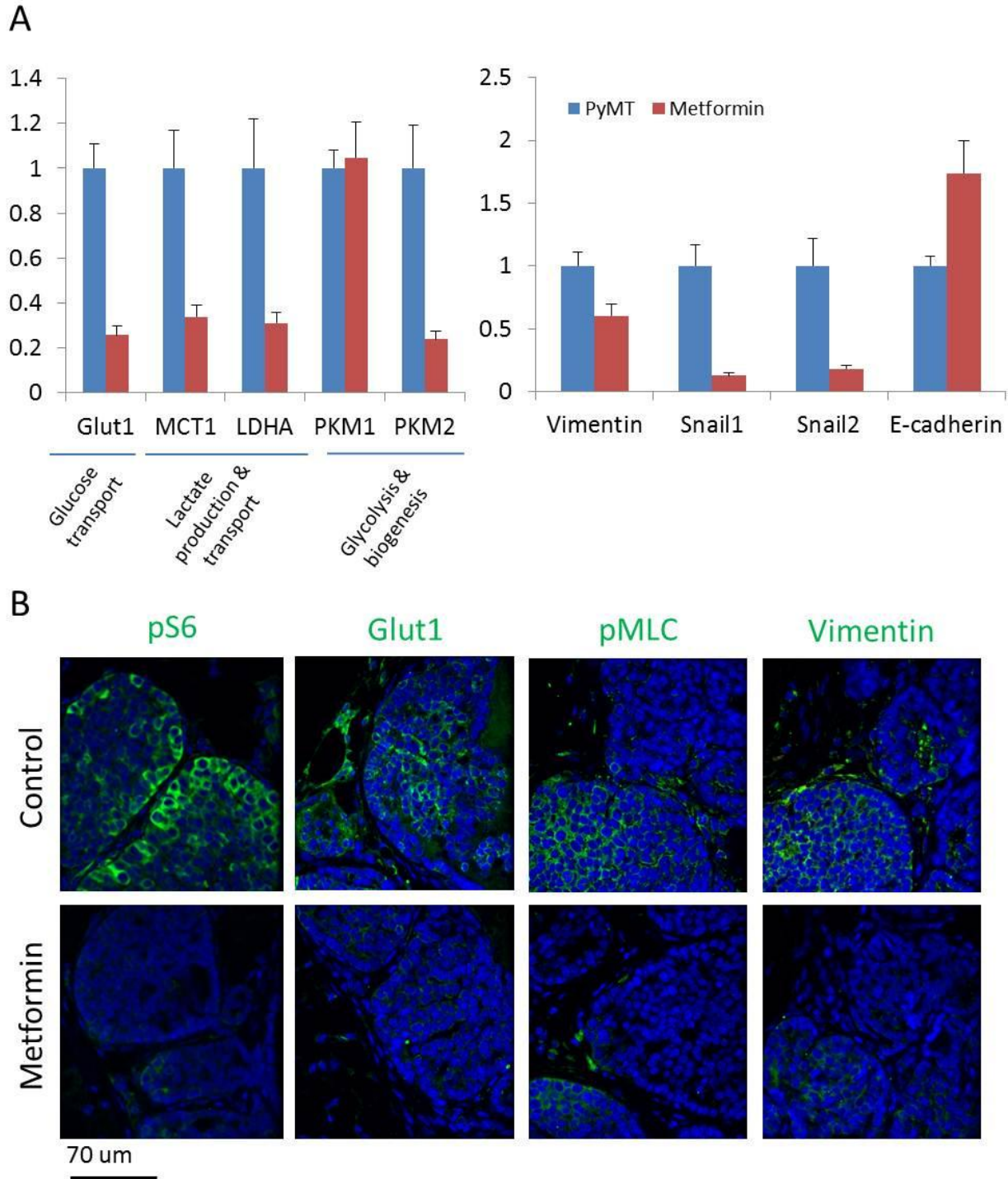


Figure 4.13 A) mRNA expression analysis of metabolic and EMT targets in 11 week PyMT tumors +/- metformin **B)** Tissue staining in 11 week PyMT tumors +/- metformin to assess protein levels of Glut1 and vimentin and activation of ribosomal protein S6 and MLC.

Discussion:

In this work I have demonstrated for the first time the role of ECM mechanics in altering cell metabolism. Specifically, I have shown that ECM stiffness can significantly upregulate expression levels of key regulators of cell metabolism controlling glucose transport, glucose metabolism, lactate metabolism, and lactate transport in mammary tumor cells both *in vitro* and *in vivo*. Importantly, I have also demonstrated how these changes are important to tumor cell growth and invasion *in vitro* as tumor cell malignant phenotype can be significantly blunted with metabolic inhibition; however, this inhibition depends on both the target of the inhibition and the ECM mechanical environment of the given tumor cells. In particular, mimicking nutrient stress with 2DG was not effective in stiffened environments due to upregulation of glucose transporters with increased substrate stiffness whereas metformin which targets the fundamental mechanisms of metabolic adaptation (Hif1a, MYC, mTor) previously reported for mammary tumor cells is particularly selective for tumor cells in a stiffened environment. Interestingly, I were able to show the potential for metformin specifically in treating breast cancer as it significantly reduced tumor growth, reduced pro-invasion and EMT signaling, and importantly for its potential in a clinical setting preventing metastasis.

Taken together these results provide several key new insights to both the cell metabolism and cancer biology field in particular with regards to potential therapeutic targets and diagnostic approaches. Based on these data metabolic inhibition clearly can prevent aggressive tumor phenotypes but intriguingly depends on the mechanical environment in which a tumor arises. For example, metformin is likely only suitable in patients with highly fibrotic breast tumors, which fortunately also tend to be the most aggressive. Additionally, the

metabolic pathways identified here, specifically the switch to glycolysis in the more aggressive tumors, can be screened for with techniques such as hyper polarized NMR⁵² and allow for more robust prognosis in breast cancer patients. The potential for combining the diagnostic potential of these data and the new potential therapies shown in this data is also intriguing in that a combined metabolic and tissue mechanics diagnostic tool^{1,2,53,54} could potentially allow identification of patients with the fibrotic tissue and metabolic pattern best suited for therapeutic drugs like metformin. However, the data here was solely generated using luminal breast cancer cell lines and whether these results can be translated to all breast cancers or other solid tumors not clear and in reality probably unlikely due to the wide variety of metabolic adaptations that have been observed in different tumor types.

In particular, while aberrant metabolism in tumors is well appreciated, the type of metabolic change seen is highly heterogeneous between tumor type, individual tumor, and even within and across a single tumor^{38,39,41}. Nearly every aspect of cell metabolism, balance of glycolysis to oxidative phosphorylation, energy source (glucose, glutamate, amino acids, or lipids), biogenesis, pH regulation, and molecular biogenesis can be modified in a tumor context^{24,27,29,34,55-57}. Yet, in spite of this wide variety of possible alterations the impact of aberrant metabolism in tumor growth, progression, and malignancy is well supported^{39,43,52,58}. Thus, future work in other cancer indications would have to account for different types of metabolic adaptations specific to a given tumor type.

Additionally, there are several more research questions still to be answered in this work. Specifically, how is actual cell metabolism, glucose consumption for example, altered by ECM stiffness based on the differences I observed in expression and protein level of pertinent

metabolic regulators? Also essential, through which important metabolism regulation pathways, AKT, MYC, mTor, and MYC, identified in mammary epithelial cells does stiffness act? Moreover, in previous works I have seen integrin specificity plays a key role in tumor in malignant phenotype, specifically alpha 5 integrin and its ligand fibronectin. Future studies in this project should also focus on whether integrin specificity also applies to metabolic adaptation in response to ECM stiffness. Also, in metformin treated animals I observed significantly reduced FAK and MLC activations suggesting blunted cell contractility. While collagen deposition was not significantly different it is possible fibronectin deposition may be reduced in line with previous results showing tumor cells on fibronectin coated surfaces have enhanced focal adhesion formation and contractility which in turn drives malignant phenotype.

With regards to the potential clinical strategies with metformin, are the changes I observed to mammary tumor cell signaling enough to explain why metformin prevented metastasis? Or is it a combination of systemic effects on other cell types as well affecting other key events in tumor development like angiogenesis or immune response or is it localized to the lung metastatic niche, possibly altering the microenvironment preventing secondary tumor formation? While these questions are beyond the scope of the work presented here they do provide interesting research directions for the future.

Methods:

Cell culture

MMTV PyMT mice were sacrificed at 11 week and the #4 mammary glands were collected and digested for tumor organoids isolated as previously described. Once acini were isolated they were seeded in the collagen bioreactor or seeded onto 2D polyacrylamide gels and cultured for 2 days. For bioreactor studies after 2 days they were paraformaldehyde fixed and stained with propidium iodide and alexa488 phalloidin for imaging on the two-photon microscope.

Polyacrylamide gel cultures were also stopped after 2 days with a 2% SDS lysis buffer used to collect protein lysates or Trizol for RNA expression analysis.

Studies in which metabolic inhibition was required 2DG or metformin were resuspended in sterile H₂O and added to cell culture media for a final concentration of 500uM-5mM and 10mM-50mM respectively.

Tissue Immunofluorescence Staining and quantification

Antibodies and Reagents. Antibodies were as follows: Primary MLCpS19 (Rabbit Cell Signaling), Glut1 (Mouse Cell Signaling), Vimentin (Hamster Cell Signaling) secondary AlexaFluor goat anti-mouse, anti-rabbit, and anti-hamster (488 conjugates) and DAPI (Sigma). Immunofluorescence staining and imaging of FFPE tissue sections was performed as recently described²⁸.

Image Acquisition

All immunofluorescence images were acquired using a Nikon 40x water immersion objective (NA=1.15) on a Nikon spinning disk microscope.

Mouse Studies

Starting at 4 weeks of age, mice were treated with metformin (0.5mg/ml; Spectrum) in the drinking water. Mice were sacrificed at 11 weeks of age or when total tumor burden reach 2mm^3 , at which time the 4th mammary gland was paraformaldehyde fixed; paraffin sections were analyzed for histology and parallel sections were stained as described, and the 2/3 mammary gland was collected for PCR and immunoblot analysis and as a cell source for tumor cells. For mice sacrificed at a total tumor burden of 2mm^3 lungs were also collected for PCR analysis of metastasis.

RT-PCR analysis

Random-primed cDNA was prepared from total isolated RNA using Trizol reagent (Invitrogen) and target cDNA sequences were quantified via real-time PCR using SYBR Green I reagent (Roche) according to the manufacturer's protocol. Eppendorf Realplex2 quantitative PCR machine was used for all studies.

Immunoblot analysis

Immunoblot analysis was done with a 3% BSA block solution and the following primary antibodies: pHistone H3 (Rabbit Cell Signaling), pS6 (Rabbit Cell Signaling), pAMPk (Rabbit Cell Signaling), AMPk (Rabbit Cell Signaling), pmTOR (Rabbit Cell Signaling), mTOR (Rabbit Cell Signaling), pFAK 397 (Rabbit Cell Signaling) and with a horseradish peroxidase anti-rabbit secondary (Cell Signaling).

3D and 2D Substrate Preparation

Tension bioreactor studies were performed as previously described.⁸ ECM-functionalized PA gels were prepared and mechanically analyzed as described previously⁵⁹.

Statistical Analysis

Statistical analysis was performed using Prism/GraphPad Software (La Jolla, CA) at indicated p-values. Unless otherwise stated, two-tailed Student's t-tests were used for significance testing. Means were presented as +/- s.e.m of at least three independent experiments. Unless otherwise noted, sample size, n, was n=3 and statistical significance was considered at p<0.05. Adhesion strength values were specifically analyzed via ANOVA and Tukey's post-hoc test with a p-value < 0.05 considered significant.

Acknowledgements:

Work was supported by NIH F31CA183255 and the ARCS Foundation to LC, NIH R01 CA138818,

DoD W81XWH-13-1-0216, NIH U01ES019458, and NIH R01 CA085492 to VW

Works Cited:

1. Chang, J. M. *et al.* Stiffness of tumours measured by shear-wave elastography correlated with subtypes of breast cancer. *Eur Radiol* **23**, 2450–2458 (2013).
2. Lopez, J. I., Kang, I., You, W.-K., McDonald, D. M. & Weaver, V. M. In situ force mapping of mammary gland transformation. *Integr. Biol. (Camb)*. **3**, 910–21 (2011).
3. Samani, A., Zubovits, J. & Plewes, D. Elastic moduli of normal and pathological human breast tissues: an inversion-technique-based investigation of 169 samples. *Phys. Med. Biol.* **52**, 1565–76 (2007).
4. Plodinec, M. *et al.* The nanomechanical signature of breast cancer. *Nat. Nanotechnol.* **7**, 757–65 (2012).
5. Huang, S. & Ingber, D. E. Cell tension, matrix mechanics, and cancer development. *Cancer Cell* **8**, 175–6 (2005).
6. Barr, R. G. Elastography in clinical practice. *Radiol. Clin. North Am.* **52**, 1145–62 (2014).
7. Acerbi, I. *et al.* Human breast cancer invasion and aggression correlates with ECM stiffening and immune cell infiltration. *Integr. Biol. (Camb)*. (2015).
doi:10.1039/c5ib00040h
8. Cassereau, L., Miroshnikova, Y., Ou, G., Lakins, J. & Weaver, V. M. A 3D tension bioreactor platform to study the interplay between ECM stiffness and tumor phenotype. *J. Biotechnol.* **193**, 66–69 (2014).

9. Yeung, T. *et al.* Effects of substrate stiffness on cell morphology, cytoskeletal structure, and adhesion. *Cell Motil. Cytoskeleton* **60**, 24–34 (2005).
10. Samuel, M. S. *et al.* Actomyosin-mediated cellular tension drives increased tissue stiffness and β -catenin activation to induce epidermal hyperplasia and tumor growth. *Cancer Cell* **19**, 776–91 (2011).
11. Paszek, M. J. *et al.* Tensional homeostasis and the malignant phenotype. *Cancer Cell* **8**, 241–54 (2005).
12. Levental, K. R. *et al.* Matrix crosslinking forces tumor progression by enhancing integrin signaling. *Cell* **139**, 891–906 (2009).
13. Netti, P. A., Berk, D. A., Swartz, M. A., Grodzinsky, A. J. & Jain, R. K. Role of extracellular matrix assembly in interstitial transport in solid tumors. *Cancer Res* **60**, 2497–2503 (2000).
14. Janmey, P. A., Wells, R. G., Assoian, R. K. & McCulloch, C. A. From tissue mechanics to transcription factors. *Differentiation* **86**, 112–120 (2013).
15. Provenzano, P. P., Inman, D. R., Eliceiri, K. W. & Keely, P. J. Matrix density-induced mechanoregulation of breast cell phenotype, signaling and gene expression through a FAK-ERK linkage. *Oncogene* **28**, 4326–4343 (2009).

16. Gallant, N. D., Michael, K. E. & García, A. J. Cell adhesion strengthening: contributions of adhesive area, integrin binding, and focal adhesion assembly. *Mol. Biol. Cell* **16**, 4329–40 (2005).
17. Paszek, M. J. *et al.* The cancer glyocalyx mechanically primes integrin-mediated growth and survival. *Nature* **511**, 319–25 (2014).
18. Guo, W. & Giancotti, F. G. Integrin signalling during tumour progression. *Nat. Rev. Mol. Cell Biol.* **5**, 816–26 (2004).
19. Martino, M. M. *et al.* Controlling integrin specificity and stem cell differentiation in 2-D and 3-D environments through regulation of fibronectin domain stability. **30**, 1089–1097 (2010).
20. Desgrosellier, J. S. & Cheresch, D. a. Integrins in cancer: biological implications and therapeutic opportunities. *Nat. Rev. Cancer* **10**, 9–22 (2010).
21. Keely, P. J. Mechanisms by which the extracellular matrix and integrin signaling act to regulate the switch between tumor suppression and tumor promotion. *J Mammary Gland Biol Neoplasia* **16**, 205–219 (2011).
22. Chappell, W. H. *et al.* Ras/Raf/MEK/ERK and PI3K/PTEN/Akt/mTOR inhibitors: rationale and importance to inhibiting these pathways in human health. *Oncotarget* **2**, 135–64 (2011).

23. Chou, C.-C. *et al.* AMPK reverses the mesenchymal phenotype of cancer cells by targeting the Akt-MDM2-Foxo3a signaling axis. *Cancer Res.* **74**, 4783–95 (2014).
24. Elstrom, R. L. *et al.* Akt stimulates aerobic glycolysis in cancer cells. *Cancer Res.* **64**, 3892–9 (2004).
25. McCubrey, J. A. *et al.* Roles of the Raf/MEK/ERK pathway in cell growth, malignant transformation and drug resistance. *Biochim. Biophys. Acta* **1773**, 1263–84 (2007).
26. Engelman, J. A. Targeting PI3K signalling in cancer: opportunities, challenges and limitations. *Nat. Rev. Cancer* **9**, 550–62 (2009).
27. Mukherjee, J. *et al.* Pyruvate kinase M2 expression, but not pyruvate kinase activity, is up-regulated in a grade-specific manner in human glioma. *PLoS One* **8**, e57610 (2013).
28. Mouw, J. K. *et al.* Tissue mechanics modulate microRNA-dependent PTEN expression to regulate malignant progression. *Nat Med* **20**, 360–367 (2014).
29. Semenza, G. L. Tumor metabolism: cancer cells give and take lactate. *J. Clin. Invest.* **118**, 3835–7 (2008).
30. Diehn, M. *et al.* Association of reactive oxygen species levels and radioresistance in cancer stem cells. *Nature* **458**, 780–3 (2009).
31. Morais-Santos, F. *et al.* Differential sensitivities to lactate transport inhibitors of breast cancer cell lines. *Endocr. Relat. Cancer* **21**, 27–38 (2014).

32. Chandel, N. S. Mitochondria as signaling organelles. *BMC Biol.* **12**, 34 (2014).
33. Zordoky, B. N. M., Bark, D., Soltys, C. L., Sung, M. M. & Dyck, J. R. B. The anti-proliferative effect of metformin in triple-negative MDA-MB-231 breast cancer cells is highly dependent on glucose concentration: implications for cancer therapy and prevention. *Biochim. Biophys. Acta* **1840**, 1943–57 (2014).
34. Muniyappa, H., Song, S., Mathews, C. K. & Das, K. C. Reactive oxygen species-independent oxidation of thioredoxin in hypoxia: inactivation of ribonucleotide reductase and redox-mediated checkpoint control. *J. Biol. Chem.* **284**, 17069–81 (2009).
35. Doherty, J. R. *et al.* Blocking lactate export by inhibiting the Myc target MCT1 Disables glycolysis and glutathione synthesis. *Cancer Res.* **74**, 908–20 (2014).
36. De Saedeleer, C. J. *et al.* Glucose deprivation increases monocarboxylate transporter 1 (MCT1) expression and MCT1-dependent tumor cell migration. *Oncogene* **33**, 4060–8 (2014).
37. Sommermann, T. G., O'Neill, K., Plas, D. R. & Cahir-McFarland, E. IKK β and NF- κ B transcription govern lymphoma cell survival through AKT-induced plasma membrane trafficking of GLUT1. *Cancer Res.* **71**, 7291–300 (2011).
38. Loo, J. M. *et al.* Extracellular Metabolic Energetics Can Promote Cancer Progression. *Cell* **160**, 393–406 (2015).

39. Pinheiro, C. *et al.* GLUT1 and CAIX expression profiles in breast cancer correlate with adverse prognostic factors and MCT1 overexpression. *Histol. Histopathol.* **26**, 1279–86 (2011).
40. Lüftner, D. *et al.* Tumor type M2 pyruvate kinase expression in advanced breast cancer. *Anticancer Res.* **20**, 5077–82
41. Denko, N. C. Hypoxia, HIF1 and glucose metabolism in the solid tumour. *Nat. Rev. Cancer* **8**, 705–13 (2008).
42. Leone, A., Di Gennaro, E., Bruzzese, F., Avallone, A. & Budillon, A. New perspective for an old antidiabetic drug: metformin as anticancer agent. *Cancer Treat. Res.* **159**, 355–76 (2014).
43. Lea, M. A., Pourat, J., Patel, R. & desBordes, C. Growth inhibition of colon cancer cells by compounds affecting AMPK activity. *World J. Gastrointest. Oncol.* **6**, 244–52 (2014).
44. Rubashkin, M. G. *et al.* Force engages vinculin and promotes tumor progression by enhancing PI3K activation of phosphatidylinositol (3,4,5)-triphosphate. *Cancer Res.* **74**, 4597–611 (2014).
45. Shyu, K.-G., Chao, Y.-M., Wang, B.-W. & Kuan, P. Regulation of discoidin domain receptor 2 by cyclic mechanical stretch in cultured rat vascular smooth muscle cells. *Hypertension* **46**, 614–21 (2005).

46. Damiano, L. *et al.* Oncogenic targeting of BRM drives malignancy through C/EBP β -dependent induction of α 5 integrin. *Oncogene* **33**, 2441–2453 (2014).
47. Stambolic, V., Woodgett, J. R., Fantus, I. G., Pritchard, K. I. & Goodwin, P. J. Utility of metformin in breast cancer treatment, is neoangiogenesis a risk factor? *Breast Cancer Res. Treat.* **114**, 387–9 (2009).
48. Anisimov, V. N. *et al.* Metformin extends life span of HER-2/neu transgenic mice and in combination with melatonin inhibits growth of transplantable tumors in vivo. *Cell Cycle* **9**, 188–97 (2010).
49. Doherty, J. R. *et al.* Blocking lactate export by inhibiting the myc target MCT1 disables glycolysis and glutathione synthesis. *Cancer Res.* **74**, 908–920 (2014).
50. Shintani, Y. *et al.* Collagen I-mediated up-regulation of N-cadherin requires cooperative signals from integrins and discoidin domain receptor 1. *J. Cell Biol.* **180**, 1277–89 (2008).
51. Willis, B. C. & Borok, Z. TGF-beta-induced EMT: mechanisms and implications for fibrotic lung disease. *Am. J. Physiol. Lung Cell. Mol. Physiol.* **293**, L525–L534 (2007).
52. Asghar Butt, S. *et al.* Monitoring mammary tumor progression and effect of tamoxifen treatment in MMTV-PymT using MRI and magnetic resonance spectroscopy with hyperpolarized [1-(13) C]pyruvate. *Magn. Reson. Med.* (2014). doi:10.1002/mrm.25095
53. Venkatesh, S. K. *et al.* MR elastography of liver tumors: preliminary results. *AJR. Am. J. Roentgenol.* **190**, 1534–40 (2008).

54. Balleyguier, C. *et al.* Breast elasticity: principles, technique, results: an update and overview of commercially available software. *Eur J Radiol* **82**, 427–434 (2013).
55. Cairns, R. A., Harris, I. S. & Mak, T. W. Regulation of cancer cell metabolism. *Nat. Rev. Cancer* **11**, 85–95 (2011).
56. Wallace, D. C. Mitochondria and cancer. *Nat. Rev. Cancer* **12**, 685–98 (2012).
57. Schumacker, P. T. Reactive oxygen species in cancer cells: live by the sword, die by the sword. *Cancer Cell* **10**, 175–6 (2006).
58. Le, A. *et al.* Tumorigenicity of hypoxic respiring cancer cells revealed by a hypoxia-cell cycle dual reporter. *Proc. Natl. Acad. Sci. U. S. A.* **111**, 12486–91 (2014).
59. Tse, J. R. & Engler, A. J. Preparation of hydrogel substrates with tunable mechanical properties. *Curr Protoc Cell Biol* **Chapter 10**, Unit 10.16 (2010).

Chapter 5: Human Breast Cancer Invasion and Aggression Correlates with ECM Stiffening and Immune Cell Infiltration

L Cassereau¹

In collaboration with: I Acerbi¹, I Dean¹, Q Shi^{2,5}, A Au³, C Park⁴, YY Chen⁵, J Liphardt^{2,5}, ES Hwang⁷

Under the supervision of: VM Weaver^{1,2,8}

¹Center for Bioengineering and Tissue Regeneration, Department of Surgery, UCSF, San Francisco, CA

²Bay Area Physical Sciences Oncology Center.

³Department of Pathology, UCSF, San Francisco, California

⁴Department of Radiation Oncology, UCSF, San Francisco, CA

⁵Department of Pathology, UCSF, San Francisco, CA

⁶Department of Bioengineering, Stanford University, Palo Alto, CA

⁷Department of Surgery, Duke University Comprehensive Cancer Center, Durham, North Carolina, USA

⁸Departments of Anatomy and Bioengineering and Therapeutic Sciences, Eli and Edythe Broad Center of Regeneration Medicine and Stem Cell Research, and UCSF Helen Diller Comprehensive Cancer Center, UCSF, San Francisco, California, USA.

Adapted from previously published work: Cassereau et al., Integrative Biology May 201553

Abstract

Tumors are stiff and data suggest that the extracellular matrix stiffening that correlates with experimental mammary malignancy drives tumor invasion and metastasis. Nevertheless, the relationship between tissue and extracellular matrix stiffness and human breast cancer progression and aggression remains unclear. I undertook a biophysical and biochemical assessment of stromal-epithelial interactions in noninvasive, invasive and normal adjacent human breast tissue and in breast cancers of increasingly aggressive subtype. My analysis revealed that human breast cancer transformation is accompanied by an incremental increase in collagen deposition and a progressive linearization and thickening of interstitial collagen. The linearization of collagen was visualized as an overall increase in tissue birefringence and was most striking at the invasive front of the tumor where the stiffness of the stroma and cellular mechanosignaling were the highest. Amongst breast cancer subtypes we found that the stroma at the invasive region of the more aggressive Basal-like and Her2 tumor subtypes was the most heterogeneous and the stiffest when compared to the less aggressive Luminal A and B subtypes. Intriguingly, we quantified the greatest number of infiltrating macrophages and the highest level of TGF beta signaling within the cells at the invasive front. We also established that stroma stiffness and the level of cellular TGF beta signaling positively correlated with each other and with the number of infiltrating macrophages, which was highest in the more aggressive tumor subtypes. These findings indicate that human breast cancer progression and aggression, collagen linearization and stromal stiffening are linked and implicate tissue inflammation and TGF beta.

Introduction

Human tumors are stiffer than normal tissue and this characteristic has been used to detect and stage cancer^{1,2}. Experimental models indicate that altered tumor mechanics reflects increased interstitial pressure and compression loading, extracellular matrix (ECM) stiffening, and elevated cell contractility and rheology³⁻⁵. Mouse studies further suggest that the aberrant mechanics in cancerous tissue contributes to tumor aggression and compromises treatment efficacy⁷⁻⁹. These findings emphasize the need to characterize the origins of the altered tumor mechanics so that strategies to normalize tissue force can be identified for clinical use.

A major contributor to tumor mechanics is the abundant collagen-rich ECM which is a characteristic trait of many solid cancers¹⁰⁻¹³. This phenotype is particularly evident in human breast cancers which are characterized by a profound desmoplastic response that is accompanied by greater amounts of ECM and increased remodeling and cross-linking. We and others showed that the ECM progressively stiffens in mouse models of mammary cancer and that this stiffened ECM can foster tissue transformation and metastasis^{5,9,14}. Consistently, unconfined compression analysis indicates that as human breast tissue transforms it progressively stiffens and suggests that tumor stiffness reflects a more aggressive cancer^{15,16}. Moreover, micro indentation Atomic Force Microscopy (AFM) scanning studies of human breast and mouse mammary cancers suggests that there may be heterogeneous stiffening of the mammary gland and these works postulate that tumor aggression is inversely correlated with tumor tissue stiffness¹⁷. Thus, the relevance of tumor mechanics and in particular ECM stiffness to human cancer remains unresolved.

In the earliest of breast cancers, linearized thick collagen fibers perpendicular to the tumor boundary in ductal carcinoma in situ (DCIS) lesions promote a higher propensity for progression to invasive breast cancer¹⁸. Moreover, collagen abundance in the primary breast tumor is a significant risk factor for patient mortality¹⁹. Breast cancer patients with high levels of the collagen cross-linker lysyl oxidase (LOX) have a higher probability of developing metastatic lesions^{14,20-23}. Because collagen stiffness increases as a function of concentration, fiber width and with LOX-mediated cross-linking these findings imply that ECM stiffness promotes malignancy and enhances tumor aggression in breast cancer patients⁷. Consistently, higher grade DCIS lesions, which have a higher frequency of malignant transformation often have detectable levels of activated focal adhesion kinase (FAK) and p130Cas; two mechanically-activated kinases²⁴⁻²⁷. Moreover, breast cancer patients with abundant beta 1 integrin and activated FAK demonstrate a poor overall prognosis^{28,29}. However, although these findings argue that breast cancer progression and aggression are in fact linked to ECM stiffening no study to date has systemically linked collagen status, ECM mechanics and mechanosignaling to human breast cancer progression and tumor subtype. My goal here is to interrogate the existence of mechanical heterogeneity of the ECM in human breast tumors and to quantitatively correlate these measurements with ECM architecture and mechanosignaling and to place these measurements within the context of tumor biology.

As detailed in this chapter, I performed a comprehensive biophysical and histological analysis of human breast tissue to assess the biomechanical tissue characteristics relative to tumor progression and subtype. Human breast tumor biopsies with adjacent normal, DCIS and invasive breast cancer were examined to establish correlations between ECM and collagen

architecture, ECM stiffness, mechanosignaling and tumor progression. Human breast biopsy tissues from normal mammary reduction mammoplasty and prophylactic mastectomy tissue with normal histological features were compared to stage matched, breast cancer samples from Luminal A, Luminal B, Her2 and Basal-like invasive breast cancers to establish associations with tumor subtype and aggression. The mechanical properties of the ECM, including ECM architecture and elasticity, were compared with indicators of pro-invasion tumor cell signaling and a tissue inflammatory response. My data reveal, for the first time, that human breast cancer transformation is not only accompanied by a progressive deposition and remodeling of type I collagen and mechanosignaling, but that these phenotypes associate positively with a stiffened "heterogeneous" ECM that is the most rigid at the invasive front of the lesion. Moreover, amongst breast cancer subtypes I observed that the invasive front in the most aggressive subtypes (Basal-like, Her2) are the stiffest and contain cells with the highest mechanosignaling as compared to the less aggressive subtypes (Luminal A, Luminal B). I quantified abundant infiltrating immune cells and the highest tissue levels of TGF beta signaling within the cells at the invasive front; regardless of subtype, and showed that both ECM stiffness and cellular TGF beta signaling correlated positively with the number of infiltrating macrophages. These findings demonstrate a positive association between breast tumor progression and aggression, collagen linearization and tissue mechanics and implicate inflammation and TGF beta in this phenotype.

Results

Human luminal breast cancer progression is accompanied by collagen deposition and remodelling

I conducted a biophysical analysis of interstitial collagens as a function of breast transformation in archived, human breast tumor biopsies (n=20, luminal subtype, stage matched, BRCA mutation negative) containing invasive breast cancer, ductal carcinoma in situ (DCIS) and adjacent normal tissue. Regions with confirmed invasive luminal ductal carcinoma (IDC) breast cancer lesions, DCIS and adjacent normal tissue were identified on H&E stained sections (Figure 5.1; top panel). Quantification of the amount of interstitial collagen surrounding each region in serial sections using by trichrome staining demonstrated that the stromal region bordering the DCIS lesions contained significantly more collagen that increased further in the IDC lesions (Figure 1A; second panel; quantified in Figure 1B; top bar graph). Polarized imaging of picosirius red stain parallel sections revealed that these collagens were assembled into thicker fibers (Figure 5.1A; third panel; quantified in Figure 5.1B; lower bar graph). Second harmonics generation (SHG) imaging using two-photon microscopy additionally revealed that the collagen fibers surrounding the DCIS lesions were more linearized as compared to the collagens associated with the adjacent normal breast tissue and that these linearized collagens appeared thicker in the stroma within the transformed IDC tissue region (Figure 5.1A; fourth panel). Using ImageJ (NIH³⁰) and CT-Fire (LOCI, UW Madison) image processing software to render the collagen topography as imaris images revealed that these linearized collagen fibers were significantly longer in the DCIS stroma and more uniform

in the stroma surrounding the invasive lesions (Figure 5.1A; fifth panel; Figure 5.1C). These findings reveal a progressive increase in the amount and a linear reorganization of interstitial collagen in human breast cancer as the tissue progresses from normal through DCIS to fully invasive IDC.

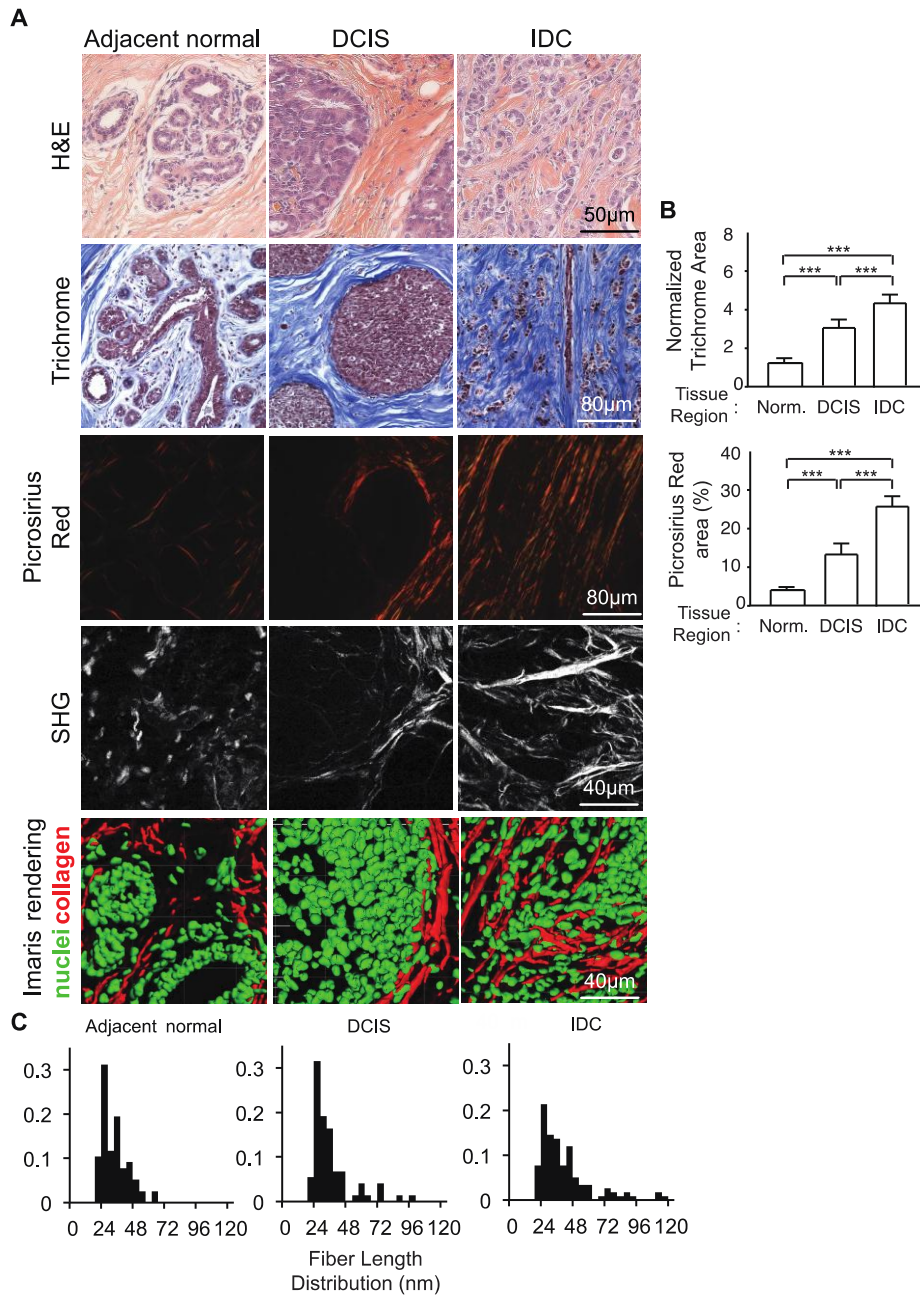


Figure 5.1: Tumor progression correlates with significant ECM remodeling.

(A) Immunohistological staining (H&E, trichrome, picrosirius red, and SHG imaging) of human tumors featuring areas of normal, DCIS and invasive ductal carcinoma (IDC). (B) Quantitative analysis of trichrome and picrosirius red staining. (***) denotes $P < 0.05$ (C) Quantitative analysis of collagen fiber length from second harmonic generation imaging represented as a histogram.

Human breast cancer progression is accompanied by elevated mechanosignaling and an increase in tissue birefringence

Quantitative polarization microscopy (Q-POL) is a method for quantifying the birefringence of a material in a way that is insensitive to the orientation of the sample relative to the microscope^{31,32}. The birefringence of a gel or a matrix is determined by both fiber concentration and fiber alignment. Once materials become aligned, such as cells pulling on the ECM, the birefringence increases. The highest birefringence is generated by dense bundles of aligned fibers. Maps of the retardance reveal areas of ordered and/or concentrated fibrous material, especially ECM components such as collagen. Since Q-POL is a wide-field technique, it can be used to rapidly quantify collagen fiber concentration/alignment in relatively large samples with lateral dimensions of several millimetres³³. Consistent with my PS and SHG analysis, Q-POL imaging of the normal adjacent, DCIS and IDC luminal breast lesions revealed a progressive increase in birefringence of the DCIS regions within the tissue and showed that this increased significantly in the tissue within the invasive lesions; findings that likely reflect the increased orientation of the fibrillar collagens³⁴(Figure 5.2A; top panel; quantified in 5.2B; top bar graphs).

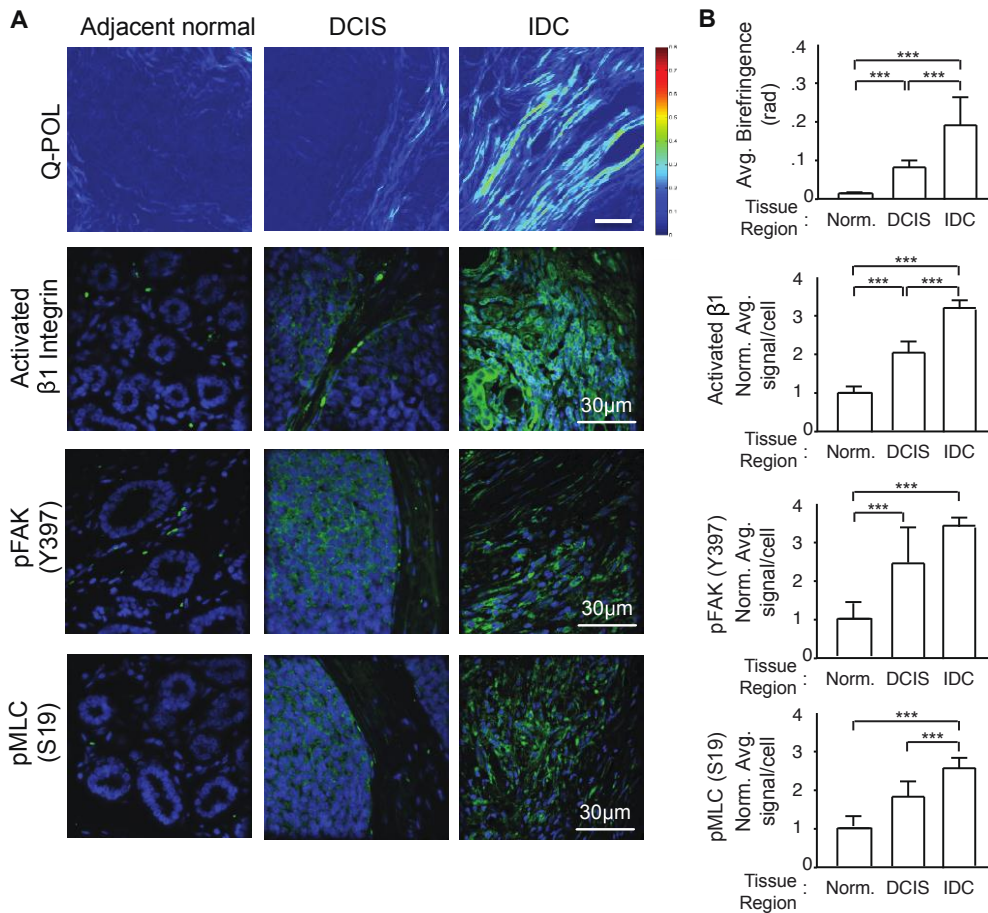


Figure 5.2: Human tumor progression is accompanied by increased stromal density and enhanced mechanosignaling.

(A) SIM-POL and immunofluorescence imaging of human tumor samples. SIM-POL images shown as a heat map of birefringence reflecting increased stromal density, alignment, and stiffness. Immunofluorescence imaging for mechanosignaling in the tumors includes activated beta 1 integrin, pFAK (Y397), and pMLC (S19). (B) Quantification of SIM-POL and immunofluorescence imaging. Immunofluorescence quantified as average signal intensity per cell. Bars represent average of 20 patient samples and error bars represent standard deviation.

(*** denotes $P < 0.05$)

Quantification of immunofluorescence images of the normal adjacent, DCIS and IDC tissue further revealed a progressive and significant increase in total levels of activated beta 1 integrin (activated β 1 integrin), activated FAK (pY397 FAK) and higher cell contractility (pS19 MLC) which all indicate an increase in cellular mechanosignaling (Figure 5.2A; lower three panels; quantified in Figure 5.2B bar graphs)^{9,35}. These findings suggest that the oriented collagen fibers exhibit a higher tensile strength that engages and activates cellular mechanosignaling.

The invasive front of human breast cancers is stiffer

I next assessed the relationship between collagen abundance and orientation and stromal stiffness in IDC specimens. Sections of snap frozen fresh human breast tissue containing luminal IDC lesions were fixed and stained by H&E and subjected to analysis by a pathologist to identify adjacent normal and the invasive front of the tumor (Figure 5.3A; left image). Serial sections of the tissue were then stained with propidium iodide to visualize the nuclei (Figure 5.3A; right image). Using these same sections Q-POL imaging was then used to identify multiple sub regions within the stroma of the tissues lacking birefringence in the adjacent normal and within noninvasive regions surrounding the tumor as well as several additional regions with high birefringence within the IDC invasive front (Figure 5.3B; regions of interest are indicated by a dashed yellow box). I then used nanoscale atomic force microscopy (AFM) mechanical testing to measure the elasticity of the stroma in $90 \times 90 \mu\text{m}^2$ grids within these identified regions and constructed force maps of these areas⁶. I noted a strong association between intense Q-POL birefringence imaging measurements and stromal stiffness; particularly in the

invasive leading edge of the IDC lesions where I quantified up to a 4 fold increase in the average elastic modulus relative to the non-invasive regions and the normal adjacent stroma (Figure 5.3C,D). Importantly, an examination of the distribution of stromal stiffness revealed a dramatic increase in stromal stiffness heterogeneity in the invasive region of the IDC tissue (Figure 5.3E). Thus, while the normal and noninvasive stroma and in the breast tissue of these cancer patients was predominantly around 400Pa; the invasive regions exhibited an elevated mean stiffness primarily due to a higher incidence of discrete, highly stiff regions (>5kPa)..

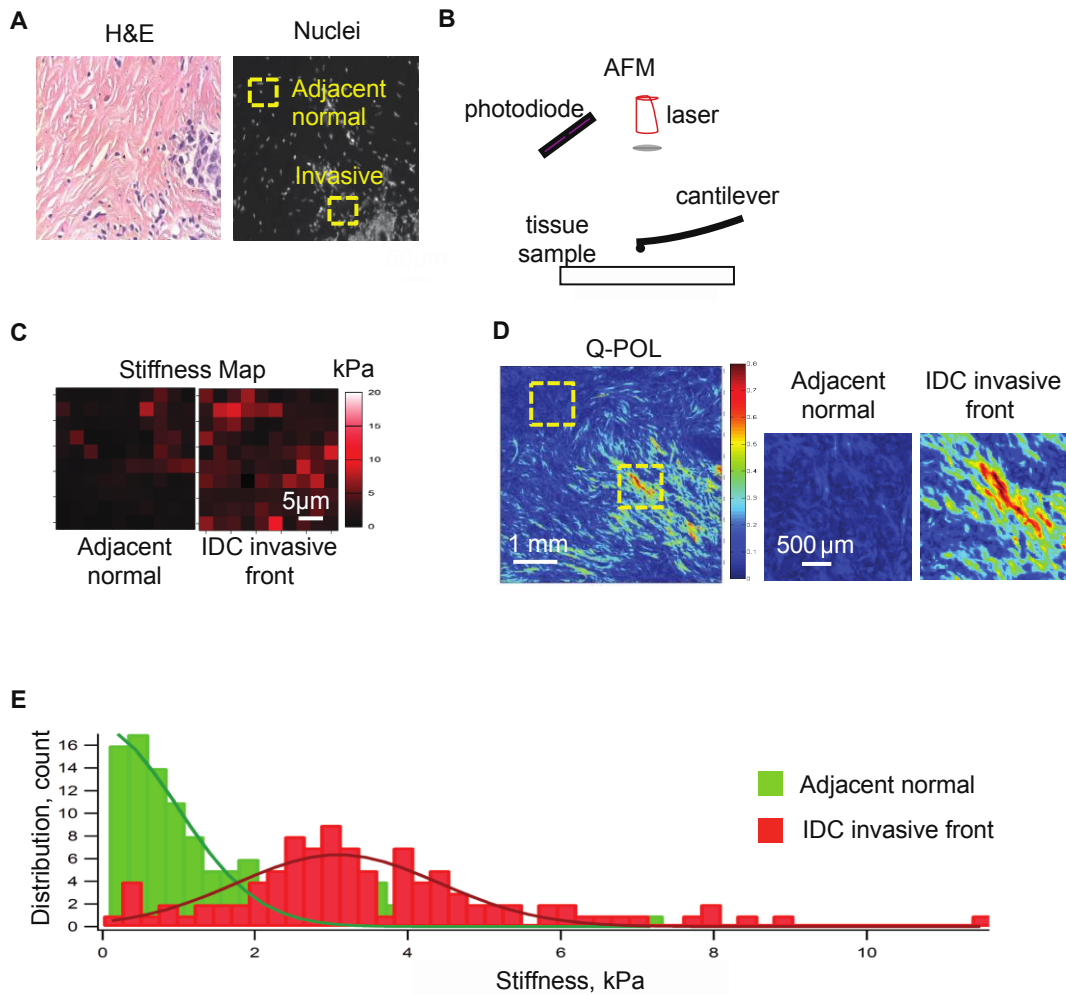


Figure 5.3: ECM remodeling at the tumor invasive front is correlated with increased ECM stiffness.

(A) H&E staining and nuclear immunofluorescence images used to determine regions for atomic force microscopy (AFM) testing comparing tumor invasive front and adjacent healthy tissue. (B) SIM-POL imaging comparing adjacent normal tissue and tumor invasive front to be measured via AFM. (C) AFM force map result represented as a heat map. (D) Histograms of stiffness values from adjacent normal tissue and tumor invasive front

Additionally, I compared the biophysical properties of the tumor invasive front and tumor core (Figure 5.4A-D) and found that the tumor core tissue had less birefringence and was overall less stiff. These findings link collagen orientation and linearization, tissue birefringence and elevated mechanosignaling to stromal stiffness. The data further emphasize the heterogeneity of the ECM and stromal stiffness in breast tumors and indicate that this phenotype is particularly evident at the invasive front of the lesion.

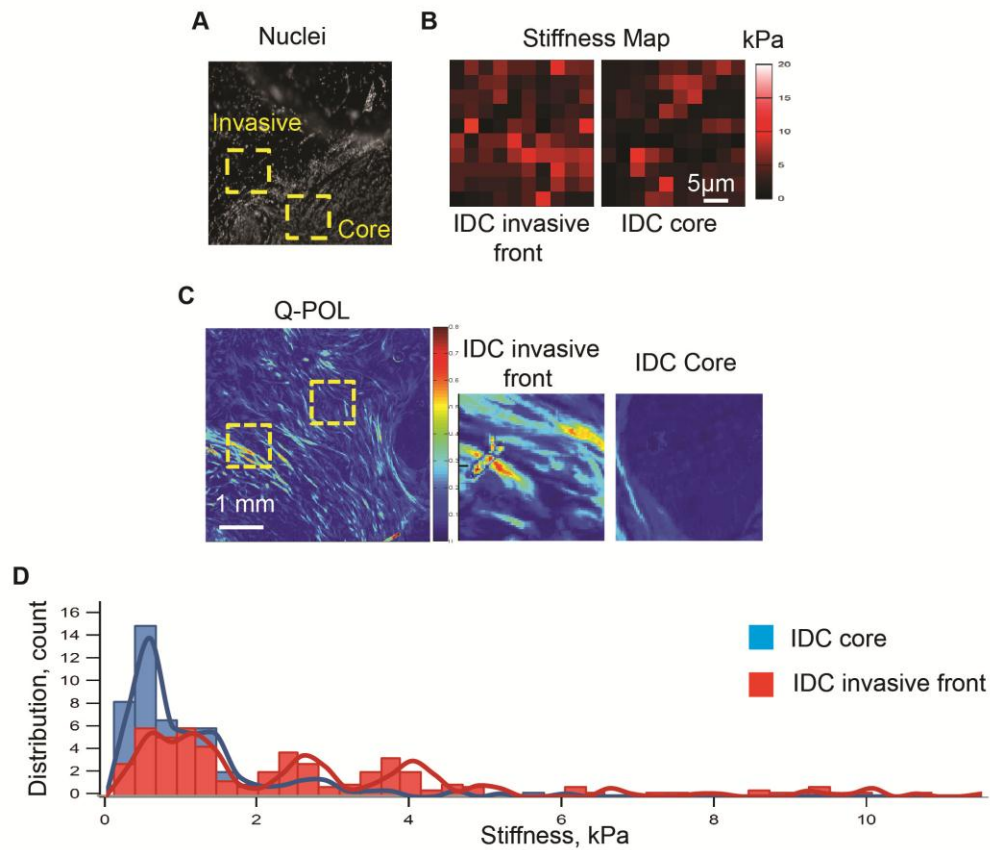


Figure 5.4: ECM remodeling at the tumor invasive front is correlated with increased ECM stiffness.

(A) H&E staining and nuclear immunofluorescence images used to determine regions for atomic force microscopy (AFM) testing comparing tumor invasive front and adjacent healthy tissue. (B) SIM-POL imaging comparing adjacent normal tissue and tumor invasive front to be measured via AFM. (C) AFM force map result represented as a heat map. (D) Histograms of stiffness values from adjacent normal tissue and tumor invasive front.

Human breast cancer progression associates with macrophage infiltration and elevated TGF beta signalling

Human breast cancers have high numbers of infiltrating immune cells and metastasis in experimental models is associated with inflammation and can be inhibited by reducing macrophage recruitment³⁶⁻³⁸. Macrophages secrete a number of soluble factors including such transforming growth factor beta (TGF beta) that stimulate cell migration and induce extracellular matrix deposition, remodeling and cross-linking to stiffen the extracellular stroma^{14,36,39}. Consistently, staining of serial sections of the breast tumor biopsies shown in figures 5.1-5.4 contained high numbers of CD45 positive immune cells (Figure 5.5A; top panel). Interestingly I noted that the CD45 positive immune cells were most abundant within the IDC region of the tissue and that they were particularly concentrated within the invasive front of these lesions where I measured the highest birefringence and stromal stiffness (Figures 5.3-5.4). CD68 staining revealed that a high proportion of the infiltrating immune cells were macrophages localized predominantly within the invasive regions of the IDC (Figure 5.5A; middle panel; quantified in bar graphs at left in B). CD163 staining confirmed these were indeed macrophages and indicated that they were activated³⁶. Moreover, immunohistochemistry analysis indicated that the cells in the invasive front of the tumors had the highest TGF beta activity as assessed by SMAD phosphorylation (Figure 5.5A; bottom panel; quantified in bar graphs at right in B)⁴⁰. These data suggest there likely exist a functional relationship between tissue mechanics, infiltrating macrophages and TGF beta signalling and malignant transformation of human breast cancers.

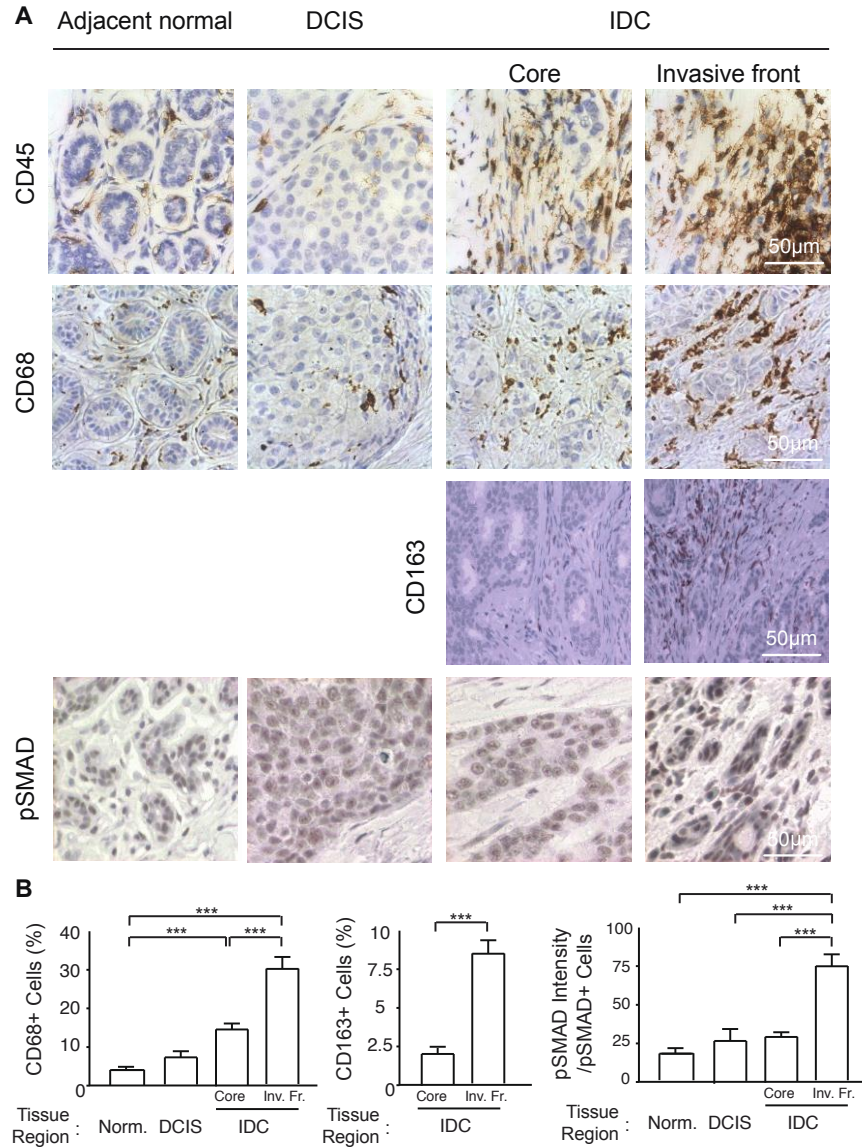


Figure 5.5: ECM remodeling and stiffening with tumor progression correlates with increased immune infiltrate.

(A) Immunohistological staining to assess total immune infiltrate (CD45), macrophage infiltrate (CD68, CD163) and associated tumor cell signaling (pSMAD) comparing healthy, DCIS and IDC tissue. IDC tissue analysis was broken down further comparing the tumor invasive front and the tumor core. (B) Quantification of CD68+ and CD163+ relative to all cells, and quantification of pSMAD signaling assessed as pSMAD staining intensity per pSMAD+ cell. (***) denotes $P < .05$.

Tissue mechanics and collagen linearization associate with human breast cancer aggression

To determine if there is a relationship between tumor aggression and tissue mechanics I examined stage and size matched, untreated, human breast cancer biopsies representing four pathologically-confirmed subtypes classified as progressively aggressive including: least aggressive luminal A, luminal B, Her2+ and the most aggressive, basal-like triple negative (TNBC) (n=5 patients/subtype, stage matched, BRCA mutation negative)⁴¹. The invasive front of each lesion was identified in H&E stained tissue sections (Figure 5.6A; top panel). Polarized imaging of picosirius red stained tissue revealed the most abundant fibrillar collagens were present at the invasive front of the Her2+ and TNBCs (Figure 5; second panel; quantified in top bar graphs shown in Figure 5B). SHG imaging revealed that these collagen fibers were more linearized and thicker in the more aggressive tumor subtypes (Figure 5.6A; third panel) a finding that was confirmed by the significant increase in tissue birefringence (Q-POL) quantified in the Her2+ and TNBCs (Figure 5.6A; bottom panel; quantified in lower bar graphs shown in Figure 5.6B). Moreover, AFM indentation indicated that the invasive front in the higher grade Her2+ and TNBCs were significantly stiffer than the less aggressive luminal breast tumors (Figure 5.6C)

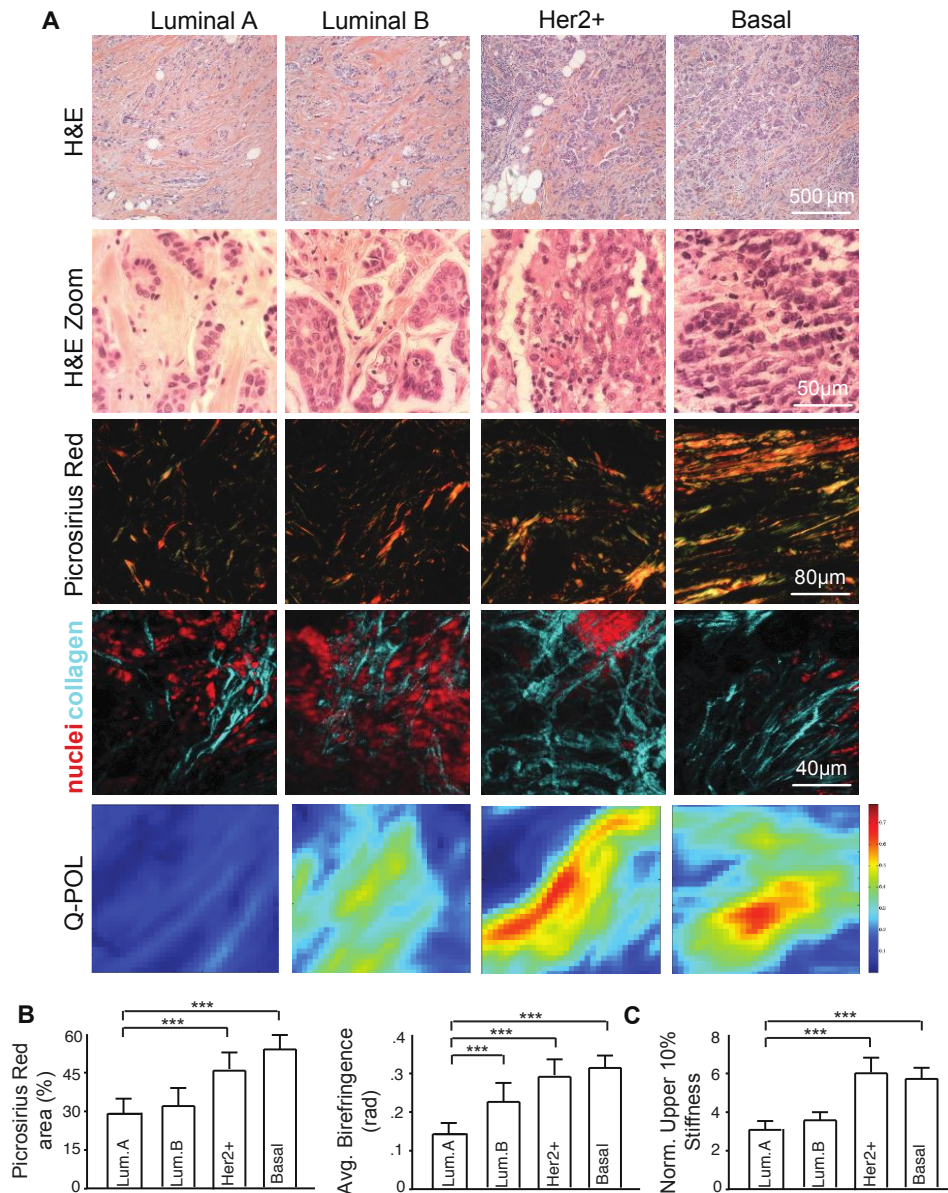


Figure 5.6: Human IDC subtype influences ECM remodeling and mechanics.

(A) Immunohistological (H&E, picrosirius red and SHG) staining of human tumor samples (Luminal A, Luminal B, Her2+ and Basal). (B) Quantification of picrosirius red area and SIM-POL imaging as a measure of collagen density, tissue birefringence. (C) Quantification of AFM measurements of human tissue samples. The upper 10% of stiffness values are shown and normalized to measurements from healthy control tissue. (***) denotes $P < 0.05$.

Furthermore, analysis of immunofluorescence images of the invasive front of the luminal A, luminal B, Her2+ and TNBC biopsied tissue revealed that the cells within the more aggressive tumor subtypes (Her2+, TNBC) had the highest levels of activated $\beta 1$ integrin (Activated $\beta 1$ integrin) and FAK (pY397 FAK) and were more contractile (pS19 MLC) indicating they were likely more mechanically activated (Figure 5.7A; images quantified in bar graphs shown in B)^{9,35}. Consistently, the higher grade tumor subtypes Her2+ and TNBC both showed much higher nuclear levels of the mechanically-activated factor Yorkie Associated Protein (YAP) than the lower grade luminal A/B tumors (Figure 5.7C; quantified in the bar graphs shown in Figure 5.7D)⁴²⁻⁴⁴. These findings confirm my earlier results which emphasize that there exists a positive correlation between stromal stiffness and the presence of linearized collagen fibers. The data also indicate that tissue mechanics and extracellular matrix modeling and collagen linearization reflect tumor aggression in human breast cancer patients.

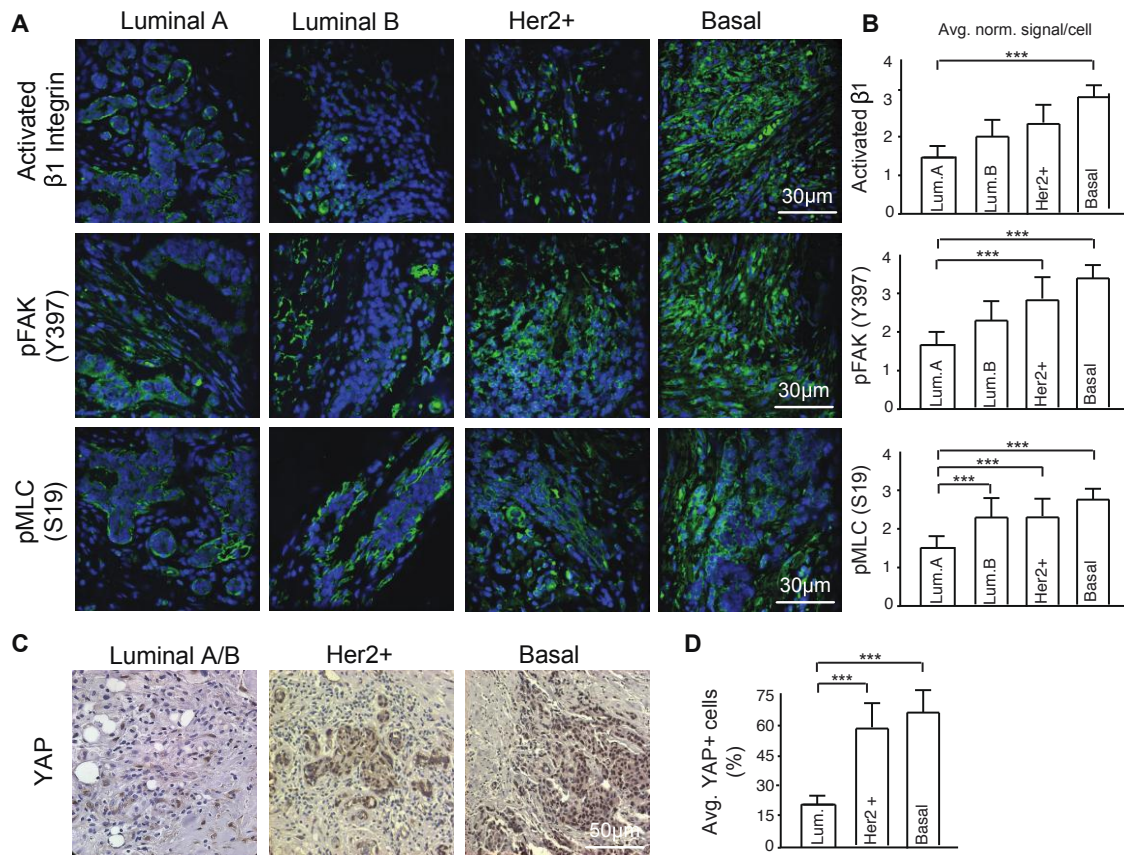


Figure 5.7: ECM remodeling associated with each subtype influences subsequent mechanosignaling.

(A) Immunofluorescence imaging for mechanosignaling in the tumors including activated beta 1 integrin, pFAK (Y397), and pMLC (S19). (B) Quantification of immunofluorescence as average signal intensity per cell. (C) Immunohistological staining for YAP. Luminal A and Luminal B tumors assessed as one group due to lack of differences in YAP intensity. (D) Quantification of YAP staining as average percentage of nuclear YAP+ cells per patient within each subtype. Bars represent an average of 5 patient samples per subtype and error bars represent standard deviation. (***) denotes $P < 0.05$)

Human breast cancer aggression correlates with a stiffer, more heterogeneous stroma and higher levels of infiltrating macrophages

Nanoscale AFM testing of the distribution and the magnitude of stromal stiffness at the invasive front of each breast tumor subtype revealed a striking increase in heterogeneity as a function of tumor aggressiveness. Thus, while AFM indentation revealed that acquisition of an invasive phenotype is consistently accompanied by a significant shift towards higher stiffness relative to prophylaxis tissue (Representative AFM indentation maps shown in Figure 5.8A), the distribution of the stromal stiffening was found to increase dramatically with tumor aggression (Figure 5.8B compare Luminal A to Luminal B to Her2+ to Basal-like (TNBC)). Thus, the two more aggressive breast tumor subtypes, Her2+ and TNBC had a much wider distribution of stiffness measurements and a greater skewing towards high values (> 5kPa).

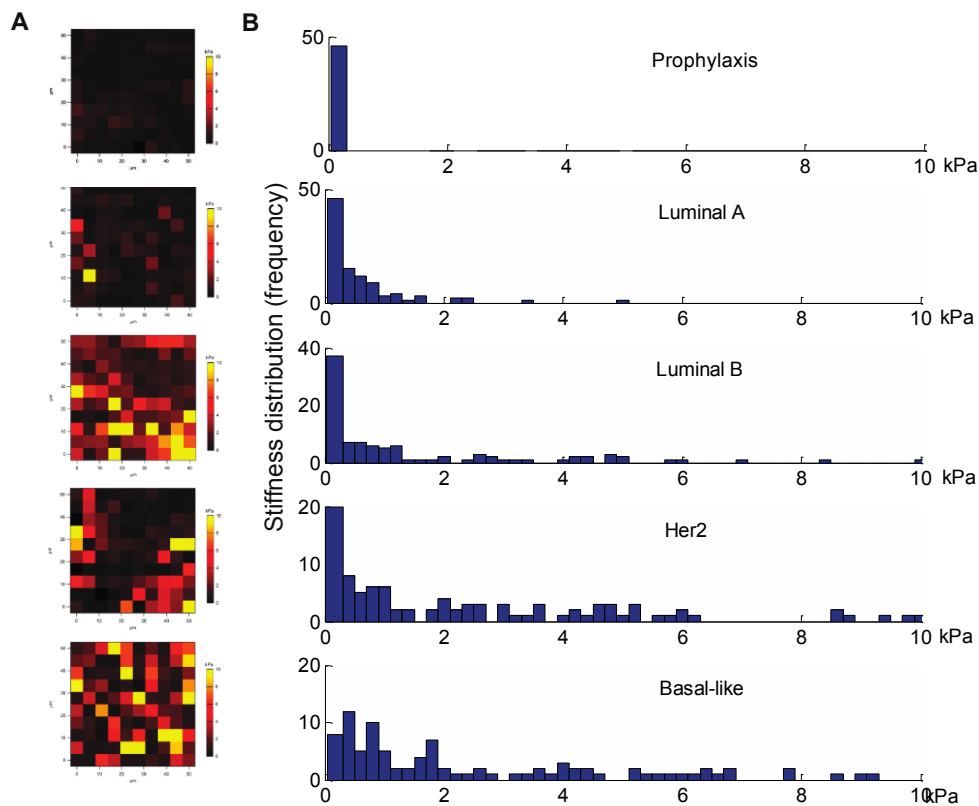


Figure 5.8: AFM testing of human tissue reveals increased mechanical heterogeneity within the more aggressive subtypes.

(A) Sample histograms of AFM mechanical measurements for human prophyllaxis tissue and human tumor tissue of each subtype. Statistical significance was determined via a Wilcoxon Rank Sum Test, with all subtypes showing statistically significant differences relative to prophyllaxis tissue ($p < 0.05$). (B) Atomic force microscopy force map result represented as a heat map

Interestingly, immunohistochemical (IHC) staining revealed that the skewed distribution towards high ECM stiffness values found in the high aggressive cancer subtypes is mirrored by an increased number of infiltrating immune cells (CD45+ cells) and specifically macrophages (CD68+ cells) that were highly concentrated at the invasive front of each of the lesions (Figure 5.9A; first two panels; CD68 + cell quantification shown in bar graphs shown at left in Figure 8B). Moreover, IHC for activated SMAD (pSMAD; a marker of TGF beta signaling in the cell⁴⁰) revealed significantly elevated TGF beta signaling in the cells within the invasive front of the more aggressive subtype (Figure 8A; bottom panel; quantified below in Figure 5.9B right bar graphs). Indeed, I observed a significant correlation between the number of infiltrating macrophages and the stiffness of the invasive tumor stroma and between the number of infiltrating macrophages and the intensity of TGF beta signaling in the cells at the invasive front of these human breast tumors (Figure 5.9C). These results show an association between tissue mechanics and inflammation and suggest they potentially cooperate to drive breast tumor aggression.

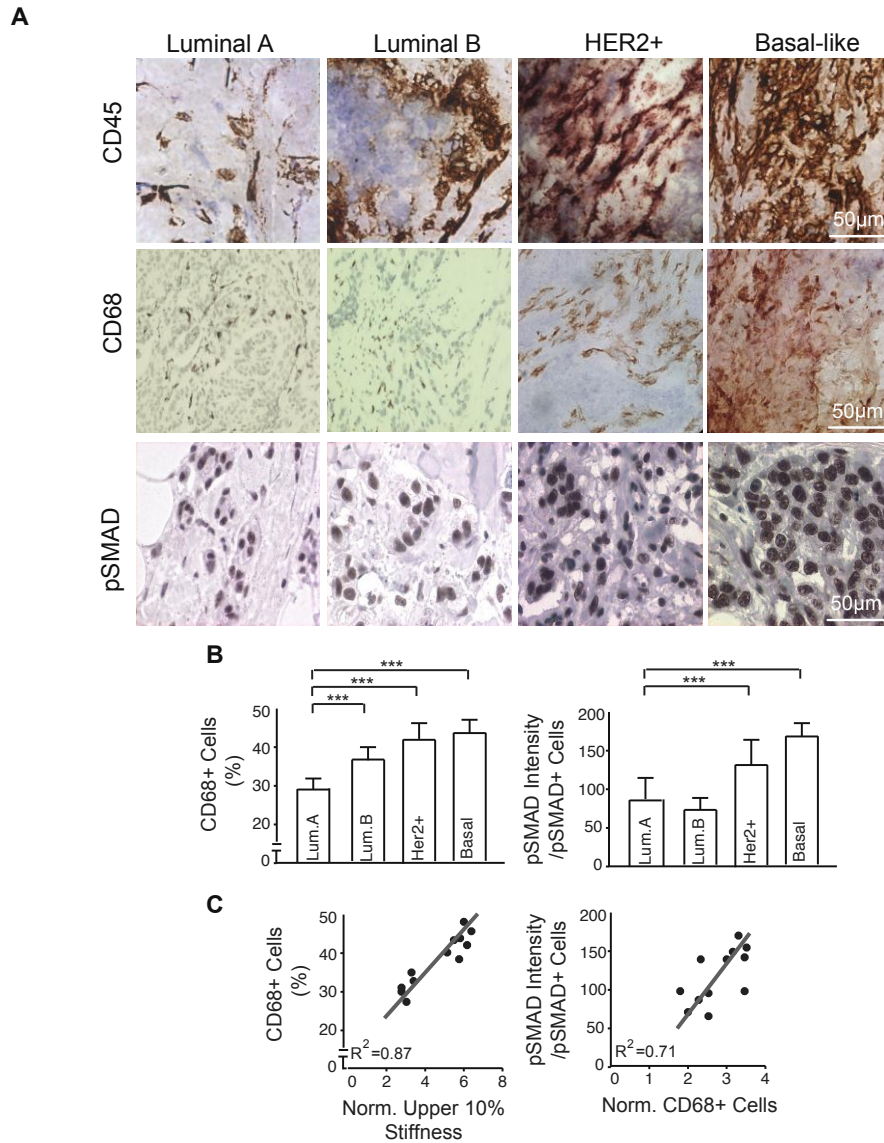


Figure 5.9: Tumor aggression and increased immune infiltrate correlates with ECM stiffness.

(A) Immunohistological staining to assess immune infiltrate (CD45), macrophage infiltrate (CD68), and associated tumor cell signaling (pSMAD) comparing breast cancer human subtype.

(B) Quantification of CD68+ relative to all cells and of pSMAD signaling assessed as pSMAD staining intensity per pSMAD+ cell.

(C) Correlation curves comparing ECM stiffness and macrophage infiltrate and macrophage infiltrate and pSMAD signaling. Curve fit via linear regression model (***) denotes $P < 0.05$

Discussion

Here, I demonstrate a correlation between the mechanical properties of the ECM, immune cell infiltrate, tumor grade, subtype and aggression in human breast cancer samples. Indeed, I found that the transition from non-malignant tissue to an invasive ductal carcinoma corresponds with significant collagen deposition, linearization and bundling which leads to a stiffening of the ECM. Subsequently, these mechanical alterations parallel enhanced activation of mechanically-sensitive signaling pathways associated with focal adhesions, YAP and growth factor receptor signaling. Accompanying this profound ECM remodeling and stiffening were significant immune cell infiltrate, predominantly comprised of macrophages. I found this influx of macrophages correlates with upregulated SMAD signaling in tumors, suggesting elevated TGF β signaling. This presents a possible mechanistic explanation for the fibrosis and stiffening of the ECM via TGF β -stimulated production of collagen and the collagen crosslinking enzyme lysyl oxidase (LOX)⁴⁵. Interestingly, I also found that the relationship between ECM stiffness, immune infiltrate and tumor progression also depends on tumor subtype. Compared to Her2 and basal-like cancers, luminal breast cancers displayed less ECM remodeling and stiffening, and consistently less immune infiltrate and pro-invasion signaling. Further investigation into a causal relationship between ECM stiffening and the more aggressive breast cancer subtypes would present a new set of potential prognostic parameters.

Current clinical techniques interrogate tissue stiffness as a passive feature to detect cancer⁴⁶⁻⁴⁸. Yet, experimental models contend that tissue mechanics plays more than just a passenger role in tumor progression^{9,35,49,50}. Amongst breast cancer subtypes, I found that the ECM at the invasive regions of the more aggressive Basal-like and Her2 tumor subtypes was the

most heterogeneous and the stiffest when compared to the less aggressive Luminal A and B subtypes. While shear wave elastography (SWE) yields quantitative information capable of discerning benign and malignant lesions⁵¹, my study demonstrates the need for region-specific measurements in deconstructing breast cancer mechanosignaling. The topographical variations in the mechanical landscape of the collagen-rich ECM could not have been detected by techniques such as SWE.

Interestingly, the mechanical heterogeneity within tumors observed in my study parallels the genomic intratumor heterogeneity observed in human cancers⁵². I found that geographically-distinct regions of the same tumor displayed different constituents, architectures and mechanical properties of the ECM. These results are consistent with previous publications demonstrating increased tumor stiffness relative to healthy tissue and further demonstrate the necessity for nanoscale mechanical testing and imaging to observe the heterogeneous structures and features contributing to tumor stiffness. My findings, combined with evidence that multiple measures of heterogeneity are associated with poor patient prognosis, suggest the need for future exploration of how the resident stromal and immune environments influence tumor progression and fate. Correlating local mechanical measurements with regional histopathological analyses may provide the most efficacious approach to relating tumor behavior with ECM mechanics.

Experimental Methods

Human Breast Tissue. Fresh human breast tissue samples from prophylaxis mastectomy or breast tumor mastectomy were either embedded in OCT (Tissue-Tek) aqueous embedding compound within a disposable plastic base mold (Fisher) and were snap frozen by direct immersion into liquid nitrogen and kept at -80 degrees until cryosectioning for analysis, or formalin fixed and paraffin-embedded. All human breast tissue samples were prospectively collected from patients undergoing surgery at UCSF or Duke University Medical Center between 2010 and 2014. The selected samples were de-identified, stored and analyzed according to the procedures described in Institutional Review Board Protocol #10-03832 and #10-05046, approved by the UCSF Committee of Human Resources and the Duke IRB (Pro00034242).

Tissue preparation for AFM measurements of ECM stiffness

Human breast tissue samples were analyzed following cryopreservation. Frozen tissue blocks were then cut into 20 μm sections using disposable low profile microtome blades (Leica, 819) on a cryostat (Leica, CM1900-3-1). Prior to the AFM measurement, each section was fast thawed by immersion in PBS at thawed at room temperature. The samples were maintained in proteinase inhibitor in PBS (Protease Inhibitor Cocktail Roche Diagnostics, 11836170001), with Propidium Iodide (SIGMA P4170, 20 $\mu\text{g}/\text{ml}$) during the AFM session. Five patient's samples for each breast cancer subtype were used for AFM quantification of Young's elastic modulus of the cancer-associated stroma.

AFM measurements of ECM stiffness on tissue sections

All AFM indentations were performed using an MFP3D-BIO inverted optical AFM (Asylum Research) mounted on a Nikon TE2000-U inverted fluorescent microscope, as previously

described ⁵. Briefly, I used silicon nitride cantilevers with spring constant of 0.06 N/m with borosilicate glass spherical tip with 5 μm in diameter (Novascan Tech). The cantilever was calibrated using the thermal oscillation method prior to each experiment. Samples were indented at 20 $\mu\text{m/s}$ loading rate, with a maximum force of 2 nN. Ten AFM force maps were typically obtained on each sample, each map as a 50x50 μm raster series of indentations utilizing the FMAP function of the IGOR PRO build supplied by Asylum Research. The Hertz model was used to determine the elastic properties of the tissue (E1). Tissue samples were assumed to be incompressible and a Poisson's ratio of 0.5 was used in the calculation of the Young's elastic modulus.

Two-photon microscopy image acquisition and analysis

For two-photon imaging 20 μm fresh tissue sections were fixed post-AFM indentation in 4% neutral buffered formalin, and mounted with Permount Mounting Medium. I used custom resonant-scanning instruments based on published designs containing a five-PMT array (Hamamatsu, C7950) operating at video rate.² The setup was used with two channel Qultaneous video rate acquisition via two PMT detectors and an excitation laser (2W MaiTai Ti-Sapphire laser, 710-920nm excitation range). Second harmonics imaging was performed on a Prairie Technology Ultima System attached to an Olympus BX- 51 fixed stage microscope equipped with a 25 \times (NA 1.05) water immersion objective. Tissue samples were exposed to polarized laser light at a wavelength of 830nm and emitted light was separated with a filter set (short pass filter, 720nm; dichroic mirror, 495nm; band pass filter, 475/40nm). Images of x-y planes of 284 by 284 μm at a resolution of 0.656 $\mu\text{m}/\text{pixel}$ were captured using Micro-Manager Open Source Microscopy Software (Micro-Manager) in at least 3 locations on each human

tissue sample. Quantification of collagen fibers was achieved by setting a minimal threshold in the second harmonic signal. The threshold was maintained for all images across all conditions. The area of regions that was covered by the minimal threshold was calculated and 3 images per sample were averaged together (Image J, Image Processing and Analysis in Java). Collagen fiber diameters data were visualized and analyzed using Imaris (Bitplane AG) and MATLAB (MathWorks). Statistical analysis was performed using Prism software (GraphPad Software, Inc.).

Q-POL image acquisition and analysis

Retardance maps of tissue samples were obtained using custom-written Matlab program to analyze the images acquired by an Olympus microscope (IX81) with a 10x objective as described previously (Qui et al., PNAS 2014). Briefly the light (632nm LED) is incident on the sample after passing through a linear top polarizer. After the sample, there is a circular polarizer consisting of a quarter waveplate and a linear polarizer with relative alignment angle of $\pi/4$. Rotation of the top polarizer (rotation angle ϑ) results in a sinusoidal modulation of the light intensity at each pixel^{31,32}:

$$I(\theta) = \frac{I_0}{2} (1 + \sin \delta \cdot \sin(2\theta + 2\phi)) \quad (1)$$

where, ϕ is the principal axis and δ is the phase retardance (in radian) defined by

$$\delta = \frac{2\pi}{\lambda} \cdot \Delta n \cdot d, \quad (2)$$

The polarizer stage steps in 4° per step with a total of 200° . The light intensity modulation of each pixel on the image was fitted with equation 1 to generate the retardance map.

Picrosirius Red Staining and quantification. Flash frozen OCT embedded frozen tissues were crio-sectioned at $5 \mu\text{m}$, fixed in 4% neutral buffered formalin and stained using 0.1% picrosirius

red (Direct Red 80, Sigma) and counterstained with Weigert's hematoxin, as previously described³⁴. Polarized light images were acquired using an Olympus IX81 microscope fitted with an analyzer (U-ANT) and polarizer (U-POT, Olympus) oriented parallel and orthogonal to each other. Images were quantified using ImageJ. Briefly, a minimal intensity threshold was used to eliminate background and then fiber density was measured as image % area coverage. For analysis of tumor progression samples 5 images per tissue region (normal, DCIS, IDC) were taken for all 20 patients. Results per tissue region type were then pooled and averaged and normalized to adjacent normal tissue values. For analysis of breast cancer subtypes, 10 images were taken per patient with 5 patients per subtype. Results for each subtype were pooled and averaged and then normalized to data from prophylaxis tissue serving as a non-tumor control.

Trichrome Staining and quantification. Paraffin-embedded samples were sectioned at 5 μm and Masson's trichrome staining was performed following the optimized protocol (<https://www.bcm.edu/research/labs/jeffrey-rosen/protocols>). For quantitative morphometric analysis, ten sections of trichrome slides were imaged with color camera, using an Olympus IX81 microscope and bright field light. Three fields acquired in each of the histological regions of defined by my pathologist (Dr. YY Chen). Each RGB image was subsequently analyzed using Image J (version 1.32j) software (National Institutes of Health, USA <http://rsb.info.nih.gov/ij/>). The amount of fibrosis was then estimated from the RGB images with a macro written by the authors (IA) by converting pixels of the image with substantially greater (> 1.5) blue than red intensity ratio, and calculating the area over the threshold (Supplemental Figure I).

Immunohistochemistry staining and quantification

Antibodies and Reagents. Antibodies were as follows: CD45 (antibody clone X16/99 from Leica) CD68(antibody clone 514H12 from Leica), YAP (Rabbit Cell Signaling), pSMAD (Rabbit Cell Signaling). Immunohistochemistry staining and imaging of FFPE tissue sections was performed as recently described.

Quantification. pSMAD intensity was quantified as the integrated density divided by the total number of positive pSMAD-stained cancer cells. The integrated density was measured using ImageJ software (NIH). The integrated density was divided by the total number of positive pSMAD-stained cancer cells. Average YAP+ cells were quantified by the number of nuclear-stained YAP+ cancer cells divided the total number of cancer cells. The ratio of positive nuclear-stained YAP cells divided by the total number of cells was multiplied by 100 to generate a percentage.

Immunofluorescence Staining and quantification

Antibodies and Reagents. Antibodies were as follows: activated β 1 integrin (Rat R&D Systems); FAKpY397 (Rabbit Invitrogen); Phospho Akt Substrate (Rabbit Cell Signaling); MLCpS19 (Rabbit Cell Signaling) secondary AlexaFluor goat anti-mouse, anti-rabbit, and anti-rat (488 conjugates) and DAPI (Sigma). Immunofluorescence staining and imaging of FFPE tissue sections was performed as recently described.

Quantification. Images were quantified in ImageJ. Briefly a minimal intensity threshold for real signal based on the max intensity of secondary only controls was used and then signal intensity per cell was quantified as image fluorescent intensity integrated density divided by the total number of cells in the image. For analysis of tumor progression samples 5 images per tissue region (normal, DCIS, IDC) were taken for all 20 patients. Results per tissue region type were

then pooled and averaged and normalized to adjacent normal tissue values. For analysis of breast cancer subtypes, 10 images were taken per patient with 5 patients per subtype. Results for each subtype were pooled and averaged and then normalized to data from prophylaxis tissue serving as a non-tumor control.

Statistics

Statistical significance comparing different histological regions representing tumor progression within the same patient was assessed either using a two-tailed paired Mann-Whitney non-parametric test or ANOVA. Statistical significance comparing tissue samples from different tumor subtypes was assessed either using a two-tailed unpaired Mann-Whitney non-parametric test, Wilcoxon Rank Sum Test, or ANOVA as appropriate. Means are presented \pm standard deviation of multiple measurements and statistical significance was considered at $P < 0.05$.

Acknowledgements

I thank the Dr. Janna Mouw and Dr. Michael Pickup as well as all members of the Weaver lab for helpful discussions and the tissue pathology cores at UCSF for support of tissue sectioning and staining. This work was supported by Susan G. Komen Postdoctoral Fellowship PDF12230246 (I.A.), ME National Institutes of Health grant NCI F31 CA183255 (L.C.), ARCS Foundation Fellowship (L.C.), ME National Institutes of Health grant T32 CA108462-11 (I.D.), ME Department of Defense Breast Cancer Research Program (DOD BCRP) grant W81XWH-05-1-0330 and W81XWH-13-1-0216 (V.M.W.), ME National Institutes of Health (NIH) NCI grants R01 CA085492 and U01 ES019458 (V.M.W.), NIH NCI grant U54 CA143836 (V.M.W. and J.L.), NIH NCI grant R01 CA174929 (V.M.W. and C.P.) and Susan G. Komen grant KG110560PP (V.M.W. and E.S.H.).

Works Cited

- [1] J. H. Youk, E. J. Son, H. M. Gweon, H. Kim, Y. J. Park and J. -A. Kim, "Comparison of strain and shear wave elastography for the differentiation of benign from malignant breast lesions, combined with B-mode ultrasonography: qualitative and quantitative assessments", *Ultrasound Med Biol*, 40, no. 10, p. . 2336-44, 2014.
- [2] J. M. Chang, W. K. Moon, N. Cho, A. Yi, H. R. Koo, W. Han, D. -Y. Noh, H. -G. Moon and S. J. Kim, "Clinical application of shear wave elastography (SWE) in the diagnosis of benign and malignant breast diseases", *Breast Cancer Res Treat*, 129, no. 1, p. . 89-97, 2011.
- [3] P. P. Provenzano, C. Cuevas, A. E. Chang, V. K. Goel, D. D. Von Hoff and S. R. Hingorani, "Enzymatic targeting of the stroma ablates physical barriers to treatment of pancreatic ductal adenocarcinoma", *Cancer Cell*, 21, no. 3, p. . 418-29, 2012.
- [4] J. M. Tse, G. Cheng, J. A. Tyrrell, S. A. Wilcox-Adelman, Y. Boucher, R. K. Jain and L. L. Munn, "Mechanical compression drives cancer cells toward invasive phenotype", *Proc Natl Acad Sci U S A*, 109, no. 3, p. . 911-5, 2012.
- [5] M. S. Samuel, J. I. Lopez, E. J. McGhee, D. R. Croft, D. Strachan, P. Timpson, J. Munro, E. Schröder, J. Zhou, V. G. Brunton, N. Barker, H. Clevers, O. J. Sansom, K. I. Anderson, V. M. Weaver and M. F. Olson, "Actomyosin-mediated cellular tension drives increased tissue stiffness and β -catenin activation to induce epidermal hyperplasia and tumor growth", *Cancer Cell*, 19, no. 5, p. . 776-91, 2011.
- [5] J. I. Lopez, I. Kang, W. -K. You, D. M. McDonald and V. M. Weaver, "In situ force mapping of mammary gland transformation", *Integr Biol (Camb)*, 3, no. 9, p. . 910-21, 2011.

- [7] H. F. Dvorak, V. M. Weaver, T. D. Tlsty and G. Bergers, "Tumor microenvironment and progression", *J Surg Oncol*, 103, no. 5, p. . 468-74, 2011.
- [8] P. Lu, K. Takai, V. M. Weaver and Z. Werb, "Extracellular matrix degradation and remodeling in development and disease", *Cold Spring Harb Perspect Biol*, 3, no. 12, 2011.
- [9] K. R. Levental, H. Yu, L. Kass, J. N. Lakins, M. Egeblad, J. T. Erler, S. F. T. Fong, K. Csiszar, A. Giaccia, W. Weninger, M. Yamauchi, D. L. Gasser and V. M. Weaver, "Matrix crosslinking forces tumor progression by enhancing integrin signaling", *Cell*, 139, no. 5, p. . 891-906, 2009.
- [10] Z. Werb, C. J. Simpson, C. M. Alexander, N. Thomasset, L. R. Lund, A. MacAuley, J. Ashkenas and M. J. Bissell, "Extracellular matrix remodeling and the regulation of epithelial-stromal interactions during differentiation and involution", *Kidney Int Suppl*, 54, no., p. . S68-74, 1996.
- [11] P. J. Keely, "Mechanisms by which the extracellular matrix and integrin signaling act to regulate the switch between tumor suppression and tumor promotion", *J Mammary Gland Biol Neoplasia*, 16, no. 3, p. . 205-19, 2011.
- [12] T. Hasebe, "Tumor-stromal interactions in breast tumor progression--significance of histological heterogeneity of tumor-stromal fibroblasts", *Expert Opin Ther Targets*, 17, no. 4, p. . 449-60, 2013.
- [13] J. A. Rudnick and C. Kuperwasser, "Stromal biomarkers in breast cancer development and progression", *Clin Exp Metastasis*, 29, no. 7, p. . 663-72, 2012.
- [14] M. W. Pickup, H. Laklai, I. Acerbi, P. Owens, A. E. Gorska, A. Chytil, M. Aakre, V. M. Weaver and H. L. Moses, "Stromally derived lysyl oxidase promotes metastasis of transforming growth factor- β -deficient mouse mammary carcinomas", *Cancer Res*, 73, no. 17, p. . 5336-46, 2013.

- [15] A. Samani, J. Bishop, C. Luginbuhl and D. B. Plewes, "Measuring the elastic modulus of ex vivo small tissue samples", *Phys Med Biol*, 48, no. 14, p. . 2183-98, 2003.
- [16] A. Samani, J. Zubovits and D. Plewes, "Elastic moduli of normal and pathological human breast tissues: an inversion-technique-based investigation of 169 samples", *Phys Med Biol*, 52, no. 5, p. . 1565-76, 2007.
- [17] M. Plodinec, M. Loparic, C. A. Monnier, E. C. Obermann, R. Zanetti-Dallenbach, P. Oertle, J. T. Hyotyla, U. Aebi, M. Bentires-Alj, R. Y. H. Lim and C. -A. Schoenenberger, "The nanomechanical signature of breast cancer", *Nat Nanotechnol*, 7, no. 11, p. . 757-65, 2012.
- [18] M. W. Conklin, J. C. Eickhoff, K. M. Ricking, C. A. Pehlke, K. W. Eliceiri, P. P. Provenzano, A. Friedl and P. J. Keely, "Aligned collagen is a prognostic signature for survival in human breast carcinoma", *Am J Pathol*, 178, no. 3, p. . 1221-32, 2011.
- [19] T. Hasebe, H. Tsuda, Y. Tsubono, S. Imoto and K. Mukai, "Fibrotic focus in invasive ductal carcinoma of the breast: a histopathological prognostic parameter for tumor recurrence and tumor death within three years after the initial operation", *Jpn J Cancer Res*, 88, no. 5, p. . 590-9, 1997.
- [20] J. T. Erler and V. M. Weaver, "Three-dimensional context regulation of metastasis", *Clin Exp Metastasis*, 26, no. 1, p. . 35-49, 2009.
- [21] J. T. Erler and A. J. Giaccia, "Lysyl oxidase mediates hypoxic control of metastasis", *Cancer Res*, 66, no. 21, p. . 10238-41, 2006.
- [22] M. Decitre, C. Gleyzal, M. Raccurt, S. Peyrol, E. Aubert-Foucher, K. Csiszar and P. Sommer, "Lysyl oxidase-like protein localizes to sites of de novo fibrinogenesis in fibrosis and in the early stromal reaction of ductal breast carcinomas", *Lab Invest*, 78, no. 2, p. . 143-51, 1998.

- [23] G. L. Semenza, "Cancer-stromal cell interactions mediated by hypoxia-inducible factors promote angiogenesis, lymphangiogenesis, and metastasis", *Oncogene*, 32, no. 35, p. . 4057-63, 2013.
- [24] S. van der Flier, A. Brinkman, M. P. Look, E. M. Kok, M. E. Meijer-van Gelder, J. G. Klijn, L. C. Dorssers and J. A. Foekens, "Bcar1/p130Cas protein and primary breast cancer: prognosis and response to tamoxifen treatment", *J Natl Cancer Inst*, 92, no. 2, p. . 120-7, 2000.
- [25] G. Tornillo, B. Bisaro, M. D. P. Camacho-Leal, M. Galiè, P. Provero, P. Di Stefano, E. Turco, P. Defilippi and S. Cabodi, "p130Cas promotes invasiveness of three-dimensional ErbB2-transformed mammary acinar structures by enhanced activation of mTOR/p70S6K and Rac1", *Eur J Cell Biol*, 90, no. 2-3, p. . 237-48, 2011.
- [26] M. H. Oktay, K. Oktay, D. Hamele-Bena, A. Buyuk and L. G. Koss, "Focal adhesion kinase as a marker of malignant phenotype in breast and cervical carcinomas", *Hum Pathol*, 34, no. 3, p. . 240-5, 2003.
- [27] M. D. Planas-Silva, R. D. Bruggeman, R. T. Grenko and J. Stanley Smith, "Role of c-Src and focal adhesion kinase in progression and metastasis of estrogen receptor-positive breast cancer", *Biochem Biophys Res Commun*, 341, no. 1, p. . 73-81, 2006.
- [28] D. Barkan and A. F. Chambers, " β 1-integrin: a potential therapeutic target in the battle against cancer recurrence", *Clin Cancer Res*, 17, no. 23, p. . 7219-23, 2011.
- [29] N. Cordes and C. C. Park, "beta1 integrin as a molecular therapeutic target", *Int J Radiat Biol*, 83, no. 11-12, p. . 753-60, 2007.
- [30] C. A. Schneider, W. S. Rasband and K. W. Eliceiri, "NIH Image to ImageJ: 25 years of image analysis", *Nature Methods*, 9, no. 7, p. . 671-675, 2012.

- [31] I. H. Shin, S. M. Shin and D. Y. Kim, "New, simple theory-based, accurate polarization microscope for birefringence imaging of biological cells", *J Biomed Opt*, 15, no. 1, p. . 016028, 2010.
- [32] A. M. Glazer, J. G. Lewis and W. Kaminsky, "An Automatic Optical Imaging System for Birefringent Media", *Proceedings of the Royal Society of London A: Mathematical, Physical and Engineering Sciences*, 452, no. 1955, p. . 2751-2765, 1996.
- [33] Q. Shi, R. P. Ghosh, H. Engelke, C. H. Rycroft, L. Cassereau, J. A. Sethian, V. M. Weaver and J. T. Liphardt, "Rapid disorganization of mechanically interacting systems of mammary acini", *Proc Natl Acad Sci U S A*, 111, no. 2, p. . 658-63, 2014.
- [34] K. Király, M. M. Hyttinen, T. Lapveteläinen, M. Elo, I. Kiviranta, J. Dobai, L. Módis, H. J. Helminen and J. P. Arokoski, "Specimen preparation and quantification of collagen birefringence in unstained sections of articular cartilage using image analysis and polarizing light microscopy", *Histochem J*, 29, no. 4, p. . 317-27, 1997.
- [35] M. J. Paszek, N. Zahir, K. R. Johnson, J. N. Lakins, G. I. Rozenberg, A. Gefen, C. A. Reinhart-King, S. S. Margulies, M. Dembo, D. Boettiger, D. A. Hammer and V. M. Weaver, "Tensional homeostasis and the malignant phenotype", *Cancer Cell*, 8, no. 3, p. . 241-54, 2005.
- [36] B. Ruffell, A. Au, H. S. Rugo, L. J. Esserman, E. S. Hwang and L. M. Coussens, "Leukocyte composition of human breast cancer", *Proc Natl Acad Sci U S A*, 109, no. 8, p. . 2796-801, 2012.
- [37] B. Ruffell, D. Chang-Strachan, V. Chan, A. Rosenbusch, C. M. T. Ho, N. Pryer, D. Daniel, E. S. Hwang, H. S. Rugo and L. M. Coussens, "Macrophage IL-10 blocks CD8+ T cell-dependent responses to chemotherapy by suppressing IL-12 expression in intratumoral dendritic cells", *Cancer Cell*, 26, no. 5, p. . 623-37, 2014.

- [38] J. W. Pollard, "Macrophages define the invasive microenvironment in breast cancer", *J Leukoc Biol*, 84, no. 3, p. . 623-30, 2008.
- [39] M. Pickup, S. Novitskiy and H. L. Moses, "The roles of TGF β in the tumour microenvironment", *Nat Rev Cancer*, 13, no. 11, p. . 788-99, 2013.
- [40] M. E. Engel, P. K. Datta and H. L. Moses, "Signal transduction by transforming growth factor-beta: a cooperative paradigm with extensive negative regulation", *J Cell Biochem Suppl*, 30-31, no., p. . 111-22, 1998.
- [41] A. Goldhirsch, W. C. Wood, A. S. Coates, R. D. Gelber, B. Thürlimann, H. J. Senn and Panel members, "Strategies for subtypes--dealing with the diversity of breast cancer: highlights of the St. Gallen International Expert Consensus on the Primary Therapy of Early Breast Cancer 2011", *Ann Oncol*, 22, no. 8. England, p. . 1736-47, 2011.
- [42] P. A. Janmey, R. G. Wells, R. K. Assoian and C. A. McCulloch, "From tissue mechanics to transcription factors", *Differentiation*, 86, no. 3, p. . 112-20, 2013.
- [43] K. H. Wrighton, "Mechanotransduction: YAP and TAZ feel the force", *Nat Rev Mol Cell Biol*, 12, no. 7, p. . 404, 2011.
- [44] B. C. Low, C. Q. Pan, G. V. Shivashankar, A. Bershadsky, M. Sudol and M. Sheetz, "YAP/TAZ as mechanosensors and mechanotransducers in regulating organ size and tumor growth", *FEBS Lett*, 588, no. 16, p. . 2663-70, 2014.
- [45] P. Lijnen and V. Petrov, "Transforming growth factor-beta 1-induced collagen production in cultures of cardiac fibroblasts is the result of the appearance of myofibroblasts", *Methods Find Exp Clin Pharmacol*, 24, no. 5, p. . 333-44, 2002.

- [46] P. A. Fasching, K. Heusinger, C. R. Loehberg, E. Wenkel, M. P. Lux, M. Schrauder, T. Koscheck, W. Bautz, R. Schulz-Wendtland, M. W. Beckmann and M. R. Bani, "Influence of mammographic density on the diagnostic accuracy of tumor size assessment and association with breast cancer tumor characteristics", *Eur J Radiol*, 60, no. 3, p. . 398-404, 2006.
- [47] J. M. Chang, I. A. Park, S. H. Lee, W. H. Kim, M. S. Bae, H. R. Koo, A. Yi, S. J. Kim, N. Cho and W. K. Moon, "Stiffness of tumours measured by shear-wave elastography correlated with subtypes of breast cancer", *Eur Radiol*, 23, no. 9, p. . 2450-8, 2013.
- [48] A. Evans, P. Whelehan, K. Thomson, D. McLean, K. Brauer, C. Purdie, L. Jordan, L. Baker and A. Thompson, "Quantitative shear wave ultrasound elastography: initial experience in solid breast masses", *Breast Cancer Res*, 12, no. 5, p. . R104, 2010.
- [49] J. K. Mouw, Y. Yui, L. Damiano, R. O. Bainer, J. N. Lakins, I. Acerbi, G. Ou, A. C. Wijekoon, K. R. Levental, P. M. Gilbert, E. S. Hwang, Y. -Y. Chen and V. M. Weaver, "Tissue mechanics modulate microRNA-dependent PTEN expression to regulate malignant progression", *Nat Med*, 20, no. 4, p. . 360-7, 2014.
- [50] P. P. Provenzano, D. R. Inman, K. W. Eliceiri and P. J. Keely, "Matrix density-induced mechanoregulation of breast cell phenotype, signaling and gene expression through a FAK-ERK linkage", *Oncogene*, 28, no. 49, p. . 4326-43, 2009.
- [51] C. Balleyguier, S. Canale, W. Ben Hassen, P. Vielh, E. H. Bayou, M. C. Mathieu, C. Uzan, C. Bourgier and C. Dromain, "Breast elasticity: principles, technique, results: an update and overview of commercially available software", *Eur J Radiol*, 82, no. 3, p. . 427-34, 2013.
- [52] N. McGranahan and C. Swanton, "Biological and Therapeutic Impact of Intratumor Heterogeneity in Cancer Evolution", *Cancer Cell*, 27, no. 1, p. . 15-26, 2015.

Chapter 6: Investigating a link between tissue mechanics and tumor immune response in breast cancer

Luke Cassereau^{1,2}

In collaboration with: Ori Maller¹, Brian Ruffell³, Lisa M. Coussens³, Jonathan Lakins¹

Under the supervision of: Valerie M. Weaver^{1,2,4,5,6}

¹Center for Bioengineering and Tissue Regeneration, Department of Surgery, UCSF, San Francisco, California, USA.

²University of California San Francisco/University of California Berkeley Joint Graduate Group in Bioengineering, San Francisco, CA, USA.

³Department of Cell, Developmental, and Cancer Biology and Knight Cancer Institute, Oregon Health and Science University, Portland, OR 97034.

³Department of Anatomy, and Department of Bioengineering and Therapeutic Sciences, UCSF, San Francisco, California, USA.

⁴Eli and Edythe Broad Center of Regeneration Medicine and Stem Cell Research, UCSF, San Francisco, California, USA.

⁵UCSF Helen Diller Comprehensive Cancer Center, UCSF, San Francisco, California, USA.

Abstract:

Human breast tumors are highly fibrotic and their extracellular matrix (ECM) is stiffer relative to benign lesions. A major contributor to tumor mechanics is fibrillar collagen-rich ECM. During tumor progression, fibrillar collagen content increases and its organization is characterized by bundles of aligned collagen fibers that are oriented perpendicular, particularly on the invasive fronts in both mouse models of breast cancer and human disease. I demonstrated that a stiffened ECM and elevated mechanosignaling (e.g. $\beta 1$ integrin-focal adhesion kinase signaling axis) promoted mammary tumorigenesis, whereas reducing ECM stiffening impeded tumor formation. More recently, I established a positive correlation between the number and location of infiltrating CD45 and CD68 immune cells and ECM stiffness in human breast tumors.

Infiltrating immune cells have been previously implicated in ECM remodeling associated with mammary gland development and tumorigenesis. This has led me to hypothesize that immune cells promote tumor-associated fibrosis that induces inflammatory signaling, resulting in a feed-forward loop to stimulate a pro-tumor immune response. Using the MMTV-PyMT mouse model, I found that lysyl oxidase (LOX) inhibitor treatment — an inhibitor of collagen crosslinking — attenuated ECM stiffness and caused a shift in the cytokine milieu consistent with an anti-tumor immune response. Macrophage depletion early in PyMT tumorigenesis not only ablated metastasis, but demonstrated an anti-fibrotic role for macrophages as depicted by a decrease in fibrillar collagen and a reduction in ECM stiffness. Interestingly, I also found that MMTV-PyMT primary organoids embedded in stiff collagen gels induced M0 macrophage (bone marrow derived cells previously cultured with M-CSF) differentiation and invasion suggesting a reciprocal relationship between macrophage infiltrate and ECM remodeling. In accordance with the macrophage depletion data, STAT3 phosphorylation levels in tumor cells decreased in

mammary tumors when mice were treated with a LOX inhibitor. Furthermore, the ECM adjacent to mammary tumor cells that lacked STAT3 was softer and a quantitative cytokine profiling of these tumors revealed a shift toward an anti-tumor immune response. Moreover, I demonstrated that ECM stiffness directly caused STAT3 phosphorylation in tumor cells *in vitro* by using ECM-coated polyacrylamide gels and that STAT3 signaling is essential for macrophage infiltrate in collagen gel co-cultures. Collectively, my data provide multiple lines of evidence to argue that macrophage infiltration promotes tumor-associated fibrosis that stimulates inflammatory signaling in tumor cells in early mammary tumorigenesis — and this feed-forward loop induces a pro-tumor immune response. These findings suggest that early treatment with an anti-fibrotic agent could mitigate immune suppression associated with late tumorigenesis and may enhance the efficacy of immunotherapy.

Introduction:

Human tumors are highly fibrotic and previous work in our lab has shown a strong correlation between tissue mechanical properties and breast tumor aggression¹⁻³. Specifically, we have demonstrated that collagen cross-linking and extracellular matrix (ECM) stiffness is necessary for metastasis in *in vivo* breast cancer models and that altered tissue organization and mechanics are associated with increasing tumor aggression in human patient samples. Yet, the ECM is not solely a protein rich matrix, but also contains stromal cell populations such as fibroblasts and immune cells⁴⁻⁷. Critically, these stromal cell populations can have a potent effect on tumor aggression through secreted cytokines which alter tumor cell signaling to influence tumor cell survival, drug resistance, invasion, and motility⁸⁻¹⁵. However this relationship exists within a dynamically changing micro environment and how the ECM mechanical changes that occur with tumor progression regulate stromal cell – tumor interactions to influence metastatic progression remains poorly understood and is the focus of this work.

I previously demonstrated a direct relationship between the increased stiffness and reorganization of the ECM in the most aggressive human tumors and significant immune cell infiltration in the form of macrophages¹⁶. Interestingly, immune cells are potent regulators of ECM remodeling through a pro-fibrotic inflammatory cytokine milieu¹⁷⁻²², suggesting immune infiltrate may support tumor aggression by inducing ECM stiffening. Specifically, my work in this thesis and previous work in our lab has demonstrated that ECM stiffness can directly affect tumor aggression through regulation of pro-tumorigenic MAPk signaling to support tumor cell growth, metabolism, motility, and ultimately metastasis *in vivo*. Moreover, ECM mechanics can

also modulate stromal cell phenotype^{4,7,10,23}, suggesting the relationship between immune cell infiltrate and ECM stiffness may be reciprocal.

In this work I aimed to explore this relationship between immune infiltrate and ECM mechanics in tumor malignant phenotype through the following hypothesis: infiltrating immune cells promote tumor-associated fibrosis that induces inflammatory signaling, resulting in a feed-forward loop to stimulate a pro-tumor immune response. To test this hypothesis, I utilized a combination of breast cancer *in vivo* models in which I could modulate ECM mechanics, immune cell infiltrate, and inflammatory signaling and then measured ECM structural and mechanical properties, tumor cell signaling, and evidence of metastatic progression. To supplement my animal studies I also used tunable hydrogel substrates *ex vivo* in which I could tune ECM stiffness to elucidate the importance of substrate mechanics in modulating immune cell – tumor cell interactions.

From these studies I observed that infiltrating macrophage play a critical role in ECM remodeling and tumor metastatic progression. Interestingly, the relationship between immune cell infiltrate and ECM remodeling is reciprocal and mediated through tumor cell inflammatory response via tumor cell Stat3 signaling. These results provide important new insights into the role of tissue inflammation and tumor aggression and metastatic progression.

Results:

Macrophage infiltration is necessary for stromal remodeling and tumor metastatic progression

Having previously observed that increased stromal stiffness in human patient samples correlated with macrophage infiltrate I aimed to determine whether macrophage recruitment regulated ECM mechanical properties. To test this I used the MMTV PyMT breast cancer model +/- an anti-CSF1 antibody which depletes infiltrating macrophage and collected tissues at 11 weeks of tumor progression (early stage carcinoma). To assess mechanical and structural changes in the stroma bordering the tumor I used a combination of atomic force microscopy (AFM) and second harmonic generation (SHG) collagen imaging with a two-photon microscope. From these analyses I measured a significant decrease in tissue elastic modulus in the collagen rich stroma bordering the tumor and corresponding structural changes suggesting smaller less bundled collagen fibers with macrophage depletion (Figure 6.1 A-B). These results suggested macrophage play an important role in determining the mechanical microenvironment during tumor development.

To determine how macrophage depletion alters metastatic progression I collected lung tissue from late stage MMTV PyMT animals (13 weeks) and used qPCR to test for the presence of the PyMT transgene. Interestingly, I observed a highly significant decrease in metastasis in anti-CSF1 treated mice underscoring the importance of immune infiltrate in tumor malignant phenotype (Figure 6.1C). Moreover, this result is consistent with inhibiting collagen cross-linking (Figure 4.3) suggesting that the impact of immune infiltrate on tumor metastasis may be through ECM remodeling.

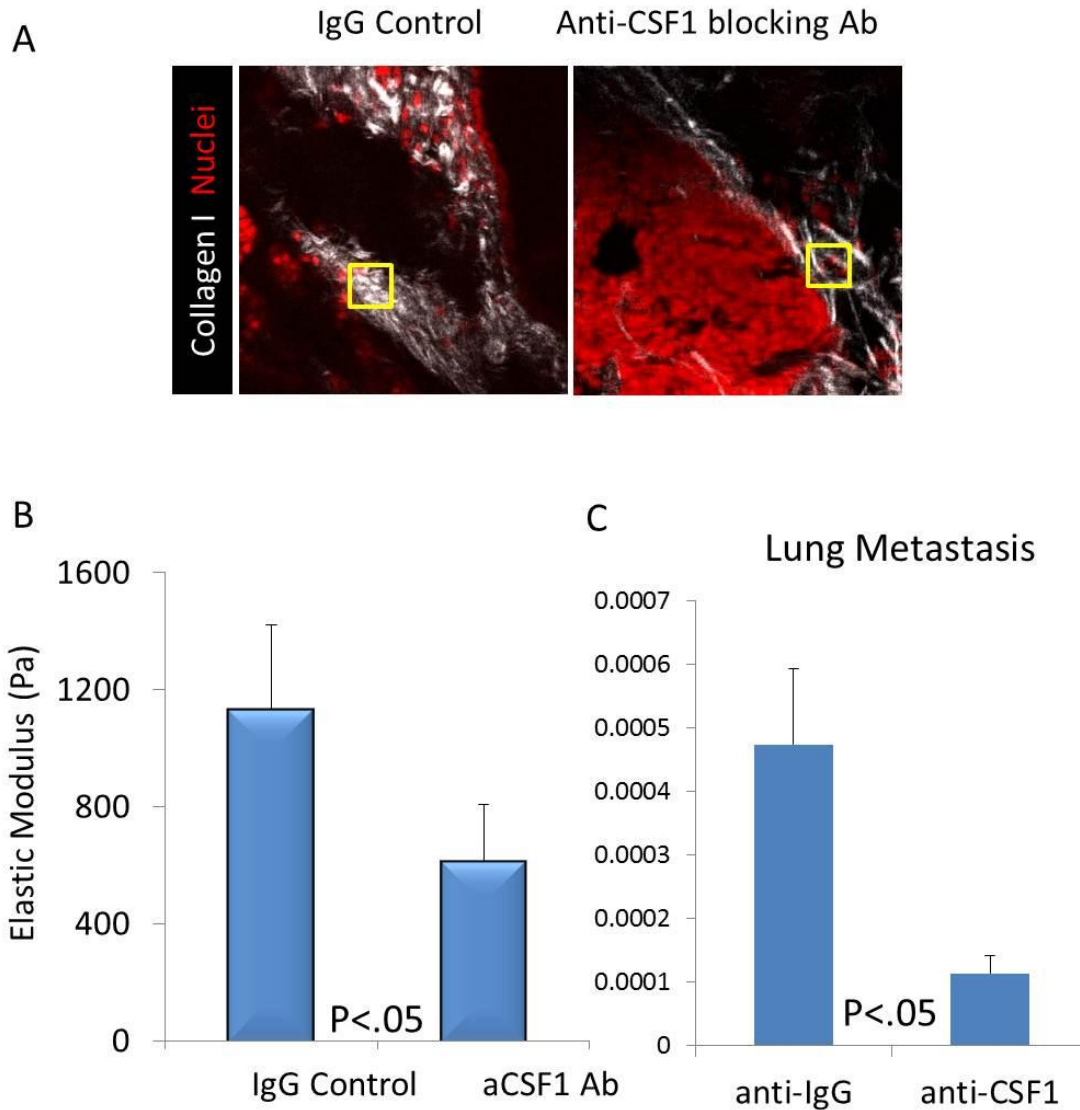


Figure 6.1. A) Two photon imaging of 11 week PyMT tumor tissue +/- macrophage depletion, collagen imaged via SHG and nuclei by propidium iodide fluorescent stain. Yellow grid represents sample AFM testing region focused on tumor stroma border. **B)** Quantification of average stroma elastic modulus representing 5 animals in each group with one mammary gland per animal tested with 1000 measurements per gland taken at 11 weeks. **C)** Lung metastasis quantified by PyMT transgene expression in lung tissue of late stage (13 week) animals.

Substrate stiffness and tumor cell cytokine secretion potentiates macrophage infiltration in an *ex vivo* co-culture model.

Having demonstrated an important role for immune infiltrate in ECM remodeling, I next wanted to explore the reciprocal relationship. In particular, previous works have implicated ECM mechanical properties can regulate stromal cell phenotype^{4,7,10,23} and I aimed specifically to determine if the stiffness of the matrix could alter macrophage infiltration.

To do this in a highly controllable setting, I altered my tension bioreactor system²⁴ to work as a co-culture between macrophage and isolated tumor cells. Briefly, macrophage were derived from bone marrow isolates cultured for 7 days with M-CSF and then seeded on top of collagen gels tuned to either normal or tumor associated mammary gland stiffness and with or without embedded isolated tumor organoids as previously described²⁵ (Figure 6.2).

Interestingly, the combination of stiffened substrate and tumor organoids lead to significantly greater macrophage adhesion to the collagen gel and subsequent infiltration of macrophage into the hydrogel than either stiffness or embedded tumor cells individually. From this I inferred that there may be a stiffness mediated upregulation of pro-inflammatory signaling in the tumor cells to potentiate cytokine secretion and macrophage infiltration, thus explaining why I only observed macrophage infiltration with a stiffened ECM and embedded tumor cells rather than either individually. I next aimed to assess which inflammatory signaling pathways *in vivo* were alte

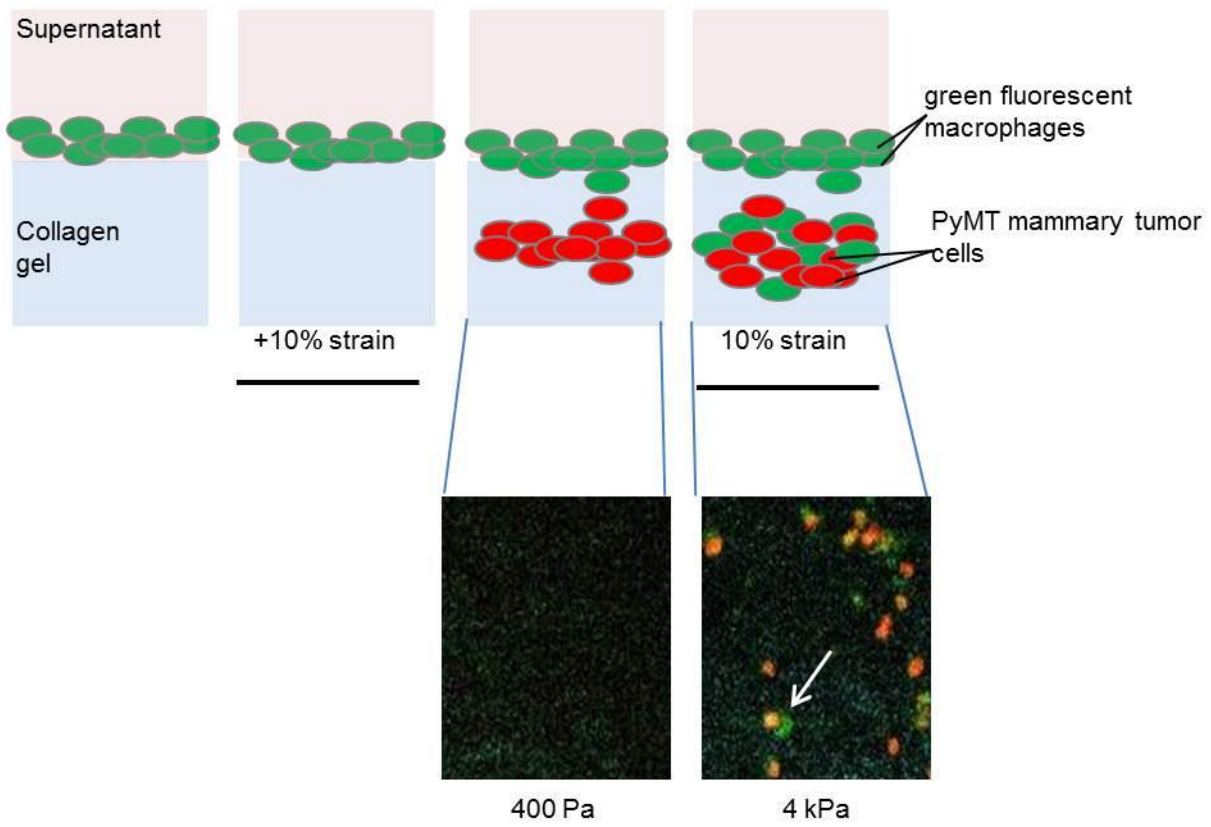


Figure 6.2. Macrophage – tumor cell co culture demonstrates the importance of both tumor cell cytokine secretion and ECM stiffness in enhancing immune cell infiltrate. Tumor cells were PyMT organoids and gels were tuned to either 400Pa or 4kPa. Z-projections were made from z-stack images taken via two-photon, with imaging starting 10um below the surface of the collagen gel and ranging to 350 um deep.

Tumor cell Stat3 signaling is altered by ECM stiffness and dependent on integrin focal adhesion signaling.

I next aimed to assess which inflammatory signaling pathways *in vivo* were altered in response to ECM stiffness to determine which tumor cell signaling mechanisms might be regulating immune infiltrate. Using the same MMTV PyMT +/- collagen cross-linking inhibitor mammary gland samples described in chapter 4, I assessed via tissue staining potential differences in tumor inflammatory signaling and found a significant decrease in pStat3 levels with decreased ECM stiffness (Figure 6.3A). Stat3 signaling has been implicated as a critical regulator of pro-inflammatory cytokine secretion^{26,27,28} and thus an attractive possible mechanism for the phenotype I observed in our co culture. However, Stat3 signaling can also be induced in response other inflammatory cytokines^{11,29,30} and thus I next aimed to determine the role of stiffness alone on Stat3 signaling in tumor cells.

To assess the impact of ECM stiffness on tumor cell Stat3 signaling specifically I seeded isolated MMTV PyMT on mechanically tunable polyacrylamide (PA) gels calibrated to either normal or tumor associated mammary gland stiffness. After 24 hours of culture I collected protein lysates for immunoblotting quantification and I measured a significant increase of activated Stat3 signaling (ratio of pStat3 to total Stat3) with increased substrate stiffness (Figure 6.3B). To determine if this enhanced Stat3 activation was due directly to cell-ECM interactions through focal adhesions or through canonical Stat3 activation by EGFr signaling²⁸ I quantified stiffness mediated Stat3 phosphorylation in the presence of JAK1/2 (canonical Stat3 activation pathway), pFAK or pEGFr inhibition. Consistently, I found that FAK inhibition significantly reduced Stat3 activation on stiff substrates while EGFr signaling inhibitors had little to no effect on pStat3 levels (Figure 6.3B). These data support ECM stiffness as a potent regulator of tumor

cell inflammatory signaling and suggest a possible positive feedback loop in which infiltrating macrophage secrete soluble factors to induce fibrosis that in turn increases tumor cell Stat3 signaling, which can potentiate the release of additional pro-inflammatory cytokines.

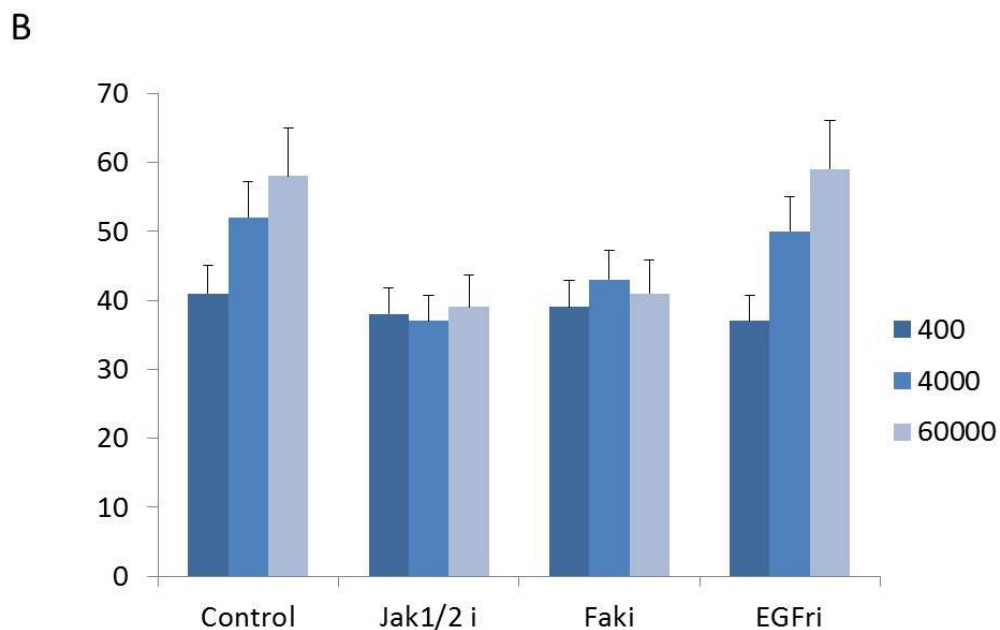
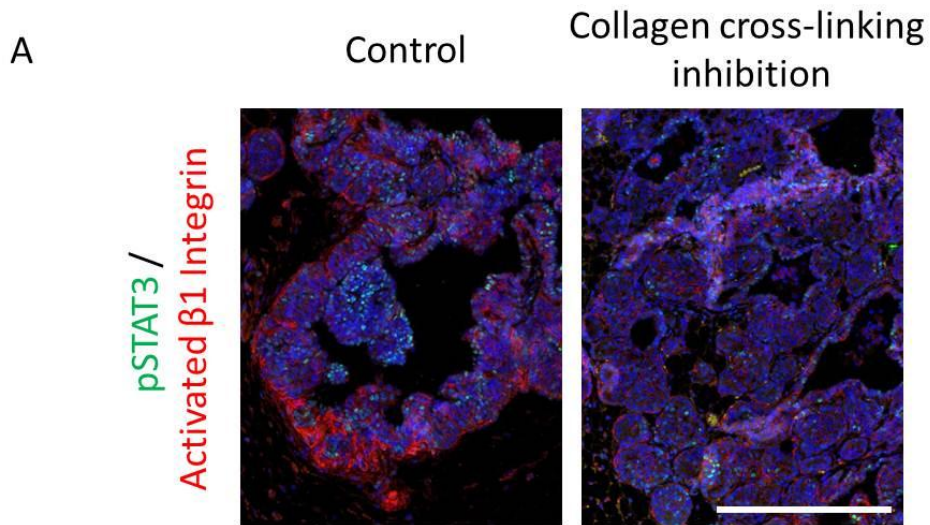


Figure 6.3 A) pSTAT3 and activated β 1 integrin tissue staining of 11 week PyMT tumors +/- BAPN treatment for collagen cross-linking inhibition. Scale bar 80 μ m. **B)** Measurement of Stat3 signaling quantified as ratio pStat3 to total Stat3 determined via western blot. MMTV PyMT cells were seeded on PA gels of increasing stiffness and culture for 24 hours in either standard culture media or with an addition of a Jak1/2, Fak, or EGFr inhibitor. Bars represent 3 biological replicates for each group.

Stat3 signaling is required for ECM remodeling and tumor metastasis

Building on previous experiments implicating Stat3 signaling as a possible mediator of immune infiltrate and I next aimed to determine how Stat3 contributes to ECM remodeling and tumor malignant progression.

As in the macrophage depletion studies, I utilized my MMTV PyMT animal model +/- a genetic knockout of Stat3 signaling in the tumor epithelium and collected tissues at 11 weeks. Structural and mechanical changes in the stroma with the loss of Stat3 signaling were determined via AFM and SHG imaging. Consistent with my results from the macrophage depletion studies, the Stat3 KO tumors had significantly less stiff stroma than control tumors as well as reduced collagen bundling and linearization (Figure 6.4). Importantly, these changes also correlated with significantly less evidence of lung metastasis (Figure 6.4).

Combining these observations, my data suggest that while Stat3 is regulated by ECM stiffness it also plays an important role in supporting ECM remodeling and subsequently malignant progression. Additionally, these results closely match the data from PyMT tumors in which we ablated macrophage infiltration again suggesting an important relationship between immune infiltrate, Stat3 signaling, ECM stiffness, and ultimately metastasis. To build on these data I next aimed to determine how Stat3 contributed to macrophage infiltrate.

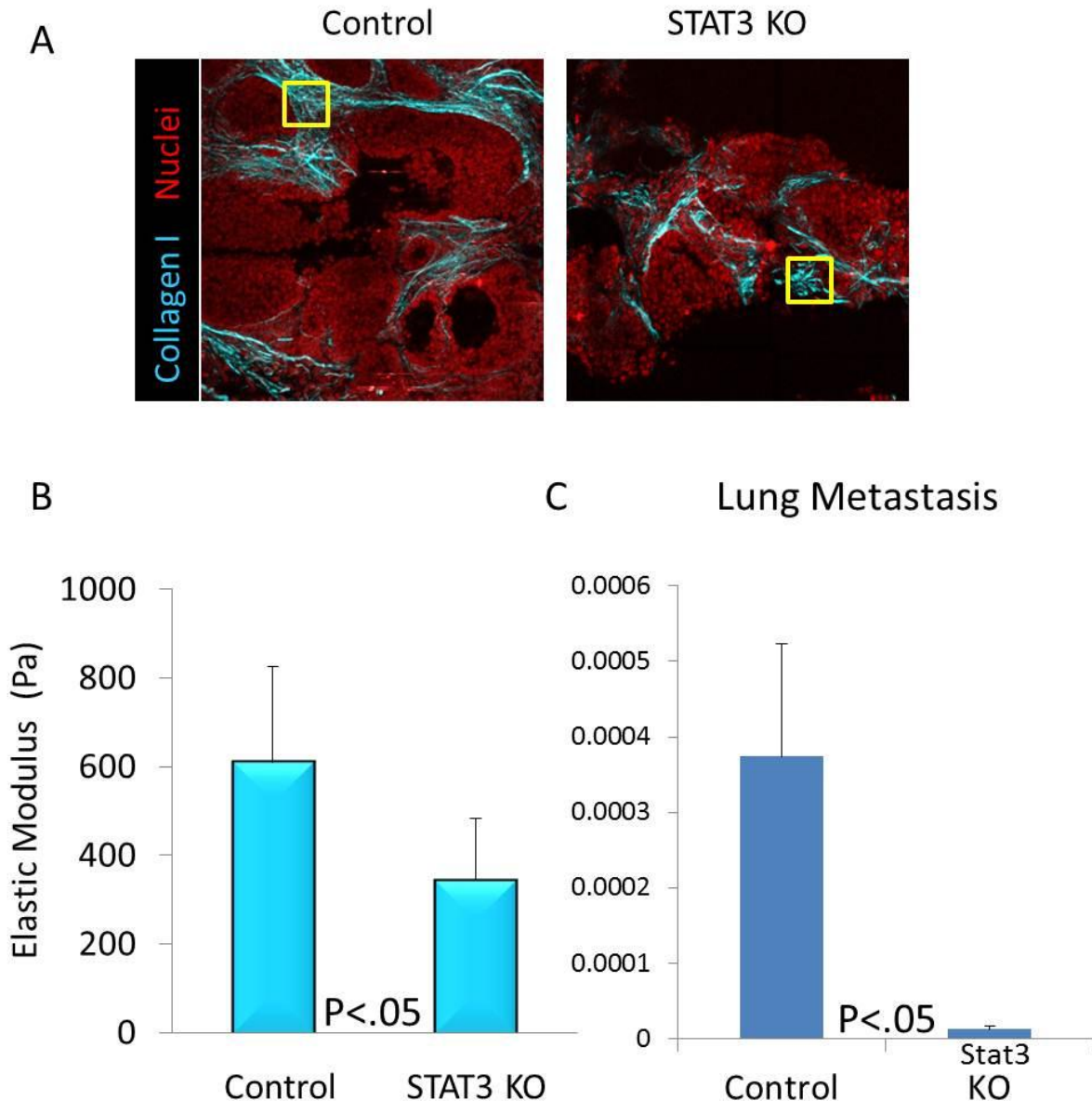


Figure 6.4 **A)** Two photon imaging of 11 week PyMT tumor tissue +/- Stat3 KO, collagen imaged via SHG and nuclei by propidium iodide fluorescent stain. Yellow grid represents sample AFM testing region focused on tumor stroma border. **B)** Quantification of average stroma elastic modulus representing 5 animals in each group with one mammary gland per animal tested with 1000 measurements per gland taken at 11 weeks. **C)** Lung metastasis quantified by PyMT transgene expression in lung tissue of late stage (13 week) animals.

ECM stiffness mediated macrophage infiltrate depends on tumor cell Stat3 signaling

Building on previous results, I aimed to determine if mechanistically tumor cell inflammatory signaling regulated ECM stiffness through altered immune cell infiltrate. Specifically, I assessed the importance of Stat3 signaling to macrophage infiltrate both *in vivo* and *in vitro*.

Interestingly, tissue staining in 11 week PyMT tumors +/- Stat3 KO showed nearly no macrophage infiltrate with loss of Stat3 signaling (Figure 6.5), supporting my previous results that both loss of macrophage infiltrate and loss of Stat3 prevent ECM stiffening. To dynamically assess the impact of substrate stiffness on macrophage-tumor cell interactions and the role of Stat3 signaling, I again utilized my tension bioreactor adapted for a macrophage – tumor cell co-culture (Figure 6.5). Interestingly, the combination of stiffened substrate and tumor organoids lead to significantly greater macrophage adhesion to the collagen gel and subsequent infiltration of macrophage into the hydrogel than either stiffness or embedded tumor cells individually. Consistent, with previous results, Stat3 was essential in this model for macrophage behavior as collagen gel co-cultures with Stat3 KO tumor organoids had significantly blunted macrophage infiltration (Figure 6.5).

From these results, it is clear there exists a dynamic interplay between infiltrating macrophage, tumor cell signaling, and tissue mechanical properties with each being interrelated and each critical for tumor malignant progression.

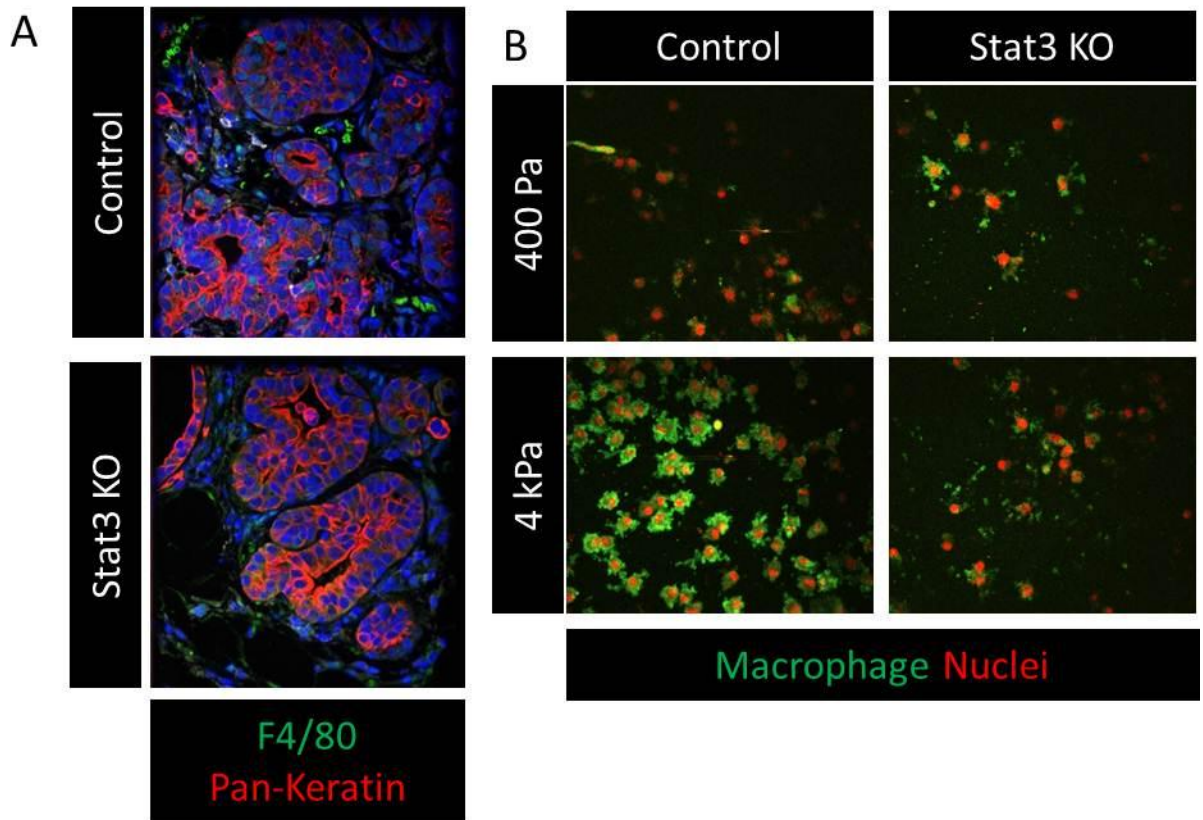


Figure 6.5 A) Macrophage infiltrate determined by F4/80 tissue stain in PyMT tumor tissue +/- Stat3 KO. **B)** Z-projected images of macrophage infiltration into the collagen gel in macrophage – tumor cell co-culture. PyMT organoids +/- Stat3 KO and gels were tuned to either 400Pa or 4kPa. Z-projections were made from z-stack images taken via two-photon, with imaging starting 10um below the surface of the collagen gel and ranging to 350 um deep.

Discussion:

In this work I aimed to better understand the interrelated roles of macrophage, tumor cell signaling, and stromal remodeling and stiffness in tumor aggression. Based on previous data there is a clear correlation between stromal stiffness, inflammatory signaling, and immune infiltrate and critically each has been implicated in tumor malignant progression and metastatic phenotype^{11,29-31}. However, how these factors are regulated relative to each other and potential synergistic effects or the possibility of feed forward loops was unclear. Here I have made several key observations, which clarify the nature of these relationships.

By using AFM and SHG imaging with tumor tissue samples in which macrophage were depleted I observed significant reduction in the ECM remodeling and stiffening concordant with tumor progression. Consistently, with the reduction of infiltrating macrophage I observed a severe reduction in tumor Stat3 activation, a major inflammatory signaling mechanism^{26,27}. Interestingly, using a genetic KO of Stat3 in tumor cells I not only measured a reduced ECM stiffness but the loss of Stat3 signaling also significantly hindered macrophage infiltrate suggesting the relationship between macrophage infiltrate and tumor Stat3 signaling is bi-directional and both have a key role in inducing ECM remodeling.

Further, when I tested the effects of substrate stiffness on tumor cell Stat3 activation I saw stiffness alone significantly enhanced Stat3 signaling dependent on cell-ECM adhesion and focal adhesion signaling. Consistently, in a macrophage-tumor cell co-culture model using my tension bioreactor, I observed significantly enhanced macrophage infiltration with stiffened collagen gels embedded with tumor cells with Stat3 signaling intact.

Importantly, these data shows for the first time that ECM stiffness is a critical regulator of tumor cell immune cell interactions. These results also suggest an interesting positive feedback loop in which infiltrating macrophage drive Stat3 signaling but also require Stat3 signaling with both pathways feeding into ECM remodeling as well as being tuned by ECM stiffness. Importantly, this loop directly contributes to malignant progression, as each one of the axes of this loop is necessary for metastasis in animal models and correlates with tumor progression and aggression in human patient samples.

However, to build upon and translate these results into possible clinical therapies there is still more work to be done to better understand the mechanistic underpinnings of the interactions between macrophage, tumor cells, and ECM stiffness. In particular, through which cytokines do macrophage stimulate Stat3 activation and conversely which soluble factors draw in infiltrating macrophage? Moreover, which cell populations drive the ECM remodeling and how is this activity influenced by macrophage tumor cell interactions?

Future studies using ELISA and mass spectrometry to assess the cytokine milieu in my variety of models presented here should better elucidate which cytokines and subsequently cell signaling mechanisms are involved. Moreover, previous results from my work have strongly implicated integrin specificity and cell metabolic changes as key to tumor cell malignant phenotype with ECM stiffening. How these factors contribute to tumor cell – immune cell interactions is not yet understood and should be explore in future follow up experiments.

Methods:

Cell culture

MMTV PyMT mice were sacrificed at 11 week and the #4 mammary glands were collected and digested for tumor organoids isolated as previously described²⁴. Once acini were isolated they were seeded in the collagen bioreactor or seeded onto 2D polyacrylamide gels and cultured for 2 days. For bioreactor studies after 2 days they were paraformaldehyde fixed and stained with propidium iodide and alexa488 phalloidin for imaging on the two-photon microscope.

Polyacrylamide gel cultures were also stopped after 2 days with a 2% SDS lysis buffer used to collect protein lysates.

Studies in which pharmacological inhibition was required, I used Ruxolitinib at 5uM to inhibit Stat3 signaling, PND 1186 at 1uM to inhibit FAK, and Tryphosin AG 1478 at 0.5uM to inhibit EGFR.

AFM measurements of ECM stiffness on tissue sections

All AFM indentations were performed using an MFP3D-BIO inverted optical AFM (Asylum Research) mounted on a Nikon TE2000-U inverted fluorescent microscope, as previously described⁶. Briefly, I used silicon nitride cantilevers with spring constant of 0.06 N/m with borosilicate glass spherical tip with 5 μm in diameter (Novascan Tech). The cantilever was calibrated using the thermal oscillation method prior to each experiment. Samples were indented at 20 $\mu\text{m/s}$ loading rate, with a maximum force of 2 nN. Ten AFM force maps were typically obtained on each sample, each map as a 90x90 μm of 10x10 indentations in a raster

series of indentations utilizing the FMAP function of the IGOR PRO build supplied by Asylum Research. The Hertz model was used to determine the elastic properties of the tissue (E1). Tissue samples were assumed to be incompressible and a Poisson's ratio of 0.5 was used in the calculation of the Young's elastic modulus.

Two-photon microscopy image acquisition and analysis

For two-photon imaging 20 μm fresh tissue sections were fixed post-AFM indentation in 4% neutral buffered formalin, and mounted with Permount Mounting Medium. I used custom resonant-scanning instruments based on published designs containing a five-PMT array (Hamamatsu, C7950) operating at video rate. The setup was used with two channel Qultaneous video rate acquisition via two PMT detectors and an excitation laser (2W MaiTai Ti-Sapphire laser, 710-920nm excitation range). Second harmonics imaging was performed on a Prairie Technology Ultima System attached to an Olympus BX- 51 fixed stage microscope equipped with a 25 \times (NA 1.05) water immersion objective. Tissue samples were exposed to polarized laser light at a wavelength of 830nm and emitted light was separated with a filter set (short pass filter, 720nm; dichroic mirror, 495nm; band pass filter, 475/40nm). Images of x-y planes of 284 by 284 μm at a resolution of 0.656 $\mu\text{m}/\text{pixel}$ were captured using Micro-Manager Open Source Microscopy Software (Micro-Manager) in at least 3 locations on each human tissue sample. Quantification of collagen fibers was achieved by setting a minimal threshold in the second harmonic signal. The threshold was maintained for all images across all conditions. The area of regions that was covered by the minimal threshold was calculated and 3 images per sample were averaged together (Image J, Image Processing and Analysis in Java). Collagen fiber

diameters data were visualized and analyzed using Imaris (Bitplane AG) and MATLAB (MathWorks). Statistical analysis was performed using Prism software (GraphPad Software, Inc.).

Tissue Immunofluorescence Staining and quantification

Antibodies and Reagents. Immunofluorescence staining and imaging of FFPE tissue sections was performed as recently described³².

Image Acquisition

All immunofluorescence images were acquired using a Nikon 40x water immersion objective (NA=1.15) on a Nikon spinning disk microscope

Mouse Studies

Mice were sacrificed at which time the 4th mammary gland was paraformaldehyde fixed; paraffin sections were analyzed for histology and parallel sections were stained as described, and the 2/3 mammary gland was collected for PCR and immunoblot analysis and as a cell source for tumor cells. For mice sacrificed at a total tumor burden of 2mm³ lungs were also collected for PCR analysis of metastasis.

Immunoblot analysis

Immunoblot analysis was done with a 3% BSA block solution and the following primary antibodies: pStat3 (Rabbit Cell Signaling), Stat3 (Rabbit Cell Signaling) and with a horseradish peroxidase anti-rabbit secondary (Cell Signaling).

3D and 2D Substrate Preparation

Tension bioreactor studies were performed as previously described²⁴. For co-culture studies, I culture BMDC (bone marrow derived cells) based on previously established protocols.²⁵ Briefly, I use 26G needle to flesh the bone (femur from a Mac GFP mouse) and culture the BMDC in DMEM/F12+10% FBS+1%A/A and with 100ng/mL murine M-CSF for 7 days. I change media on the 3rd day (the day of isolation is day 0).

I then plated approximately 200K cells on top of each gel in the bioreactor on day 1 (one day after starting to culture the PyMT organoids). Cultures are then fixed and stained on day 3 followed by large field two photon images to assess infiltration of macrophage into the gel. As for the cell sorting Ori has gotten data but I are still very much in the optimizing phase.

ECM-functionalized PA gels were prepared and mechanically analyzed as described previously³³.

Statistical Analysis

Statistical analysis was performed using Prism/GraphPad Software (La Jolla, CA) at indicated p-values. Unless otherwise stated, two-tailed Student's t-tests were used for significance testing. Means were presented as +/- s.e.m of at least three independent experiments. Unless otherwise noted, sample size, n, was n=3 and statistical significance was considered at p<0.05. Adhesion strength values were specifically analyzed via ANOVA and Tukey's post-hoc test with a p-value < 0.05 considered significant.

Acknowledgements

NIH/NCI F31 CA183255 (L.C.), ARCS Foundation Fellowship (L.C.), ME DOD BCRP Postdoctoral Fellowship W81XWH-14-1-0056 (O.M.), ME NIH T32 CA 108462-10 (O.M.), ME DOD BCRP W81XWH-05-1-0330 and W81XWH-13-1-0216 (V.M.W.), ME NIH/NCI R01 CA192914-01 (V.M.W.), NIH/NCI R01 CA174929 (V.M.W. and C.P.) and Susan G. Komen KG110560PP (V.M.W. and E.S.H.)

Works Cited:

1. Paszek, M. J. *et al.* Tensional homeostasis and the malignant phenotype. *Cancer Cell* **8**, 241–54 (2005).
2. Lopez, J. I., Kang, I., You, W.-K., McDonald, D. M. & Weaver, V. M. In situ force mapping of mammary gland transformation. *Integr. Biol. (Camb)*. **3**, 910–21 (2011).
3. Levental, K. R. *et al.* Matrix crosslinking forces tumor progression by enhancing integrin signaling. *Cell* **139**, 891–906 (2009).
4. Ewald, A. J., Werb, Z. & Egeblad, M. Dynamic, long-term in vivo imaging of tumor-stroma interactions in mouse models of breast cancer using spinning-disk confocal microscopy. *Cold Spring Harb. Protoc.* **2011**, pdb.top97 (2011).
5. Hasebe, T. Tumor-stromal interactions in breast tumor progression--significance of histological heterogeneity of tumor-stromal fibroblasts. *Expert Opin Ther Targets* **17**, 449–460 (2013).
6. Rudnick, J. A. & Kuperwasser, C. Stromal biomarkers in breast cancer development and progression. *Clin Exp Metastasis* **29**, 663–672 (2012).
7. Semenza, G. L. Cancer-stromal cell interactions mediated by hypoxia-inducible factors promote angiogenesis, lymphangiogenesis, and metastasis. *Oncogene* **32**, 4057–4063 (2013).

8. Walker, R. A., Dearing, S. J. & Gallacher, B. Relationship of transforming growth factor beta 1 to extracellular matrix and stromal infiltrates in invasive breast carcinoma. *Br J Cancer* **69**, 1160–1165 (1994).
9. Pickup, M. W. *et al.* Stromally derived lysyl oxidase promotes metastasis of transforming growth factor- β -deficient mouse mammary carcinomas. *Cancer Res* **73**, 5336–5346 (2013).
10. Provenzano, P. P. *et al.* Enzymatic targeting of the stroma ablates physical barriers to treatment of pancreatic ductal adenocarcinoma. *Cancer Cell* **21**, 418–429 (2012).
11. Radisky, E. S. & Radisky, D. C. Stromal induction of breast cancer: inflammation and invasion. *Rev Endocr Metab Disord* **8**, 279–287 (2007).
12. Rønnov-Jessen, L., Petersen, O. W. & Bissell, M. J. Cellular changes involved in conversion of normal to malignant breast: importance of the stromal reaction. *Physiol Rev* **76**, 69–125 (1996).
13. Ruffell, B. *et al.* Leukocyte composition of human breast cancer. *Proc Natl Acad Sci U S A* **109**, 2796–2801 (2012).
14. Pollard, J. W. Macrophages define the invasive microenvironment in breast cancer. *J Leukoc Biol* **84**, 623–630 (2008).
15. Arihiro, K., Oda, H., Kaneko, M. & Inai, K. Cytokines facilitate chemotactic motility of breast carcinoma cells. *Breast Cancer* **7**, 221–230 (2000).

16. Acerbi, I. *et al.* Human breast cancer invasion and aggression correlates with ECM stiffening and immune cell infiltration. *Integr. Biol. (Camb)*. (2015).
doi:10.1039/c5ib00040h
17. Ioachim, E. *et al.* Immunohistochemical expression of extracellular matrix components tenascin, fibronectin, collagen type IV and laminin in breast cancer: their prognostic value and role in tumour invasion and progression. *Eur. J. Cancer* **38**, 2362–2370 (2002).
18. Singh, P., Carraher, C. & Schwarzbauer, J. E. Assembly of fibronectin extracellular matrix. *Annu. Rev. Cell Dev. Biol.* **26**, 397–419 (2010).
19. Guo, C.-L. *et al.* Long-range mechanical force enables self-assembly of epithelial tubular patterns. *Proc Natl Acad Sci U S A* **109**, 5576–5582 (2012).
20. Lu, P., Takai, K., Weaver, V. M. & Werb, Z. Extracellular matrix degradation and remodeling in development and disease. *Cold Spring Harb Perspect Biol* **3**, (2011).
21. Egeblad, M., Rasch, M. G. & Weaver, V. M. Dynamic interplay between the collagen scaffold and tumor evolution. *Curr Opin Cell Biol* **22**, 697–706 (2010).
22. Netti, P. A., Berk, D. A., Swartz, M. A., Grodzinsky, A. J. & Jain, R. K. Role of extracellular matrix assembly in interstitial transport in solid tumors. *Cancer Res* **60**, 2497–2503 (2000).
23. Quail, D. F. & Joyce, J. A. Microenvironmental regulation of tumor progression and metastasis. *Nat. Med.* **19**, 1423–37 (2013).

24. Cassereau, L., Miroshnikova, Y., Ou, G., Lakins, J. & Weaver, V. M. A 3D tension bioreactor platform to study the interplay between ECM stiffness and tumor phenotype. *J. Biotechnol.* **193**, 66–69 (2014).
25. Zhang, X., Goncalves, R. & Mosser, D. M. The Isolation and Characterization of Murine Macrophages. *Curr. Protoc. Immunol.* **83**, 1–18 (2008).
26. McCubrey, J. A. *et al.* Targeting survival cascades induced by activation of Ras/Raf/MEK/ERK, PI3K/PTEN/Akt/mTOR and Jak/STAT pathways for effective leukemia therapy. *Leukemia* **22**, 708–22 (2008).
27. Charpin, C. *et al.* A signature predictive of disease outcome in breast carcinomas, identified by quantitative immunocytochemical assays. *Int J Cancer* **124**, 2124–2134 (2009).
28. Sommermann, T. G., O'Neill, K., Plas, D. R. & Cahir-McFarland, E. IKK β and NF- κ B transcription govern lymphoma cell survival through AKT-induced plasma membrane trafficking of GLUT1. *Cancer Res.* **71**, 7291–300 (2011).
29. López-Novoa, J. M. & Nieto, M. A. Inflammation and EMT: an alliance towards organ fibrosis and cancer progression. *EMBO Mol. Med.* **1**, 303–14 (2009).
30. Pickup, M. W., Mouw, J. K. & Weaver, V. M. The extracellular matrix modulates the hallmarks of cancer. *EMBO Rep* **15**, 1243–1253 (2014).

31. Willis, B. C. & Borok, Z. TGF-beta-induced EMT: mechanisms and implications for fibrotic lung disease. *Am. J. Physiol. Lung Cell. Mol. Physiol.* **293**, L525–L534 (2007).
32. Mouw, J. K. *et al.* Tissue mechanics modulate microRNA-dependent PTEN expression to regulate malignant progression. *Nat Med* **20**, 360–367 (2014).
33. Tse, J. R. & Engler, A. J. Preparation of hydrogel substrates with tunable mechanical properties. *Curr Protoc Cell Biol* **Chapter 10**, Unit 10.16 (2010).

Chapter 7: Conclusions & Future Directions

This thesis aimed to build on previous data suggesting a key role for extracellular matrix (ECM) mechanics in driving breast tumor aggression through focal adhesion signaling enhancing tumor cell invasion, migration, and ultimately metastasis^{1-3,4}. Consistently, previous work in our lab and others have implicated cell-ECM interactions as potent effectors of tumor cell proliferation, motility, metabolic adaptation, and immune system response through modulation of stromal immune cells and secreted cytokines^{4,5-9}. In particular, we have previously demonstrated cell-ECM adhesions through integrins as critical mechanical sensors of the remodeled ECM associated with tumor progression and aggression, which serve as potent signal transducers to drive tumor cell malignant phenotype^{5,7,10-13,14-18}. In spite of this mounting evidence supporting tissue physical properties as essential drivers of tumor development and malignancy, several questions remained unanswered:

1. How to engineer and implement an *ex vivo* system that recapitulates the complex heterogeneity, structure, and mechanics of the tumor ECM while still being highly controllable for the study of tumor cell-ECM interactions?
2. In considering integrin based mechanosignaling driving tumor aggression are there specific integrin dimer-ligand combinations that are key for malignant progression?
3. Downstream of integrin signaling, what cell signaling pathways are regulated by ECM mechanics and which are pertinent to tumor cell invasion and malignant phenotype?
4. In the remodeled ECM of the stroma, how are other cell types affected and how do they contribute to tumor aggression?

5. How can I accurately measure and assess the mechanical changes and remodeling that occurs with tumor progression and can I relate specific modifications to malignant progression?

This thesis addressed these questions and aimed to test the overall hypothesis that ECM mechanical properties influence tumor malignant progression through integrin focal adhesion signaling and subsequent downstream signaling affecting tumor motility and invasion, tumor metabolism, and immune cell response. I tested this hypothesis across five separate research projects ranging from the design of experimental systems to best study tumor cell-ECM interactions, determining which integrin dimers enhance tumor malignancy, the effects of ECM mechanics on tumor cell signaling downstream of integrins (specifically, growth factor receptors signaling and cell metabolism), and the role of tissue mechanical properties on stromal immune cells and the subsequent impact on tumor malignancy.

The combined results across these projects provide novel insight into how ECM biomechanics influence tumor cell phenotype and which signaling mechanisms are sensitive to ECM stiffness and contribute to malignant progression. Additionally, each of these projects has promising future directions with potential for development of experimental systems, which accurately recapitulate the entire tissue microenvironment, novel therapeutic targets, and new insights to tumor aggression and tissue mechanics allowing more accurate diagnostic tests. The results and future directions of each project are summarized individually in the following sections.

Development of a bioreactor to study mechanically sensitive cell-ECM interactions in 3D

Initially, one of the critical technical hurdles of this thesis work was the lack of appropriate *ex vivo* systems in which to study ECM stiffness and its effects on tumor cell behavior. The standard systems available at the inception of this work were either experimentally intractable to control and assess dynamically, such as *in vivo* animal models, or did not adequately capture the complex, multi component, and 3D structure of native tissue^{10,19-21}. While a growing number of 3D hydrogel systems had tried to address this many suffered from lack of independent control of stiffness and topology (natural ECM hydrogels) or were not as bioactive nor biocompatible as native tissue (synthetic hydrogels)²²⁻²⁷. With these limitations in mind I designed a tension bioreactor system in which I could tune collagen hydrogel stiffness through strain hardening without altering pore size. This system provided several key advantages as collagen is amenable to growth factor and adhesion ligand tethering, cell remodeling, and is the primary structural component of the mammary gland. Using this system combined with pre-malignant and malignant mammary epithelial cells (MEC) I demonstrated that ECM stiffness alone could enhance tumor cell invasion and that the tension bioreactor could serve as a suitable *in vitro* intermediate between higher throughput 2D hydrogel systems and *in vivo* models¹⁰.

In its current state, the bioreactor is limited to studying general tumor cell invasion, whereas in a tumor vasculature provides chemoattractant gradients for directed cell migration as well as sites for intravasation. Recapitulating this tissue element in the bioreactor would be a key technological leap forward for the physiological relevance of the phenotypes observed with the bioreactor. Other groups have also been experimenting with

this through 3D printing of scaffolds for endothelial cell tube formation and subsequent embedding of this primitive vascular network in a full collagen gel with tumor cells^{28,29}. This network is then amenable to perfusion and long term culture in which tumor cell invasion and migration can be monitored and tumor cells entering “circulation” can be quantified. However, several technical challenges still exist such as how to determine the shape, density, and geometry of the vascular network, optimizing perfusion flow profile and what media type to use for a endothelial-tumor co-culture, and for the case of the bioreactor how would the endothelial network react under tension? Yet, such improvements would dramatically improve bioreactor physiological relevance and enhance functionality for studying tumor cell-ECM interactions and in particular tumor cell invasion.

The role of $\alpha 5$ integrin - FN interactions in tumor malignant phenotype

While several previous works in my lab and others had implicated integrin signaling as a key mechanotransduction mechanism in tumor cells, there exist 24 integrin heterodimer-ligand pairs, and whether they are all equally important to tumor progression or whether specific pairs were critical drivers of malignant phenotype remained unclear^{2,12,30,31}. I had seen specific up regulation of alpha 5 integrin and its ligand fibronectin with oncogenic transformation, and I then aimed to determine whether alpha 5-FN binding was uniquely important for tumor cell malignant progression and if so how? Critically, I found that specifically overexpressing alpha 5 in the presence of fibronectin induces a malignant phenotype in normal MEC while blocking alpha 5 – FN binding reverts malignant tumor cells to a normal phenotype demonstrating alpha 5 – FN is both necessary and sufficient for tumor malignant progression. Alpha 5 – FN binding is distinct from other

integrin ligand adhesions in that alpha 5 engages both the RGD domain and a secondary synergy site, PHSRN, causing a catch-bond effect^{17,32,33,34}. I showed that this catch-bond causes integrin clustering, higher strength of adhesion, enhanced cell contractility, and subsequently enhanced pro-invasion cell signaling (Akt and Erk). Importantly, these alterations in cell signaling resulted in enhanced tumor cell invasion dependent on the increased cell contractility from alpha 5 – FN binding. Critically, I also found that full engagement of the synergy site required a stiffened substrate, such as collagen bundles in the tumor stroma, as even with alpha 5 FN binding, cells plated on soft substrates did not recapitulate the malignant phenotype.

These results have several important clinical implications and potential translational impacts in both breast tumor prognostics and therapeutics. Here I demonstrated how up regulation of alpha 5 and FN both correlate with a malignant phenotype making them attractive potential targets for human tumor pathology^{15,31,35,36,37}. Moreover, new probes targeting specific conformations of FN can allow detection of synergy site engagement thus allowing for the alpha 5 – FN binding and the pro-invasion phenotype it potentiates to be detected^{38,39}. However, several of the findings in this work would need to be validated in large patient cohorts. Relatedly, the alpha 5 – FN interaction can be targeted therapeutically via the small molecule inhibitor of synergy site binding ATN-161^{17,36}, which I used in this work and was originally designed for clinical applications. However, integrin-FN binding is also critical to other fundamental biological processes such as wound healing and immune process limiting the potential of drugs such as ATN-161 when used systemically. Further research into local delivery of compounds

such as ATN-161 directly into the tumor microenvironment would better assess their clinical efficacy and potential.

Tumor metabolism is tuned by ECM mechanical properties and is a key mediator of tumor invasion and metastasis

While there exist many shared hallmarks of tumors between different indications and subtypes, few hallmarks are as critical to tumor development and as varied across tumor type as aberrant metabolism⁴⁰. Whether it be up regulation of glycolysis and lactic acid production, enhanced mitochondrial respiration, or increased ROS production, a wide variety of aberrant metabolic phenotypes have been observed in different tumors or even across a single tumor⁴¹⁻⁴⁷. Combining this variety with the fact that altered cell metabolism has been shown to be a marker of poor prognosis in clinical samples in several different indications and it is clear that a better understanding of tumor metabolism is critical for patient care⁴⁸⁻⁵⁰.

In this project, I aimed to build on previous data demonstrating ECM mechanics as potent regulators of cell signaling pathways, Akt, Hif1a, MYC, which have been shown to play a key role in controlling cell metabolism^{42,46,47,51-54}. Consistently, I demonstrated that breast tumor cells on stiffened matrices have significantly higher levels of key metabolic regulators such as the glucose transporters, glycolytic enzymes, lactic acid fermentation enzymes, and lactic acid transporters. These changes are consistent with previous data suggesting breast tumors are highly dependent on glycolysis and I hypothesized that this change might be to support the increased energy demands and biogenesis required for the enhanced cell proliferation and invasion seen in stiffened microenvironments.

To test this hypothesis I postulated that cells on stiff substrates would be more sensitive to metabolic inhibition, specifically nutrient deficiency, but interestingly I found the opposite. In fact, tumor cells in stiff substrates were less sensitive to nutrient stress suggesting that the metabolic change with stiffness actually allows tumor cell flexibility and adaptability when nutrients may be low such as early in tumorigenesis when vascularization might be poor. However, I next showed that by targeting the metabolic adaptation directly, via metformin⁵⁵, tumor cell invasion and proliferation in stiff ECMs are significantly blunted. Importantly, this also translates *in vivo* as metformin treatment prevented tumor growth, EMT, and metastasis in the MMTV PyMT breast carcinoma model.

Future directions in this work will further explore the mechanistic underpinnings of the observed phenotypes and more in depth look at functional metabolic changes. Specifically, while I have strong evidence of metformin preventing metastasis, its mechanism of action (AMPk activation) interacts with many pathways (Akt, MYC, Hif1a, mTor) making it difficult with the current data to determine which pathways are most critical⁵⁶⁻⁵⁸. Additionally, the fundamental changes I have observed in tumor cell metabolism downstream of integrin signaling are likely influenced by specific integrin-ligand dimer pairs as I showed alpha 5 – FN as a key driver of Akt signaling for example. In the future I would like to determine any integrin specificity that may exist in tumor cell metabolic adaptation in response to stiffness.

Also, most observations here regarding metabolic changes have focused on protein and expression levels of key regulators (glucose transporters for example) and I have yet to assess changes on functional metabolism such as glucose metabolism, oxygen consumption, or ATP production for example. Existing technologies, mass spectroscopy and H¹-NMR, and newer

technologies, Seahorse metabolic profiler and C¹³ hyperpolarized NMR, would allow static and dynamic profiling of metabolite profile and metabolic rates⁴⁹. This type of data would provide strong credence to my protein and expression level data and dovetail with proposed new diagnostic technologies. Specifically, the metabolic profile defined here related to malignant progression and tissue stiffness could be measured with hyperpolarized NMR in a clinical setting and allow better assessment of patient risk. Additionally, metformin itself has been shown to have protective effects in human tumor patients⁵⁵⁻⁵⁸. The data here supports this concept of metformin as potentially useful as a preventative measure in high risk patients pending large scales human clinical trials.

A quantitative mechanical and structural analysis of human tumor tissue remodeling accompanying malignant transformation

Having established ECM remodeling and stiffening as correlating with metastatic progression *in vivo*² and several other stiffness based metrics demonstrating this translates to a clinical setting⁵⁹⁻⁶⁴ I aimed to quantitatively assess what ECM remodeling is occurring in human breast tumors and how this translates to tissue mechanical changes with tumor progression and aggression. I found consistent with previous results^{65,66}, human tumors demonstrate significant collagen fibrosis with tumor progression. Specifically, I observed increased collagen linearization and bundling, which correlated with significantly increased elastic modulus and as expected enhanced tumor cell mechanosignaling. Intriguingly, these trends also hold across subtypes with the most aggressive subtypes (Her2+, triple negative) demonstrating significantly more fibrosis and subsequent stiffening. Coincident with this fibrosis, I observed dramatic

macrophage infiltration and activation scaling with the degree of collagen remodeling and stiffening.

These critical observations have interesting implications for potential patient therapies and prognostic approaches. Techniques that measure tumor rigidity could potentially allow better assessment of patient risk for a given tumor. Additionally, the correlation between immune infiltrate and ECM stiffening suggests a possible role for macrophage in inducing ECM remodeling and driving tumor progression, supporting current clinical trials using anti-CSF1 treatments. Moreover, this suggests that patients with highly fibrotic tumors could potentially benefit most from anti-CSF1 treatment.

Investigating a link between tissue mechanics and tumor immune response in breast cancer malignant progression

Following up on my observation that in human breast tumors there is significant ECM remodeling concordant with tumor progression and aggression and this is associated with significant immune infiltrate⁴, I next aimed to explore the relationship between ECM mechanics, immune cell response, and how they relate to tumor malignant phenotype. Interestingly, I found that ECM stiffness, infiltrating macrophage, and tumor cell inflammatory signaling via Stat3 are all dependent on each other and all necessary for metastasis. These results provide several interesting possible therapeutic targets as both preventing macrophage infiltrate or targeting the downstream signaling in the tumor cells themselves, Stat3, both prevented metastasis in breast cancer animal models. Whether these treatments would work in

a clinical setting or whether similar therapies targeting immune cell infiltrate and subsequent inflammatory setting is not yet clear but promising.

In future work I would want to explore how other elements of the ECM influence these interactions, specifically integrin-FN interactions, or how downstream cell signaling in the tumor altered by ECM mechanics, such as tumor cell metabolism, determines tumor cell immune cell interaction. I have demonstrated previously a distinct role for specifically alpha 5 integrin – FN focal adhesion signaling in driving tumor cell malignant phenotype and would like to connect those findings with the results from this project in which there is a clear relationship between ECM mechanics and tumor – immune cell interactions with a potent effect on malignant progression. In particular, is FN deposition a prerequisite for the relationship between immune cell response and tumor aggression I observed here? Does altered tumor cell metabolism play an important role in both the tumor's response to secreted cytokines and the soluble factors the tumor secretes?

Beyond breast cancer

While the work presented here is solely focused on breast cancer, many of the findings or the experimental systems developed could be expanded to other cancer types or other fields entirely.

ECM mechanics in other carcinomas

Fibrosis in solid carcinomas such as pancreatic, liver, prostate, or ovarian cancer have also been implicated as correlating with poor prognosis such as in breast cancer^{63,67,68,69,70,71-73}. Thus, many of the results and systems used in this thesis could be adapted to studying other

cancers, but several technical challenges still exist. Outside of just needing a different cell source, tissue composition also varies widely between all of these organ types with a variety of collagen subtypes (I, III, V) being the dominant structural component depending on the system^{20,23}. Additionally relative amounts of other ECM adhesion ligands such as fibronectin or tenascin C would also have to be tuned^{21,23,74}. Moreover, the stiffness appropriate for each tissue and its relative tumor associated stroma also are system specific^{75,76}. Thus, experimental models like the tension bioreactor would have to be significantly altered to achieve the appropriate composition and mechanics.

Additionally, while the signaling mechanisms shown here related to ECM mechanics give a good starting point for looking at stiffness mediated tumor cell signaling, I can't assume that these trends are automatically a given in all tumor types. For example, in pancreatic cancer severe fibrosis was actually shown to blunt tumor progression⁷⁰. Also again considering the variety of ECM compositions across these tissues, integrin specific signaling will have to be accounted for.

ECM mechanics in tissue engineering and regenerative medicine

The effects of stiffness on cell behaviors I have shown here, proliferation, migration, metabolism, while studied in a tumor context could also be of interest in a tissue engineering or regenerative medicine context^{10,24-27,29}. In particular, many of my observations could be implemented when designing synthetic materials for replacement tissues, such as a cardiac patch or a skin graft, or used to enhance stem or progenitor cell culture^{27,77,78}. Additionally, systems like the tension bioreactor could be adapted to study wound healing as many of the same mechanisms of fibrosis at work in cancer are normally regulated to control proper wound

healing through scarring^{11,39,74}. Overall, this work and the technologies used provide a new potential area of research outside of cancer entirely if adapted to suit the model system

Conclusions and Final Comments

Here I aimed to explore the relationship between tissue mechanics and tumor malignancy, building on previous data closely linking the two. In this work I engineered and optimized several *in vitro* systems allowing me to carefully tune substrate composition and mechanical properties. I then used these systems combined with *in vivo* animal models and clinical samples to carefully and quantitatively assess tumor cell – ECM interactions and both how a tumor cell senses and interacts with its environment and how this alters its signaling and behavior to drive tumor progression. From my work I was able to identify specific integrin-ECM interactions, which drive tumor aggression as well as implicating ECM mechanics as altering tumor metabolism and host immune response all of which were critical for tumor metastasis. These results provide new insight for the breast cancer field and clearly underline the importance of considering the ECM and its physical properties. Several new exciting directions are also in progress, which will further develop the observations, made here. Future endeavors can also translate these results or systems used to have an impact on research in other cancer indications or other fields entirely, such as tissue engineering, which might also benefit from a clearer understanding of mechanosignaling in driving cell and tissue behavior.

Works Cited:

1. Paszek, M. J. *et al.* Tensional homeostasis and the malignant phenotype. *Cancer Cell* **8**, 241–54 (2005).
2. Levental, K. R. *et al.* Matrix crosslinking forces tumor progression by enhancing integrin signaling. *Cell* **139**, 891–906 (2009).
3. Dvorak, H. F., Weaver, V. M., Tlsty, T. D. & Bergers, G. Tumor microenvironment and progression. *J Surg Oncol* **103**, 468–474 (2011).
4. Acerbi, I. *et al.* Human breast cancer invasion and aggression correlates with ECM stiffening and immune cell infiltration. *Integr. Biol. (Camb)*. (2015).
doi:10.1039/c5ib00040h
5. Yeung, T. *et al.* Effects of substrate stiffness on cell morphology, cytoskeletal structure, and adhesion. *Cell Motil. Cytoskeleton* **60**, 24–34 (2005).
6. Rubashkin, M. G. *et al.* Force engages vinculin and promotes tumor progression by enhancing PI3K activation of phosphatidylinositol (3,4,5)-triphosphate. *Cancer Res.* **74**, 4597–611 (2014).
7. Mouw, J. K. *et al.* Tissue mechanics modulate microRNA-dependent PTEN expression to regulate malignant progression. *Nat Med* **20**, 360–367 (2014).

8. Pickup, M. W., Mouw, J. K. & Weaver, V. M. The extracellular matrix modulates the hallmarks of cancer. *EMBO Rep* **15**, 1243–1253 (2014).
9. Damiano, L. *et al.* Oncogenic targeting of BRM drives malignancy through C/EBP β -dependent induction of α 5 integrin. *Oncogene* **33**, 2441–2453 (2014).
10. Cassereau, L., Miroshnikova, Y., Ou, G., Lakins, J. & Weaver, V. M. A 3D tension bioreactor platform to study the interplay between ECM stiffness and tumor phenotype. *J. Biotechnol.* **193**, 66–69 (2014).
11. Barker, T. H. *et al.* SPARC regulates extracellular matrix organization through its modulation of integrin-linked kinase activity. *J. Biol. Chem.* **280**, 36483–93 (2005).
12. Weaver, V. M. *et al.* Reversion of the malignant phenotype of human breast cells in three-dimensional culture and in vivo by integrin blocking antibodies. *J. Cell Biol.* **137**, 231–45 (1997).
13. Samuel, M. S. *et al.* Actomyosin-mediated cellular tension drives increased tissue stiffness and β -catenin activation to induce epidermal hyperplasia and tumor growth. *Cancer Cell* **19**, 776–91 (2011).
14. Mierke, C. T., Frey, B., Fellner, M., Herrmann, M. & Fabry, B. Integrin α 5 β 1 facilitates cancer cell invasion through enhanced contractile forces. *J. Cell Sci.* **124**, 369–83 (2011).

15. Nam, J.-M., Onodera, Y., Bissell, M. J. & Park, C. C. Breast cancer cells in three-dimensional culture display an enhanced radioresponse after coordinate targeting of integrin alpha5beta1 and fibronectin. *Cancer Res.* **70**, 5238–48 (2010).
16. Park, C. C. *et al.* Beta1 integrin inhibitory antibody induces apoptosis of breast cancer cells, inhibits growth, and distinguishes malignant from normal phenotype in three dimensional cultures and in vivo. *Cancer Res.* **66**, 1526–35 (2006).
17. Stoeltzing, O. *et al.* Inhibition of integrin alpha5beta1 function with a small peptide (ATN-161) plus continuous 5-FU infusion reduces colorectal liver metastases and improves survival in mice. *Int. J. Cancer* **104**, 496–503 (2003).
18. Maschler, S. *et al.* Tumor cell invasiveness correlates with changes in integrin expression and localization. *Oncogene* **24**, 2032–41 (2005).
19. Wolf, K. *et al.* Physical limits of cell migration: control by ECM space and nuclear deformation and tuning by proteolysis and traction force. *J Cell Biol* **201**, 1069–1084 (2013).
20. Kadler, K. E., Hill, A. & Canty-Laird, E. G. Collagen fibrillogenesis: fibronectin, integrins, and minor collagens as organizers and nucleators. *Curr. Opin. Cell Biol.* **20**, 495–501 (2008).
21. Singh, P., Carraher, C. & Schwarzbauer, J. E. Assembly of fibronectin extracellular matrix. *Annu. Rev. Cell Dev. Biol.* **26**, 397–419 (2010).

22. Ulrich, T. A., Jain, A., Tanner, K., MacKay, J. L. & Kumar, S. Probing cellular mechanobiology in three-dimensional culture with collagen-agarose matrices. *Biomaterials* **31**, 1875–1884 (2010).
23. Dallas, S. L., Chen, Q. & Sivakumar, P. Dynamics of Assembly and Reorganization of Extracellular Matrix Proteins. *Curr. Top. Dev. Biol.* **75**, 1–24 (2006).
24. Miroshnikova, Y. A. *et al.* Engineering strategies to recapitulate epithelial morphogenesis within synthetic three-dimensional extracellular matrix with tunable mechanical properties. *Phys Biol* **8**, 26013 (2011).
25. Guo, C.-L. *et al.* Long-range mechanical force enables self-assembly of epithelial tubular patterns. *Proc Natl Acad Sci U S A* **109**, 5576–5582 (2012).
26. Tse, J. R. & Engler, A. J. Preparation of hydrogel substrates with tunable mechanical properties. *Curr Protoc Cell Biol* **Chapter 10**, Unit 10.16 (2010).
27. Young, J. L. & Engler, A. J. Hydrogels with time-dependent material properties enhance cardiomyocyte differentiation in vitro. *Biomaterials* **32**, 1002–1009 (2011).
28. Kim, C., Kasuya, J., Jeon, J., Chung, S. & Kamm, R. D. A quantitative microfluidic angiogenesis screen for studying anti-angiogenic therapeutic drugs. *Lab Chip* **15**, 301–10 (2015).
29. Jeon, J. S. *et al.* Human 3D vascularized organotypic microfluidic assays to study breast cancer cell extravasation. *Proc. Natl. Acad. Sci. U. S. A.* **112**, 214–9 (2015).

30. Gallant, N. D., Michael, K. E. & García, A. J. Cell adhesion strengthening: contributions of adhesive area, integrin binding, and focal adhesion assembly. *Mol. Biol. Cell* **16**, 4329–40 (2005).
31. Dingemans, A.-M. C. *et al.* Integrin expression profiling identifies integrin alpha5 and beta1 as prognostic factors in early stage non-small cell lung cancer. *Mol. Cancer* **9**, 152 (2010).
32. García, A. J., Huber, F. & Boettiger, D. Force required to break alpha5beta1 integrin-fibronectin bonds in intact adherent cells is sensitive to integrin activation state. *J. Biol. Chem.* **273**, 10988–93 (1998).
33. Friedland, J. C., Lee, M. H. & Boettiger, D. Mechanically activated integrin switch controls alpha5beta1 function. *Science* **323**, 642–4 (2009).
34. Kong, F., García, A. J., Mould, a P., Humphries, M. J. & Zhu, C. Demonstration of catch bonds between an integrin and its ligand. *J. Cell Biol.* **185**, 1275–84 (2009).
35. Desgrosellier, J. S. & Cheresh, D. a. Integrins in cancer: biological implications and therapeutic opportunities. *Nat. Rev. Cancer* **10**, 9–22 (2010).
36. Barkan, D. & Chambers, A. F. β 1-integrin: a potential therapeutic target in the battle against cancer recurrence. *Clin Cancer Res* **17**, 7219–7223 (2011).
37. Cordes, N. & Park, C. C. beta1 integrin as a molecular therapeutic target. *Int J Radiat Biol* **83**, 753–760 (2007).

38. Cao, L. *et al.* Phage-based molecular probes that discriminate force-induced structural states of fibronectin in vivo. *Proc. Natl. Acad. Sci. U. S. A.* **109**, 7251–6 (2012).
39. Bachman, H., Nicosia, J., Dysart, M. & Barker, T. H. Utilizing Fibronectin Integrin-Binding Specificity to Control Cellular Responses. *Adv. wound care* **4**, 501–511 (2015).
40. Cairns, R. A., Harris, I. S. & Mak, T. W. Regulation of cancer cell metabolism. *Nat. Rev. Cancer* **11**, 85–95 (2011).
41. Semenza, G. L. Tumor metabolism: cancer cells give and take lactate. *J. Clin. Invest.* **118**, 3835–7 (2008).
42. Denko, N. C. Hypoxia, HIF1 and glucose metabolism in the solid tumour. *Nat. Rev. Cancer* **8**, 705–13 (2008).
43. Diehn, M. *et al.* Association of reactive oxygen species levels and radioresistance in cancer stem cells. *Nature* **458**, 780–3 (2009).
44. Wallace, D. C. Mitochondria and cancer. *Nat. Rev. Cancer* **12**, 685–98 (2012).
45. Mukherjee, J. *et al.* Pyruvate kinase M2 expression, but not pyruvate kinase activity, is up-regulated in a grade-specific manner in human glioma. *PLoS One* **8**, e57610 (2013).
46. Le, A. *et al.* Tumorigenicity of hypoxic respiring cancer cells revealed by a hypoxia-cell cycle dual reporter. *Proc. Natl. Acad. Sci. U. S. A.* **111**, 12486–91 (2014).

47. Doherty, J. R. *et al.* Blocking lactate export by inhibiting the Myc target MCT1 Disables glycolysis and glutathione synthesis. *Cancer Res.* **74**, 908–20 (2014).
48. Pinheiro, C. *et al.* GLUT1 and CAIX expression profiles in breast cancer correlate with adverse prognostic factors and MCT1 overexpression. *Histol. Histopathol.* **26**, 1279–86 (2011).
49. Asghar Butt, S. *et al.* Monitoring mammary tumor progression and effect of tamoxifen treatment in MMTV-PymT using MRI and magnetic resonance spectroscopy with hyperpolarized [1-(13) C]pyruvate. *Magn. Reson. Med.* (2014). doi:10.1002/mrm.25095
50. Lüftner, D. *et al.* Tumor type M2 pyruvate kinase expression in advanced breast cancer. *Anticancer Res.* **20**, 5077–82
51. Lea, M. A., Pourat, J., Patel, R. & desBordes, C. Growth inhibition of colon cancer cells by compounds affecting AMPK activity. *World J. Gastrointest. Oncol.* **6**, 244–52 (2014).
52. Muniyappa, H., Song, S., Mathews, C. K. & Das, K. C. Reactive oxygen species-independent oxidation of thioredoxin in hypoxia: inactivation of ribonucleotide reductase and redox-mediated checkpoint control. *J. Biol. Chem.* **284**, 17069–81 (2009).
53. Elstrom, R. L. *et al.* Akt stimulates aerobic glycolysis in cancer cells. *Cancer Res.* **64**, 3892–9 (2004).

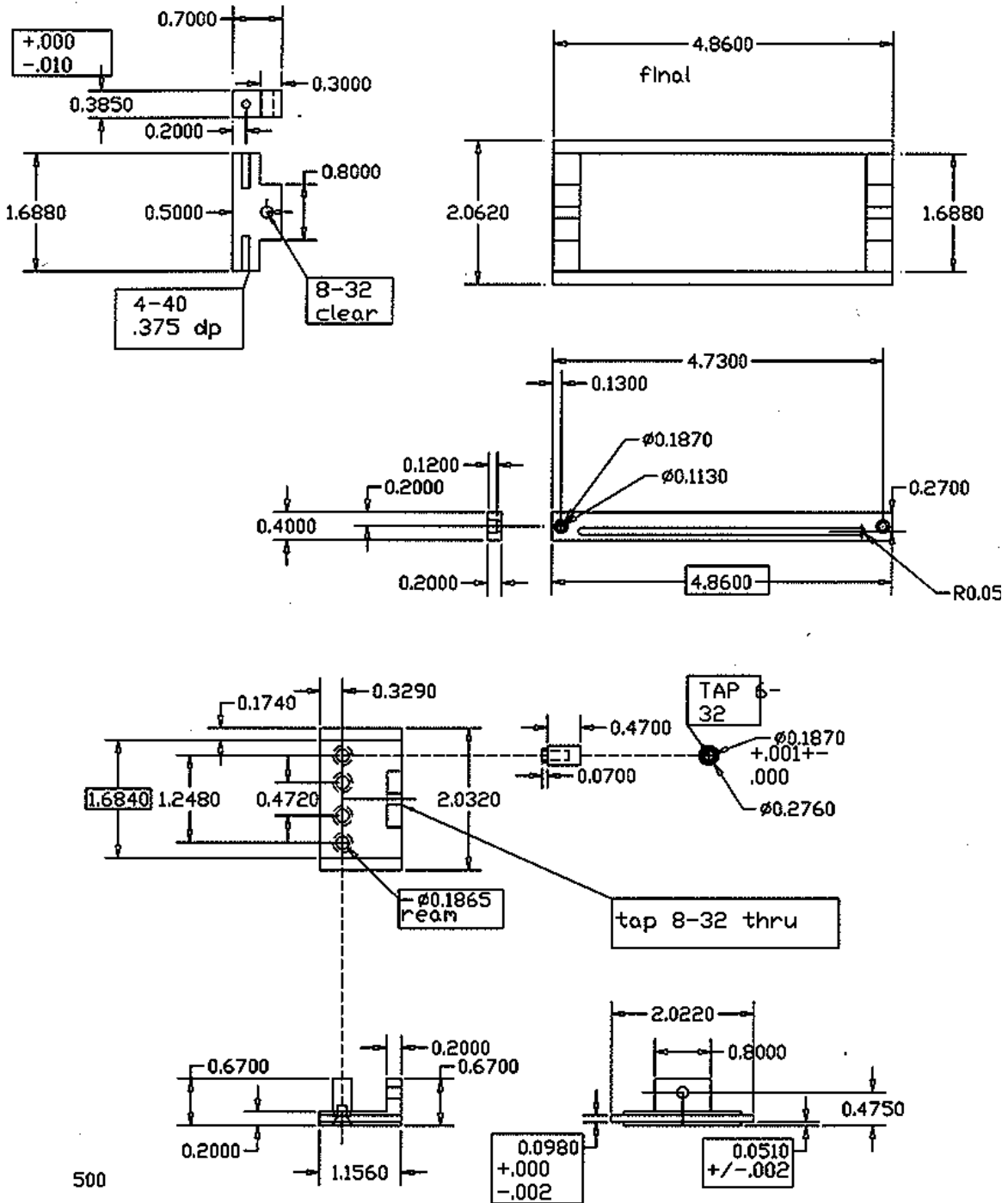
54. Sommermann, T. G., O'Neill, K., Plas, D. R. & Cahir-McFarland, E. IKK β and NF- κ B transcription govern lymphoma cell survival through AKT-induced plasma membrane trafficking of GLUT1. *Cancer Res.* **71**, 7291–300 (2011).
55. Leone, A., Di Gennaro, E., Bruzzese, F., Avallone, A. & Budillon, A. New perspective for an old antidiabetic drug: metformin as anticancer agent. *Cancer Treat. Res.* **159**, 355–76 (2014).
56. Zakikhani, M., Dowling, R., Fantus, I. G., Sonenberg, N. & Pollak, M. Metformin is an AMP kinase-dependent growth inhibitor for breast cancer cells. *Cancer Res.* **66**, 10269–73 (2006).
57. Anisimov, V. N. *et al.* Metformin extends life span of HER-2/neu transgenic mice and in combination with melatonin inhibits growth of transplantable tumors in vivo. *Cell Cycle* **9**, 188–97 (2010).
58. Zordoky, B. N. M., Bark, D., Soltys, C. L., Sung, M. M. & Dyck, J. R. B. The anti-proliferative effect of metformin in triple-negative MDA-MB-231 breast cancer cells is highly dependent on glucose concentration: implications for cancer therapy and prevention. *Biochim. Biophys. Acta* **1840**, 1943–57 (2014).
59. Chang, J. M. *et al.* Stiffness of tumours measured by shear-wave elastography correlated with subtypes of breast cancer. *Eur Radiol* **23**, 2450–2458 (2013).

60. Lopez, J. I., Kang, I., You, W.-K., McDonald, D. M. & Weaver, V. M. In situ force mapping of mammary gland transformation. *Integr. Biol. (Camb)*. **3**, 910–21 (2011).
61. Samani, A., Zubovits, J. & Plewes, D. Elastic moduli of normal and pathological human breast tissues: an inversion-technique-based investigation of 169 samples. *Phys. Med. Biol.* **52**, 1565–76 (2007).
62. Plodinec, M. *et al.* The nanomechanical signature of breast cancer. *Nat. Nanotechnol.* **7**, 757–65 (2012).
63. Venkatesh, S. K. *et al.* MR elastography of liver tumors: preliminary results. *AJR. Am. J. Roentgenol.* **190**, 1534–40 (2008).
64. Balleyguier, C. *et al.* Breast elasticity: principles, technique, results: an update and overview of commercially available software. *Eur J Radiol* **82**, 427–434 (2013).
65. Conklin, M. W. *et al.* Aligned collagen is a prognostic signature for survival in human breast carcinoma. *Am J Pathol* **178**, 1221–1232 (2011).
66. Provenzano, P. P. *et al.* Collagen density promotes mammary tumor initiation and progression. *BMC Med* **6**, 11 (2008).
67. Nakagawa, H. *et al.* Loss of liver E-cadherin induces sclerosing cholangitis and promotes carcinogenesis. *Proc. Natl. Acad. Sci. U. S. A.* 2–7 (2014). doi:10.1073/pnas.1322731111
68. Barr, R. G. Elastography in clinical practice. *Radiol. Clin. North Am.* **52**, 1145–62 (2014).

69. Silva, S. A. *et al.* Prostate hyperplasia caused by long-term obesity is characterized by high deposition of extracellular matrix and increased content of MMP-9 and VEGF. *Int. J. Exp. Pathol.* **96**, 21–30 (2015).
70. Ozdemir, B. C. *et al.* Depletion of carcinoma-associated fibroblasts and fibrosis induces immunosuppression and accelerates pancreas cancer with reduced survival. *Cancer Cell* **25**, 719–34 (2014).
71. Raglow, Z. & Thomas, S. M. Tumor matrix protein collagen XI α 1 in cancer. *Cancer Lett.* **357**, 448–53 (2015).
72. Tilbury, K. & Campagnola, P. J. Applications of second-harmonic generation imaging microscopy in ovarian and breast cancer. *Perspect. Medicin. Chem.* **7**, 21–32 (2015).
73. Welge, W. A. *et al.* Diagnostic potential of multimodal imaging of ovarian tissue using optical coherence tomography and second-harmonic generation microscopy. *J. Med. imaging (Bellingham, Wash.)* **1**, 025501 (2014).
74. Lu, P., Takai, K., Weaver, V. M. & Werb, Z. Extracellular matrix degradation and remodeling in development and disease. *Cold Spring Harb Perspect Biol* **3**, (2011).
75. Egeblad, M., Rasch, M. G. & Weaver, V. M. Dynamic interplay between the collagen scaffold and tumor evolution. *Curr Opin Cell Biol* **22**, 697–706 (2010).

76. Netti, P. A., Berk, D. A., Swartz, M. A., Grodzinsky, A. J. & Jain, R. K. Role of extracellular matrix assembly in interstitial transport in solid tumors. *Cancer Res* **60**, 2497–2503 (2000).
77. Lijnen, P. & Petrov, V. Transforming growth factor-beta 1-induced collagen production in cultures of cardiac fibroblasts is the result of the appearance of myofibroblasts. *Methods Find Exp Clin Pharmacol* **24**, 333–344 (2002).
78. Miklas, J. W. *et al.* Bioreactor for modulation of cardiac microtissue phenotype by combined static stretch and electrical stimulation. *Biofabrication* **6**, 24113 (2014).

Appendix 1: Tension bioreactor schematics and protocols
Loading frame schematic



500

Creating fibrillar Col I hydrogels in bioreactor

Materials:

- 5% Glutaraldehyde in PBS
- 10% APTES in EtOH
(Keep all hydrogel reagents on ice)
- Acid solubilized rat tail collagen I (3.1-5 mg/ml)
- 1N NaOH
- 10X DMEM buffer
- Fibronectin 1mg/ml (optional)
- BSA
- Matrigel

Protocol:

1. Plasma clean inserts for 5 minutes on high setting
2. Add 200 ul 10% APTES in EtOH in each well in membrane and heat to 60°C for 1 hour
(Check status at 30 min and every following 10 min, remove before all liquid has evaporated)
3. Thoroughly rinse with dH₂O, 5x 5 min
4. Add 200 ul 5% Glutaraldehyde in PBS incubate at room temperature for 30 min
5. Thoroughly rinse with dH₂O, 5x 5 min
6. Mix in this order (based on worksheet values)
 1. 10x DMEM
 2. 1N NaOH
 3. npH₂O
 4. BSA
 5. Matrigel
 6. FN
 7. Col I
 8. 1 N NaOH titrate in small volumes (5-10ul at a time) mixing well in between until the gel is a light pink/peach color
7. Add 100 ul of collagen solution per well as a base layer to prevent cells from sinking
8. Polymerize gel at 37°C for 30 min
9. Resuspend acini in collagen gel and add additional 100 ul per well
10. Polymerize gel at 37°C for 30 min
11. Add media on top of gels and culture for 2-5 days

Appendix 2: List of PCR primers used

- Mouse MCT1 (gene: SLC16A1)
 - TATTGGAGGTCTTGGGCTTG
 - GCCAGTGGTCGCTTCTTGTA

- Mouse MCT4 (gene: SLC16a3)
 - GGTCAGCGTCTTTTCAAGG
 - GGTCCTGTGCCATAGAGCAT

- Mouse LDH A
 - GACTCCAGTGTGCCTGTGTG
 - TCCTTCCACTGCTCCTTGTC

- Mouse LDH B
 - CCAACCCAGTGGATATTCTGA
 - GGAATCGAGCAGAATCCAGA

- Mouse Ca9 (pH balance- Hif1a target)
 - GTTTCCCTGCTGAGATCCAC
 - CAGAAAGGCAGCCAAAAGT

- Human Trx1 (key antioxidant system protein)
 - hTrx1 F CCTCACAGGATTAAGGCAACA
 - hTrx1 R TTCTTTGTCACCAGGGATGC

- Human PKM-1 (potentiates glycolysis)
 - hPKM1 F ACCGCAAGCTGTTTGAAGAA
 - hPKM1 R TCCATGAGGTCTGTGGAGTG

- Human PKM-2 (slows glycolysis to potentiate PPP for biogenesis)
 - hPKM2 F GAGGCCTCCTTCAAGTGCT
 - hPKM2 R CCAGACTTGGTGAGGACGAT

- Mouse PKM-1 (potentiates glycolysis)

- mPKM1 F ATTACCAGCGACCCACAG
- mPKM1 R TAGAAGAGGGGCTCCAGAGG

- Mouse PKM-2 (slows glycolysis to potentiate PPP for biogenesis)
 - mPKM2 F AGGATGCCGTGCTGAATG
 - mPKM2 R TAGAAGAGGGGCTCCAGAGG

- Mouse Trx1 (key antioxidant system protein)
 - mTrx1 F TCGAGAGCAAGGAAGCTTTT
 - mTrx1 R TGATCATTTTGCAAGGTCCA

- Mouse Slc1a5 (Neutral Amino Acid and Glutamate Transporter)
 - mSLC1A5 F CTCCTGGATTATGTGGTACGC
 - mSLC1A5 R CGGACGTCTTTCATCTCCAC

- Human Slc1a5 (Neutral Amino Acid and Glutamate Transporter)
 - hSLC1A5 F TGGGACCTCTTCCAGTTC
 - hSLC1A5 R ATGAAACGGCTGATGTGCTT

Publishing Agreement

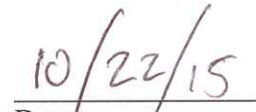
It is the policy of the University to encourage the distribution of all theses, dissertations, and manuscripts. Copies of all UCSF theses, dissertations, and manuscripts will be routed to the library via the Graduate Division. The library will make all theses, dissertations, and manuscripts accessible to the public and will preserve these to the best of their abilities, in perpetuity.

Please sign the following statement:

I hereby grant permission to the Graduate Division of the University of California, San Francisco to release copies of my thesis, dissertation, or manuscript to the Campus Library to provide access and preservation, in whole or in part, in perpetuity.



Author Signature



Date